VISCOSITY MEASUREMENTS AT PRESSURES UP TO 14 000 BAR USING AN AUTOMATIC FALLING CYLINDER VISCOMETER

A thesis submitted to the
Faculty of Engineering
of the
University of Glasgow

for the degree of
Doctor of Philosophy

by

JOHN BRUCE IRVING

Department of Electronics
& Electrical Engineering

June 1977

ProQuest LLC.
789 East Eisenhower Parkway
P.O. Box 1346
Ann Arbor, MI 48106 – 1346

SUMMARY

The thesis describes a new method for measuring the viscosity of liquids in a pressure vessel capable of reaching 14 000 bar, and results are presented for six liquids at 30°C, up to viscosities of 3000 P.

The technique is based on the well-tried principle of a cylindrical sinker falling in a viscometer tube. It departs from earlier systems in that the sinker is retrieved electromagnetically rather than by rotating the whole pressure vessel, and the sinker is held by a semi-permanent magnet before a fall time measurement is made. The sinkers do not have guiding pins, but rely on self-centering forces to ensure concentric fall. Another novel aspect is that a sinker with a central hole to produce faster fall times has been introduced for the first time. An analysis for such a sinker is presented, and when the diameter of the hole is mathematically reduced to zero, the equation of motion for the solid sinker is obtained. The solution for the solid cylinder is compared with earlier approximate analyses. The whole cycle of operation - retrieval, holding, releasing, sinker detection, and recording is remotely controlled and entirely automated.

With unguided falling weights it is essential that the viscometer tube is aligned vertically. The effects of non-vertical alignment are assessed both experimentally and theoretically. An original analysis is presented to explain the rather surprising finding that when a viscometer tube is inclined from the vertical, the sinker falls much more quickly. The agreement between experiment and theory is to within one per cent.

From the analysis of sinker motion, appropriate allowances for the change in sinker and viscometer tube dimensions under pressure are calculated; these are substantially linear with pressure. The viscometer was calibrated at atmospheric pressure with a variety of liquids whose viscosities were ascertained with calibrated suspended-level viscometers. Excellent linearity over three decades of viscosity was found for both sinkers. A careful analysis of errors shows that the absolute accuracy of measurement is to within ±1.8 per cent.

The fall time of the sinker is also a function of the buoyancy of the test liquid. Therefore a knowledge of the liquid density is required, both at atmospheric pressure and at elevated pressures. The linear differential transformer method for density measurement formed the basis of a new apparatus designed to fit into the high pressure vessel. Up to pressures of 5 kbar measurements are estimated to be within ±0.14 per cent, and above this pressure uncertainty could be as high as 0.25 per cent.

The last chapter deals with empirical and semi-theoretical viscosity-pressure equations. Two significant contributions are offered. The first is a new interpretation of the free volume equation in which physically realistic values of the limiting specific volume, v_o, are derived by applying viscosity and density data to the equation isobarically, not isothermally as most have done in the past. This led to a further simplification of the free volume equation to a two constant equation.

The second contribution is a purely empirical equation which describes the variation of viscosity as a function of pressure:

$$\ln(\eta/\eta_o)_t = A(e^{BP} - e^{-KP})$$

where η_o is the viscosity at atmospheric pressure, and A, B and K are constants. This 'double-exponential' equation is shown to describe data to within experimental error for viscosities which vary by as much as four decades with pressure. It also describes the different curvatures which the logarithm of viscosity exhibits when plotted as a function of pressure: concave towards the pressure axis, convex, straight line, or concave and then convex. The many other equations in existence cannot describe this variety of behaviour.

A C K N O W L E D G E M E N T S

The author expresses gratitude to Professor John Lamb for his permission to carry out this research, and for his encouragement during its progress.

The supervision of Dr A J Barlow, who initiated this study and discussed freely all its aspects, is gratefully acknowledged.

The author also wishes to thank his colleague Dr W C Pursley not only for many fruitful discussions and useful suggestions, but also for his patience in bringing the 14 kbar high-pressure vessel into working order. The assistance of departmental staff is sincerely acknowledged.

This work was supported by a Science Research Council grant for the first three years, and by a Post Graduate Fellowship from the Faculty of Engineering at Glasgow University for the fourth; both are gratefully acknowledged.

C O N T E N T S

Note: Section headings within chapters are listed at the beginning of each chapter

C H A P T E R 1

INTRODUCTION

List of Figures

List of Tables

CHAPTER 1

INTRODUCTION

1.1 The Importance of the Variation of Viscosity with Pressure

Viscosity is one of the fundamental transport properties of a fluid, and as such it has been the subject of considerable interest, both experimental and theoretical, since the nineteenth century. Early studies involved the measurement of viscosity under ambient conditions, but gradually the range of measurement has been extended to include high and low temperatures and increasing hydrostatic pressures.

The behaviour of liquid viscosity is of importance in many fields of engineering. One such area of interest is that of lubrication where liquids are often highly stressed, such as in gears, roller bearings, and other applications. In such situations an elastohydrodynamic régime prevails, and now that the thickness of lubricant in a contact zone can be predicted, a knowledge of its viscosity must be known to enable the friction of contact to be calculated. When gear teeth mesh, or when the surfaces of roller bearings meet, the hydrostatic pressure on the thin film of lubricating fluid separating the moving parts can be as high as 300 000 lbf in^{-2} (≈20 kbar)[1], according to Galvin, Jones and Naylor (1968)[2], and Trachman (1975). At such pressures the viscosity of the lubricant increases by several orders of magnitude, and it is thus self-evident that under such conditions this property of the lubricant is of dominant interest.

Viscosity is also of intrinsic scientific interest being one of the physical property variables in different theories of liquid behaviour. One such recent subject of study has been the effect of pressure on the

---

[1] Conversion factors for pressure are tabulated at the end of Chapter 7.

[2] In this thesis references are listed in alphabetical order.

viscoelastic properties of liquids, and experimental results from this work have been used for testing viscoelastic models such as that of Barlow, Erginsav and Lamb (1967).

1.2 Review of High-pressure Viscometry

Since the early work of Flowers (1914) many techniques have been devised for the measurement of the viscosity of liquids under hydrostatic pressure. The choice of method used is determined mainly by the maximum pressure involved and the viscosity range required. The upper limit of viscosity measurement of liquid under pressure was until recently about 3000 P[1]. The extension of this limit to about 10^7 P is discussed later. For viscosities up to 3000 P, weights falling or rolling under gravity are usually employed, the position of the weight and hence the time of fall being determined electrically by simple electrical contact or inductive methods.

The method that has been used most frequently for measuring liquid viscosity under pressure is the falling cylinder; it is based on a fundamental concept and thus has the advantage of simplicity, and in addition it permits operation in an entirely closed apparatus. The first recorded apparatus was that used by Lawaczeck (1919). He used guiding pins on the cylinder to ensure concentric fall, but it was not until 1943 that an unguided cylinder - a falling needle - was used by Seeder for measuring water and superheated steam viscosities.

Apart from the falling body, other methods have been developed, particularly in recent years. For example, there is the falling plate viscometer of Wilson (1967) and a capillary viscometer by Jones, Johnson, Winer, and Sanborn (1974) for use up to pressures of 5.4 kbar. Falling ball or rolling ball viscometers have also been widely used but the latter have the disadvantage that at higher viscosities there may be uncertainty as to whether the ball is rolling or sliding down the viscometer tube.

---

[1] Viscosity units with conversion factors are in section 1.6 of this Chapter.

The falling cylinder type of viscometer for measurements under pressure has proved to be the most successful, and this type of apparatus has provided two outstanding sources of viscosity-pressure data. The first is Bridgman of Harvard who was the pioneer of high-pressure techniques and a prolific author. He made measurements up to 12 kbar on many liquids, Bridgman (1926). The second is the ASME (American Society of Mechanical Engineers) who published data on forty-four liquids in 1953 at pressures up to 10 kbar covering a wide temperature range from 32 to 425°F.

1.2.1 Falling cylinder viscometers

The fall time of a cylinder in a closely fitting viscometer tube is related to fluid viscosity by the relationship

$$\frac{\eta}{(\rho_1 - \rho_2)} = KT \qquad (1.1)$$

where K is a constant, and ρ_1 and ρ_2 are the densities of the cylinder and the fluid through which it falls. The constant K which is a term dependent upon the geometry can be calculated (c.f. Chapter 3), but is usually found by calibration. Provided that the sinker and liquid densities are known, it is a straightforward operation to derive dynamic viscosity η from a fall time measurement.

In Table 1.1 there is a list in chronological order of those who adopted the falling cylinder viscometer with guiding pins or other protuberances to ensure concentric fall within the viscometer tube.

Table 1.1

List of workers who used guided falling cylinder viscometers

Author	Date	Maximum pressure kbar	Temperature range °C	Tube dia. mm	b/a*	Remarks
Lawaczeck	1919	atm	-	10	.952	
Heinz	1925	Thesis (in German) not seen				
Bridgman	1926	12	30-75	6	.958 .75	Hollow sinker filled with gold or tungsten
Kiesskalt	1927	This reference has not been seen				
Stakelbeck	1933	0.1	-20 to 40	12	.981 .984	
Hawkins, Solberg & Potter	1935	0.24	160-540	10.4	.961 .978	
Mason	1935	0.27	——— Not stated ———			No measurements reported
Bolarovich	1940	1.0	60	Reference (in Russian) unobtainable		
Steiner	1949	atm	——— Not stated ———			
Bradbury, Mark & Kleinschmidt	1951	10	0-218	-	-	} Preview of ASME Report
ASME Report	1953	10	0-218	6.5	.663 .959	} 5.400 P limit ±2% error
Heiks and Orban	1956	12.7	90-288	12.3	.968	
Swift(a)	1959		-185 to 90	8	.955 .980	
Huang	1966	0.3	-170 to -37.8	8	.979 .983	
Cappi	1964	10	0-100	7.67	.958 .970	
Kozlov and Yakovlev	1966		20-280	Not stated		
Gabibov and Tsaturyants	1968	1.6	250	8.2	.982	
Galvin, Jones & Naylor	1968	8	-	6.35	-	Design & construction only
Künzel	1969	6	4-20	4.0	.836 .926	Pressure & temperature Private communication (1971)

*b/a is the sinker to tube diameter ratio

(a) See also papers by Swift et al 1959, 1960
Lohrenz et al 1960, 1962
Chen et al 1968, 1972 and Lescarboura & Swift 1968

There is some doubt as to whether Hawkins et al (1935) did have guiding pins on their sinkers. In their paper they state that a 'Lawaczeck viscometer was selected', but do not state if there were guiding pins as there were on the original cylinders of Lawaczeck. The paper illustrates five different cylinder shapes but does not show any pins. If, however, there were no guiding pins, it is surprising that specific mention of this fact was not made because this would have been the first instance of unguided sinkers, and would have pre-dated the falling needle viscometer of Seeder (1943).

The second class of falling cylinder viscometer is where the sinker does not have guiding pins, but relies on the flow round the cylinder to produce self-centering. Provided the viscometer tube is truly vertical and the ratio of sinker to tube diameters is large (greater than about 0.95), then concentric fall occurs. The advantage is that the uncertainty due to turbulence and drag effects caused by guiding pins is eliminated, as are the difficulties in manufacturing the guiding pins to the required high precision.

In Table 1.2 there are three who used the falling needle viscometer. This is a particular case of the falling cylinder, where a sinker in the shape of a gramophone needle (Fig. 1.1) falls freely in a tube of about 1 mm diameter. It differs from the more usual falling cylinder in that the sinker is sharply pointed, and in that the viscometer tube is much narrower.

Table 1.2

List of workers who used unguided falling cylinder viscometers

Author	Date	Maximum pressure kbar	Temperature range °C	Tube dia. mm	b/a*	Remarks
Seeder	1943	This reference has not been seen				Needle viscometer
Jobling and Lawrence	1951	3	30-90	Not stated		
Boelhouwer and Toneman	1957	1.4	30-150	1	~.90	Needle viscometer
Scott	1959	This reference was seen but figures were not recorded				
Galvin, Naylor & Wilson	1963/4	1.0	30-100	Not stated		Needle viscometer
Bessouat and Elberg	1964	0.02	500	20.6	.961, .985	
Chaudhuri, Stager & Mathur	1968	1.4	20-27	4.71	.928	
McDuffie and Barr	1969	3.5	-60 to 100	4.83	.936	With 0.127 mm axial hole
Irving and Barlow	1971	7.1	30	6.305	.938, .964	With 2.468 mm axial hole
Isdale and Spence	1975	10.0	25-100	7.785	.959, .971	
Mclachlan	1975	3.5	30	6.65	.95	With 4.62 mm axial hole

*b/a is the sinker to tube diameter ratio

Sinker shapes

A wide variety of shapes have been used in falling body viscometry. The original viscometer of Lawaczeck (1919) had a sinker with flat ends as illustrated in Fig. 1.1(A), with the edges chamferred to reduce the rapidity of constriction of the fluid as it enters the narrow annulus between the sinker and tube. This flat-ended type of sinker was also used by Scott (1959), and by Kozlov and Yakolev (1966). One of the several sinker designs employed by Swift and his co-workers was a flat-ended magnesium cylinder with a 0.0005 inch taper, Swift, Lohrenz and Kurata (1960).

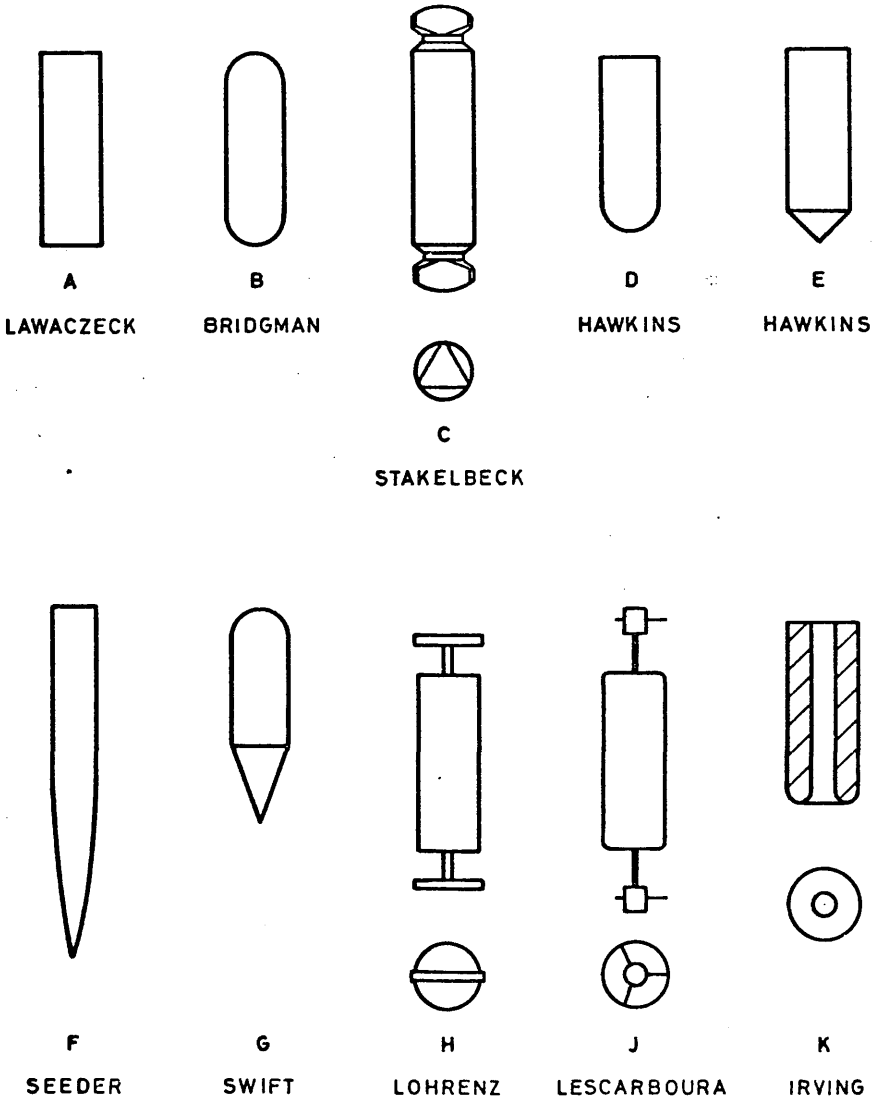

Fig 1.1 Sinker designs used in falling body viscometers

Bridgman (1926) was the first to use a sinker with hemispherical ends as shown in Fig. 1.1(B). This design has been copied by a large number of workers, namely Hawkins et al (1935), Mason (1935), Steiner (1949), Jobling and Lawrence (1951), ASME (1953), Heiks and Orban (1956), Cappi (1964), Gabibov and Tsaturyants (1968), Galvin et al (1968), and Chaudhuri et al (1968). This type of sinker is symmetrical and usually measurements were made with the sinker falling in both directions after alternate inversion of the viscometer tube. The fall time invariably differed in either direction because it is very difficult to machine a sinker so that both ends are identically hemispherical. Bridgman, for example, found a directional difference of 1 per cent.

A novel design of sinker was introduced by Stakelbeck (1933) who placed centering guides outside the annulus of the cylinder, type C in Fig. 1.1. This was an excellent improvement since the velocity of the fluid around the stabilizers is less than in the annulus where guiding pins are usually placed. Thus drag is less in this new configuration. It is surprising that this type of design was allowed to lie dormant for almost thirty years until Lohrenz and Kurata introduced a similar one in 1962 as shown schematically in Fig. 1.1(H). One possible reason for this omission is that Stakelbeck published in a lesser-known German journal.

The next type of sinker, D in Fig. 1.1, differs from the first three in that it is not symmetrical; it has a hemispherical nose but has a flat upper surface. This too constitutes a significant contribution to sinker design because this sinker is inherently stable since its centre of gravity is below the centre of action of the viscous forces in the annulus, whereas the symmetrical sinkers are more prone to irregular fall because they are in neutral equilibrium. The type D design was used by Hawkins et al (1935), Bessouat and Elberg (1964), Isdale and Spence (1975), and was adopted in this work.

The pointed, asymmetrical sinker, E, is one of the several designs tried by Hawkins et al (1935). It causes a sudden constriction of fluid on entry to the annulus, and is not so good as those sinkers with curved profiles which cause a gradual acceleration of fluid.

The falling-needle viscometer found favour with Dutch workers such as Seeder (1943), and Boelhouwer and Toneman (1957). It was used briefly by Galvin, Naylor and Wilson (1963/4). The needle, shown in Fig. 1.1(F), is like a gramophone needle both in shape and size. One advantage of its small size is that the needle can be brought to the top of the viscometer tube by means of an external magnet.

Swift et al (1960) made glass sinkers with conical noses and hemispherical upper ends for measuring liquid methane, ethane, and propane, G in Fig. 1.1. Not only did they have stabilizing lugs, they also were of hollow construction. From the practical point of view these must have been difficult to make.

Several sinker designs emanated from the University of Kansas and among these are type H and J. These are ones where the guiding pins are outside the annulus, to minimise frictional drag on the pins by placing them away from the area of high fluid velocity. Lohrenz and Kurata (1962) were able to show that frictional forces on the guiding pins are negligible when they are mounted away from the annulus. The first type (H) was by Lohrenz and Kurata, and the second (J) by Lescarboura and Swift (1968). The latter was specially made with pins of adjustable lengths to enable the sinker to be forced to fall eccentrically. This is an interesting facet of falling body viscometry, and is investigated in depth in Chapter 5.

The last type of sinker was designed during this research programme. It has an axial central hole as shown in Fig. 1.1(K). This design is to allow fluid to pass through the central hole to reduce the resistance to the fall so that viscous liquids can be measured. By having a hole rather than enlarging the gap between sinker and tube wall it is found (Chapter 4) that stable, repeatable fall times can be recorded without having to use guiding pins. McDuffie and Barr (1969) also had a sinker with a narrow axial hole, but did not mention the reason for it. Recently Mclachlan (1975) has developed this type of falling body design to enable viscosities up to 10^7 P to be measured.

Sinker material and construction

Many different materials have been used in the manufacture of sinkers such as glass, aluminium, magnesium, chromium plated steel, brass, mild steel, and stainless steel. The choice of material depends upon the fluids to be studied, the method of detection, and the method of retrieval. Ideally the viscometer tube and the sinker should be of the same material to avoid differential compressibilities or coefficients of expansion.

In the previous section the shape of sinkers was discussed, that is the outline, but many of them are of hollow manufacture. There are two main reasons for this; firstly, a hollow sinker enables it to be loaded with materials of varying densities such as tungsten or gold in the case of Bridgman. This means that the same sinker can be used over different viscosity ranges. Clearly the heavier the ballast, the greater the viscosity that can be measured in a given fall time. Cappi (1964) used two sinkers in his viscometer, one of high and the other of low density so that measurements of both fluid density and viscosity could be made. The second reason is because detection methods sometimes require a particular material in the sinker. Several workers used an induction-type of detector system which required a magnetic core such as ferrite, and in the single case of Heiks and Orban (1956) a core of radioactive cobalt-60 was employed. Jobling and Lawrence (1951) used a tungsten ballast as well as an Alnico magnet, in a brass casing.

1.2.2 Methods of detection

Falling body or rolling ball viscometers usually use electrical detection such as simple contact or induction methods. For pressures up to about 3.5 kbar the availability of non-magnetic pressure tubing makes possible very simple viscometers, since the detection system may be mounted outside the high-pressure region (McDuffie and Barr 1969). At higher pressures such methods are precluded by restrictions imposed by material strength and the large ratio of wall thickness to internal diameter of pressure vessels.

The contact method was used by Bridgman (1926), Stakelbeck (1933), and by the team who produced the ASME Report (1953). When the sinker comes to rest after its fall, it comes into contact with an insulated metal contact and the timing device is triggered as soon as the circuit is completed between the contact and the wall of the viscometer through the sinker. The guiding pins assist rapid completion of the circuit. One disadvantage of this method is that electrically conducting liquids cannot be measured. Chaudhuri et al (1968) adopted the same method with unguided cylinders using 'modified electrical contacts'. Timing commences as soon as the sinker moves from the top contact in the tube, and this means that during the first moments the sinker is accelerating to its terminal velocity which produces uncertainty, especially for a rapidly falling sinker.

The induction method has been used by the majority of workers. It offers the advantage that the coils are wound round the outside of the viscometer tubes, sometimes in specially machined grooves, so there is no contact with the test fluid. The coils can be placed along the tube where uniform velocity is assured. The earliest application of induction for detection was by Hawkins, Solberg, and Potter (1935) and it has been used for falling body and rolling ball applications alike, and is still prevalent, Isdale and Spence (1975).

Other detection methods have been tried, such as radioactive devices. Heiks and Orban (1956) placed a cobalt-60 source inside their sinker, and Rowe (1966) used a 2 mm diameter cobalt falling ball. The Geiger detection tubes were placed outside the pressure vessel in both cases. To determine the position of his flat falling plate Wilson (1967) used a capacitance method which had the main disadvantage that he had to measure the effect of pressure upon the dielectric constant of the test liquid as well.

More recently McDuffie and Barr (1969) and Mclachlan (1975) have used a linear differential transformer for sinker detection. In the first case the transformer was mounted outside the pressurised viscometer tube, and could be moved to allow several measurements to be made during one descent of the sinker. Mclachlan's transformer was situated inside the pressure

vessel and was able to detect very small sinker movements, thus enabling high viscosity determinations without unduly long fall times.

1.3 Description of the Viscometer

The viscometer described here was designed to allow measurements to be made in a fixed pressure vessel capable of being pressurised to 14 kbar. It is of the simple falling cylinder type in which the time of fall under gravity is determined over a fixed distance by the induction method. Successive measurements are obtained without rotation or disconnection of the pressure system. After falling, the sinker is retrieved electromagnetically and held at the top of the viscometer tube by a semi-permanent magnet. The sequence of operations is automated and remotely controlled, so that once temperature and pressure are set, any number of measurements may be made and recorded without further attention.

The only moving part in the system is the sinker itself. The pressure vessel required to be static because its bulk made rotation an impracticable proposition and the wall thickness of over 4 inches made external magnetic lifting impossible. Another design constraint was that the closure of the vessel carries only four connections into the high-pressure chamber. The viscometer comprises a brass viscometer tube surrounded by nine lifting coils, connected in three staggered sets of three in series. One set of these coils is also used for detecting the fall of the iron sinker. A tenth coil, on top of the lifting/detection stack of coils is used to magnetise a semi-permanent holding magnet, and to demagnetise it to initiate a fall time measurement after thermal equilibrium has been reached. Two types of sinker are used. The first is a solid cylinder with a hemispherical end; the second has a similar shape but with a central hole. The viscosity ranges are 0.01-10 P and 10-3000 P with maximum fall times of about 100 minutes.

The viscometer, the control system, and the mode of operation are described in Chapter 3.

1.4 Additional Papers

"An automatic high-pressure viscometer".
J. B. Irving, A. J. Barlow. J. Phys E, (1971) 4, 232-236.

"The effect of non-vertical alignment on the performance of a falling cylinder viscometer".
J. B. Irving. J. Phys D, (1972) 5, 214-224.

Copies of the above papers are submitted with this thesis.

"The effect of pressure on the viscoelastic properties of liquids".
A. J. Barlow, G. Harrison, J. B. Irving, M. G. Kim, J. Lamb, and W. C. Pursley.
Proc. R. Soc. Lond. A, (1972) 327, 403-412.

The author has also published two papers on the viscosity of binary liquid mixtures.

"Viscosities of binary liquid mixtures: a survey of mixture equations".
J. B. Irving, National Engineering Laboratory (1977), NEL Report No 630, pp 27.

"Viscosities of binary liquid mixture: the effectiveness of mixture equations".
J. B. Irving, National Engineering Laboratory (1977), NEL Report No 631, pp 86.

1.5 Explanatory Note

This project was begun on 1 October 1964 and all experimental work was completed by 31 December 1968. It is evident that a considerable time has elapsed up to the submission date of this thesis. During the intervening period, the two main papers referred to in section 1.4 were published, so the new viscometry technique, results, double-exponential equation etc do have a priority date, 1971.

Mclachlan (1975), also working in the Electrical Engineering Department of Glasgow University extended the viscosity range of measurements to 10^7 P by reducing the length over which the fall of a sinker with a central hole is measured. Isdale and Spence (1975) discarded sinkers with guiding pins in favour of the unguided variety on a private recommendation by the author. The viscometer has been duplicated by a group of Russian workers, (Golik, Adamenko, and Varetskii, 1976), who have published results up to 2.5 kbar for n-paraffins in the temperature range 20 to 140^{o}C.

1.6 Conversion Factors for Viscosity

For convenience, dynamic viscosity η is commonly referred to as 'viscosity'. This convention is adopted throughout this thesis. The practical viscosity unit of poise (P), and sometimes the centipoise (cP) is adhered to because it is the unit which predominates the literature and it is more easily written and more readily comprehended by the reader in its abbreviated form than the SI units of Newton per second per metre squared (N s/m^2) or pascal second (Pa s).

The table below gives conversion factors for the more commonly used units.

	dyne s/cm^2	P	cP	N s/m^2	Pa s
dyne s/cm^2 =	1	1	100	0.1	0.1
poise (P) =	1	1	100	0.1	0.1
centipoise (cP) =	0.01	0.01	1	0.001	0.001
N s/m^2 =	10	10	1000	1	1
pascal second (Pa s) =	10	10	1000	1	1

These are force units of viscosity. Occasionally mass units are used, such as the g cm^{-1} s^{-1} which is the mass-equivalent unit of the dyne s/cm^2.

Kinematic viscosity, ν, often used in the oil industry, is found by dividing dynamic viscosity by the fluid density,

$$\nu = \eta/\rho .$$

C H A P T E R 2

THE THEORY OF THE FALLING-BODY VISCOMETER

List of Figures

List of Tables

CHAPTER 2

THE THEORY OF THE FALLING-BODY VISCOMETER

Of the workers who used the falling-cylinder method of viscometry, some have produced laws of motion which show remarkable differences in form. These differences are due to the methods adopted to solve the equations of fluid flow. An early approximate solution by Lawaczeck (1919) was based on the assumption that the flow through the annulus is equivalent to the flow between rectangular parallel plates. A further expression is quoted in the American Society of Mechanical Engineers Report (hereafter referred to as the ASME Report) of 1953, although the derivation is not given. Boelhouwer and Toneman (1957) gave another original expression, and in 1964 Bessouat and Elberg quoted an approximate form of Lawaczeck's equation. In the thesis of Cappi (1964) another equation appears which is in error. The treatment adopted by Smith (1957) provides what is now the accepted law of motion. The equation has been frequently derived subsequently: Swift, Lohrenz, and Kurata (1960), Huang (1966), Künzel (1969), and Chee and Rudin (1970). The different equations are compared in section 2.2.

All the known solutions to date are for a solid cylinder falling in a vertical viscometer tube. The following analysis is for a cylinder with an axial hole through the centre of the cylinder. This novel arrangement allows the cylinder to fall more rapidly through liquids of high viscosities such as those encountered at high pressures so that fall times are not excessively long without sacrificing stability which happens when sinker diameter is reduced to produce faster velocities of fall. By mathematically reducing the radius of the central hole to zero the solution reduces to the accepted law of motion for a solid cylinder already referred to.

2.1 Analysis for a Sinker with Central Hole

To obtain a law of flow of a Newtonian liquid round a falling cylinder with a central hole, the same assumptions are made as for flow in a capillary. That is, the flow is Poiseuille (fully developed laminar flow), and is parallel with the axis.

The Navier-Stokes equation which is the momentum equation for a continuous material, is solved to provide the required law of flow. A condition of the Navier-Stokes equation is that there is no relative motion between a solid surface and the contacting fluid particles, and the effects of fluid entering and leaving the annulus are assumed to be negligible. The momentum equations for a liquid of negligible compressibility when expressed in cylindrical coordinates are as follows:

In the r-direction

$$\frac{\partial u}{\partial t} + u\frac{\partial u}{\partial r} + \frac{v}{r}\frac{\partial u}{\partial \theta} + w\frac{\partial u}{\partial z} - \frac{v^2}{r} = -\frac{\partial}{\partial r}\left(\frac{p}{\rho} + gh\right) + \nu\left(\nabla^2 u - \frac{u}{r^2} - \frac{2}{r^2}\frac{\partial v}{\partial \theta}\right), \qquad (2.1)$$

where $$\nabla^2 = \frac{\partial^2}{\partial r^2} + \frac{1}{r}\frac{\partial}{\partial r} + \frac{1}{r^2}\frac{\partial^2}{\partial \theta^2} + \frac{\partial^2}{\partial z^2}.$$

u, v, w are the particle velocities in the r, θ, and z directions and ν is the kinematic viscosity. The density of the fluid is ρ and $\partial p/\partial r$ is the pressure gradient, where p is the pressure due to fluid motion and includes the pressure due to differences in fluid levels. The term $\partial(gh)/\partial r$ takes the direction of gravitational force into account, and for the present will remain in this general form.

The flow in the annular region where flow is parallel with the z-axis is considered in the analysis, and therefore there are no tangential or radial velocity components. Thus the left-hand side of equation 2.1 is zero. For the same reason $\nu(\nabla^2 u - u/r^2 - 2/r^2\ \partial v/\partial\theta)$ on the right-hand side of the equation is also zero. Thus

$$-\frac{\partial}{\partial r}\left(\frac{p}{\rho} + gh\right) \equiv 0.$$

This means that $(p/\rho + gh)$ is independent of r.

In the θ-direction

$$\frac{\partial v}{\partial t} + u\frac{\partial v}{\partial r} + \frac{v}{r}\frac{\partial v}{\partial \theta} + w\frac{\partial v}{\partial z} + \frac{uv}{r} = -\frac{\partial}{r\partial\theta}\left(\frac{p}{\rho} + gh\right) + \nu\left(\nabla^2 v + \frac{2}{r^2}\frac{\partial u}{\partial \theta} - \frac{v}{r^2}\right). \qquad (2.2)$$

By similar reasoning it is evident that

$$-\frac{\partial}{\partial\theta}\left(\frac{p}{\rho} + gh\right) \equiv 0.$$

Therefore $(p/\rho + gh)$ is also independent of θ.

In the z-direction

$$\frac{\partial w}{\partial t} + u\frac{\partial w}{\partial r} + \frac{v}{r}\frac{\partial w}{\partial \theta} + w\frac{\partial w}{\partial z} = -\frac{\partial}{\partial z}\left(\frac{p}{\rho} + gh\right) + \nu\nabla^2 w. \qquad (2.3)$$

In the steady state the fluid velocity in the z-direction, w, is a function of r alone, and since u is zero it follows that

$$0 \equiv -\frac{\partial}{\partial z}\left(\frac{p}{\rho} + gh\right) + \nu\left(\frac{\partial^2 w}{\partial r^2} + \frac{1}{r}\frac{\partial w}{\partial r} + \frac{1}{r^2}\underbrace{\frac{\partial^2 w}{\partial\theta^2}}_{\equiv 0} + \underbrace{\frac{\partial^2 w}{\partial z^2}}_{\equiv 0}\right). \qquad (2.4)$$

Therefore the Navier-Stokes equation reduces to the following equation for which a solution is required

$$\nu\left(\frac{\partial^2 w}{\partial r^2} + \frac{1}{r}\frac{\partial w}{\partial r}\right) = \frac{d}{dz}\left(\frac{p}{\rho} + gh\right). \qquad (2.5)$$

$(p/\rho + gh)$ is a function of z only, since it is independent of both r and θ.

Consider a cylinder falling concentrically in a vertical tube as shown in Fig. 2.1. Because of the fall of the cylinder a pressure is exerted on the fluid causing it to flow up through the annulus and the central hole; this pressure, along with the hydrostatic pressure due to the difference in fluid levels is included in p of equation 2.5. On re-arrangement of this equation one has

$$\eta\left(\frac{\partial^2 w}{\partial r^2} + \frac{1}{r}\frac{\partial w}{\partial r}\right) = -\frac{dp}{dz} + \rho_2 g. \qquad (2.6)$$

The dynamic viscosity η equals the product of kinematic viscosity and fluid density, ρ_2. $d(gh)/dz$ becomes equal to g as the cylinder is falling vertically under the force of gravity, and a negative sign is ascribed to dp/dz to indicate that the pressure differential acts in

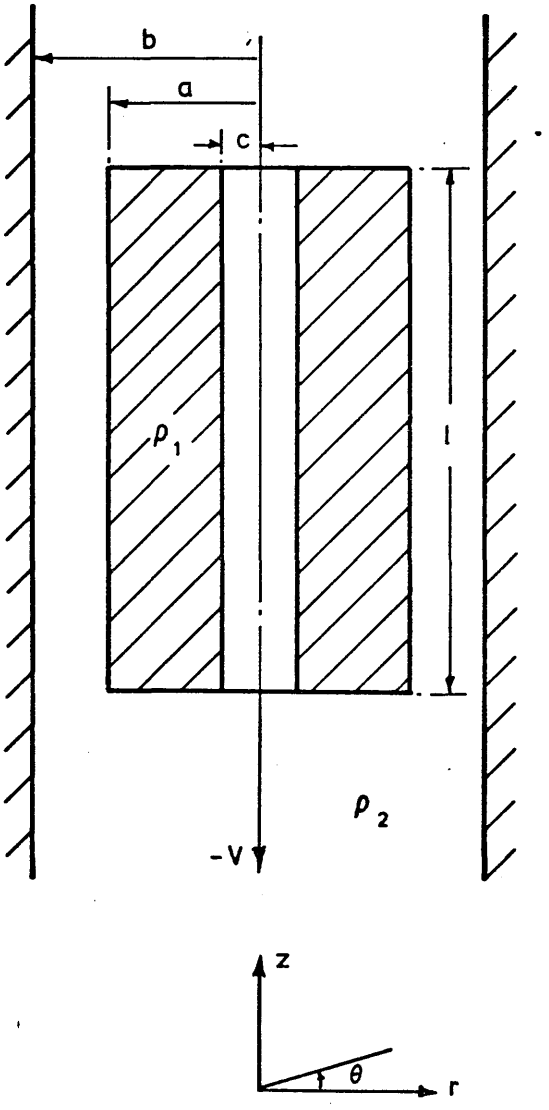

FIG 2.1 Sinker with central hole
with cylindrical coordinates

opposition to the downward gravitational force.

The end effect due to the finite length of the tube has been considered by Barr (1931) who found that it could be neglected if the velocity of fall was measured at a point removed several lengths of the falling body from the lower end of the containing vessel. In the analysis which follows end effects are ignored because his condition is met in the viscometer which is described in the following chapter.

Let the radii of cylinder, tube, and central hole be a, b, and c respectively. The cylinder is long compared with its diameter and the width of the annulus is small. Let the densities of the cylinder and fluid be ρ_1 and ρ_2 respectively. The cylinder falls with a terminal velocity of -V.

Integrating equation 2.6 one has

$$\frac{dw}{dr} = -\frac{Ar}{2\eta} + \frac{C}{r}, \tag{2.7}$$

where $A = dp/dz - \rho_2 g$ is introduced for ease of manipulation, C is a constant of integration and is a function of r only. dw/dr is the velocity gradient or rate of shear at point r in the fluid.

Integrating again one has

$$w = -\frac{Ar^2}{4\eta} + C \ln r + D. \tag{2.8}$$

D is a further constant of integration, and w is the fluid velocity at any point in the areas under consideration.

The flowrate of fluid past the sinker equals the flowrate through the annulus plus the flowrate through the central hole.

i The annulus

The volume of fluid passing through the annulus in unit time is

$$\dot{Q}_a = \int_0^{2\pi} \int_a^b w\, r\, dr\, d\theta$$

$$= 2\pi \int_a^b \left[-\frac{Ar^2}{4\eta} + C \ln r + D \right] r\, dr. \qquad (2.9)$$

On integration, and imposition of the boundary conditions which are that at r = b the fluid velocity is zero, and that at r = a the fluid velocity is -V, the terminal velocity of the cylinder, the following expression is obtained

$$\dot{Q}_a = \pi \left[\frac{A}{8\eta}(b^4 - a^4) - \frac{A(b^2 - a^2)^2}{8\eta \ln b/a} - \frac{V(b^2 - a^2)}{2 \ln b/a} + a^2 V \right]. \qquad (2.10)$$

ii The central hole

The volume of liquid passing through the central hole in unit time is

$$\dot{Q}_h = \int_0^{2\pi} \int_0^c w\, r\, dr\, d\theta$$

$$= 2\pi \int_0^c \left[-\frac{Ar^2}{4\eta} + C \ln r + D \right] r\, dr. \qquad (2.11)$$

Due to symmetry the velocity gradient at r = o is zero. Thus by equation 2.7 it is evident that C equals zero. The second boundary condition is that at r = c, the fluid velocity is -V. By integrating equation 2.11 and imposing these boundary conditions one obtains the following identity

$$\dot{Q}_h = \pi c^2 \left[\frac{Ac^2}{8\eta} - V \right]. \qquad (2.12)$$

Now the total flowrate past the sinker in unit time relative to the tube is the volume of liquid displaced by the sinker in unit time, that is,

$$V\pi(a^2 - c^2).$$

Thus

$$V\pi(a^2 - c^2) = \dot{Q}_a + \dot{Q}_h$$

therefore

$$\frac{A}{8\eta}(b^4 - a^4 + c^4) - \frac{A(b^2 - a^2)^2}{8\eta \ln b/a} - \frac{V(b^2 - a^2)}{2 \ln b/a} = 0. \qquad (2.13)$$

This equation relates viscosity with terminal velocity, tube and sinker dimensions, and the constant A which is as yet unknown. A is determined by consideration of the forces on the sinker.

The rate of shear at the outer sinker surface is given by equation 2.7 with r = a:

$$\left[\frac{\partial w}{\partial r}\right]_{r = a} = -\frac{Aa}{2\eta} + \frac{C}{a}.$$

The constant C is already defined by the boundary conditions described between equations 2.9 and 2.10. The shear force on the outer surface of the sinker is the surface area, $2\pi al$ (where l is the sinker length), multiplied by shear stress $\eta(\partial w/\partial r)_{r = a}$. Thus the shear force is

$$\eta\left[\frac{\partial w}{\partial r}\right]_{r = a} \cdot 2\pi al = 2\pi l\left[-\frac{Aa^2}{2} + \left\{\frac{A}{4}(b^2 - a^2) + V\eta\right\}\Big/\ln b/a\right]. \qquad (2.14)$$

The rate of shear at the inner surface of the sinker is given by equation 2.7 with r = c. Since the constant of integration C is zero in this region the shear rate is

$$\left[\frac{\partial w}{\partial r}\right]_{r = c} = -\frac{Ac}{2\eta}.$$

Therefore the shear force on the inner surface of the sinker is given by

$$\eta\left[\frac{\partial w}{\partial r}\right]_{r = c} \cdot 2\pi cl = -\pi lAc^2. \qquad (2.15)$$

In physical terms these shear forces both oppose the downward motion of the sinker. The shear forces are proportional to the rates of shear at the surfaces, that is, to the velocity gradients. Because the reference axis is along the central hole the velocity gradient at the outer surface is positive, but negative at the inner surface with respect to radius r.

Because of the axis position not being in the solid part of the cylinder, the shear forces appear in opposing directions. To avoid this contradiction the sign of inner shear force must be altered so that both shear forces act upwards to oppose the downward gravitational force on the sinker.

The upward forces acting upon the sinker are the two shear forces and the forces due to the pressure gradient which, for steady flow conditions, are balanced by the gravitational force on the sinker. The pressure gradient term includes the buoyancy of the cylinder. Thus

[outer surface force] + [inner surface force] + [pressure difference]

= [gravitational force], and so

$$\left[2\pi l\left\{-\frac{Aa^2}{2}+\left(\frac{A}{4}(b^2-a^2)+V\eta\right)\Big/\ln b/a\right\}\right]-\left[-\pi l A c^2\right]+$$

$$+\left[\frac{dp}{dz}l\pi(a^2-c^2)\right]=\left[\pi(a^2-c^2)l\rho_1 g\right]. \qquad (2.16)$$

Since $dp/dz = A + \rho_2 g$ this equation yields

$$A=\frac{2}{(b^2-a^2)}\left[(\rho_1-\rho_2)(a^2-c^2)g\ln b/a-2V\eta\right]. \qquad (2.17)$$

On substituting A into equation 2.13 the final expression is obtained.

$$\eta=\frac{(\rho_1-\rho_2)(a^2-c^2)g\left[(b^4-a^4+c^4)\ln b/a-(b^2-a^2)^2\right]}{2V(b^4-a^4+c^4)}. \qquad (2.18)$$

By equations 2.13 and 2.17 A may alternatively be expressed as

$$A=\frac{(\rho_1-\rho_2)(a^2-c^2)(b^2-a^2)g}{(b^4-a^4+c^4)}. \qquad (2.17a)$$

All the quantities in equation 2.18 may be determined experimentally; the fluid viscosity is thus defined in terms of sinker and tube dimensions, the densities of fluid and sinker, and the terminal velocity of the sinker.

The equation for a solid sinker is obtained by reducing radius c to zero. Equation 2.18 then becomes

$$\eta=\frac{(\rho_1-\rho_2)a^2g[(b^2+a^2)\ln b/a-(b^2-a^2)]}{2V(b^2+a^2)}. \qquad (2.19)$$

This equation is identical to the accepted solution obtained by Smith (1957), Swift et al. (1960), Huang (1966), Künzel (1969), and Chee et al. (1970) which applies to a solid sinker.

For convenience, the above two equations may be written as follows

$$\eta = \frac{(\rho_1 - \rho_2)(a^2 - c^2)g\theta'}{2V(b^4 - a^4 + c^4)}, \qquad (2.18a)$$

where $\theta' = [(b^4 - a^4 + c^4)\ln b/a - (b^2 - a^2)^2]$,

and

$$\eta = \frac{(\rho_1 - \rho_2)a^2 g\theta}{2V(b^2 + a^2)}, \qquad (2.19a)$$

where $\theta = [(b^2 + a^2)\ln b/a - (b^2 - a^2)]$.

2.1.1 Velocity profile

The velocity of the fluid at any point in the annulus or in the central hole can be readily obtained from the analysis.

i The annulus

The velocity in this region is described in general terms by equation 2.8. By applying the boundary condition stated between equations 2.9 and 2.10 and eliminating A by equation 2.17, the following expression for fluid velocity is obtained:

$$w = \frac{V}{\theta'}\left[(b^2 - a^2)(b^2 - r^2) - (b^4 - a^4 + c^4)\ln b/r\right]. \qquad (2.20)$$

The profile described by this is approximately parabolic in nature with velocity zero at r = b, and velocity -V at r = a. The profile is shown diagrammatically in Fig. 2.2(a). The point of maximum velocity occurs at $r = \sqrt{(b^4 - a^4 + c^4)/2(b^2 - a^2)}$. This is where dw/dr = 0, where the shear rate is zero.

ii The central hole

By imposing the boundary conditions stated between equations 2.11 and 2.12 upon the general velocity equation, the velocity in the central hole is similarly obtained.

$$w = V\left[\frac{(b^2 - a^2)(c^2 - r^2)}{\theta'} - 1\right]. \qquad (2.21)$$

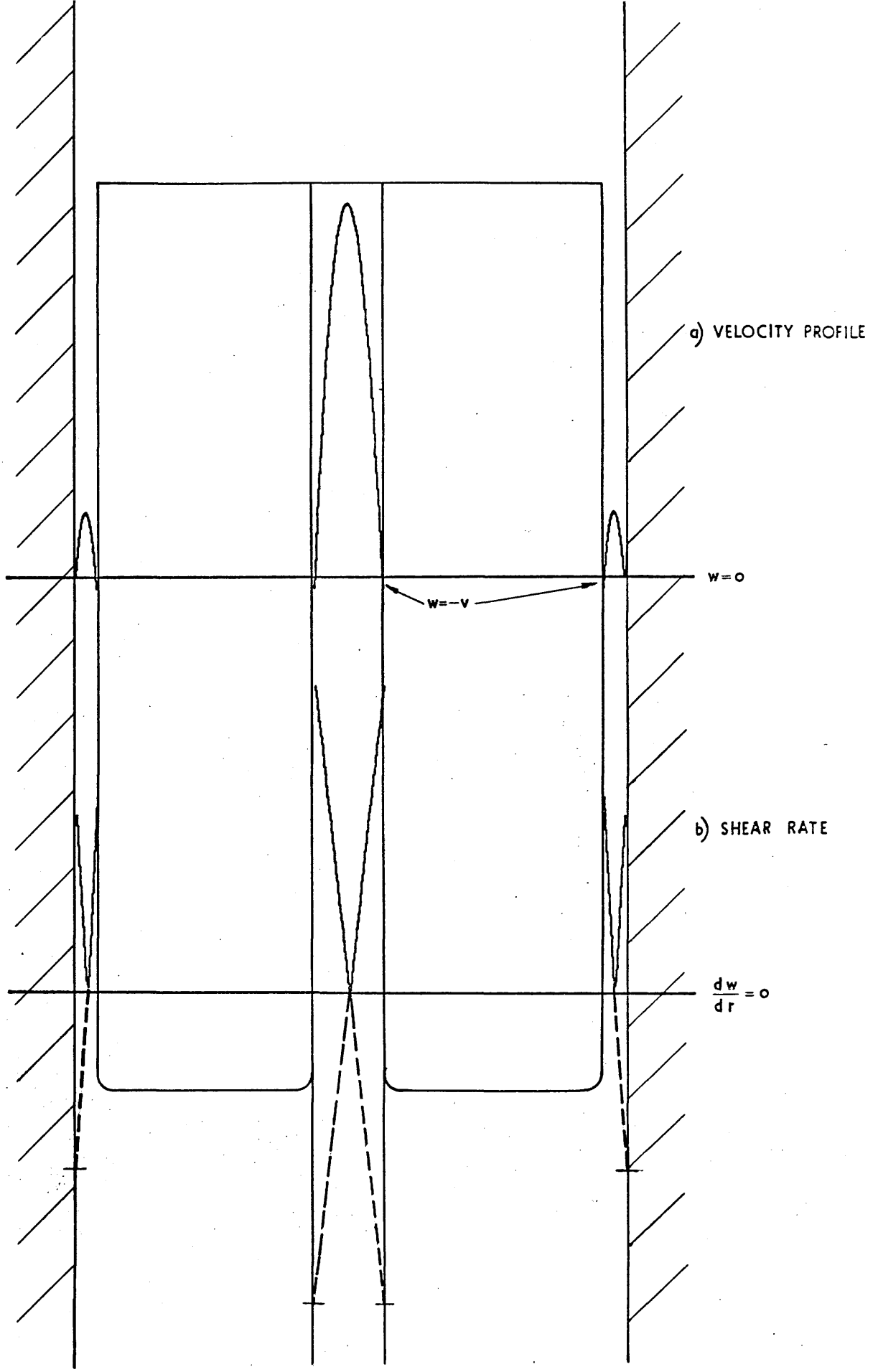

FIG 2.2 Sinker with central hole

a) Velocity profile

b) Shear rate

This profile is parabolic with the velocity on the inner sinker surfaces at -V. The velocity profile, which is drawn by computer, is also shown in Fig. 2.2 where it is clear that the point of maximum velocity is at r = o.

iii The solid sinker

The velocity in the annular space between a solid sinker and the tube walls is obtained by reducing c to zero in equation 2.20. Thus

$$w = -V\left[\frac{(b^2 + a^2)\ln b/r - (b^2 - r^2)}{\theta}\right]. \qquad (2.22)$$

The maximum velocity is at $r = \sqrt{(b^2 + a^2)/2}$.

2.1.2 Shear rate (velocity gradient)

The shear rate at any point in the fluid is given by the equation

$$\frac{dw}{dr} = -\frac{Ar}{2\eta} + \frac{C}{r}. \qquad (2.7)$$

The constant A may be eliminated by equation 2.17, and C is obtained from the boundary conditions appropriate to the regions under consideration as already described.

i The annulus

$$\frac{dw}{dr} = \frac{V}{r}\left[\frac{(b^4 - a^4 + c^4) - (b^2 - a^2)2r^2}{\theta'}\right]. \qquad (2.23)$$

This shear rate is zero at $r = \sqrt{(b^4 - a^4 + c^4)/2(b^2 - a^2)}$, and is greatest at r = a.

ii The central hole

$$\frac{dw}{dr} = -\frac{2Vr(b^2 - a^2)}{\theta'}. \qquad (2.24)$$

Here the shear rate is linear and is zero at r = o. It is at its greatest magnitude at r = c.

iii The solid sinker

The shear rate in the annulus of a solid sinker is given by

$$\frac{dw}{dr} = \frac{V(b^2 + a^2 - 2r^2)}{r\theta}. \qquad (2.25)$$

Its numerical value varies with increase of r from $V(b^2 - a^2)/a\theta$ at the sinker surface, through zero at $r = \sqrt{(b^2 + a^2)/2}$, to $-V(b^2 - a^2)/b\theta$ at the tube wall. Thus the maximum rate of shear is at the surface of the sinker.

The shear rates are shown diagrammatically in Fig. 2.2(b). The broken lines show the shear rate described by equations 2.23 and 2.24 where it is negative by virtue of the chosen datum position of the radius r. That the shear forces act upwards on the surfaces is shown by mirror image of these broken lines.

It is pertinent to mention here that for a given geometry, namely with fixed values of a, b, and c, that the shear forces acting on the sinker and tube surfaces are constant no matter what viscosity of liquid. This is because that at any surface the shear rate is $dw/dr = Vf(a,b,c)$, and since shear force is $\tau \times$ (surface area) which equals $\eta dw/dr \times$ (surface area), then shear force equals $\eta Vf(a,b,c) \times$ (surface area). But ηV is constant as shown by equation 2.18, and therefore shear force, or shear stress, is independent of the viscometer liquid.

2.2 Comparison with Other Equations

The equations of motion derived by workers for this type of viscometry relate to a solid cylinder in a viscometer tube. The equations fall naturally into a common form in which the difference is determined by a dimensionless term which is a function of the cylinder and viscometer tube radii only. For example, the equation for the solid cylinder which is derived in the preceding analysis is

$$\eta = \frac{(\rho_1 - \rho_2)a^2g[(b^2 + a^2)\ln b/a - (b^2 - a^2)]}{2V(b^2 + a^2)}. \qquad (2.19a)$$

This may be put in the form

$$\eta = \eta' f(\kappa) \qquad (2.26)$$

where $\eta' = (\rho_1 - \rho_2)a^2g/2V$ which has the dimensions of dyne sec cm^{-2} (Poise). $f(\kappa) = [(b^2 + a^2)\ln b/a - (b^2 - a^2)]/(b^2 + a^2)$. This equals $[(1 + \kappa^2)\ln 1/\kappa - (1 - \kappa^2)]/(1 + \kappa^2)$, where κ is dimensionless: $\kappa = a/b$

where $\kappa < 1$.

Therefore

$$\eta = \eta' \frac{[(1 + \kappa^2)\ln 1/\kappa - (1 - \kappa^2)]}{(1 + \kappa^2)}. \qquad (2.26a)$$

In comparing the equations of others, it is sufficient to produce $f(\kappa)$ as follows

1 Lawaczeck (1919)

Lawaczeck considered the flow to be taking place between parallel plates to obtain an approximate solution

$$f(\kappa) = \frac{4(1 - \kappa)^3}{\kappa[7(1 + \kappa^2) - 2\kappa]}. \qquad (2.27)$$

The equation of Lawaczeck is incorrectly quoted by Heiks and Orban (1956).

2 Bessouat and Elberg (1964)

The solution is an approximation of Lawaczeck's equation

$$f(\kappa) = \frac{1}{3}\left[\frac{1}{\kappa} - 1\right]^3. \qquad (2.28)$$

3 ASME (1953)

$$f(\kappa) = \frac{(1 - \kappa)^3}{3\kappa^2}\left[1 - \frac{1}{2}(1 - \kappa) - \frac{13}{20}(1 - \kappa)^2 - \frac{13}{40}(1 - \kappa)^3 - \ldots\right]. \qquad (2.29)$$

The derivation of this equation is not given.

4 Boelhouwer and Toneman (1957)

$$f(\kappa) = \frac{1}{3}\left[\frac{1 - \kappa^2}{1 + \kappa^2}\right]^3. \qquad (2.30)$$

The equation quoted by the authors is in error by a factor of four due a diameter term in the numerator which should be $(\text{radius})^2$. Equation 2.30 is in the correct form.

5 Cappi (1964)

$$f(\kappa) = \frac{(1 + \kappa^2)\ln 1/\kappa - (1 - \kappa^2)}{(3 - \kappa^2)}. \qquad (2.31)$$

The difference between this equation and equation 2.32 is due to Cappi's assumption that the flowrate through the annulus is $V\pi b^2$. This is, however, the flowrate relative to the moving sinker. The frame of reference for the analysis is the fixed tube, and the flowrate is in fact $V\pi a^2$.

6 This work

The geometric function has already been shown to be

$$f(\kappa) = \frac{(1 + \kappa^2)\ln 1/\kappa - (1 - \kappa^2)}{(1 + \kappa^2)}. \qquad (2.32)$$

This is obtained from the analysis for a sinker with a central hole where the radius of the central hole is reduced to zero. This is identical to the version of Smith (1957).

7 Smith (1957)

The numerator of equation 2.32 occurs as the difference between two relatively large quantities which are nearly equal. For ease of calculation, Smith obtained the following approximation:

$$f(\kappa) = \frac{1}{3}\frac{(1 - \kappa^2)(1 - \kappa)^2}{\kappa(1 + \kappa^2)} \qquad (2.33)$$

2.2.1 Evaluation of the equations

Although the seven equations differ widely in mathematical form, on substitution of a value for κ, they show very close agreement, especially those of the ASME Report, Boelhouwer, this work and Smith. A value of $\kappa = 0.95$ is typical in falling body viscometry. The values of $f(\kappa)$ for each equation are compared below

Table 2.1

Comparison of $f(\kappa)$ for $\kappa = 0.95$

	Equation	$f(\kappa)$
1	Lawaczeck	4.6097×10^{-5}
2	Bessouat & Elberg (approximation of 1)	4.8598
3	ASME Report	4.4939
4	Boelhouwer & Toneman	4.4866
5	Cappi	4.1704
6	This work (equation 2.32)	4.4937
7	Smith (approximation of 6)	4.4955

$\kappa = a/b$ where a is the radius of the sinker and b the radius of the viscometer tube. Special care must be taken in evaluating the functions, particularly equations 5 and 6 which involve the difference between two large but almost equal quantities. Seven figure logarithmic tables are not sufficiently accurate (especially in the case of a very narrow annulus when κ approaches unity) and a digital computer with double length number storage for extra precision was therefore used to ensure accurate calculation.

The agreement among the ASME equation, equation 2.32, and Smith's approximation of the latter is very close, as shown in Table 2.1. The agreement between the ASME equation and equation 2.32 suggests that the ASME equation is also an approximation of equation 2.32.

2.3 Reynolds Number

In fluid flow two types of flow exist: one, at relatively low velocities in which the flow is Poiseuille; and the second, at relatively higher velocities in which particles execute a sinuous and then finally a nearly random fluctuating motion about a mean velocity. The two types of motion are called laminar and turbulent respectively. Reynolds pointed out that the existence of the two flow types depend not just on the velocity but rather on a dimensionless parameter called the Reynolds number.

For flow in a pipe, the Reynolds number is defined as $\bar{V}D/\nu$ where D is the diameter of the pipe. ν is kinematic viscosity, and $\bar{V}$ the average fluid velocity. When Reynolds number exceeds about 2000 turbulent flow is encountered in a pipe.

It is our concern to design the falling body viscometer so that the flow will be laminar and not turbulent. If turbulence is present then a linear calibration of viscosity as a function of fall time is no longer possible since fall times become larger than would be predicted.

The Reynolds number for a falling cylinder in a tube cannot be readily defined since ambiguity arises in the diameter to be used. The definition of diameter is arbitrary provided that a corresponding critical Reynolds

number Re_{crit} is known. Several definitions of equivalent diameter and corresponding critical Reynolds numbers have been used in this type of viscometry.

2.3.1 Equivalent diameter definitions for the solid sinker

$$Re = \frac{\bar{V}D_E}{\nu} = \frac{\bar{V}\rho D_E}{\eta}. \tag{2.35}$$

The equivalent diameter D_E, has been variously defined as follows.

i Swift, Christy and Kurata (1959)

For the falling-cylinder viscometer a modified Reynolds number used by Hubbard and Brown (1943) for a rolling ball viscometer, was employed from which one obtains

$$D_E = \frac{2a^2}{(a + b)}. \tag{2.36}$$

Swift et al. established from experiment that the critical Reynolds number was about 280 on the basis of this definition.

ii Lohrenz and Kurata (1962)

$$D_E = 2a\sqrt{2[\ln b/a - (b^2 - a^2)/(b^2 + a^2)]}. \tag{2.37}$$

The critical Reynolds number corresponding to this definition of D_E is 0.2 for cylinders with guiding pins. For uninterrupted flow, however, the value Re_{crit} is stated to be about 10.

iii Trombetta (1971)

$$D_E = 2(b - a). \tag{2.38}$$

For an annulus the author uses the term 'hydraulic diameter'. No value for Re_{crit} is offered. This equivalent diameter is twice the annular gap. The general law for obtaining the hydraulic diameter is defined as follows

$$D_E = \frac{4 \times (\text{area of flow})}{\text{wetted perimeter}}.$$

For annular flow, therefore,

$$D_E = \frac{4\pi(b^2 - a^2)}{2\pi(b + a)}.$$

Thus $$D_E = 2(b - a).$$

The 'hydraulic diameter' definition has also been used by Mitsuishi and Aoyagi (1973) in a study of fluid flow in an eccentric annulus.

The compatibility of definitions (i) and (ii) can be examined by virtue of the re-arranged definition of Reynolds number,

$$\frac{Re}{D_E} = \frac{\bar{V}}{\nu}.$$

It is evident that Re/D_E should be constant, since the right-hand side of the equation must be fixed for a given set of conditions. Table 2.2 shows a comparison of D_E, Re_{crit}, and their ratio for the three definitions. Dimensions a and b are arbitrarily set at 0.3711 cm and 0.4 cm respectively.

Table 2.2

Critical Reynolds numbers and equivalent diameter

		D_E	Re_{crit}	Re_{crit}/D_E
i	Swift	0.357	285	798
ii	Lohrenz	0.0124	10	806
iii	Hydraulic	0.0578		

Taking Re_{crit}/D_E as 800, the critical Reynolds number for the third definition is therefore approximately 46.

Since the definitions of equivalent diameter are arbitrary, the hydraulic diameter definition as used by Trombetta will be used since it is the most easily calculated.

Thus the design criterion is according to the definition that

$$Re = \frac{\bar{V}\rho}{\eta} 2(b - a), \qquad (2.39)$$

and Re < 46 for laminar flow.

The average velocity is given in terms of the solid sinker velocity by

$$\bar{V} = \frac{a^2 V}{(b^2 - a^2)}.$$

2.3.2 Critical Reynolds number for sinker with central hole

With a sinker with a central hole there exist two separate areas of flow. The flow regimes in the annulus and in the central hole can be examined separately for the onset of turbulence. For the annulus

$$Re = \frac{\bar{V}\rho 2(b - a)}{\eta}, \text{ where } Re_{crit} = 46. \tag{2.39}$$

For the central hole which may be regarded as a pipe

$$Re = \frac{\bar{V}\rho 2c}{\eta}, \text{ where } Re_{crit} = 2000. \tag{2.40}$$

In the annulus the average fluid velocity is relative to the fixed viscometer tube, while in the central hole the average fluid velocity is relative to the falling sinker since the sinker itself is the pipe through which flow takes place.

In practice most of the fluid passes through the central hole as shown in the velocity profile of Fig. 2.2(a). The average fluid velocity in the central hole, relative to the sinker is by equation 2.12.

$$\bar{V} = \frac{Ac^2}{8\eta}, \tag{2.41}$$

where the constant A is given by equation 2.17(a).

The average velocity in the annulus is given by

$$\bar{V} = \frac{\dot{Q}_a}{\pi(b^2 - a^2)}, \tag{2.42}$$

where $\dot{Q}_a$ is defined in equation 2.9.

These formulae for Reynolds number are an aid to the calculation of dimensions of a sinker which will allow a given viscosity to be measured without turbulence. Or alternatively, the minimum viscosity and the

corresponding sinker velocity can be calculated for a given set of dimensions.

The latter procedure is illustrated. The dimensions of a, b, and c are those of the only sinker with a central hole which was used for measurements.

$a = 0.29555$ cm therefore $a/b = 0.9375 = \kappa$

$b = 0.31525$ cm

$c = 0.12340$ cm

Let $\rho_1 = 7$ g cm^{-3}, and

$\rho_2 = 1$ g cm^{-3}

assume that $\eta = 1000$ P.

Therefore constant $A = 4121.0$, dyne cm^{-3} (equation 2.17)

Sinker velocity, $V = 0.001\ 297$ cm sec^{-1} (equation 2.18)

Flowrate through annulus, $\dot{Q}_a = -0.000\ 0190$ cm^3 sec^{-1} (equation 2.9)

Therefore average annular velocity = $-0.000\ 501$ cm sec^{-1} (equation 2.42)

Therefore in the annulus $Re = 0.613 \times 10^{-6}$ (equation 2.39)

Flowrate through central hole $Q = \pi c^4 A/8\eta = 0.000\ 375$ cm^3 sec^{-1}

Therefore average velocity in hole = $0.007\ 84$ cm sec^{-1} (equation 2.41)

Therefore in central hole $Re = 1.93 \times 10^{-6}$ (equation 2.40)

For a fixed geometry it may be shown that $(\eta^2 Re)$ is constant. Thus the critical viscosity, η_{crit}, which is the viscosity at which turbulence is encountered, may be calculated.

For the annulus,

$$\eta^2_{crit} = \frac{\eta^2 Re}{Re_{crit}}$$

$$= \frac{0.613 \times 10^{-6} \times 10^6}{46}$$

thus $\eta_{crit} = 0.1154$ P.

For the central hole,

$$\eta^2_{crit} = \frac{1.93 \times 10^{-6} \times 10^6}{2000}$$

thus $\eta_{crit} = 0.031$ P.

The results show that turbulence is encountered in the annulus at 0.1154 P, before turbulence is reached in the central hole. Thus the minimum viscosity which can be measured with the stipulated fixed geometry is 0.115 P.

The corresponding maximum sinker velocity is

$$V = \frac{V_1 \eta_1}{\eta_{crit}}$$

$$= \frac{0.001\ 297 \times 1000}{0.1154}$$

$$= 11.24 \text{ cm/sec.}$$

Thus for the sinker with the central hole, turbulence is first encountered in the annulus at the comparatively high sinker velocity of about 11 cm sec^{-1}. This is outwith the range of velocity measured in practice (not greater than 0.5 cm sec^{-1}).

It is of interest to note that for this geometry the flowrate, and consequently the average velocity, in the annulus is negative with respect to the viscometer tube. This is because the annular gap is small compared with the central hole.

2.4 The Effects of Pressure

The viscometer geometry is affected by pressure in two ways. Firstly, the diameters of both tube and sinker are reduced thus narrowing the annulus, and secondly, the length of the viscometer tube is shortened. The effect of narrowing the annulus is to restrict fluid flow thus causing a greater fall-time, while the effect of shortening the tube length is to decrease the time of fall. The two effects of pressure are therefore self-cancelling to a certain extent. The annular effect is,

however, predominant as can be seen from the equation

$$\eta = \frac{(\rho_1 - \rho_2)a^2 g}{2V} f(\kappa) \qquad (2.26)$$

$$= \frac{(\rho_1 - \rho_2)a^2 gT}{2L} f(\kappa),$$

where T is the measured fall-time over tube distance L. In terms of geometrical dimensions the expression on the right-hand side has $a^2/L \triangleq$ length, which is reduced under pressure.

The effect of pressure on $f(\kappa)$ is zero only if the tube and sinker are of the same material, since $\kappa = a/b$. In this work design criteria require that the tube and sinker be of different materials, namely brass and iron respectively. The correction for pressure effects on the viscometer performance is applied to the general case, that is to the sinker with a central hole. The general equation is

$$\eta = \frac{(\rho_1 - \rho_2)(a^2 - c^2)g[(b^4 - a^4 + c^4)\ln b/a - (b^2 - a^2)^2]T}{2L(b^4 - a^4 + c^4)}. \qquad (2.18)$$

This may be expressed as

$$\frac{\eta}{(\rho_1 - \rho_2)} = KT. \qquad (2.43)$$

The constant of proportionality at atmospheric pressure is K. Under pressure, this constant is multiplied by the quotient of

$$(a^2 - c^2)[(b^4 - a^4 + c^4)\ln b/a - (b^2 - a^2)^2] \Big/ L(b^4 - a^4 + c^4) \qquad (2.44)$$

at a given pressure and its value at atmospheric pressure. For this calculation the compressibilities of brass and iron are required.

2.4.1 Compressibilities of brass and iron

The relative decrease in length of a material is $-\Delta\ell/\ell = \varepsilon$. The value of ε may be calculated from

$$\varepsilon = \frac{(1 - 2\mu)P}{E}, \qquad (2.45)$$

where E is Young's modulus, P is pressure, and μ is Poisson's ratio. It is common practice to define linear compressibility β as $\beta = \varepsilon/P$

so that length under pressure is given by $\ell = \ell_{p=0}(1 - \beta P)$.

Calculated values of ε are shown in the following table:

Table 2.3

Elastic constants of brass and Swedish iron

Material	Young's modulus $E(N/m^2)$	Poisson's ratio μ	$\varepsilon = -\Delta\ell/\ell$	
			per N/m^2	per bar
Brass	10.4×10^{10}	0.374	2.42×10^{-12}	2.42×10^{-7}
Iron	21.2×10^{10}	0.29	1.98×10^{-12}	1.98×10^{-7}

The data are from the American Institute of Physics Handbook (1957). Measurements show that $\Delta\ell/\ell$ is not precisely a linear function of pressure. The deviation from the straight line relationships for iron is about 0.000 25 per cent at 10 kbar, and is negligibly small. The value of $\Delta\ell/\ell$ for iron was found by Bridgman (1940) to be 1.98×10^{-7} per bar, and by Vaidya and Kennedy (1970) to be 1.95×10^{-7} per bar.

2.4.2 Calculation of pressure corrections

The changes in dimensions in a, b, c and L are calculated, and by equation 2.44 the corrections for pressure obtained. Viscometer dimensions b and L, being of brass, are reduced more than the sinker dimensions a and c.

By reducing the sinker hole diameter to zero the correction for a solid sinker is obtained. The corrections for one of the sinkers used for measurements, sinker 1, are shown in Table 2.4. This table also shows the change of dimensions and the variation of $f(\kappa)$.

Table 2.4

Pressure corrections for solid sinker (sinker 1)

p/bar	a/cm	b/cm	c/cm	Ratio	Gap-thou	f(κ)	Corr.
						× 10^{-6}	
0	0.303 76	0.315 25	0.000 00	0.963 55	4.52	1.5733	1.0000
2000	0.303 64	0.315 10	0.000 00	0.963 64	4.51	1.5616	0.9926
4000	0.303 52	0.314 94	0.000 00	0.963 72	4.50	1.5500	0.9852
6000	0.303 40	0.314 79	0.000 00	0.963 81	4.49	1.5385	0.9779
8000	0.303 28	0.314 64	0.000 00	0.963 89	4.47	1.5270	0.9706
10000	0.303 16	0.314 49	0.000 00	0.963 98	4.46	1.5156	0.9633
12000	0.303 04	0.314 33	0.000 00	0.964 06	4.45	1.5042	0.9561
14000	0.302 92	0.314 18	0.000 00	0.964 15	4.43	1.4928	0.9489

The correction at 14 kbar is 0.949, which means that the sinker takes about 5 per cent longer to fall due to the narrowing of the gap between the tube and sinker. The table shows that the gap changes 0.0009 inch, that is from 0.004 52 to 0.004 43 inch. In practice the viscosity range of the sinker is such that it is not used above 3 kbar, and consequently the maximum correction applicable to sinker 1 is about 0.99 or 1 per cent.

Table 2.5 contains the corrections for the hollow sinker used for measurements.

Table 2.5

Pressure corrections for hollow sinker (sinker 2)

p/bar	a/cm	b/cm	c/cm	Ratio	Gap-thou	f(κ)	Corr.
						× 10^{-4}	
0	0.295 52	0.315 25	0.123 40	0.937 41	7.77	4.4126	1.0000
2000	0.295 40	0.315 10	0.123 35	0.937 50	7.75	4.4111	0.9997
4000	0.295 29	0.314 94	0.123 30	0.937 58	7.74	4.4097	0.9993
6000	0.295 17	0.314 79	0.123 25	0.937 66	7.73	4.4083	0.9990
8000	0.295 05	0.314 64	0.123 20	0.937 75	7.71	4.4068	0.9987
10000	0.294 93	0.314 49	0.123 16	0.937 83	7.70	4.4054	0.9984
12000	0.294 82	0.314 33	0.123 11	0.937 91	7.68	4.4039	0.9980
14000	0.294 70	0.314 18	0.123 06	0.937 99	7.67	4.4025	0.9977

The correction terms due to pressure are small, 0.23 per cent at 14 kbar. This is because the annular gap is comparatively large, and thus changes in the gap have a smaller effect than in the previous case, but mainly

because most of the flow is through the central hole of which the area is reduced only slightly.

The variation of the correction factors is substantially linear with pressure as illustrated in Fig. 2.3. The correction for a sinker with the same annular gap as sinker 2, but without the central hole is also shown in Fig. 2.3. This illustrates that a sinker with a central hole has the advantage that the correction term is greatly reduced.

The effect of temperature is similar to the effect of pressure, but produces an increase rather than a decrease of the dimensions in the correction formula given by equation 2.44. Therefore the correction term is greater than unity for measurements made at higher temperatures.

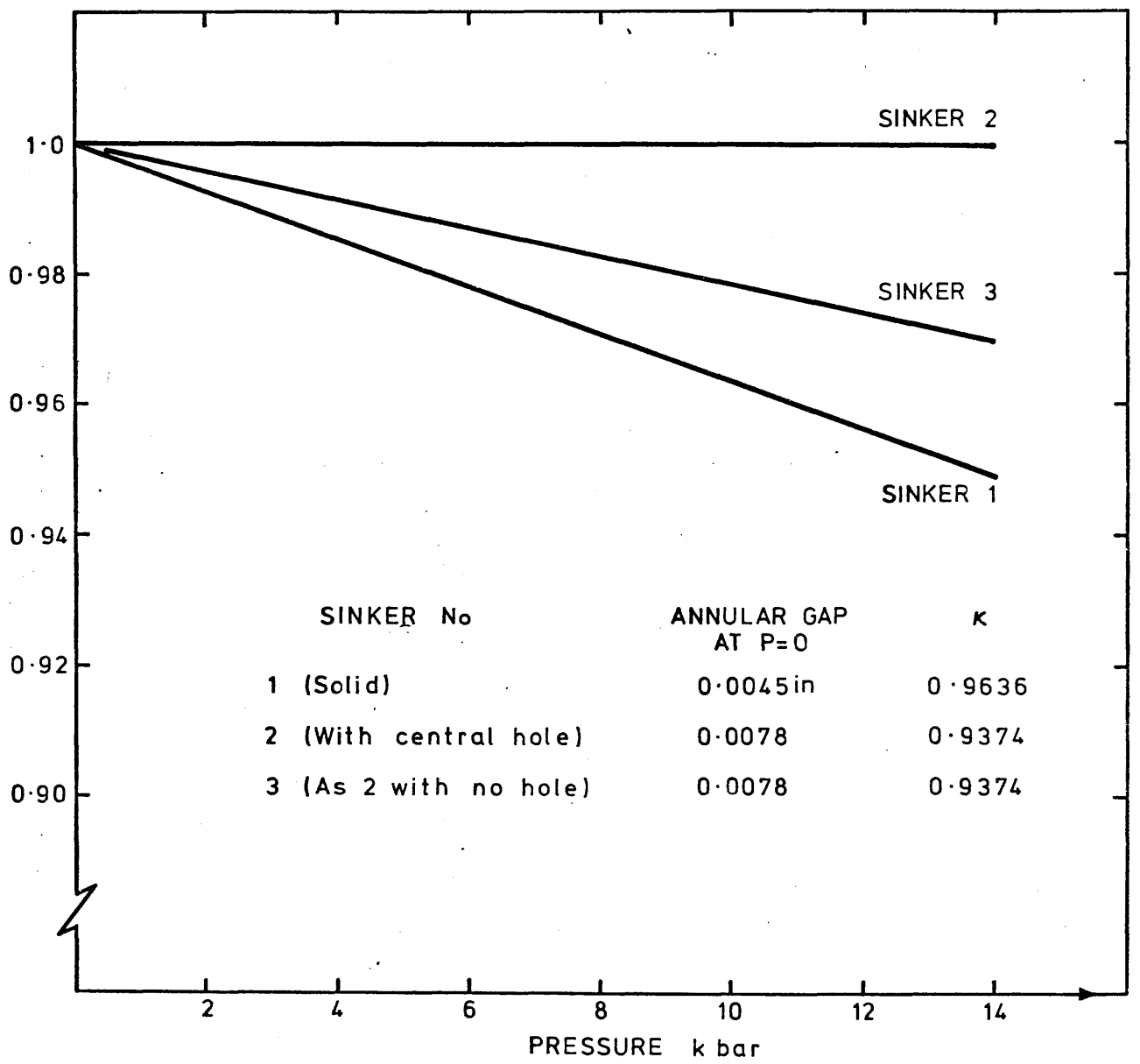

FIG 2.3 Viscometer constant correction as a function of pressure

CHAPTER 3

VISCOMETER DESIGN AND CONTROL

List of Figures

List of Tables

CHAPTER 3

VISCOMETER DESIGN AND CONTROL

3.1 General Description

This falling cylinder viscometer is unique in that the only moving part in the entire cycle of measurement and retrieval is the sinker itself. Before making a measurement the sinker is lifted electromagnetically by a series of coils along the viscometer tube. After the sinker is released its fall time is detected inductively by the same coils. The operating cycle is remotely controlled, and a predetermined number of measurements at a given pressure may be made automatically. One sinker is used in the viscosity range 0.01 to 10 P, and a second sinker with a central hole is used to extend the upper limit to 3000 P.

3.2 Viscometer Assembly

A diagram of the viscometer is given in Fig. 3.1. The liquid under test is contained in tube 1, which is closed at the top by an O-ring seal and the screw 2, and at the bottom by the flexible bellows 3, again with an O-ring. The test liquid is thus separated from the pressure transmitting fluid, and the pressure difference is minimized by using an extra flexible grade of bellows. The viscometer is of precision bore hard-drawn brass. Two types of sinkers are used, both of soft iron. The first type is a solid cylinder with a hemispherical end; the second has a similar shape but with a central hole, as illustrated in Fig. 3.1. The first sinker covers the range 0.01 to 10 P, the second 10 to 3000 P, with maximum fall times of about 100 minutes. The sinkers are unguided, since it was found during preliminary experiments that coaxial fall occurs if the sinker and tube are cylindrical and the tube is vertical. The upper and lower centering rings, 4 and 5, which are soldered on to tube 1, are sliding fits in the pressure vessel; vertical alignment of the vessel bore therefore ensures correct positioning of the viscometer.

Before being released, the sinker is held by a semi-permanent magnet 6, and at the end of the fall it rests on the brass spacer which is supported

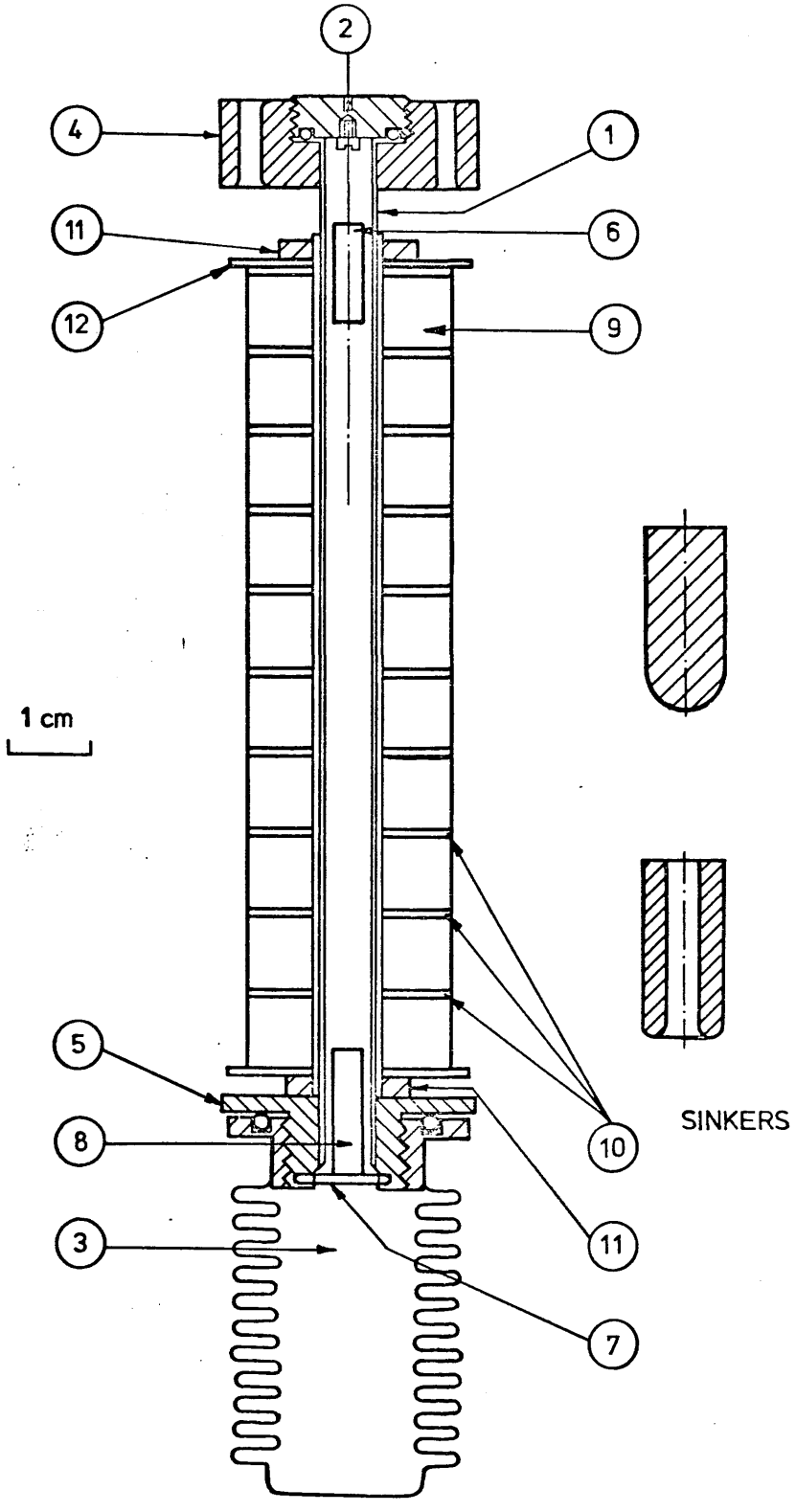

Fig 3.1 High pressure viscometer.

by a bar 8. A thin brass tube surrounds the viscometer tube, and carries ten nylon coil formers 9 which are separated by soft iron discs 10, forming parts of the magnetic circuits for the coils. The coils are clamped in position by two collars 11, and the whole coil assembly is surrounded by an iron sleeve of iron of high permeability.

Each of the lower nine coils is wound with 600 turns of 34 SWG DSC (double silk covered) copper wire. These coils are used both to lift the sinker and to determine its position. To minimise the number of leads taken through the cap of the pressure vessel, the coils are connected in three sets of three coils in series. The top coil is wound with 500 turns of 30 SWG DSC wire and is used to magnetize and demagnetize the holding magnet 6. Each set of three coils and the top coil have a common earth return through the body of the vessel.

A photograph (Fig. 3.2) shows the components of the viscometer, including the two sinkers in the foreground. Also shown is a brass tube adaptor into which the viscometer assembly is inserted when measurements are to be made in the 3000 bar pressure vessel.

3.2.1 Sinkers

The sinkers are made of soft iron. The two sinkers were turned on a lathe, the surface finish being achieved by successively finer grades of emery cloth, then polished with successively finer carborundum paste, and the final finish being made with metal polish. Considerable care was taken to achieve roundness and a smooth, mirror-like surface finish. The sinkers were measured for roundness and parallelism at the National Engineering Laboratory (NEL), East Kilbride, in the Metrology Division. The sinker dimensions are shown in the following table.

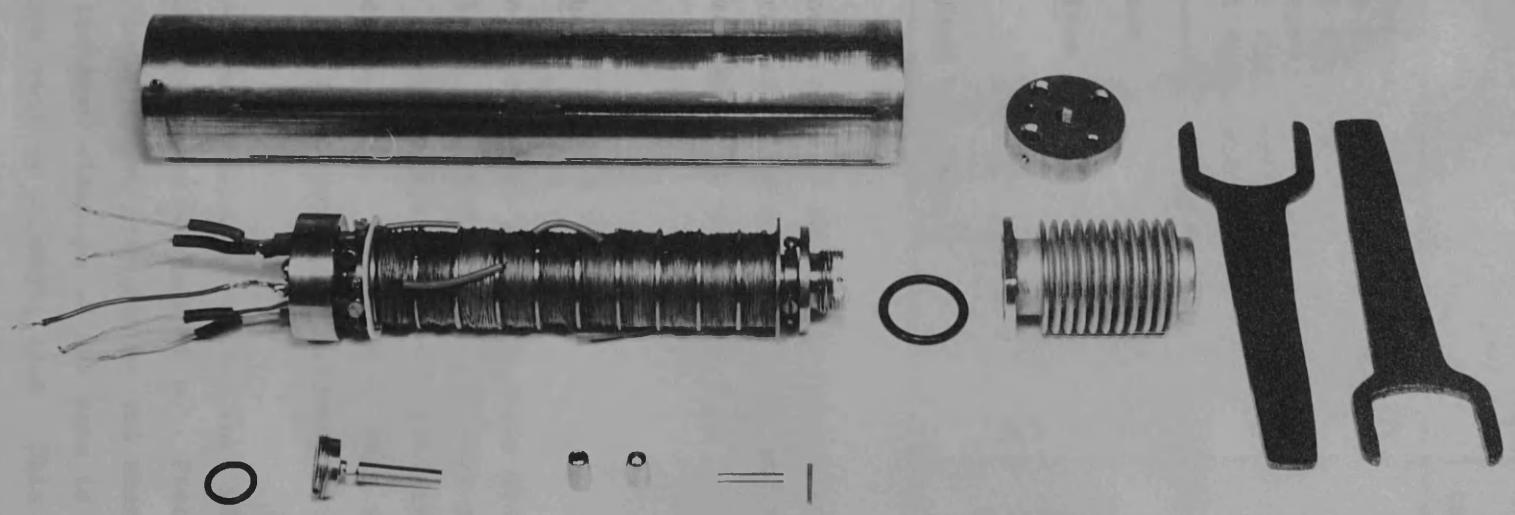

FIG. 3.2. PHOTOGRAPH OF DISMANTLED VISCOMETER

Table 3.1

Dimensions of sinkers

	Sinker 1 (solid)	Sinker 2 (central hole)
Mean diameter at flat end	0.2390_1 in	-
Maximum diameter at flat end	0.2391_2	-
Minimum diameter at flat end	0.2389_4	-
Mean diameter at round end	0.2393_4	0.2326_9 in
Maximum diameter at round end	0.2394_5	0.2327_7
Minimum diameter at round end	0.2392_7	0.2326_0
Overall mean diameter	0.2391_8 in	0.2326_9 in
	=0.6076 cm	=0.5911 cm
Maximum departure from roundness	0.0001_1 in	0.0000_9 in
	0.0003 cm	0.0002 cm
Overall length	1.00 cm	1.10 cm
Diameter of bore	-	0.2468 cm
Maximum departure from roundness	-	0.0010 cm

The departure from roundness of both sinkers is not greater than 0.0001_1 inch (0.0003 cm). The non-parallelism of sinker 1 was found to be 0.0003_3 inch ($.0008_5$ cm); it was not measured for sinker 2.

3.2.2 Viscometer tube

The viscometer tube is No 2 precision bore hard drawn brass (H Rollet & Co Ltd, Paisley). The bore of the tube was polished with metal polish on a slowly rotating lathe, flushed with diethyl ether and polished again with dry cotton wool. Visual inspection showed any residual particles of cotton wool and these are easily removed with a warm-air blower.

The straightness, parallelism and diameter of the bore of the tube were measured at NEL after the viscometer was assembled. Precise measurements at 0.5 inch intervals up to 2 inches from either end showed from a total of 20 measurements that the mean diameter of the bore is 0.2482_3 inch, and the greatest deviation from this is $+0.0002_9$ inch. This falls well within the manufacturer's stated value of 0.248 ± 0.001 inch. The greatest deviation occurred at 0.1 inch from the top of the tube and this is due to the tube being distorted where the top seal is made. Discarding this

measurement, since it lies well outside the part of the tube where fall time measurements are made shows that the variation of tube diameter is no more than ±0.0001 inch. Thus

$$\text{tube diameter} = 0.2482_3 \pm 0.0001 \text{ inch } (= 0.6305 \pm 0.0002_5 \text{ cm}).$$

Over the 2 inch lengths measured parallelism is excellent, there being no effects greater than 0.0000_9 inch. Non-straightness in the tube also proved to be negligible.

3.2.3 Details of viscometer and its construction

Drawings of the viscometer parts are shown in Figs 3.3 and 3.4. The only items not shown are the bellows and the holding magnet. The bellows are the same as for the densimeter and the specification is in section 6.1.1(a). The bellows are soldered on to the bellows seal with Woods Metal as described in that same section. The holding magnet is described in section 3.2.4.

The coils are pre-assembled with the soft iron sleeve on a No 3 brass telescopic tube and clamped together by the two collars. The tube is then slid on to the viscometer tube (No 2 telescopic) and the top centering ring is soldered to the viscometer tube, the lower centering ring already being soldered to the bottom of the tube. The main advantages are that the coil assembly is done separately from the viscometer tube, thus avoiding accidentally damaging or bending the tube, and secondly the viscometer tube is easily and thoroughly cleaned from end to end before the bellows and top seal are screwed into place.

The O-rings for sealing the viscometer are of butadiene acrylonitrile (nitrile rubber) which may be used up to 100°C

	Edwards No	Walker No	British Standard No	i.d. (in)	section (in)
Top seal	VOR 0011	-	-	0.301	0.07
Lower seal	VOR 0116	50.116	O.S. 14	0.737	0.103.

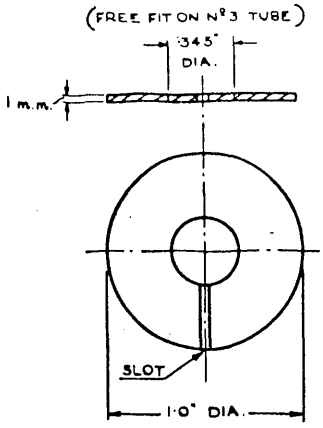

(L)

SOFT IRON DISC.

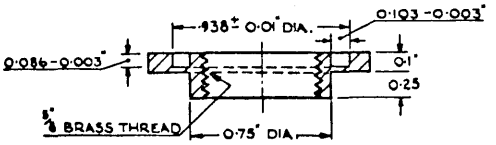

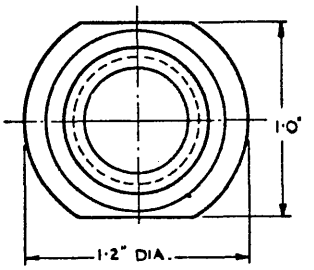

BELLOWS SEAL

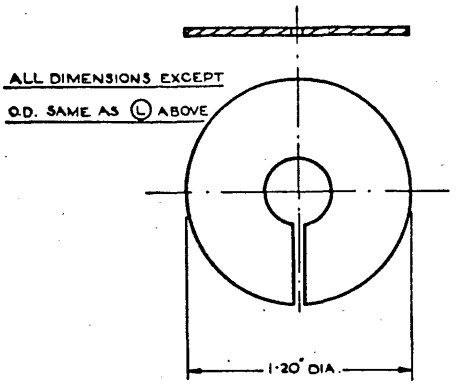

(M)

LOWER IRON DISC.

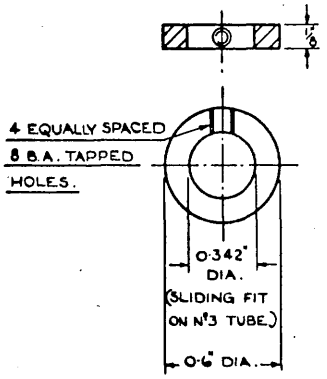

(N)

LOWER COLLAR

ITEM	No. OFF	DESCRIPTION	MATL.	REMARKS
O	1	BELLOWS SEAL	BRASS	
N	1	LOWER COLLAR	BRASS	
M	1	LOWER IRON DISC	SOFT IRON	
L	10	SOFT IRON DISC	SOFT IRON	
I	1	TOP 'O' RING SEAL	BRASS	
G	1	BOTTOM POSITIONING COLLAR	BRASS	NOTE TOLERANCES
F	1	SINKER STOP	BRASS	
D	10	COIL FORMERS	NYLON	
C	1	INSULATING DISC	NYLON	
B	1	TOP COLLAR	BRASS	
A	1	TOP POSITIONING COLLAR	BRASS	NOTE TOLERANCES

UNIVERSITY GLASGOW

ENGINEERING LABORATORIES

TITLE OF DRAWING:—DETAILS OF 14.000 ATMOSPHERE VISCOMETER.

TITLE OF PROJECT:—

DEPARTMENT:—VISCOELASTICS LABORATORY. ELECTRICAL ENG.

PROJECT No.	COST No.	WHEN QUOTING DRWG. PLEASE QUOTE LETTER OF ISSUE
		SCALE:- TWICE FULL SIZE
DRAWN BY	J.B. IRVING	A/215.
TRACED BY	E.F.	
CHECKED BY		
APPROVED BY	A.J. BARLOW	
DATE DRAWN	28TH APRIL 1967	No. OF SHEETS / SHEET No.

BE TAKEN OFF THIS DRAWING
NS ONLY TO BE WORKED TO
IVEN IN ALL CASES.
IED THUS:-
SMOOTH MACHINE
GROUND FINISH

ALL UNTOLERANCED DIMENSIONS IN DECIMALS TO BE WITHIN THE FOLLOWING LIMITS.
HOLES AND INTERNAL SURFACES. + .010"
SHAFTS AND EXTERNAL SURFACES — .010"
CENTRES OF HOLES AND CENTRES TO FACE + .005"
FRACTIONAL DIMENSIONS ± 1/64"

Fig 3.3 Workshop drawings of viscometer

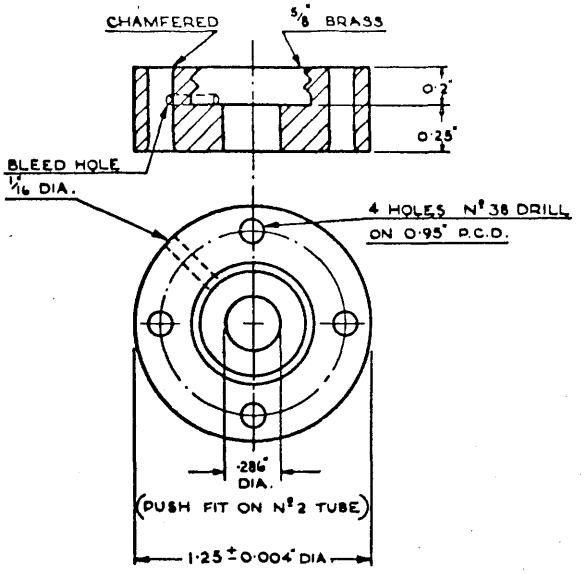

(A)

TOP POSITIONING COLLAR

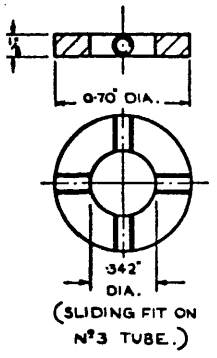

(B)

TOP COLLAR

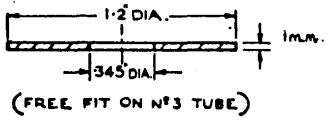

(C)

INSULATING DISC.

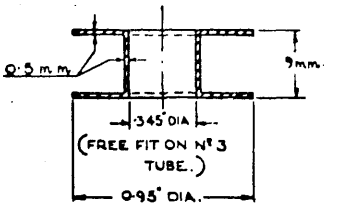

(D)

COIL FORMER

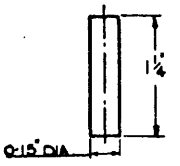

(F)

SINKER STOP

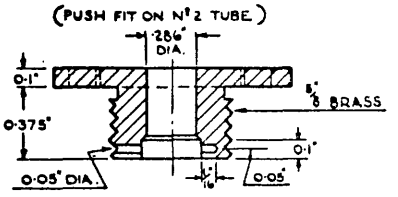

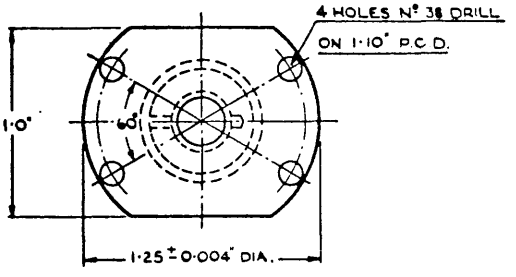

(G)

BOTTOM POSITIONING COLLAR

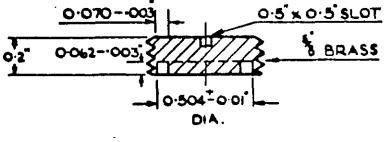

(I)

TOP 'O' RING SEAL.

Fig 3.4 Workshop drawings of viscometer.

Both seals are renewed at each filling to avoid contamination from absorbed test liquid or pressure transmitting fluid.

3.2.4 Lifting/detector coils

Each of the nine coils was wound by hand with 112 ft of 34 SWG DSC copper wire of rated resistance 361 Ω per 1000 yd. Therefore the theoretical resistance of each coil is 13.48 Ω compared with the measured average value of 12.91 Ω.

The coils are connected in series in threes so that the bottom coil is connected to the fourth coil and then to the seventh coil from the bottom, 1-4-7. The second set of coils is comprised of 2-5-8, and the third set, 3-6-9. Inductance measurements of the three sets of coils are used to detect the position of the sinker, and therefore it is necessary that all three have as nearly identical inductances as possible. The inductance and resistance of each coil was measured on a reactance bridge.

Table 3.2

Measured resistance and inductance of lifting coils

Set No	Coil No	Resist R	Inductance L	Ratio R/L	Total set inductance
1	1 4 7	12.95 Ω 13.05 12.75	4.14 mH 4.20 4.09	3.13 3.11 3.12	12.43 mH
2	2 5 8	13.00 13.07 12.79	4.14 4.20 4.10	3.14 3.11 3.12	12.44
3	3 6 9	12.70 13.00 12.86	4.04 4.23 4.16	3.14 3.07 3.09	12.43
Average		12.91 Ω	4.14 mH	3.11	12.43_3 mH

The coils were combined so that each set had as nearly the same total inductance as shown in the table above. It can be seen from the table

that the inductance totals have been equalised.

3.2.5 Holding magnet

The holding magnet is 1.4 cm long cut with a diamond saw from an $\frac{1}{8}$-inch diameter rod of high speed tool steel. It is suspended from the top seal by nichrome wire which is spot welded to the top flat surface as shown in Figs 3.1 and 3.2.

This particular material was chosen after preliminary tests with different types of steel and commercially available cylindrical magnets. The holding magnet is magnetized by passing a 3-second 25 V dc pulse through the magnetizing coil, and released for a fall time measurement by passing a decaying sinusoidal current through the same coil. The high speed tool steel was the only material of those tested which could be magnetized enough to hold the sinker, and yet be demagnetized sufficiently to release it.

3.3 Viscometer Control System and Mode of Operation

A simplified schematic diagram of the control system is given in Fig. 3.5. The transitions between the four main parts of the operating cycle, ie lifting, holding, releasing and falling, are governed by a stepping relay (Post Office type, 50 V uniselector).

Initially, the sinker is at rest in coil a. The inductance bridge (Marconi TF 2700) is connected to the set of coils adg, and the presence of the sinker in coil a causes the bridge to be unbalanced. The out of balance signal (at 1000 Hz) is amplified, rectified, and is used to operate a relay which energizes the stepping relay. A current of up to 1 A dc is applied to the set of coils beh, and the sinker is lifted into coil b. When the sinker leaves coil a, the bridge returns to balance and the consequential loss of energizing current causes the stepping relay to advance to the next position. In this second position the lifting current is transferred to coils cfi, and the bridge connection to beh. By successive steps of this kind the sinker is lifted until it reaches coil i. At this point a current is applied to coil j so that the

magnet is magnetized and the sinker held. After about 3 seconds the magnetizing current is removed.

The time taken to lift the sinker varies from a few seconds to a few minutes, depending on the viscosity of the liquid under test and the sinker used. As a safety precaution the lifting time is limited, and the cycle is stopped if the sinker has not reached the top of the tube within this time. During lifting about 30 W are dissipated (mainly in the coils), and the sinker must be held whilst the temperature returns to its original value. The resistance of one set of the coils is monitored by connecting it to a Wheatstone bridge. The bridge is balanced before lifting occurs. When the temperature differs from its original value by less than $0.5^{\circ}C$, a timer is started by the diminution of the out-of-balance signal from the bridge. This timer introduces an additional delay to ensure that thermal equilibrium is reached. The delay is adjustable, and is made at least ten times the lifting period. At the end of this delay the sinker is released. Coil j is connected as the resistive component of a damped tuned circuit, consisting of an inductance and a capacitor. The capacitor is initially charged to 300 V dc. A transient decaying oscillatory current passes through the coil, and the holding magnet is demagnetized. The heating effect of this current is negligible.

When the sinker leaves coil i the inductance bridge is connected to the set of coils beh and the motor of the chart recorder is started. The variation of the out-of-balance signal caused by the sinkers passing through coils h, e, and b is displayed as three peaks of the chart. The peaks are broad and similar in shape. Timing pulses from a clock are also recorded on the chart at intervals of one minute so that the chart speed can be accurately determined.

The chart recorder motor is stopped when the sinker reaches coil a, and the system is then ready for the start of a new cycle. A counter is used so that a predetermined number of cycles are completed without intervention.

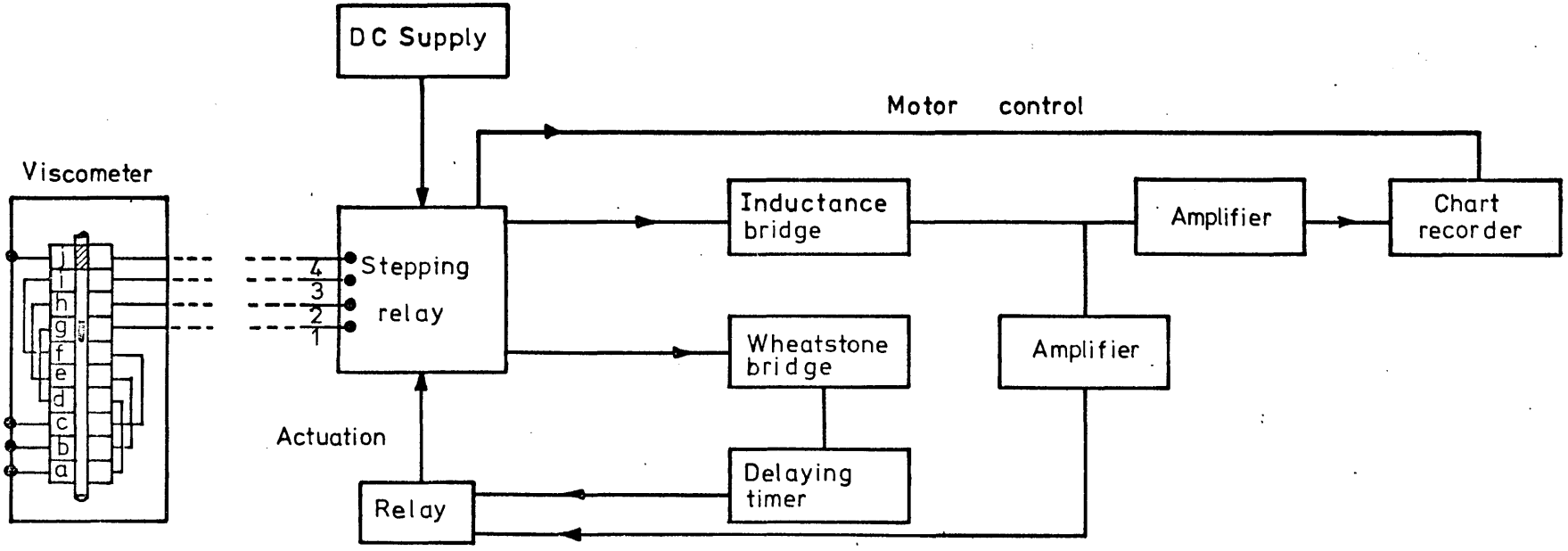

Fig 3:5 Schematic diagram of viscometer control.

3.3.1 Main control circuit

The out-of-balance signal from the inductance bridge, caused by the presence of the sinker, is amplified and rectified by a 5-stage transistor circuit. When the signal is sufficiently out-of-balance, the dc level at the output closes the armature of a miniature relay which forms the load of the output stage. The circuitry and peripheral connections are shown in Fig. 3.6.

i Sequential shift

This mode of shift is the most important aspect of the automatic viscometer. It is the mode of shift adopted during the lift of the sinker, and during its fall. In this mode, the uniselector can only move to the next position after the previous step has been carried out. For example during the lifting sequence the lifting current is transferred to the next coil only when the required upward movement of the sinker has been successfully accomplished.

In this sequential shift mode the -30 V supply is connected to the emitter of transistor BFY 11 via a 1.8 kΩ resistor. This n-p-n transistor acts as a dc coupler. When the presence of the sinker is detected the output relay armature is closed. This drives a slave relay (SR) which energises the armature of the uniselector. When energised, a catch lever extends to engage the next tooth of a ratchet wheel. When the sinker departs from the detector coil, upwards during lifting or downwards during a fall time measurement, the bridge becomes balanced, the output relay drops out followed by the slave relay, which de-energises the uniselector coil. The ratchet wheel of the uniselector is then drawn round to the next position. Thus the uniselector is moved to the next position only when the bridge is balanced after having first been out of balance.

ii Self-shift

This mode is used to perform steps such as moving over unused uniselector contacts to return to the zero position. It is used at intermediate stages of the cycle to be described later.

Self-shift is achieved by biasing the output transistor so that the miniature output relay is on. As shown in Fig. 3.6 this is done by

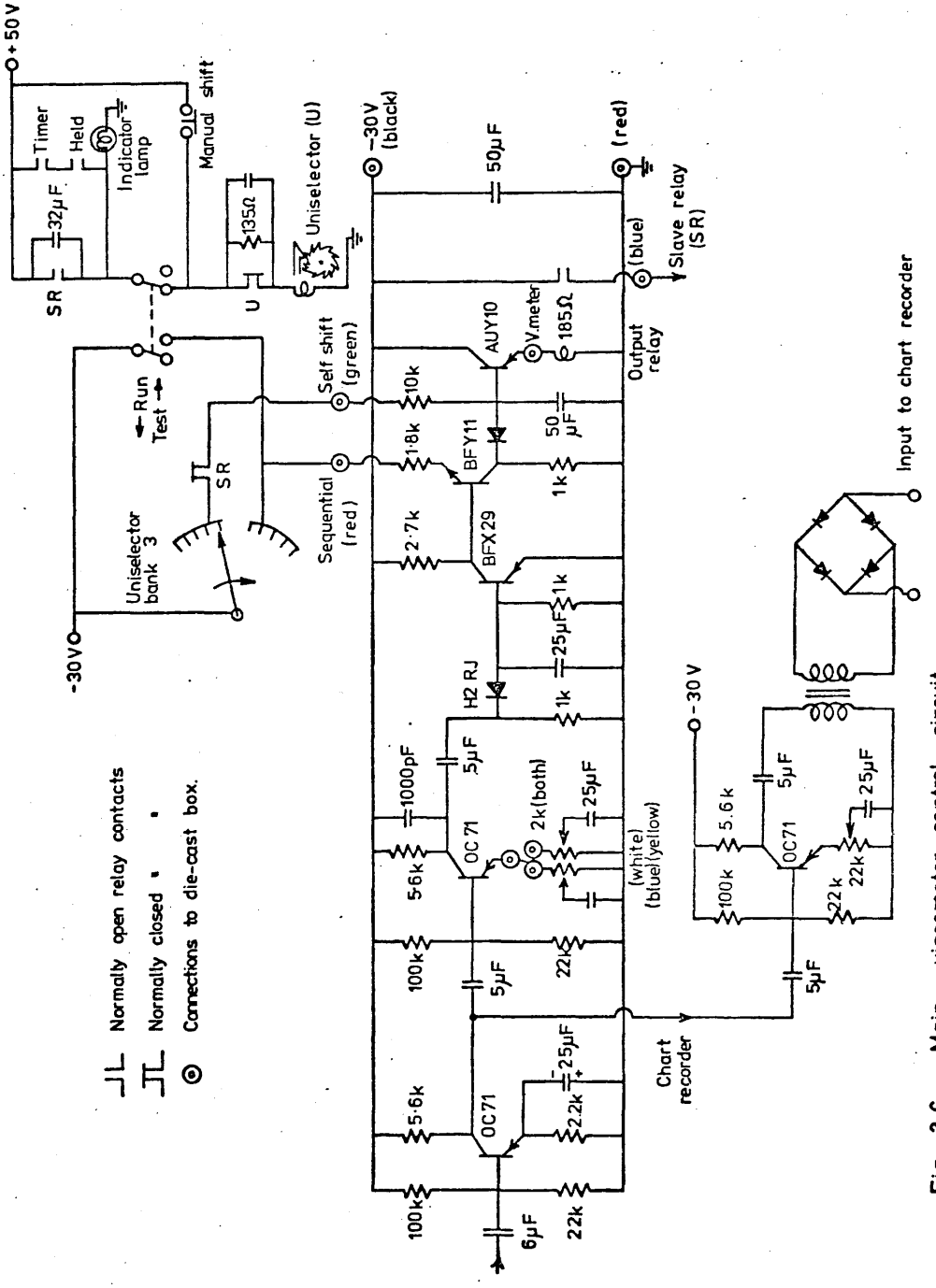

Fig 3.6 Main viscometer control circuit.

connecting the base of the transistor through 10 kΩ to the -30 V supply through the normally closed (NC) contacts of the slave relay. Thus the -30 V biasing supply is interrupted whenever the miniature relay is energised causing the uniselector to move by one position each time. The presence of the 50 μF capacitor restricts the rate of switching to about two steps per second. Self-shift continues while the bias is applied, through bank 3 of the uniselector.

iii Test/run switch

In the test position the uniselector coil is isolated. This allows switching levels to be adjusted if required without actually stepping the uniselector. An indicator lamp shows when the slave relay is energised. In this position the sequential shift mode is connected, as shown in Fig. 3.6. For automatic running the switch is in the run position.

iv Manual shift

Pressing and releasing the shift push button (NO - normally open) advances the uniselector sweep contacts by one position allowing any position in the cycle to be reached for test purposes.

To prevent the uniselector coil from overheating, a 135 Ω, 30 W resistor is connected in parallel with the uniselector normally closed contacts. Thus, when energised, the voltage across the coil is reduced, but is sufficient to hold the armature closed.

3.3.2 Peripheral controls governing sequence of operation

Operational sequence is determined by the uniselector position. There are five banks of uniselector contacts as shown below.

Bank 1	Earth	
Bank 2	-30 V	Supplies indicator lights and relays
Bank 3	-30 V	Shift mode supply, sequential or self-shift connections
Bank 4	Inductance bridge	Connects viscometer coils to inductance bridge
Bank 5	-30 V	Supplies relays which distribute lifting current.

Fig. 3.7 shows the uniselector sequence. The main steps of the cycle are as shown by separate indicator lights controlled from bank 2. Operation falls naturally into these steps and is therefore described under those headings starting at the zero position.

i Zero

In the zero position the sinker is at rest at the bottom of the viscometer tube. It is therefore in coil set 1. A coil selector switch allows the inductance bridge to be connected to either of the three sets of lifting coils, as shown in Fig. 3.8. The bridge is balanced at coils 2 or 3, and out of balance at coil 1 due to the presence of the sinker. With the test/run switch at test, the amplifier gain in the main control may be adjusted so that the shift relay closes, this is shown by the 'shift' indicator light (Fig. 3.6). When the selector switch is returned to coils 2 or 3 balance is again achieved, the shift relay is de-energised, and the indicator lamp goes out.

A measurement cycle starts from the zero position. The test/run switch is put to the run mode. If one measurement only is required, the next position may be reached by pressing the manual shift button. Alternatively, if several complete runs are to be made a manual/self-start switch is put in the self-mode. This moves the uniselector to position 2 by self-shift as described in section 3.3.1. When the cycle is complete and the uniselector reaches the zero position it will automatically move on to position 2 and so restart the measurement cycle.

ii Lifting

Lifting is achieved by passing a direct current of up to 1 A through the coils so that the sinker is lifted by 8 successive steps, the controller being in the sequential shift mode. Power is supplied from a 50 V dc unit. It is carried to the lifting coils through contactors which are used to withstand the continual breaking of up to 1 A.

Fig. 3.9 shows the method of current distribution whereby two contactors carry the lifting current. The controlling relays A and B are energised through the contacts of bank 5; they control the contactors C1 and C2.

Bank		1	2	3	4	5	6	7	8	9	10	11	12	13	14	15	16	17
1	EARTH (black)	0	———															
2	LIGHTS & RELAYS -30 V (brown)	ZERO	———			LIFTING			———		MAG RELAY	HOLD RELAYS	READY RELAY		RELEASE RELAY (1)	—— FALLING ——		
					LIFT	CONTROL		RELAY	and supply to 1-2-3 minute timer							RELAY		
3	SHIFT MODE -30 V	SELF OR MANUAL	———			SEQUENTIAL			———		SELF via NC Lift I relay	SELF after delay	—SELF—		SEQ	—SEQ—— SEQ OR SELF		SELF
4	INDUCTANCE BRIDGE (violet)	1-2-3	1	2	3	1	2	3	1	2	2	1-2-3	—— 2 ——		3	——— 2 ——— Fall detector coil		
5	LIFT CONTROL -30 V	0	2	3	1	2	3	1	2	3								

(1) Via diode to 1-2-3 minute timer

Fig 3.7 Sequence diagram for the 5 bank uniselector

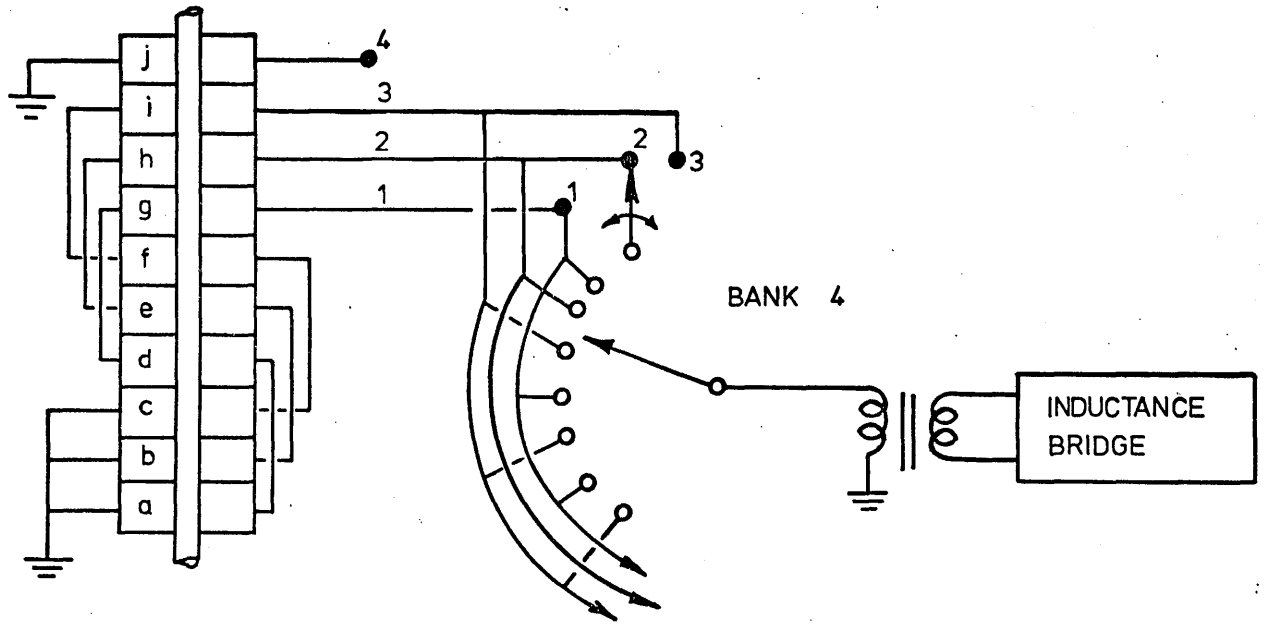

Fig 3.8 Inductance bridge connections.

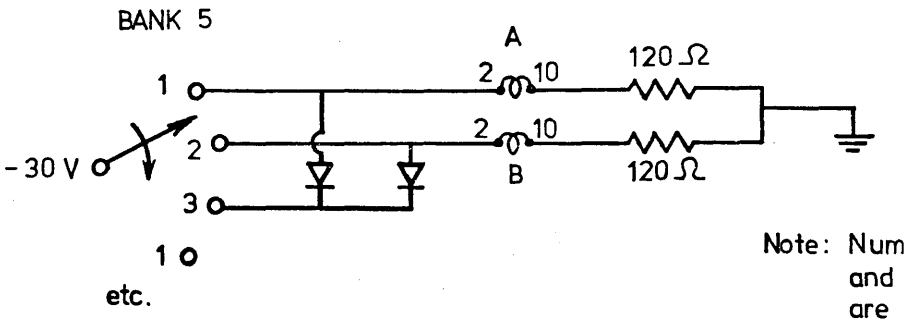

Note: Numbers on coils and relay contacts are the relay pin numbers.

(a) Slave relays A and B

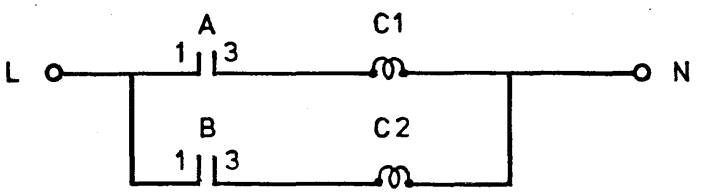

(b) Contactors C 1 & C2

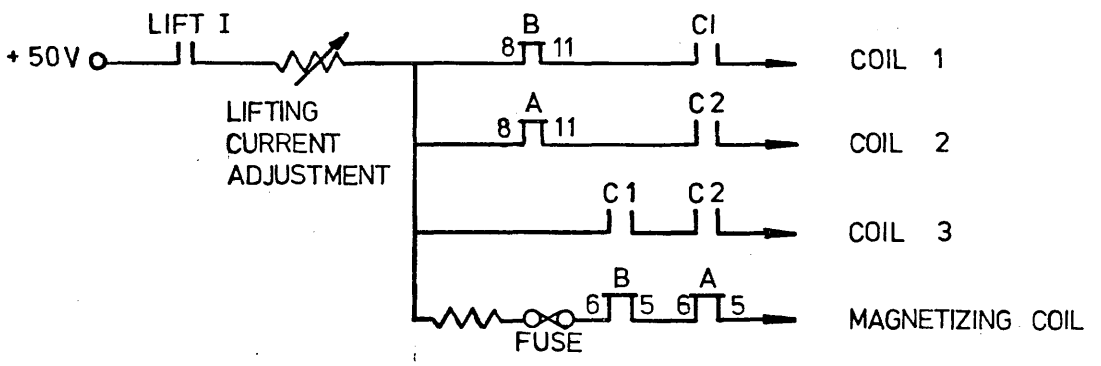

(C) Distribution of lifting current.

Fig 3.9 Lifing current control circuits.

Lifting current limitation

30 W are dissipated in the coils due to the lifting current. To avoid the possibility of overheating the period of lifting is restricted to one, two or three minutes, the period being determined by the viscosity of the test liquid and the size of sinker used.

A 1-2-3 minute timer was built for this purpose. It provides an output which is closed for the duration selected on a 3-way switch. The circuit diagram, logic diagram, and switch arrangement are shown in Fig. 3.10. The operation is self-explanatory.

There are six wires to the unit housed in a die-cast box with six miniature relays. The timer is triggered by connecting point 5 to earth through the contacts of a relay (1 minute timer relay) which is momentarily closed at minute intervals by a mechanical clock. An over-riding push-button is incorporated for test purposes. The connection labelled 6 provides a -30 V pulse after 3 minutes have elapsed, the function of which is included in section 3.3.2 (v).

Lifting current control relay

When the lifting period is started by the one minute clock the lift control relay is closed. This activates a 3-second delay switch (thermally operated relay) which closes a second relay, the lift current relay as

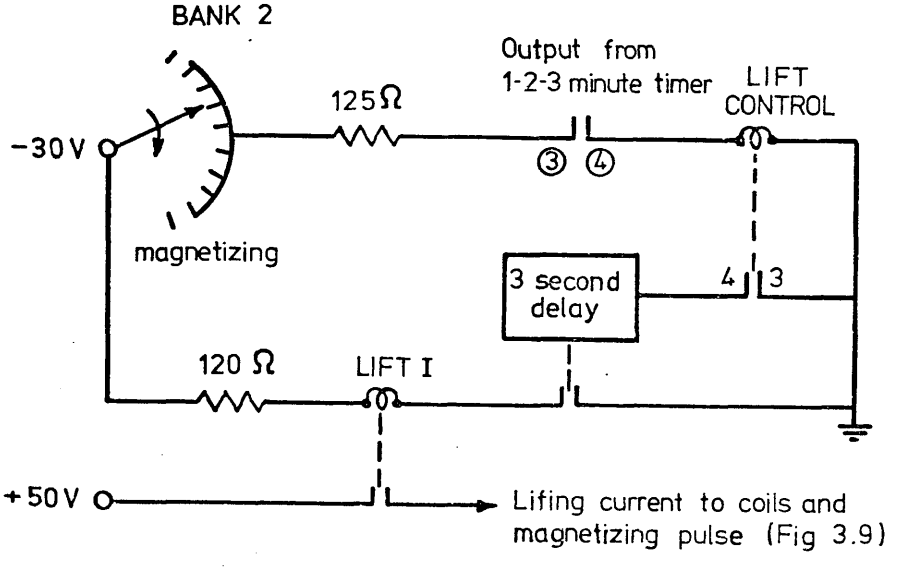

Fig. 3.11 Lifting current control relay

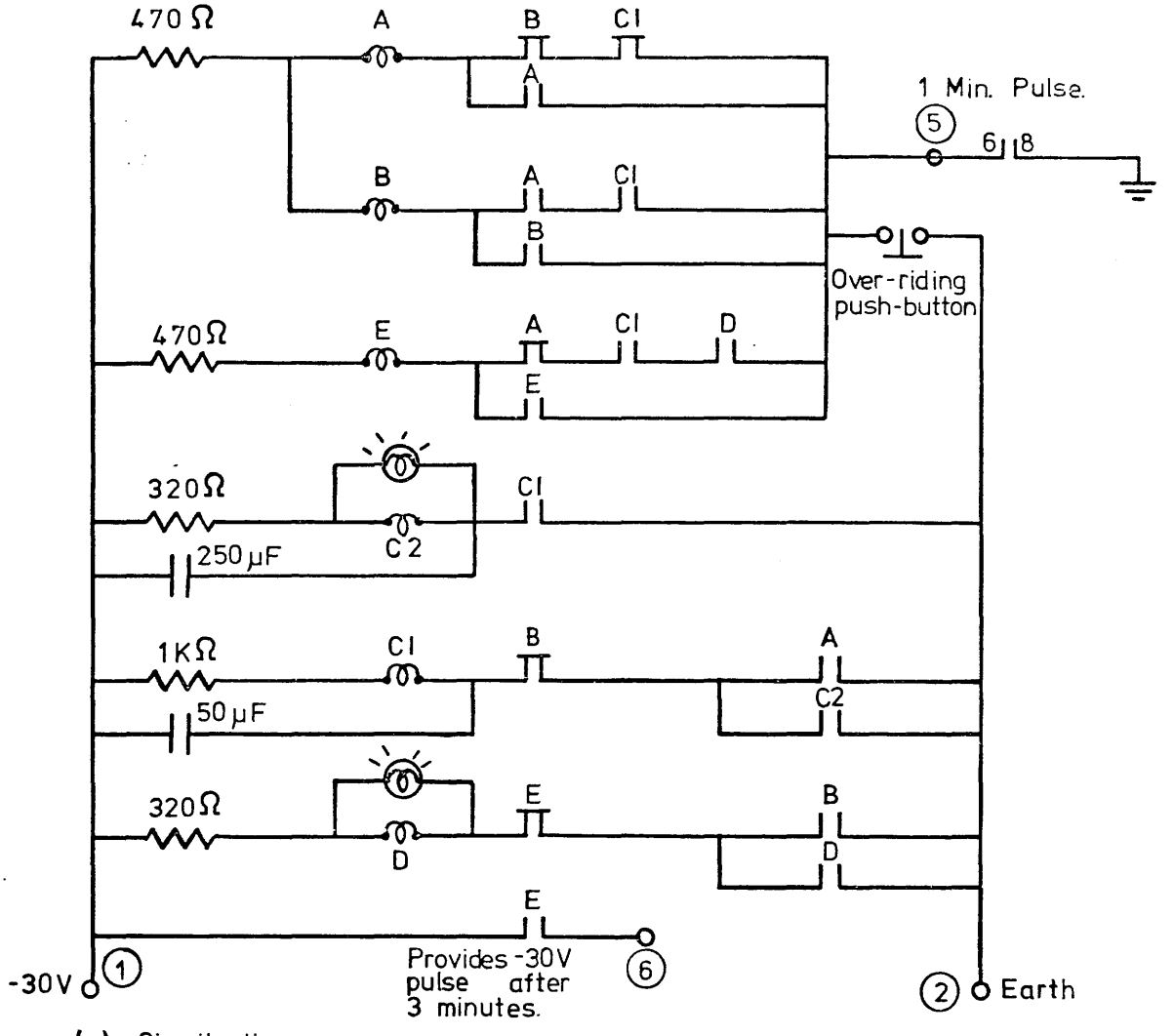

(a) Circuit diagram.

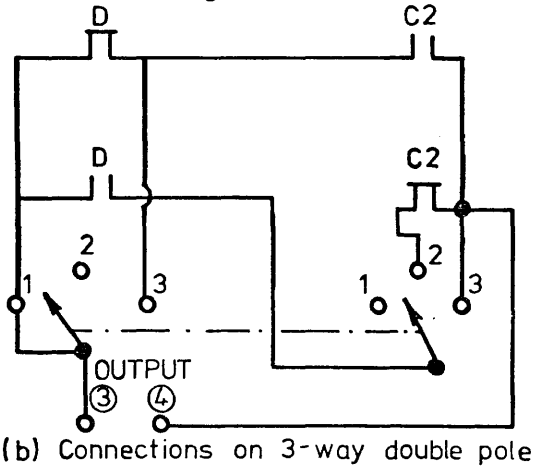

For 1 minute $C.\bar{D}$

2 " $C.\bar{D} \neq \bar{C}.D \subset C \neq D$

3 " $C \neq D$

. and $\bar{A}$ not A $\neq$ or $\not\equiv$ not same as

(b) Connections on 3-way double pole switch for output.

Pulse No.	Relays A	B	C	D	E	Indicator lights 1 min.	2 min.	Indicated time (binary code)
1	(1)		1			1		First minute
2		(1)	0	1		0	1	Second "
3	(1)		1	1		1	1	Third "
4		(1)	0	0	(1)	0		

(c) Relay logic (1) = on only during pulse.

Fig 3.10 1-2-3 minute timer.

shown in Fig. 3.11. The purpose of the 3-second delay becomes apparent in section 3.3.2 (iii) (magnetizing). The contacts of the lifting current relay then supply the lifting current to the coils as already described in the previous section. In the event of lifting not being completed the lifting current is disconnected after the pre-set interval of 1, 2 or 3 minutes.

iii Magnetizing

When the sinker is drawn to the topmost lifting coil, its departure from the coil below is detected, and the uniselector moves to the next position which is the magnetizing position. Here the lifting current supply is directed to the magnetizing coil, coil 4, as shown in Fig. 3.9(c), through the normally closed contacts of relays A and B. In this position, however, the supply to the lift control relay is disconnected on bank 2, so that connection to the thermal relay in Fig. 3.11 is broken. Thus, after a delay of 3 seconds, the lifting current relay drops out so that the magnetizing current is discontinued.

The 3 second current pulse to the magnetizing coil magnetizes the holding magnet and the sinker is drawn up by this magnetizing field. The sinker is then held in contact with the now-magnetized holding magnet.

The switching of the uniselector to the next position is by self-shift connected through normally-closed contacts of the lifting current relay. Thus the uniselector can only move on to the 'held' position after magnetization has taken place.

iv Hold

The sinker is held by the holding magnet until the viscometer and test fluid reach the equilibrium temperature of the bath. Initial cooling is monitored by the change of resistance of one of the lifting coils, arbitrarily chosen. An additional delay is then imposed to ensure that true equilibrium is reached.

Wheatstone bridge

Immediately the held position is reached coil 3 is connected into a Wheatstone bridge as shown in Fig. 3.12.

The 'hold' relay connected through bank 2, also serves to connect a 5 V dc supply to the bridge. In addition a second held relay connects the Wheatstone bridge output to the chart recorder. The chart recorder is arranged to advance slowly by means of short pulses at one minute intervals from the relay activated by the clock. The arrangement is shown in detail in section 3.3.3. The current drain through coil 3 is not more than 5 mA.

The Wheatstone bridge is balanced before lifting occurs so that when the monitored temperature reaches within $0.5^{o}C$ of its original value an automatically resetting timer is triggered by a limit switch on the chart recorder. The action of starting the delay disconnects the supply to the Wheatstone bridge, and discontinues the advance of the chart recorder.

Reset timer (1-60 minute delay)

A reset timer is used which is adjustable to between 1 and 60 minutes. The delay is set so that it is at least 10 times the lifting period. A circuit diagram of the timer with peripheral components is shown in Fig. 3.13. When the timer is instantaneously triggered by the chart recorder limit switch a synchronus motor runs, and coil CL is energised. The circuit is self-maintained by the closure of contacts 5 and 6. After the set period of delay has elapsed the switch between 11 and 7 opens, and the timer resets to its original condition.

A relay (timer relay) is connected as shown. It is evident that this relay is closed during the delay period. The contacts of this relay, in series with the 'held' relay contacts, connect the 50 V supply to the uniselector coil, as shown previously in Fig. 3.6. After the delay period has elapsed, the timer re-sets, drops out the timer relay which disconnects the supply to the uniselector and so moves the uniselector to its next position.

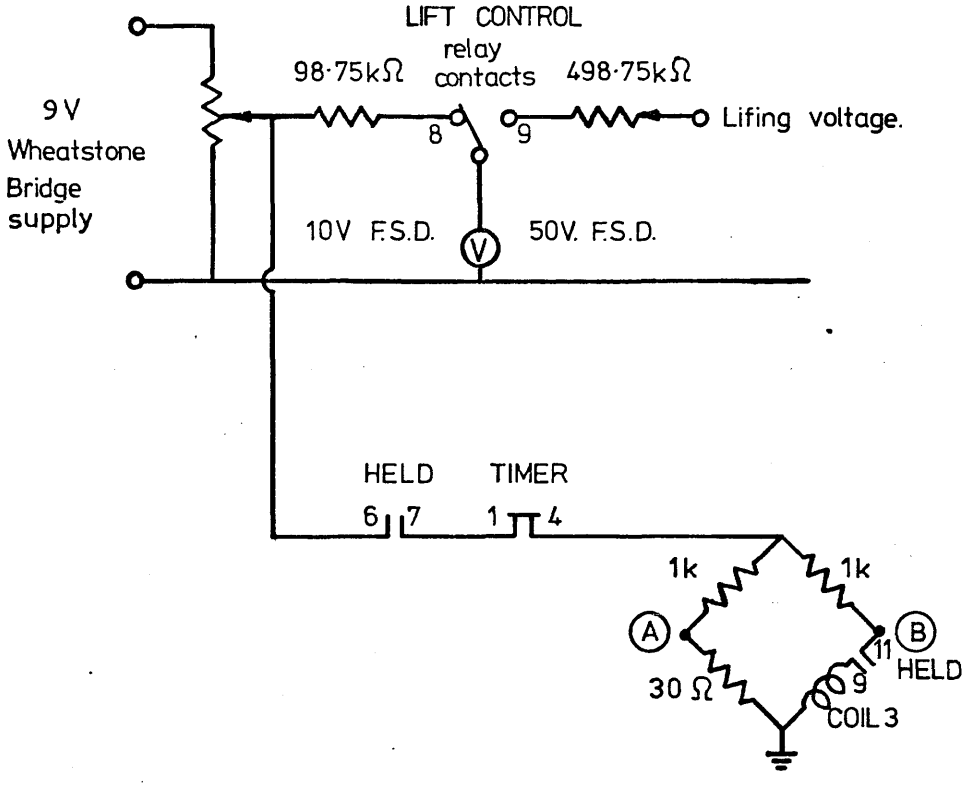

a) Connection of coil 3 into Wheatstone bridge

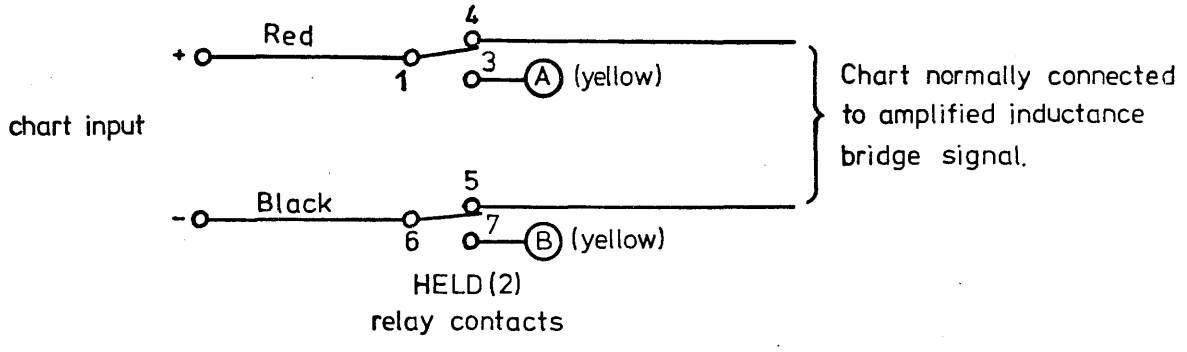

b) Bridge output connection to chart recorder.

Fig 3·12 Wheatstone bridge for monitoring temperature.

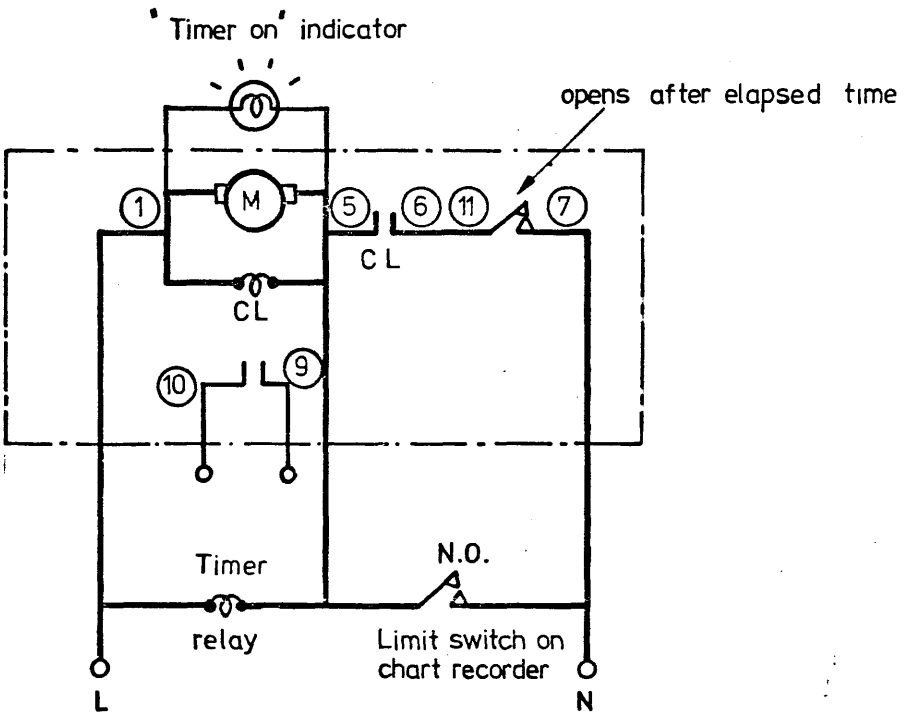

Nos. in circles refer to terminals on the timer.

Fig 3·13 1-60 minute reset timer.

v Ready and release

After the appropriate delay has been imposed the sinker is released by de-magnetizing the holding magnet. This is achieved automatically by making coil j, the coil inside which the holding magnet is placed, an integral part of a resonant R-L-C circuit with a decaying sinusoidal current.

The sequence of operation is in Fig. 3.14. In the 'ready' position the 64 μF capacitor is charged to 300 V. The 560 Ω resistance in series is to prevent too large a charging current. This charging occupies two contact positions on the uniselector to ensure sufficient time to charge the capacitor fully. The uniselector moves on by self-shift mode to the release position. Here the 300 V supply is isolated, and coil 4 completes the R-L-C circuit through the closed contacts of the 'release' relay. A transient current with decay time constant 0.4 seconds and frequency 9 Hz passes through the coil and the magnet is de-magnetized. The heating effect of this current is negligible.

The switching of the uniselector from the 'release' to 'falling' position is by sequential shift mode. Before and during release, the sinker is held by the magnet in coil 3. Coil 3 is connected to the inductance bridge so that the uniselector can only move to the next position after the sinker has departed from coil 3. This means that the cycle can only continue after the successful release of the sinker.

Abort contingency

In the event of failure to release provision is made to shut down the whole control system by an 'abort' relay. Use is made of the 1-2-3 minute lifting current timer.

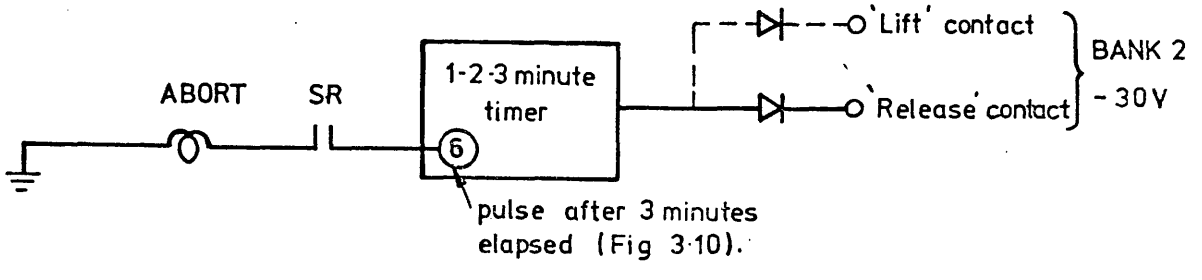

Fig. 3.15 Abort circuit

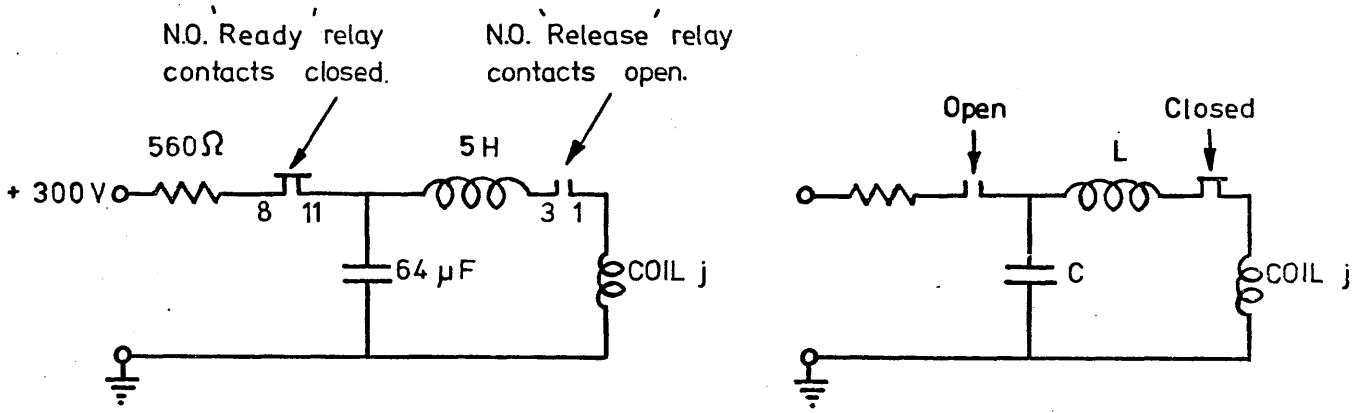

Fig 3·14 Demagnetizing circuit.

In the release position -30 V is applied via a diode to the timer as shown in Fig. 3.15. If the sinker is present in coil 3, ie is held, then the shift relay (SR) contacts will be closed. After four consecutive pulses at minute intervals contacts E are closed (described in section 3.3.2 (ii)), and then the abort relay is closed. This de-energises the contactor controlling all the dc power units and so closes down the viscometer power supplies (Fig. 3.16). Therefore, should the sinker not be released, then the control system switches off rather than allow the uniselector to move on to the falling position where it would remain until manual intervention.

vi Falling

In the falling position, the chart recorder is immediately switched on. The inductance bridge is connected to coil 2. As the sinker descends and passes through each of three coils comprising coil 2 the resulting out-of-balance signals are recorded on the chart and the uniselector is moved on by sequential shift. On departure from the lowest coil of the set, the uniselector moves by self-shift and so returns to the zero position where the cycle is restarted.

3.3.3 Control of number of measurements

At a set temperature and pressure, a pre-set number of measurements can be made. This number is governed by a countdown relay. Fig. 3.16 indicates the position of the relay in the control system. The relay may be set to any number up to 20. Each time the relay is energised, the relay moves by one position so that when zero is reached, contacts on the switch open which switches off the contactor and thus disconnects the mains supply to the dc power units.

The pulse to the countdown relay is applied in the first lifting position just before the lifting current is actually applied to coil 2. This is achieved by the path to the countdown relay being through the following relay contacts:

$$\overline{\text{LIFT CURRENT}} \cdot \text{MINUTE PULSE} \cdot \text{CONTACTOR 2(C2)} \cdot \overline{\text{DELAY TIMER}}$$

(Note: . means AND $\bar{X}$ means NOT X)

CONTROLS FOR

1) CHART MOTOR

2) COUNTDOWN RELAY

3) POWER SUPPLY CONTR.

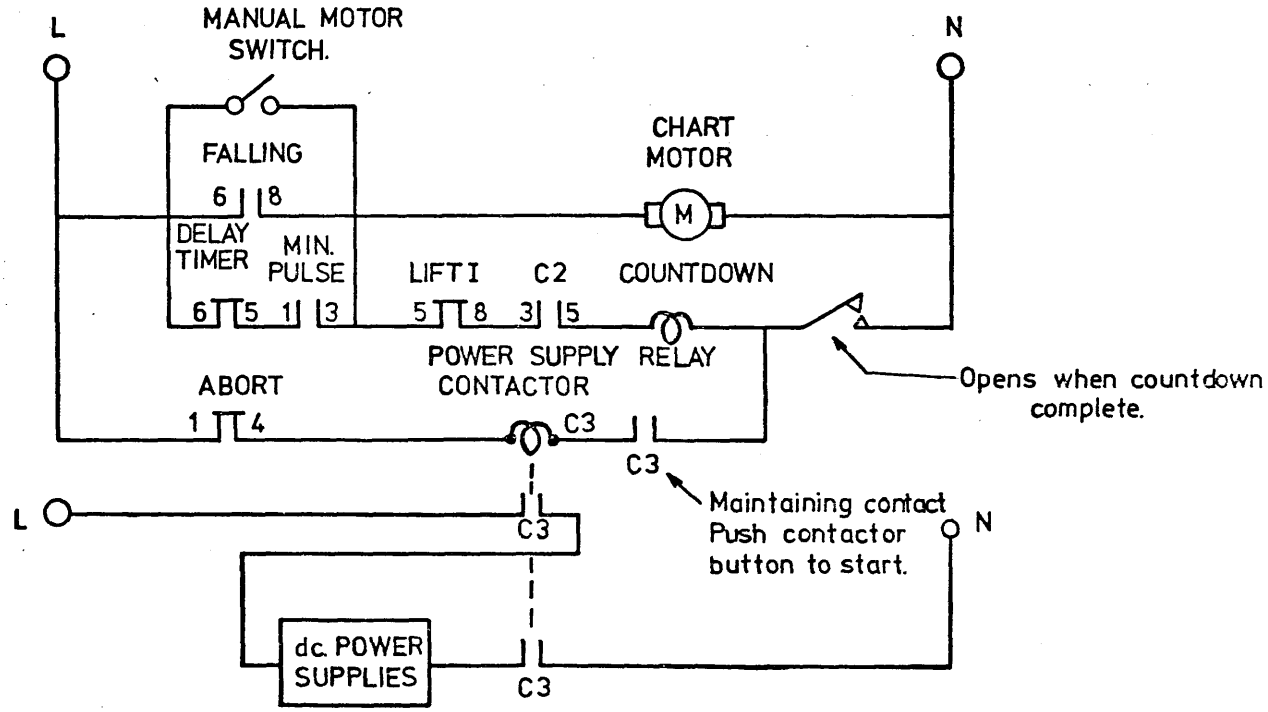

Fig 3.16 Circuits for countdown relay, chart motor, and mains supply.

These conditions ensure that the countdown relay is activated only once in a complete cycle. A connection after the timer and minute pulse relays to the chart recorder motor, steps the chart feed except during the additional cooling period, and of course during fall time measurements when the chart motor runs continuously.

The role of contactor 3(C3) in supplying the dc power units is also seen in Fig. 3.16. It should be noted that a push button on the contactor requires to be depressed to close the maintaining circuit for the contactor to supply mains to the dc power units.

3.3.4 Additional circuitry detail

Certain additional features are incorporated into the instrumentation of the viscometer which are not integral parts of the control itself. Their purpose is to facilitate the operation of the viscometer.

i Independent circuit gain during fall

During fall the Inductance bridge is connected to coil 2, and the amplified out-of-balance signal is recorded continuously on the chart. During this period switching occurs each time that the sinker departs from each of the three successive coils comprising coil 2, as is normally the case in the sequential shift mode. By including a separate gain control in the main control circuit (Fig. 3.6), it is possible to adjust this gain so that switching occurs when the sinker is well clear of the centre line of each coil which corresponds to the maximum on the trace, ensuring that a sufficient trace is obtained before the chart recorder motor is switched off. The two gains are controlled by change-over contacts on the falling relay. The position of switching is shown figuratively below.

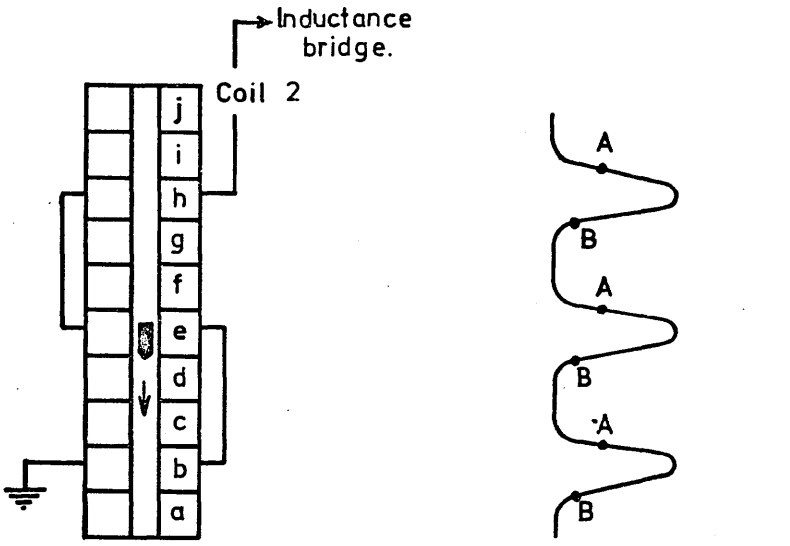

Fig. 3.17 Inductance of coil 2 during fall as displayed on chart recorder

At the points A the shift relay closes, and opens at point B. The level at which the shift relay opens is lower than the closure point because the maintaining current of a relay is less than that required for initial closure.

CHAPTER 4

PRELIMINARY INVESTIGATION, PROCEDURE, AND VISCOMETER CALIBRATION

List of Figures

List of Tables

CHAPTER 4

PRELIMINARY INVESTIGATION, PROCEDURE, AND VISCOMETER CALIBRATION

4.1 Introduction

Before calibrating the viscometer a series of preliminary investigations were required, such as finding the best sinker shape for repeatable measurements, and developing a procedure for cleaning and filling the viscometer. In addition, measurements were made with suspended level viscometers to obtain viscosities for calibration at atmospheric pressure.

4.2 Sinker Shape

In order to find the best sinker shape (ie the shape that gives the most reproducible fall times) measurements were made with variously shaped sinkers falling through air and then water in a 8 mm diameter precision bore glass tube, the timing being performed by stopwatch.

Five soft iron weights, three with flat ends and two with rounded ends, were turned on a lathe and polished until smooth. Table 4.1 shows particulars of their shape and dimensions.

Table 4.1

Dimensions of test sinkers

No	Diameter (in)	Length (in)	Shape	Length/dia
1	0.293	0.293	Flat ends	1.0
2	0.293	0.4742	Flat ends	1.619*
3	0.293	0.586	Flat ends	2.0
4	0.2927	0.587	Parabolic nose	2.0
5	0.2924	0.432	Hemisph. nose	1.48

*Ratio of length to diameter is harmonic,
(length)/(dia) = (length + dia)/(length)

The glass tube was aligned vertically against two plumb lines set at right angles, and fall time measurements were made in air at ambient. Fall times were very short, less than 4 seconds, and the scatter was large for all sinkers. This was mainly due to human error of at least 0.2 seconds at the beginning and end of fall accounting for errors of about ±10 per cent. Nevertheless it was evident at this stage that the shortest sinker fell erratically in contrast to the longer ones which appeared to remain concentric.

A further series of measurements was made with the tube filled with water. Small air bubbles were seen when raising the sinker with a magnet and a delay of about 30 seconds was allowed before each measurement to allow rising bubbles to reach the surface. The results in Table 4.2 show that as might have been expected, the round nosed sinkers give more reproducible results. This is because laminar flow is developed as the liquid enters the annular gap between sinker and tube whereas with the flat-ended sinkers there is a sudden constriction which probably causes turbulence.

Table 4.2

Fall times of five sinkers in water

Sinker No	1	2	3	4	5
Shape	Flat ended short	Flat ended medium	Flat ended long	parabolic	hemisph.
No of readings	10	10	8	10	10
Average time, s	64.5	125.9	109.8	74.3	76.1
Mean deviation, %	5.9	1.2	1.1	0.88	0.79

Since these measurements were made at room temperature, 22.4 to 26.5°C, and that the water was tap water, the repeatability of less than 0.9 per cent for the round nosed sinkers leads one to anticipate good repeatability in future measurements taken under more closely controlled conditions.

It was found that chamfering the trailing edge of the sinkers improved repeatability since this allows a gradual release of fluid from the narrow annulus, so reducing turbulence. With the hemispherically nosed sinker the mean deviation in fall time was reduced from 0.7 to 0.5 per cent.

An important feature of the round nosed sinkers is that the upper surface is flat; this improves stability since the centre of gravity lies below the plane through the middle of the cylindrical surface of the sinker along which maximum shear stress is encountered. This stabilizing influence is absent in those sinkers which are rounded at both ends and are symmetrical. Bridgman (1926) and several subsequent workers have used such sinkers, and in every case guiding pins have been required to improve stability.

In conclusion, the preliminary experiment shows that a tapered trailing edge improves stability, and a round nosed sinker is predictably superior to a flat ended one. The hemispherically nosed sinker gives marginally better repeatability than the parabolic one.

4.3 Measurement Procedure

The viscometer is designed so that it can be thoroughly cleaned. The viscometer tube, sinker, bellows, retaining bar, and top seal with holding magnet can each be cleaned separately. Most of the liquids tested were cleaned with diethyl ether, the exception being the polydimethyl siloxanes for which petroleum ether was first used as a solvent. The viscometer tube is cleaned repeatedly and finally dried and polished with cotton wool. Any dust particles are easily seen and these are removed with a warm-air blower. The bellows require particular care so that all traces are removed from the convolutions. By using an ultrasonic bath this process is accelerated. A useful test of cleanliness is to put a large drop of the solvent from the bellows on to a filter paper and dry it rapidly. If a ring is visible then the solvent contains traces of test liquid, and further rinsing is required. New O-ring seals are fitted on each filling.

The bellows are filled before joining to the viscometer, care being taken to avoid air pockets being trapped. This is effected by gently squeezing the bellows to expel any air, and for thicker liquids warming the bellows

causes air bubbles to expand and rise to the surface. For the very viscous liquids a vacuum filling method was used, combined with heat to make the liquid thinner. After attaching the viscometer tube, it is filled from the top, and the upper seal screwed into place; any surplus liquid escapes through a bleed hole. The volume of liquid to fill the viscometer is about 20 cm^3, although this can, if necessary, be reduced by placing a solid space filler in the bellows. The space filler must be short enough to allow the bellows to contract as the liquid is compressed.

The viscometer is lowered into the pressure vessel which is primed with pressure transmitting fluid, the electrical connections are made, and the vessel sealed as described in chapter 7. The vertical alignment of the pressure vessel is checked by a graduated spirit level placed on the horizontal surface of the vessel, perpendicular to the bore of the vessel. Alignment to less than 0.1^{o} from the vertical is thus achieved, and by doing so errors due to eccentric fall are made negligible. This aspect is described in detail in chapter 5.

4.3.1 Measurement of trace

During the fall of the sinker the inductance bridge is connected to the second set of coils, and the out-of-balance signal caused by the passage of the sinker through each of the three component coils is displayed on a chart recorder as already shown in Fig. 3.17. The three peaks are broad and similar in shape. A horizontal line is drawn intersecting the rise and fall of the recorded trace. The mid point of this line accurately defines the position of the peak of the out-of-balance signal. The position determined in this way does not vary with the level of the horizontal line except near the no-signal level and near the peak. In this way the distances between peaks can be determined to within ±0.02 inch, which constitutes an error of not greater than 0.2 per cent. The chart feed speed can be varied in fixed steps from 16 in h^{-1} to 960 in h^{-1} and pulses at one minute intervals are recorded on the chart so that the chart speed can be accurately determined.

In measuring fall time in two halves for each descent of the sinker their comparison is used to confirm that the speed of fall is uniform. Unequal fall times show that the sinker is falling erratically, or that there may

be contamination of the test liquid by pressurising fluid. In practice the fall times are not exactly equal because the detector coils are not dimensionally identical which produces not 1 for the ratio of second trace to the first but 0.989 which is the experimentally found average ratio from a large number of fall time measurements.

4.4 Viscosity of Calibration Liquids at Atmospheric Pressure

Accurate viscosity values are required for a range of liquids with widely varying viscosities for the calibration of the falling body viscometer at atmospheric pressure. Since liquid viscosity can be measured accurately, to within ±0.5 per cent, at atmospheric pressure, it is common practice to calibrate with a range of different liquids, rather than to calibrate with one liquid at different pressures for which the viscosity cannot, as yet, be measured with such high accuracy.

The primary calibration liquids are the polydimethyl siloxanes (MS 200 series) which cover a wide range of viscosity from 10 cSt to 100 000 cSt. They have the advantage that they are not hydroscopic and are stable, with the additional feature of changing viscosity much less with temperature than most other organic liquids, which means that errors due to temperature variations are less. All liquids whose viscosities were measured under pressure were also measured at atmospheric pressure by a suspended-level viscometer. These measurements are useful for checking against literature values where these exist, and can be used to check the calibration of the falling body viscometer.

These measurements were all made with suspended-level kinematic viscometers according to BS 188. Measurements were made at $30^{o}C \pm 0.1^{o}C$. To convert kinematic to dynamic viscosity, the density of the liquid is required; densities were also measured and the density results are reported at the beginning of chapter 9, and are also reported along with viscosity data in Table 4.3 for convenience.

Table 4.3

Viscosity of calibration liquids at 30°C

Liquid	Time (s)	ν (cSt)	ρ (g cm^{-3})	η(cP) Measured	η(cP) Literature
Polydimethyl siloxanes (MS 200 series)					
10 cSt at 25°C	309.1	9.51	0.9347	8.89	8.832[a]
20 cSt at 25°C	594.8	18.3	0.9449	17.3	17.43[a]
100 cSt at 25°C	291.2	93.84	0.9586	89.96	89.90[a] 88.0[g]
350 cSt at 25°C	307.5	328.5	0.964	317	315[a]
1000 cSt at 25°C	874	934.0	0.965	901.3	896[a] 880[g]
1437 cSt at 30°C (5.9:1 mixture of 1000 & 12500)	43.8	1437	0.9626	1383	-
12 500 cSt at 25°C	345.6	11339	0.968	10980	10850[a]
30 000 cSt at 25°C (Hopkin & Williams)	823	27003	0.9637	26100	28700[a]
100 000 cSt at 25°C	794	92740	0.966	89600	94400[a]
Mineral oils					
LVI (1964)	470.7	490.5	0.9301	457	452[b]
MVI(N) 170 TN 596/66	222.1	237.4	0.8929	212	216[a] 205[c]
HVI 330 (1964)	384.5	411.0	0.878	361	365[a]
LVI 260 TN 595/66	537.3	574.4	0.9407	540	-
Miscellaneous liquids					
di-(2-eh)phthalate	137.9	44.45	0.9760	43.48	42.0[d] 43.5[e]
di-n-butyl phthalate	415.2	12.77	1.0371	13.24	13.43[d]
castor oil (0311 First)	169.9	514.9	0.9527	490.5	-
castor oil (Castrol 111)	624.0	667.1	0.9048	604	-
OS-138	194.8	6598	1.2049	7951	-
tri-m-tolyl phosphate	-	-	1.1675[f]	-	42.0[f]

a Harrison (1964)

b Barlow (1959), measurement on a different sample

c Hutton (private communication)

d Barlow, Lamb, and Matheson (1966)

e Galvin, Naylor, and Wilson (1963)

f Erginsav (1969)

g Boelhouwer and Toneman (1957)

4.5 Calibration of Solid Sinker (sinker 1)

This sinker was designed to cover the lower range of viscosity from 10 cP to 1000 cP and the calibration was made with five liquids within this range, with corresponding fall times of between 90 seconds and 155 minutes. As described in chapter 3, this sinker has a hemispherical nose, a flat upper surface, with an overall length of 1.00 cm, and a diameter of 0.6076 cm.

Calibration measurements were made at atmospheric pressure, at 30.0 ±0.1°C with the viscometer in the 3 kbar pressure vessel. The results of calibration measurements are in Table 4.4 for 10 cSt, 20 cSt, and 100 cSt polydimethyl siloxanes, MVI(N)-mineral oil, and 1000 cSt polydimethyl siloxane. Between 3 and 8 measurements were made for each liquid. The repeatability of fall times is good, as indicated by the standard deviations shown in the last column of the table. The worst deviation from mean fall time is 0.6 per cent which occurs for the 20 cSt liquid, but nevertheless the fall time is 179.35 with a standard deviation of 0.7 seconds (0.39 per cent) which in statistical terms means that 68.3 per cent of the measurements on this liquid are within 0.7 seconds of the mean. In the case of the longest fall time (2.5 h) for the 1000 cSt silicone, the standard deviation is 1.4 per cent. This is probably because of less steady fall due to the extremely slow rate of descent which reduces the self-centering dynamic forces that normally act on the sinker.

It has been shown that the equation of the falling sinker may be reduced to the expression

$$\frac{\eta}{(\rho_1 - \rho_2)} = KT, \qquad (2.43)$$

where T is the fall time, and K is a function of the viscometer dimensions which are constant at atmospheric pressure. When T is plotted as a function of $\eta/(\rho_1 - \rho_2)$ a straight line with gradient 1/K, passing through the origin should be found if the sinker obeys the laws of motion used to derive the equation.

This calibration covers two orders of magnitude in viscosity and fall time, and it is more convenient to illustrate such a calibration curve on

Table 4.4

Fall times for sinker 1 calibration

Liquid	Chart speed (in h^{-1})	Length of chart trace (in)			Ratio	Mean fall time (sec)	Std. dev. (sec)	Max. dev. from mean (%)
		1st half	2nd half	total	2nd : 1st			
10 cSt siloxane	240	3.07	3.01	6.08	0.980	90.72	0.35	0.53
		3.04	3.01	6.05	0.990			
		3.05	2.98	6.03	0.977			
		3.03	3.00	6.03	0.990			
	average	3.04_8	3.00_0	6.04_8	0.984 ± 0.003			
	std dev.	0.01_7	0.01_4	0.02_4				
20 cSt siloxane	64	1.61	1.60	3.21	0.994	179.3	0.7	0.63
		1.60	1.59	3.19	0.994			
		1.60	1.58	3.18	0.988			
		1.59	1.60	3.19	1.006			
		1.60	1.59	3.19	0.994			
		1.58	1.59	3.17	1.006			
		1.61	1.58	3.19	0.981			
		1.60	1.58	3.18	0.988			
	average	1.59_9	1.58_9	3.18_8	0.994 ± 0.006			
	std dev.	0.01	0.00_8	0.01_2				
100 cSt siloxane	16	2.07_5	2.04	4.11_5	0.983	927.5	2.5	0.39
		2.09	2.04_5	4.13_5	0.978			
		2.07_5	2.04	4.11_5	0.983			
		2.05_5	2.05_5	4.11	1.000			
	average	2.07_4	2.04_5	4.11_9	0.986 ± 0.005			
	std dev.	0.01_4	0.00_7	0.01_1				
MVI(N)	16	4.87	4.81	9.68	0.989	2184	8.5	0.56
		4.86	4.84	9.70	0.996			
		4.90	4.86	9.76	0.992			
		4.85_5	4.80_5	9.66	0.990			
		4.88	4.84	9.72	0.992			
	average	4.87_3	4.83_2	9.70_5	0.992 ± 0.001			
	std dev.	0.01_8	0.02_2	0.03_8				
1000 cSt siloxane	16	20.15	19.95	40.10	0.990	9277	130	2.3
		21.28	20.90	42.18	0.982			
		20.91	20.51	41.42	0.981			
	average	20.78	20.45	41.23	0.984 ± 0.0005			
	std dev.	0.58	0.48	1.05				

logarithmic scales. By taking logs of both sides of equation 2.43 and treating T as the dependent variable we arrive at the expression

$$\log T = \log \frac{\eta}{(\rho_1 - \rho_2)} - \log K. \qquad (4.1)$$

Thus when the variables are both plotted on logarithmic scales, a straight line should be found with a gradient of unity, which intercepts the ordinate axis at (1/K). The five calibration points for sinker 1 are plotted in Fig. 4.1.

The viscometer constant K was found by a least-squares fit on equation 4.1. In the first instance an extra degree of freedom was allowed in that the gradient was not fixed at unity. The optimum is as follows

$$\log T = 1.000\ 57 \log \frac{\eta}{(\rho_1 - \rho_2)} + 1.8499. \qquad (4.2)$$

This indicates that the gradient is very close to the predicted value of unity.

The data were then refitted with the gradient fixed at unity to give

$$\log T = \log \frac{\eta}{(\rho_1 - \rho_2)} + 1.8505. \qquad (4.3)$$

1.8505 = -log K = log 1/K, and therefore K = 0.014 11.

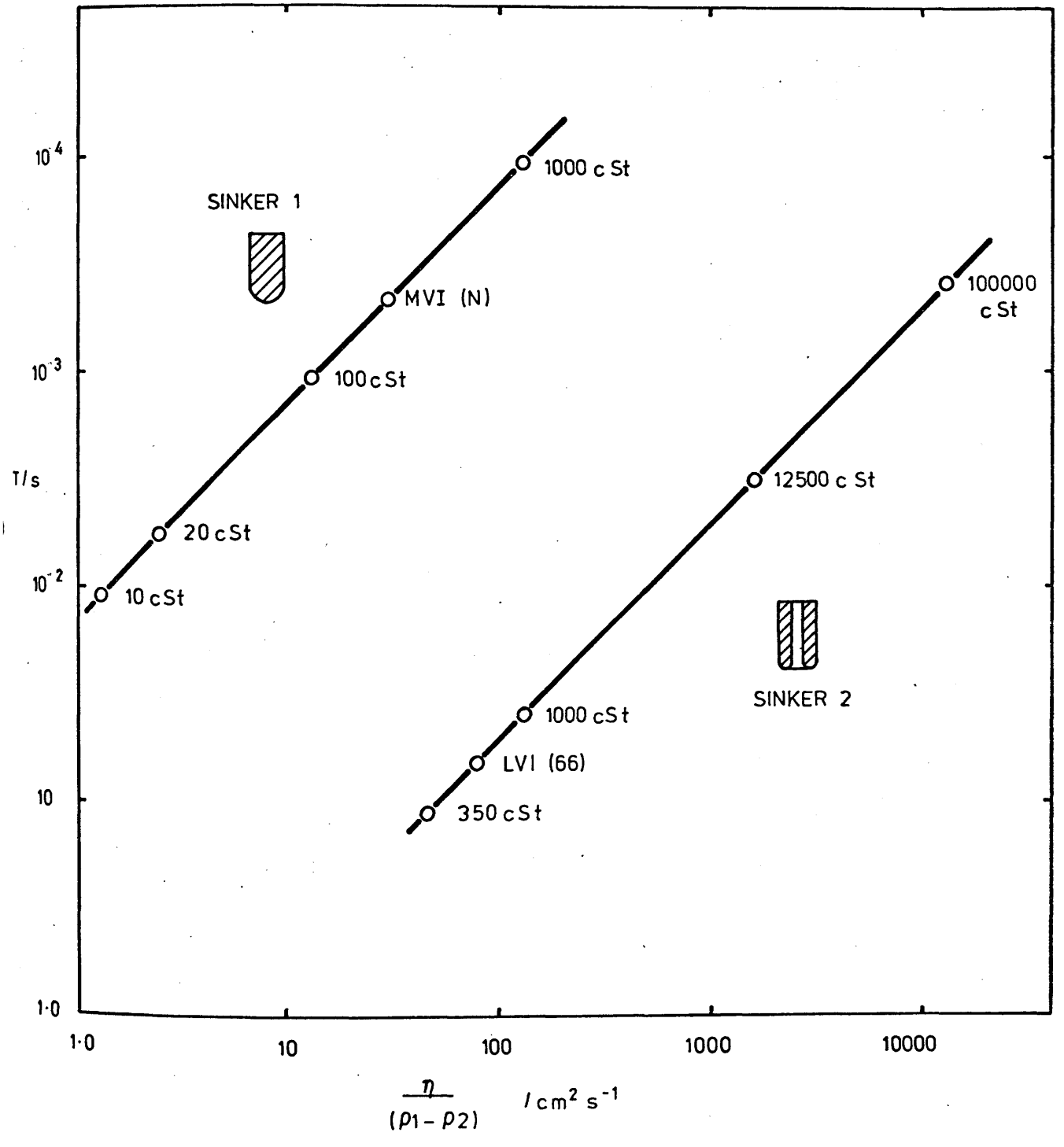

FIG 4.1 Calibration of sinkers 1 and 2

Table 4.5

Values used for calibration of sinker 1

Liquid	η (cP)	ρ_2 (g cm^{-3})	$\eta/(\rho_1 - \rho_2)$	Fall time T (sec)	η_{recalc} (cP)	*diff %
10 cSt siloxane	8.89	0.9347	1.2906	90.72	8.82	-0.82
20 cSt siloxane	17.3	0.9449	2.5152	179.3	17.4	+0.58
100 cSt siloxane	89.96	0.9586	13.1053	927.5	89.83	-0.15
MVI(N)	212.0	0.8929	30.5912	2184.0	213.6	+0.74
1000 cSt siloxane	901.0	0.965	131.3794	9277.0	897.8	-0.35

sinker density, $\rho_1 = 7.823$ g cm^{-3} *diff % = $(\eta_{calc} - \eta) \times 100/\eta$

The errors in recalculated viscosity show no systematic trend, and the value of K is to within ±1 per cent.

The errors of measurement for viscosity and fall time are proportional to their magnitudes. In performing a regression analysis on equation 4.1 where the log of η and T is used, these proportional errors are taken into account.

The linearity of the calibration is seen to be excellent over a range of two decades of viscosity for sinker 1. The repeatability of measurement is within ±0.5 per cent except in the case of excessively long fall times of greater than about 2 hours.

4.6 Calibration of Sinker with Central Hole (sinker 2)

This sinker was designed to extend the range of measurement to 300 000 cP (3000 P), providing at the same time an overlap with the range of sinker 1.

Preliminary measurements were made to check the linearity of this new design of sinker. Liquids from 350 to 100 000 cP were used for this purpose. The latter is the maximum viscosity of liquid with which it is practicable to fill the viscometer.

Table 4.6

Fall times for sinker 2 preliminary calibration

Liquid	Chart speed (in h^{-1})	Trace length (2nd half) (in)	Mean fall time (sec)	Std. dev. (sec)	Max. dev. from mean (%)
350 cSt siloxane	960	2.37 2.39 2.37 2.35 2.37 2.36_5 2.36 2.36 2.36 2.36 2.35_5	8.86_5	0.04	0.29
LVI(66)	480	2.02 2.02 2.03 2.03 2.03_5 2.01_5 2.02	15.18	0.06	0.49
1000 cSt siloxane	480	3.42 3.42 3.42 3.41 3.41 3.42	25.63	0.04	0.20
12 500 cSt siloxane	64	5.49 5.51 5.50 5.48	309.1	0.7	0.27
100 000 cSt siloxane	16	11.32 11.48 11.58 11.54	2583.0	26.0	1.04

It was found that fall time measurements had an unexpectedly high scatter, due mostly to erratic fall during the first half of the descent. The second half of the traces were quite repeatable, and these were taken to test for calibration linearity. The erratic fall over the first half of the sinker's descent is discussed later in this section.

The fall time measurements for 350 cSt silicone, LVI(66), 1000 cSt siloxane, 12 500 cSt siloxane, and 100 000 cSt siloxane are given in Table 4.6. Between 4 and 11 measurements were made for each liquid. Repeatability is good as shown by the standard deviations in the table. The maximum deviation from the mean is 0.49 per cent, except for the most viscous liquid where the maximum deviation is 1.04 per cent.

The values for the preliminary calibration are in the following table

Table 4.7

Preliminary calibration of sinker 2

Liquid	η (cP)	ρ_2 (g cm^{-3})	$\eta/(\rho_1 - \rho_2)$	Fall time T (sec)	η_{recalc} (cP)	*diff %
350 cSt siloxane	317	0.964	46.33825	8.86_5	313	-1.23
LVI(66)	540	0.9407	78.66789	15.18	538	-0.37
1000 cSt siloxane	901	0.965	131.7252	25.63	905	+0.46
12 500 cSt siloxane	10 980	0.968	1605.968	309.1	10 911	-0.63
100 000 cSt siloxane	89 600	0.966	13101.33	2583.0	91 206	+1.79

sinker density, $\rho_1 = 7.805$ g cm^{-3} *diff % = $(\eta_{recalc} - \eta) \times 100/\eta$

The optimum straight line fit to the calibration data is given by

$$\log T = \log \frac{\eta}{(\rho_1 - \rho_2)} - 0.712\ 92. \qquad (4.4)$$

Hence the viscometer calibration constant is 5.1631. The recalculated viscosities (not log viscosity) which are for the approximate range of 300 cP to 90 000 cP are remarkably good in that the average difference from the calibration values ~~to~~ is 0.9 per cent with a maximum error of

1.79 per cent. The linearity of this sinker calibration is thus confirmed, and is illustrated in Fig. 4.1.

The following steps were taken to improve the reproducibility of the fall time of the sinker with the central hole during its descent in the first half of its passage.

1 The vertical alignment of the tube was checked
2 The viscometer tube was re-polished
3 The sinker was re-polished
4 Fresh test liquid was used.

These steps did not alter the irregular first half fall times.

Further experiments were made as follows:

5 Fresh liquid of higher viscosity was used.

This was to establish if a change of viscosity would show an improvement or deterioration of fall time repeatability. It was thought that the self-centering of the sinker might be affected one way or the other by a slower descent. No systematic trend was detectable.

6 The central hole of the sinker was re-bored and polished to give a smoother finish.

No improvement in performance was observed.

7 The viscometer tube was replaced.

Again no change in performance resulted. The conclusion drawn is that due to the unusual shape of this sinker, that is its axial hole, it does not become stable until after it has passed through the first of the three detector coils. During the second half of its descent, however, repeatability is satisfactory which means that reliable results can be obtained. It was decided that since repeatable results can be obtained from the second half alone and these produce a good linear calibration for a 300 fold range in viscosity, that no more time should be spent in investigating this anomalous behaviour.

The sinker dimensions were altered, and a new viscometer tube fitted during the foregoing investigation which means that the calibration was then invalid. A second calibration was therefore necessary. The table

of results for this is given below.

Table 4.8

Second calibration of sinker 2

Liquid	η (cP)	ρ_2 (g cm^{-3})	$\eta/(\rho_1 - \rho_2)$	Fall time T (sec)	η_{recalc} (cP)	*diff %
Castor oil	490.5	0.9527	71.5818	11.31	489.2	-0.27
1000 cSt siloxane	901.3	0.965	131.769	20.95	904.5	+0.35
OS 138	7951.0	1.2049	1204.68	190.7	7944.0	-0.08

sinker density, $\rho_1 = 7.805$ g cm^{-3} *diff % = $(\eta_{recalc} - \eta) \times 100/\eta$

The optimum straight line fit to the calibration data is

$$\log T = \log \frac{\eta}{(\rho_1 - \rho_2)} - 0.800\ 16 \qquad (4.5)$$

from which the viscometer constant is K = 6.3119. The linearity of this calibration is very good and the imposed gradient of unity is quite satisfactory. Linearity has been confirmed by the preliminary calibration of sinker 2, and because of the difficulty of filling the viscometer with very viscous liquids (> 10 000 cP), and because the three point calibration above (up to about 8000 cP) is so linear, it was considered unnecessary to calibrate further.

4.7 Comparison of Theoretical and Experimental Calibration

In chapter 2 the general equation of motion for a sinker with a central hole was derived, equation 2.18. This may be expressed as

$$\frac{\eta}{(\rho_1 - \rho_2)} = KT, \qquad (2.43)$$

where

$$K = \frac{(a^2 - c^2)g[(b^4 - a^4 + c^4)\ln b/a - (b^2 - a^2)^2]}{2L(b^4 - a^4 + c^4)}. \qquad (4.6)$$

The equation for the solid sinker is obtained by reducing radius c to zero.

The calculated values of K are compared with the experimentally derived value in the table below.

Table 4.9

Calibration constants - calculated and experimental

Sinker	a/cm (sinker rad.)	b/cm (tube rad.)	c/cm (hole rad.)	K_{calc} ($cm^2\ s^{-2}$)	K_{exp}* ($cm^2\ s^{-2}$)
No 1	0.303 76	0.315 25	-	0.000 1281	0.000 1411
No 2	0.295 52	0.315 25	0.123 40	0.035 93	0.031 56

L = 6.024 cm *K_{exp} is the experimental constant divided by 100, because cP and not P units are used for calibration.

For sinker 1 the experimental K value is 9.2 per cent above the theoretical value. In the case of sinker 2 the experimental K value is 13.8 per cent below the theoretical value.

The difference between experiment and theory is not surprising because the analysis is for a cylinder with flat ends, and no account is taken of entry and exit effects. The mass of the sinker and its length do not appear in the derived equation because the sinker mass is expressed as $\pi a^2 \rho_1 l$ where l is the length of the cylinder along which laminar flow is fully developed, and the length drops out of the expression since it appears in both the numerator and demonimator. To take account of the sinker having a round nose would cause the numerator of equation 4.6 above to be greater, which means that the theoretical and experimental values of K would be in closer agreement. In the case of the solid sinker, therefore, the difference between the experimental and the theoretical calibration constant is accounted for qualitatively by the round profile of the sinker nose.

On the other hand there is the effect of the liquid being constricted as it is forced into the narrow annulus. This has the effect of slowing down the rate of sinker descent because of loss of energy. The constriction produces a smaller K value than that calculated but the effect is small. This has been proved by Chen and Swift (1972) who calculated the magnitude

of this effect, and then confirmed it by experiment. They showed that for a sinker to tube ratio of 0.921 the entry effect causes a reduction of 0.8 per cent in terminal velocity. The reduction in terminal velocity for sinker 1 where $\kappa = 0.963$ will be less than 0.8 per cent because with a narrower annulus the shear forces are larger. The experiments also revealed that a sinker with a length of greater than six times its diameter has a fall time which agrees with the theoretical value to better than 0.5 per cent.

The sinker with the central hole (No 2) has a K value below the theoretical value, which means that this sinker is falling more slowly than expected. The reason for this is not apparent.

4.8 Discussion

The two sinkers were calibrated. Sinker 1 shows good linearity from 10 cP to 1000 cP, and the calibration constant, K, is accurate to within ±1 per cent. No systematic errors are found when recalculated viscosities are compared with the reference values. The linearity of the calibration of sinker 2 was also demonstrated from 350 to 100 000 cP, and a second calibration for this sinker also shows that K is accurate to within ±1 per cent. The calibration of both sinkers show straight lines which, on a log-log plot of T, as a function of $\eta/(\rho_1 - \rho_2)$ have a gradient of one which accords with theory. It is evident therefore that a single point calibration for an unguided sinker is quite satisfactory provided that the sinker is used within the limits of its capabilities; above the point where turbulence is encountered (defined by Reynolds number in chapter 2), and below the point where excessively long fall times are encountered (greater than about 2 hours).

Some difficulty was encountered with sinker 2 in erratic first-half fall times. It was found that satisfactory results could be obtained by using only the second-half of the fall time trace with little loss of precision. This course was adopted. A useful line of investigation would be to analyse the forces acting on this type of sinker (ie with a central, axial hole) and to study the factors which govern stability. This could be supported by experiment to establish the best profile.

CHAPTER 5

THE EFFECT OF ECCENTRICITY ON THE TERMINAL VELOCITY OF A SINKER

List of Figures

List of Tables

CHAPTER 5

THE EFFECT OF ECCENTRICITY ON THE TERMINAL VELOCITY OF A SINKER

The effect of eccentricity upon terminal velocity has been appreciated from the time of Bridgman's first measurements of viscosity by the falling sinker technique. To reduce error from an eccentrically falling sinker the majority of investigators using this technique which includes Bridgman (1926), ASME Report (1953), Heiks et al. (1960), Cappi (1964), Huang (1966), Galvin et al. (1968), have used guiding pins to maintain the sinker concentric with the viscometer tube. Apart from the technical difficulties in machining the guiding pins to fine tolerances there are unknown effects due to viscous drag on the pins. For these and other reasons stated earlier, unguided sinkers are used in the present work.

Preliminary tests were made to establish the precision with which the viscometer tube must be aligned vertically in order that the unguided sinker should fall concentrically. These tests showed that the sinker becomes more and more eccentric as the tube is tilted from the vertical position showing a corresponding decrease in fall time. That is, as the sinker becomes more eccentric, the terminal velocity increases. In this chapter the results of experiments upon three liquids at varying conditions of eccentricity are presented. A vigorous analysis of behaviour under eccentric conditions produces an original solution to this problem, and by comparing experimental and theoretical results a correlation between eccentricity and angle of viscometer tube inclination is established.

5.1 The Measurement of Fall Time Variation with Tube Angle

A length of precision bore Pyrex glass tubing of inside diameter 8.0 ± 0.01 mm was aligned vertically in a temperature bath by means of two plumb lines set at right angles with respect to the tube. The parabolically nosed soft iron sinker (No 4) of outside diameter 7.422 mm was used for three sets of measurements on a series of Midland Silicones polydimethyl siloxane fluids. The silicones were of nominal viscosities 10, 20 and

100 cSt at 25°C.

Measurements were made after the tube containing the liquid had been immersed in the temperature bath for more than 30 minutes to ensure thermal equilibrium. The bath was maintained at 30 ± 0.05°C by a single element heater controlled by a mercury contact thermometer via a thermal relay. Fall time was the interval that the sinker took to pass between two marks on the glass tube (12.36 cm apart) as seen through a glass panel in the tank, and was measured with an electronic timer triggered by hand. A permanent magnet was lowered by means of a length of fine wire down the inside of the tube to retrieve the sinker after each measurement. The sinker was raised above the upper mark but not far enough to break the surface of the test liquid, and to commence another fall time measurement a sharp jerk was sufficient to detach the sinker from the magnet.

Four measurements were made for each angle of inclination starting at the vertical position, and the average value taken. For the first two degrees of tilt on either side of the vertical position measurements were made at 0.5 degree intervals increasing to 1 and the 2 degree intervals up to 36 degrees from the vertical. Normalised fall times (fall time divided by the vertical fall time) are plotted for the three liquids in Fig. 5.1.

It was not possible to tilt the tube more than 36 degrees from the vertical in the tank, and in order to observe behaviour for angles greater than this, measurements were made on one liquid (10 cSt siloxane) on a bench top at room temperature. Tube angle was increased until at approximately 70 degrees the sinker was seen to falter during its fall resulting in erratic fall times, and at greater angles it ceased to fall at all. The behaviour of fall time as a function of tube angle is shown in Fig. 5.2.

From the measurements on the three silicones it is apparent that the behaviour of the sinker is not dependent upon the viscosity of the fluid but depends rather upon the inclination of the tube to the vertical. The normalised fall time is reduced by more than 50 per cent at a tube angle of 15 degrees which is quite a surprising amount, that is, the sinker velocity more than doubles its vertical velocity. At angles less than 70 degrees the sinker descended quite steadily, and as far as could be ascertained visually it was falling parallel to the tube.

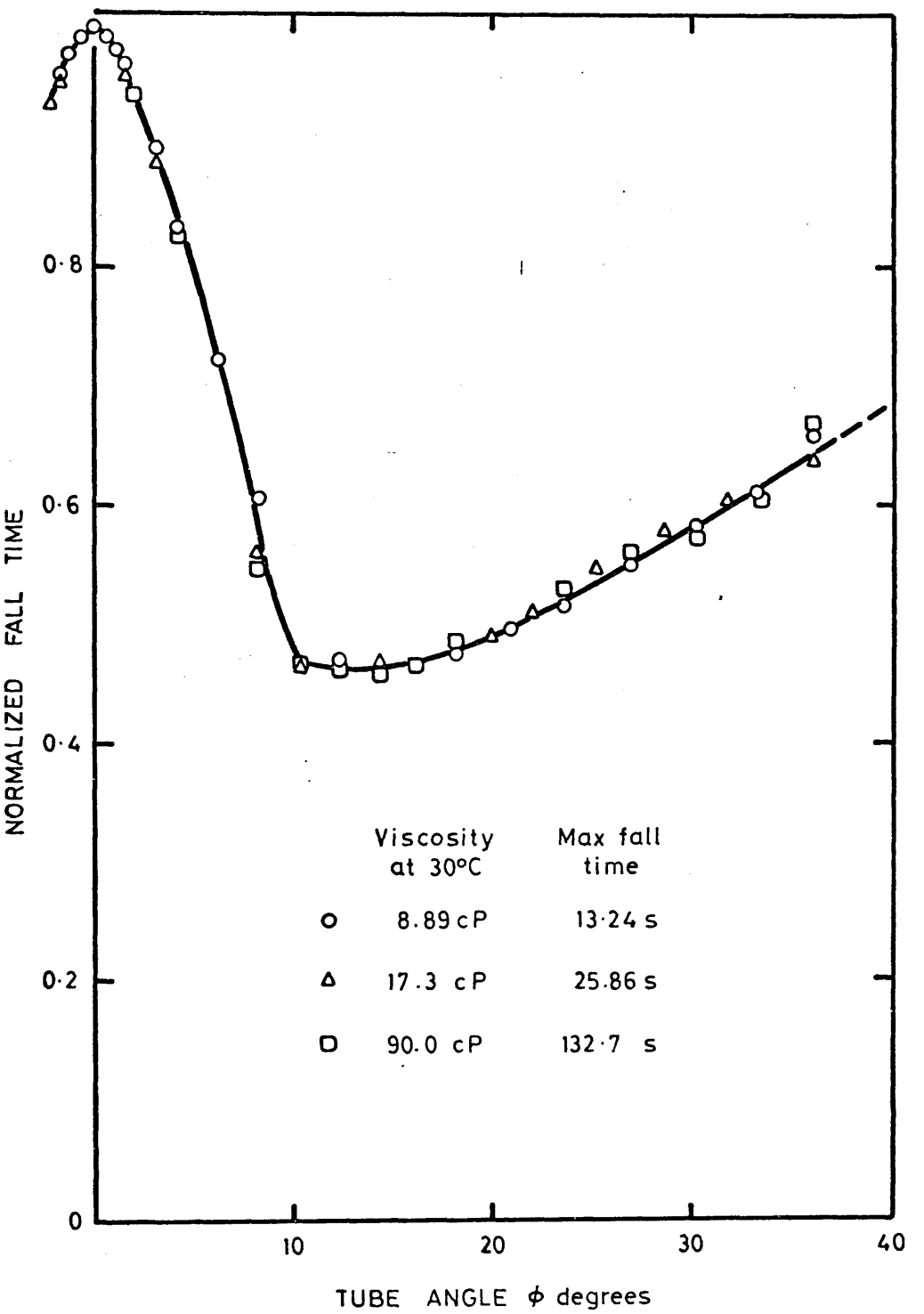

FIG 5.1 Variation of fall time with tube angle (to 36°)

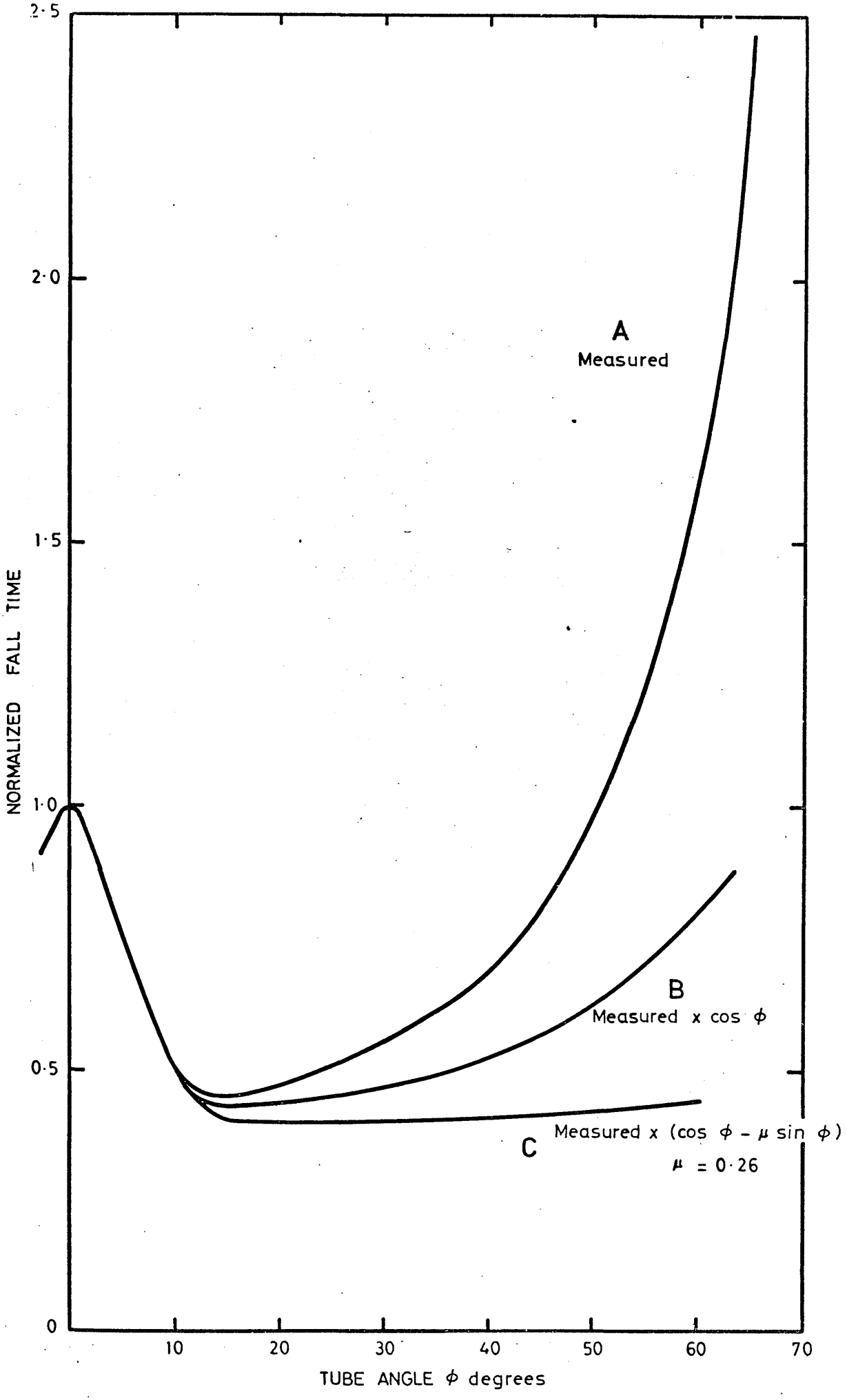

FIG 5.2 Variation of fall time with tube angle

5.2 Analysis of an Eccentrically Falling Sinker

The analysis follows the method used to establish the equation for the concentrically falling sinker. Starting with the Naiver-Stokes equation the shear rate of the liquid in the annulus is found by integration, and the velocity by a second integration. From the latter the flowrate through the annulus is calculated and by imposing appropriate boundary conditions a unique expression relating fall time, or velocity, to viscosity and physical dimensions is found. The main difference between the concentric and eccentric cases lies in the fact that the shear stress on the surface of the sinker is not constant but varies with angular position leading to more complex expressions.

The fluid in the tube is Newtonian and the sinker is falling vertically but eccentrically, parallel to the centre line of the tube. It is further assumed that perfect Poiseuille flow (ie steady and laminar) is developed along the entire length of the sinker in the annular region and that the effects of the liquid entering and leaving the annulus at either end are negligible. The sinker has a terminal velocity of -V.

i Cylindrical coordinates

The datum is taken as the centre of the sinker as shown in Fig. 5.3. Let the sinker have radius a, and the tube have inner radius b. The eccentricity is defined as the distance between the centres of tube and sinker and has the symbol ε. R is dependent upon angular position and is the distance between the centre of the sinker and the tube at angle θ.

$$R = \sqrt{b^2 - \varepsilon^2 \sin^2 \theta} - \varepsilon \cos \theta$$

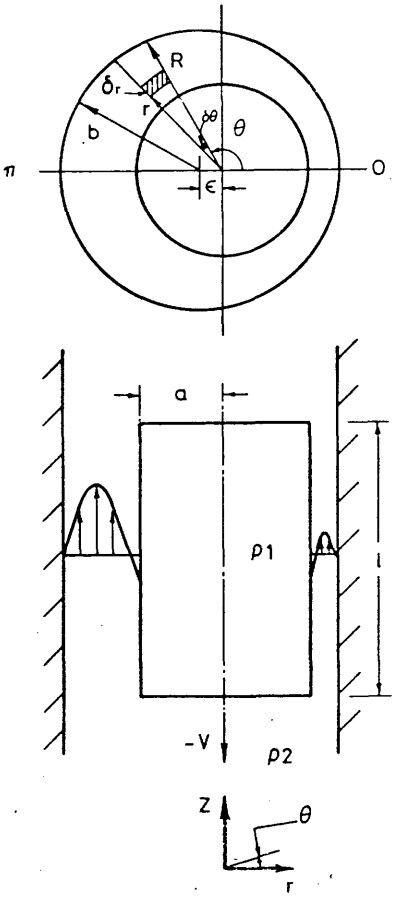

Fig. 5.3 The eccentric sinker with cylindrical coordinates

ii Forces acting on a fluid element

Consider the forces acting upon an element of fluid at radius r, angle θ, as shown in Fig. 5.3.

$$(\tau + \delta\tau)(r + \delta r)\ell\delta\theta - \tau r\ell\delta\theta + \frac{\partial p}{\partial z}\ell r\delta\theta\delta r - \rho_2 g\ell r\delta\theta\delta r = 0.$$

The first two terms are the shear forces, the third term is the upward force due to the pressure gradient, and the fourth term is the gravitational force on the element. The length of the element ℓ, equals the length of the sinker, and the fluid density is ρ_2. Neglecting the term $\ell\delta\tau\delta r\delta\theta$, the above equation becomes

$$\tau\delta r\ell\delta\theta + r\delta\tau\ell\delta\theta + \frac{\partial p}{\partial z}r\delta r\ell\delta\theta - \rho_2 g r\delta r\ell\delta\theta = 0.$$

By definition, $\tau = \eta\frac{\partial w}{\partial r}$.

Thus the forces acting upon the fluid element per unit mass are:

$$\eta\left[\frac{1}{r}\frac{\partial w}{\partial r} + \frac{\partial^2 w}{\partial r^2}\right] = -\frac{dp}{dz} + \rho_2 g. \qquad (5.1)$$

This is a simplified form of the Navier-Stokes equation in the z-direction where $w = dz/dt$, the fluid velocity, is a function of r and θ. The pressure gradient dp/dz is the pressure gradient caused by the falling sinker and includes the pressure due to the difference in levels of the liquid.

iii Shear rate

Integration of equation 5.1 yields

$$\frac{\partial w}{\partial r} = -\frac{Ar}{2\eta} + \frac{C}{r}, \qquad (5.2)$$

where $A = (dp/dz - \rho_2 g)$ for convenience, and C is a constant of integration. $\partial w/\partial r$ is the shear rate or velocity gradient of the fluid and is a function of r and θ.

iv Velocity

Integration of equation 5.2 yields

$$w = -\frac{Ar^2}{4\eta} + C \ln r + D, \tag{5.3}$$

where D is a further constant of integration.

v Flowrate through the annulus

The flowrate of the fluid element is the fluid velocity w multiplied by the cross-sectional area $\delta r \; r \; \delta\theta$. Thus the total flowrate through the annulus is given by:

$$\dot{Q} = \int_0^{2\pi} \int_a^R w \; r \; dr \; d\theta \tag{5.4}$$

$$= \int_0^{2\pi} \int_a^R \left[-\frac{Ar^2}{4\eta} + C \ln r + D\right] r \; dr \; d\theta$$

$$= \int_0^{2\pi} \left[-\frac{A}{16\eta}(R^4 - a^4) + \frac{C}{2}(R^2 \ln R - a^2 \ln a) + (\frac{D}{2} - \frac{C}{4})(R^2 - a^2)\right] d\theta. \tag{5.4a}$$

vi Boundary conditions

The constants of integration C and D can be determined from velocity boundary conditions

$$\text{At } r = a, \quad w = -V,$$
$$\text{at } r = R, \quad w = 0.$$

Thus C and D may be eliminated from equation 5.4a to give:

$$\dot{Q} = \int_0^{2\pi} \left[\frac{a^2 V}{2} + \frac{A}{16\eta}(R^4 - a^4) - \frac{(R^2 - a^2)}{4 \ln R/a}\left[V + \frac{A}{4\eta}(R^2 - a^2)\right]\right] d\theta. \tag{5.5}$$

The flowrate through the annulus equals the rate of displacement of the sinker which is $V\pi a^2$. Equating this with equation 5.5 gives the identity:

$$V\pi a^2 = V\pi a^2 + \int_0^{2\pi} \left[\frac{A}{16\eta}(R^4 - a^4) - \frac{(R^2 - a^2)}{4 \ln R/a}\left[V + \frac{A}{4\eta}(R^2 - a^2)\right]\right] d\theta.$$

Since the integral is symmetrical about π, we have:

$$V \int_0^{\pi} \frac{(R^2 - a^2)}{\ln R/a} d\theta = \frac{A}{4\eta} \int_0^{\pi} \left[(R^4 - a^4) - \frac{(R^2 - a^2)^2}{\ln R/a}\right] d\theta. \qquad (5.6)$$

The constant A is as yet unknown, but it may be found by examining the forces acting upon the sinker. Equation 5.6 relates viscosity to the velocity of fall, V.

vii Sinker forces

Since the sinker travels down the tube at constant velocity, the forces acting upon it may be equated to zero. The forces acting upon the sinker are the shear force on the walls of the sinker, the force due to gravity less buoyancy, and the force due to the pressure gradient.

The shear stress on the surface of the sinker is given by:

$$\tau_a = \eta\left[\frac{\partial w}{\partial r}\right]_{r = a}.$$

By equation 5.2 and the velocity boundary conditions we have:

$$\frac{\partial w}{\partial r} = -\frac{Ar}{2\eta} + \frac{1}{r}\left[V + \frac{A}{4\eta}(R^2 - a^2)\right] \Big/ \ln R/a.$$

Since R is a function of θ, the shear stress is dependent upon angular position.

The shear force upon the sinker is thus

$$\eta\ell \int_0^{2\pi} \left[\frac{\partial w}{\partial r}\right]_{r = a} a\,d\theta = 2\eta\ell \int_0^{\pi} \left[-\frac{Aa^2}{2\eta} + \left[V + \frac{A}{4\eta}(R^2 - a^2)\right] \Big/ \ln R/a\right] d\theta.$$

The body forces are shear force, gravitational force, and the force due to pressure gradient.

$$-Aa^2\ell \int_0^{\pi} d\theta + 2\eta\ell V \int_0^{\pi} \frac{d\theta}{\ln R/a} + \frac{A\ell}{2} \int_0^{\pi} \frac{(R^2 - a^2)}{\ln R/a} d\theta - \pi a^2 \ell \rho_1 g + \frac{dp}{dz} \ell \pi a^2 = 0,$$

where ρ_1 is the density of the sinker, and since $A = (dp/dz - \rho_2 g)$ the expression can be rearranged to the following:

$$\frac{A}{2} \int_0^{\pi} \frac{(R^2 - a^2)}{\ln R/a} d\theta = \pi a^2 (\rho_1 - \rho_2) g - 2\eta V \int_0^{\pi} \frac{d\theta}{\ln R/a}.$$

Hence A can be eliminated by substitution of the above into equation 5.6.

Therefore

$$\eta = \frac{\pi a^2 (\rho_1 - \rho_2) g}{2V \left[\int_0^{\pi} \frac{1}{\ln R/a} d\theta + \left[\int_0^{\pi} \frac{(R^2 - a^2)}{\ln R/a} d\theta \right]^2 \Big/ \int_0^{\pi} \left[(R^4 - a^4) - \frac{(R^2 - a^2)^2}{\ln R/a} \right] d\theta \right]} \qquad (5.7)$$

This equation describes variation of liquid viscosity with density and the geometry of the system, namely, the sinker and tube diameters and eccentricity, and is inversely proportional to sinker velocity. The eccentricity of the sinker is contained in the variable R where $R = \sqrt{b^2 - \varepsilon^2 \sin^2 \theta} - \varepsilon \cos \theta$.

By imposing the velocity boundary conditions upon equation 5.3 the general solution for velocity of the differential equation of fluid motion, an expression for the velocity at angular position θ, $a \leq r \leq b$ is found. This solution describing velocity at any point in the annulus is

$$w = \frac{A}{4\eta}(R^2 - r^2) - \frac{\ln R/r}{\ln R/a} \left[V + \frac{A}{4\eta}(R^2 - a^2) \right]. \qquad (5.8)$$

The velocity profile described by equation 5.8 is shown in Fig. 5.3 where it is seen to be parabolic in form with a velocity of zero at the inner surface of the tube, and a velocity of -V on the surface of the sinker.

viii The concentric case

The equation for η in the concentric case is where $\varepsilon = o$, that is to say $R = b$. On substituting b for R in equation 5.7 the evaluation of the integrals becomes trivial and therefore the equation for η is

$$\eta = \frac{(\rho_1 - \rho_2)a^2 g[(b^2 + a^2)\ln b/a - (b^2 - a^2)]}{2V(b^2 + a^2)}. \qquad (5.9)$$

This solution for the concentric case is identical to that of Smith (1957), Swift, Lohrenz, and Kurata (1960), Huang (1966), Künzel (1969), Chee and Rudin (1970), and the author, equation 2.19.

5.2.1 The effect of eccentricity variation upon fall time

To theoretically examine the dependence of fall time upon eccentricity equation 5.7 was rearranged in the following way:

$$T = k\left[B + \frac{C^2}{D - E}\right], \qquad (5.10)$$

where $k = \frac{2\eta S}{\pi a^2(\rho_1 - \rho_2)g}$, and $V = \frac{\text{Distance, } S}{\text{Time, } T}$.

The integrals are:

$$B = \int_0^{\pi} \frac{1}{\ln R/a} d\theta,$$

$$C = \int_0^{\pi} \frac{(R^2 - a^2)}{\ln R/a} d\theta,$$

$$D = \int_0^{\pi} (R^4 - a^4) d\theta,$$

$$E = \int_0^{\pi} \frac{(R^2 - a^2)^2}{\ln R/a} d\theta, \text{ where } R = f(\theta).$$

These are elliptic integrals of a non-standard type and attempts to obtain solutions by transforming the variable, θ, were unfruitful as were attempts

to use the complex variable for contour integration.

The integrals above were calculated by digital computer taking increments of 0.2^{o} in θ for values of ε (eccentricity) varying from zero to total eccentricity where $\varepsilon = (b - a)$. The values of b and a are 4.00 mm and 3.711 mm which are the experimental dimensions of tube and sinker respectively. The ratio $T/T_{\varepsilon=o}$ was thus evaluated from equation 5.10. Accuracy using 0.2^{o} steps is estimated to be within +0.01 per cent.

A graph of variation of normalised fall time as a function of the eccentricity ratio $\varepsilon/(b - a)$ is plotted on Fig. 5.4. As the sinker becomes eccentric the analysis shows that the fall time decreases by more than 50 per cent. For complete eccentricity the fall time cannot be calculated because the sinker and tube are in contact which produces a theoretically infinite shear rate, and thus an infinite shear force. The graph shows that as the sinker approaches the tube the reduction in the normalised fall time is from 1.0 to 0.42.

5.3 Other Treatments of the Eccentric Fall Problem

A recent paper by Chen and Swift (1968) has treated the eccentric case by adopting a similar analytical approach but employing bipolar coordinates. The solution of the derived equation describing the terminal velocity ratio (the inverse of rationalised fall time) was calculated by computer and is presented in tabular form as a function of eccentricity ratio and κ, which is the ratio of sinker and tube radii. The radius of the parabolic sinker 3.711 mm, and the inner radius of the glass tube 4.00 mm, provide the value of $\kappa = 0.9277$. By interpolating κ values of Chen, the rationalised fall times were calculated for an eccentricity ratio varying from zero to 0.95.

A problem is set in a book 'Fluid Flow' by Sabersky and Acosta (1964) on page 224 in which the leakage past an eccentric plunger in a cylinder is to be found. If Q_E is the flow past the eccentric plunger and Q_o is the flow with the plunger centred, the solution is $Q_E/Q_o = (1 + 3\varepsilon^2/2(b - a)^2)$ for an eccentricity ratio much less than unity. Since velocity is proportional to flowrate, it follows that the fall time ratio equals Q_o/Q_E.

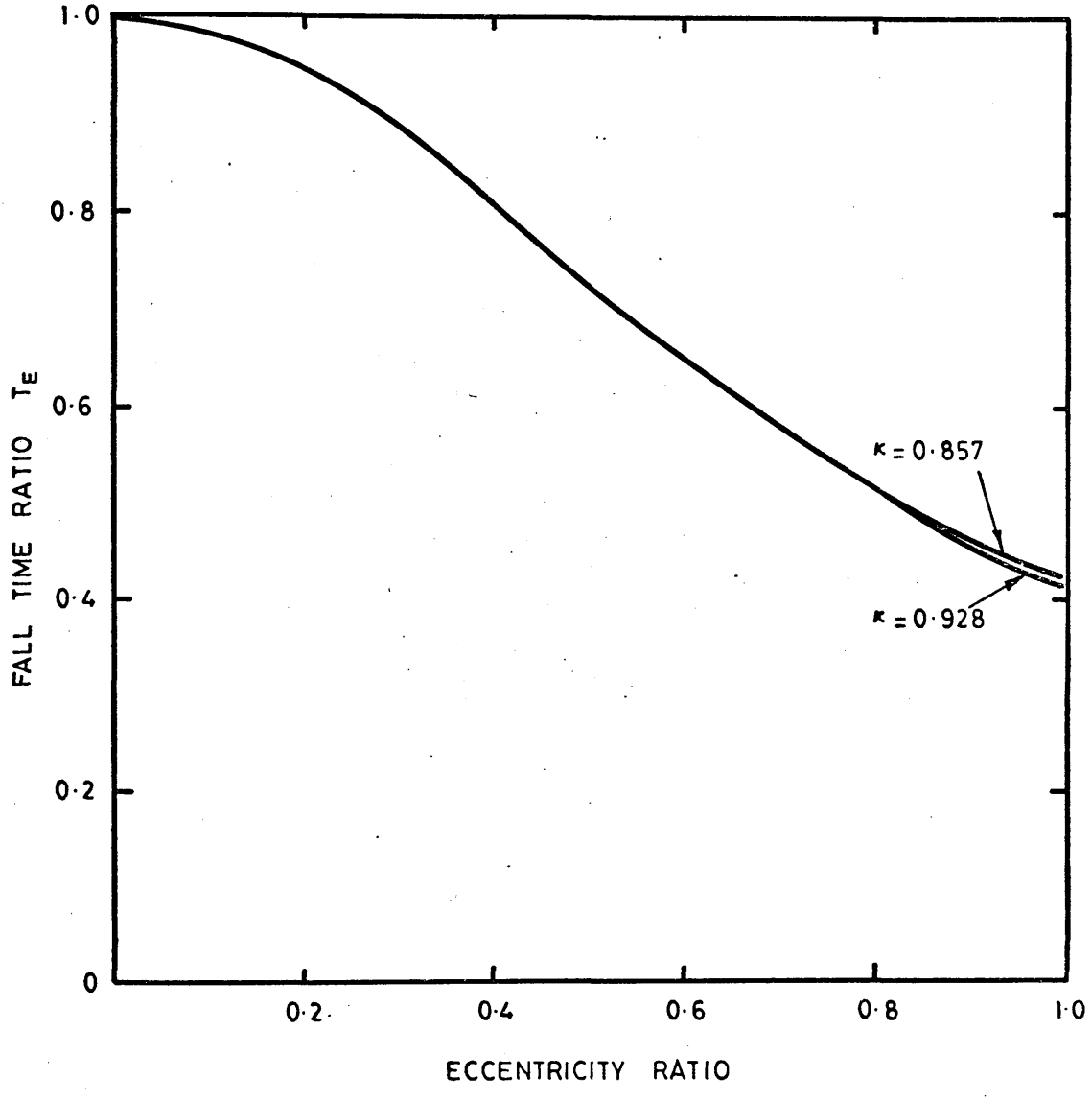

FIG 5.4 Calculated fall time as a function of eccentricity ratio

Thus

$$\frac{T}{T_{\varepsilon=o}} = \frac{1}{\left[1 + \frac{3}{2}\frac{\varepsilon^2}{(b-a)^2}\right]} \tag{5.11}$$

Values are calculated for eccentricity ratios, $\varepsilon/(b - a)$, up to 0.7.

A recent paper by Künzel (1972) gives another expression for fall time ratio based on calculations from a thesis by Heinze (1925). The expression was derived on a basis of the rectangular parallel plate approximation of Lawaczeck (1919).

$$\frac{T}{T_{\varepsilon=o}} = \frac{(b-a)^3\left[\frac{1}{\sqrt{(b-a)^2 - \varepsilon^2}} - \frac{3(1 + \frac{a}{b-a})b}{(b-a)^2\left[1 + \frac{3\varepsilon^2}{2(b-a)^2}\right]}\right]}{3b^2 + (b-a)^2}. \tag{5.12}$$

The equation is evaluated for eccentricity ratios up to 0.99.

The values of rationalised fall time, or fall time ratio, obtained from equation 5.10 from Chen et al, and from equation 5.11 and 5.12 are collected in Table 5.1. The numerical solutions of the author and Sabersky are in complete agreement up to $\varepsilon = 0.5$, while the average difference between those of the author and Chen is 0.1 per cent. The approximation of Künzel gives values slightly lower than equation 5.10 with a maximum difference of 0.55 per cent.

Table 5.1

Comparison of theoretical fall time v. eccentricity

Eccentricity ratio ($\varepsilon/(b-a)$)	Eccentric fall time ratio T_E			
	Equation 5.10	Chen et al.	Sabersky & Acosta	Künzel
0.0	1.0000	1.0000	1.0000	1.0000
0.1	0.9852	0.9852	0.9852	0.9852
0.2	0.9434	0.9436	0.9434	0.9434
0.3	0.8811	0.8814	0.8811	0.8808
0.5	0.7275	0.7281	0.7275	0.7265
0.7	0.5771	0.5780	0.5764	0.5749
0.9	0.4539	0.4553	-	0.4483
0.99	0.4162	-	-	0.3932

The analyses of both the author and Chen are based on the same assumptions and are derived from a solution of the Navier-Stokes equation, and the good agreement confirms the correctness of both mathematical treatments. That there is a slight difference in calculated values is due to the fact that the evaluation of integrals was performed by a small step by step procedure on a digital computer in the case of the author's treatment, while a converging series was also evaluated by computer in the calculations of Chen et al, both of which calculations introduce very small errors.

The relationship between rationalised fall time and eccentricity ratio of Sabersky and Acosta is accurate for small eccentricities and has the considerable advantage that being comparatively simple, it is more readily calculable.

5.4 Comparison of Experimental Results and Theory

Fig. 5.2 shows the measured variation of fall time with tube angle. For the first 15 degrees of tilt, the fall time decreases by more than 50 per cent and subsequently increases as the tube is tilted further until the sinker no longer falls. Thus the sinker velocity is seen to increase by a factor of more than two, whereas gravitational considerations alone indicate that the velocity should decrease as the tube is inclined from the vertical position since the gravitational component, mg cos ϕ, acting parallel to the tube, diminishes with tube inclination.

The theoretical analysis of fall time variation considers the case where the sinker falls eccentrically but vertically, and if theory and measurement are to be compared the gravitational effect due to tilting has to be allowed for. Multiplying the experimental normalised fall times by cos ϕ, where ϕ is the angle of tilt from the vertical, eliminates the gravitational variation of angle, and the resulting curve, B, is shown in Fig. 5.2. It is seen that the fall time still increases for angles greater than 15^{o}. In the region of ϕ greater than 15^{o} the sinker was observed to the sliding down the side of the glass tube so that the sinker is totally eccentric in this region which means that fall time behaviour is due to effects other than change of eccentricity, and since gravitational effects have been eliminated, the increase of fall time for ϕ greater than 15^{o} must be

attributable to some other factor.

When the sinker is sliding down the side of the tube it is behaving as a body on an inclined plane as shown in Fig. 5.5.

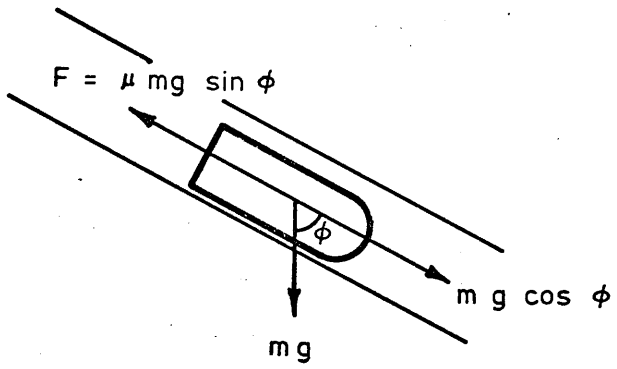

Fig. 5.5 Forces acting on a sliding sinker

Examination of kinetic behaviour shows that the forces causing motion parallel to the tube are (mg cos ϕ - μmg sin ϕ). Although the sinker is sliding down the side of the tube there is a film of liquid present which separates the two providing lubrication so that the coefficient of dynamic friction, μ, should be small.

The measured normalised fall time in which both gravitational and frictional forces have been eliminated is obtained from the following expression:

$$t' \text{(independent of gravity and friction)}$$

$$= \frac{\text{fall time} \times (mg \cos \phi - \mu mg \sin \phi)}{\text{vertical fall time} \times mg}.$$

Therefore t' = normalised fall time $\times$ (cos ϕ - μ sin ϕ).

In the region where the sinker is sliding t', the corrected fall time, should not vary with tube inclination. A value of μ = 0.26 was found

by trial and error to produce this effect and the curve, C, of normalised fall time with gravitational and frictional forces eliminated is also shown in Fig. 5.2. The value of μ compares favourably with values of dynamic frictional coefficients of lubricated surfaces quoted in the American Institute of Physics Handbook (1957), and can be further verified as follows. At the angle of tilt where the sinker just ceases to slide the only forces acting on it are gravity and friction, and since the body is in equilibrium

$$mg \cos \phi - \mu mg \sin \phi = 0$$

thus

$$\mu = \cot \phi$$

$$\phi = 75^{o} \text{ (approx.) for } \mu = 0.26.$$

As indicated by Fig. 5.2 (curve A) it is at approximately this angle of tilt that sliding no longer takes place and fall time becomes infinite.

Curve C, Fig. 5.2, represents the variation of the measured normalised fall time due only to eccentricity. Within 15^{o} of tilt the fall time drops by almost 60 per cent and then remains constant for further inclination of the tube. During this initial tilting the sinker is becoming eccentric causing the large drop in fall time, and it is this which has been derived theoretically. At 0.99 eccentricity ratio theory predicts that normalised fall time will be 0.416, and on the corrected experimental curve the normalised fall time is 0.41.

The theoretically predicted value of 0.416 at 0.99 eccentricity ratio was computed from equation 5.10. This equation is a re-arrangement of equation 5.7 which was derived by the author (section 5.2), and relates velocity with R, a function of eccentricity. The equation is restated here with V the subject of the equation:

$$V = \frac{\pi a^2(\rho_1 - \rho_2)g}{2\eta\left[\int_0^{\pi} \frac{1}{\ln R/a}d\theta + \left[\int_0^{\pi} \frac{R^2 - a^2}{\ln R/a}d\theta\right]^2 \Big/ \int_0^{\pi}\left[(R^4 - a^4) - \frac{(R^2 - a^2)^2}{\ln R/a}\right]d\theta\right]} \quad (5.7a)$$

The experimental normalised fall time value with gravitational and frictional forces eliminated, where the sinker is falling down the side of the tube at maximum eccentricity, is 0.41. This occurs at tube angles greater than 15^{o} to the vertical and is shown in Fig. 5.2, curve C.

The excellent agreement between theory and experiment is gratifying and confirms that the Navier-Stokes equation provides a useful and powerful starting point for the analysis of practical problems in fluid flow.

5.4.1 Correlation between eccentricity and viscometer tube angle

Fig. 5.4 shows the theoretically derived curve of fall time as a function of eccentricity, and Fig. 5.2, curve C, shows the experimentally obtained relationship between tube angle and fall time. By disposing of the common variable, fall time, the relationship between eccentricity and tube angle can be found graphically. This relationship is shown in Fig. 5.6 and it shows that the sinker rapidly becomes more eccentric in the first 10^{o} of tilt and then more slowly until it is totally eccentric at about 15^{o} of tilt.

The experimental results in section 5.1 show that sinker fall time is very sensitive to the inclination from the vertical of the viscometer tube, and that with the experimental sinker and tube used total eccentricity is achieved within 15^{o} of inclination. Within the limits of 0 to 15^{o} the sinker appears to remain parallel to the tube which is due to the hydrodynamic lift of the fluid flowing through the narrow part of the annular space between sinker and tube. For angles of inclination greater than 15^{o} the sinker slides down the side of the viscometer tube, while for a given angle less than 15^{o} the sinker takes up a definite eccentricity and does not deviate from that eccentricity as was demonstrated by experiment.

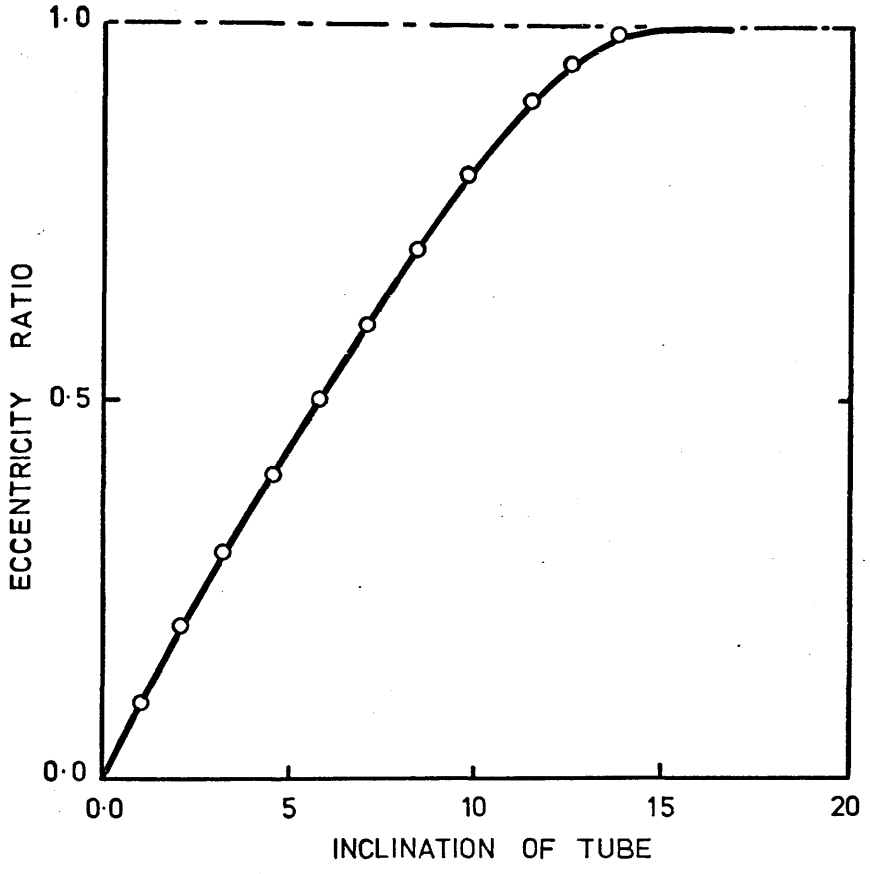

FIG 5.6 Graphically derived eccentricity ratio as a function of tube inclination

5.5 Discussion

No other reference has been found in which the eccentricity of an unguided sinker as a function of viscometer tube angle has been established. Lescaboura and Swift (1968) have examined the effect of eccentricity upon a sinker falling vertically by inducing predetermined values of eccentricity by adjusting the length of guiding pins. Good agreement with theory was obtained for four different sinkers varying in eccentricity ratio from 0 to 0.96, verifying the analysis for eccentric, vertical motion. For an eccentricity ratio less than 0.6 and in the region where κ(= sinker rad./tube rad.) is greater than or equal to 0.8, the fall time is almost independent of κ. That is, the change in fall time scarcely varies from one viscometer to another if the gap between sinker and tube is small ($\kappa \geq 0.8$) and if the eccentricity ratio is limited to a maximum of 0.6.

Cappi (1964) investigated the effects of a non-vertical viscometer with a guided sinker and found that the fall time decreased for the first 1.5° of inclination with a corresponding reduction in fall time of 0.5 per cent, and then increased. The turning point of 1.5° found by Cappi occurs because the guiding pins prevent the sinker from becoming eccentric beyond the tolerance between the tube and the guiding pins. He attributes the subsequent increase in fall time to friction.

From the measurements of fall time variation it is apparent that from Fig. 5.1 the viscometer tube should be correctly aligned. An inclination of approximately 50 minutes of angle from the vertical causes a 1 per cent difference in fall time, and it is evident therefore that the viscometer tube must be aligned accurately. As a result of these findings particular care was taken in the alignment of viscometers and it is estimated that alignment is to within 5 minutes of the vertical which can produce an error of less than 0.1 per cent.

The behaviour of a sinker falling in an inclined tube provides the phenomenon of a large variation in fall time. The normal operating point for falling body viscometers, the vertical position where $\phi = 0$, is shown again in Fig. 5.7 and occurs at a well-defined maximum. The fall time curve passes through a minimum as tube angle increases; the minimum point

occurring at about 15° in the case examined. This minimum point is more gradual than the maximum point and it follows that the error arising from a given variation of tube angle would be less at the minimum. A possible result of this is that a falling body viscometer in which the viscometer tube is set at the angle of the minimum might be developed. At this minimum the sinker would fall eccentrically and slide down the side of the tube. A viscometer working in this mode would have the following advantages:

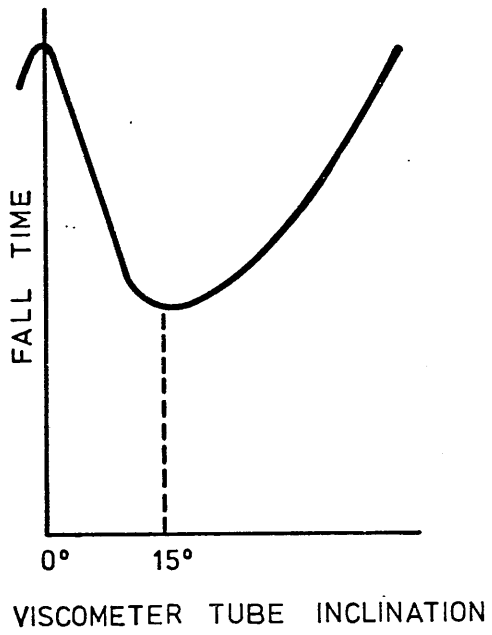

Fig. 5.7 Fall time as a function of tube inclination

i Smaller errors due to misalignment.

ii Fall time more than halved meaning that

a the upper measuring limit of the viscometer is immediately doubled, and

b time spent on the measurement of fall time is more than halved.

CHAPTER 6

THE DENSITY OF LIQUIDS UNDER PRESSURE

List of Figures

List of Tables

CHAPTER 6

THE DENSITY OF LIQUIDS UNDER PRESSURE

6.1 Introduction

The compressibility of liquids is required in order that buoyancy corrections may be made in calculating dynamic viscosity from measurements. Density data are also used in testing a viscoelastic relaxation model described by Pursley (1968).

Many methods of measuring liquid compressibility have been used and a detailed survey has been published by Tsiklis (1968).

The bellows method of Bridgman (1931) is capable of high accuracy and for this reason was adopted by the authors of the ASME Report (1953). This method has also been used in the present work. A fixed mass of test liquid is enclosed in a flexible bellows and subjected to pressure. Knowing the volume of liquid at atmospheric pressure and the cross-sectional area of the bellows, it is possible to calculate the volume change of the liquid from the change in length of the bellows. If the density of the liquid at atmospheric pressure is known, the density of the liquid may be calculated.

Bridgman used a slide-wire to determine the change in length of the bellows. Shakhovskoi, Lavrov, Puchinskii, and Gonikberg (1962) avoided the problems inherent in Bridgman's potentiometric method by determining the change in length of the bellows by a linear differential transformer in place of the slide-wire. This permits an improved resolution in the position of the bellows and volume measurement to an accuracy of ±0.1 per cent can be attained.

The measurement of change in the length of the bellows by linear differential transformer is both accurate and simple. A brass rod carrying a Swedish iron core is fastened to the top of the bellows. The brass rod is free to slide in a guiding sleeve around which is wound a central primary winding and two secondary windings which are connected in series

opposition. The net voltage output from the secondaries depends upon the position of the iron core and voltage is directly proportional to the core displacement. When the iron core is in the centre of the transformer the secondary output voltage is ideally zero.

The e.m.f. induced in the transformer is balanced by a second linear differential transformer - the reference transformer - which is similar to the bellows transformer and has an iron core whose position is adjusted by a micrometer screw. The primaries of the two transformers are connected in series, and the secondaries are connected so that the output electromagnetic forces oppose one another. The output voltages may be balanced by adjusting the position of the reference core to produce a null point. Thus a displacement of the bellows transformer may be compensated by a similar displacement of the reference core.

This technique was employed by Yazgan (1966) and has been used in this work with some modification.

6.1.1 Description of densimeter

A prototype densimeter having two bellows to contain the test liquid was first built. This was modified to a final version in which one bellows is used in order that the densimeter can be used in the very high pressure equipment (13.7 kbar).

6.1.1a Mechanical details

i Bellows assembly

An assembly drawing of the long version (prototype) densimeter is shown in Fig. 6.1. It consists of a brass coil former (A) through which a brass slider rod (B) moves. The coil former has a radial slit along its length to eliminate eddy currents. The base of the brass rod is soldered with Woods Metal to the bellows (F) and a rod of Swedish Iron (E) is screwed on to the slider. In order that the iron core should be longitudinally symmetrical 8 BA holes are tapped at either end. The composition of the Swedish Iron is:

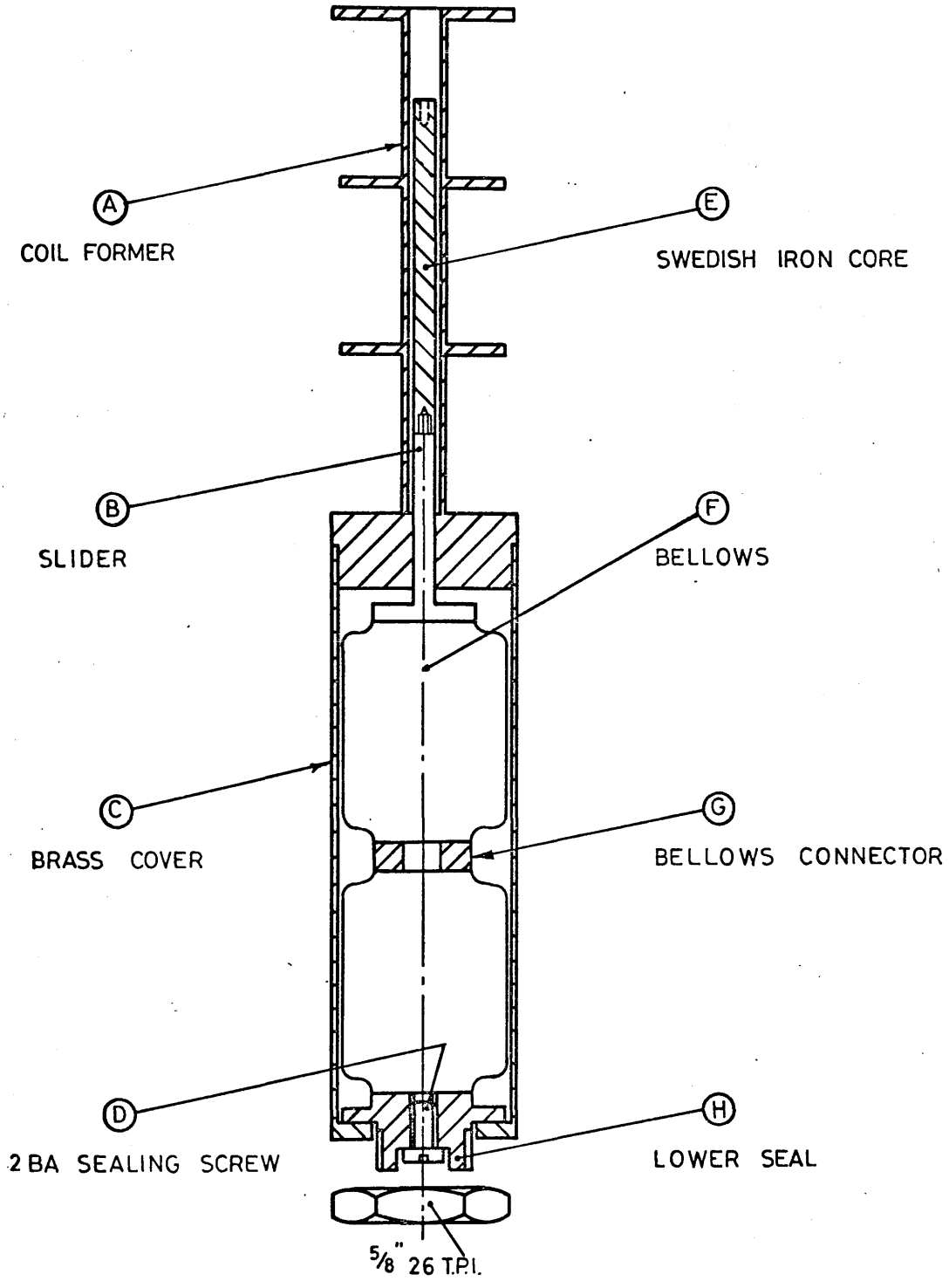

FIG 6.1 Assembly drawing of prototype densimeter

Fe: 98.84 C: 0.012 S: 0.018 Mn: 0.030 P: 0.004
Si: 0.002 O: 0.030 N: 0.0018

A brass, slotted cover (C) containing the bellows is screwed on to the lower end of the coil former. The cover consists of a cylindrical brass tube which defines the position of the lower end of the bellows with reference to the transformer. The bellows are soldered with Woods Metal to a lower seal (H) which is firmly held to the bottom of the bellows cover by a lock nut.

The brass bellows are of the 'extra flexible' type, length 1.25 inch, outside diameter 1.125 inch, with eleven convolutions, (Hydroflex Metal Bellows, Drayton Controls Ltd). The wall thickness is 0.004 inch and care has to be taken in soldering to avoid damage due to overheating. For this reason Woods Metal, melting point 70^{o}C was used for the permanent joints on the bellows and it was found that soldering could be effected by using a hand-held warm air blower, thus avoiding any possibility of damaging the bellows.

There is a filling hole through the centre of the lower seal and this is closed by a sealing screw (D) which bears upon a nitrile rubber O-ring, Edwards No VOR 2A (non British Standard). A detailed workshop drawing of the components of the densimeter is shown in Fig. 6.2.

In the long version densimeter illustrated in Figs 6.1 and 6.2 two identical bellows are joined by connecting collar (G). The final form of the densimeter differs from the long version only in that it has one bellows and a shorter brass housing. A photograph of the final densimeter which was used in the very high pressure vessel is shown in Fig. 6.3.

ii Reference transformer

This part of the apparatus consists of a rigid brass framework upon which is mounted a barrel micrometer as shown in the photograph in Fig. 6.4. The movement of the screw is transmitted via a single ball bearing to a brass rod of square section which passes through a square hole to ensure that movement is entirely vertical. A Swedish iron rod of identical dimensions with the bellows core and also tapped at both ends is attached

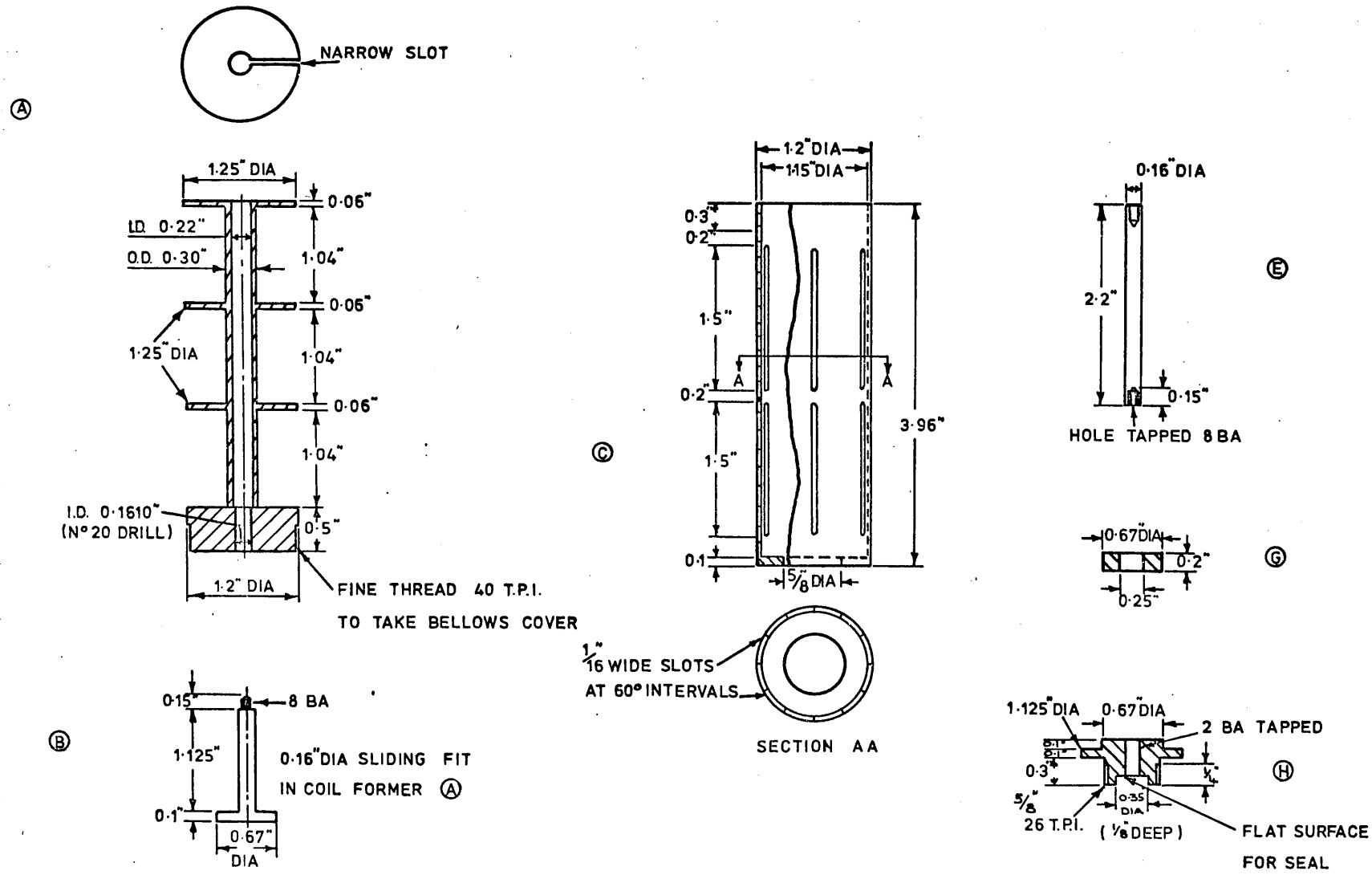

Fig 6.2 Working drawings of densimeter components

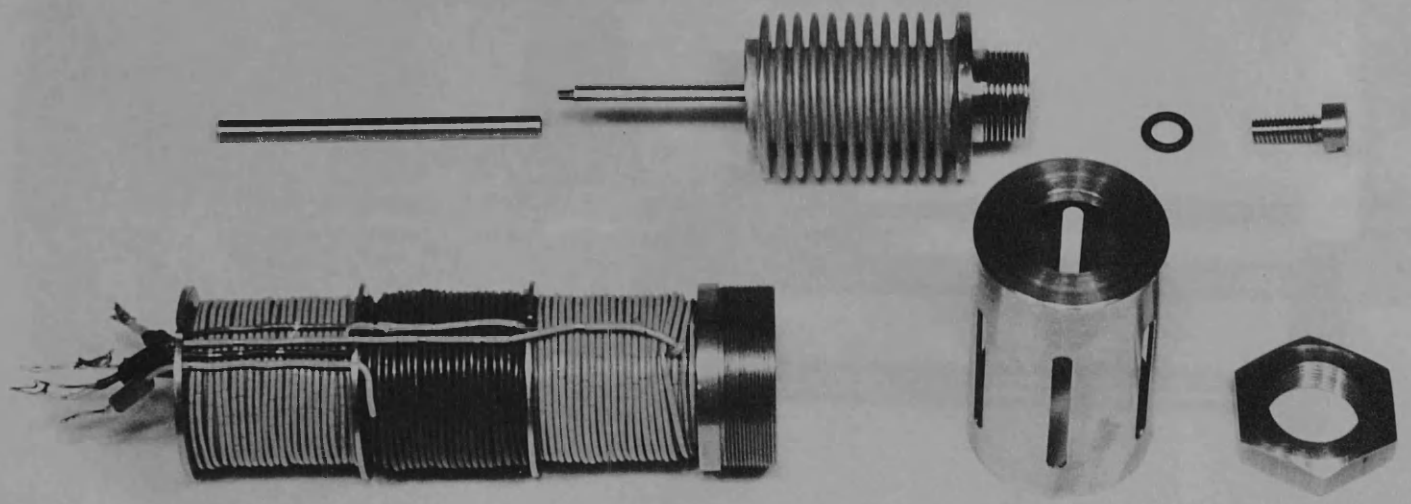

FIG. 6.3. VIEW OF THE DISMANTLED DENSIMETER

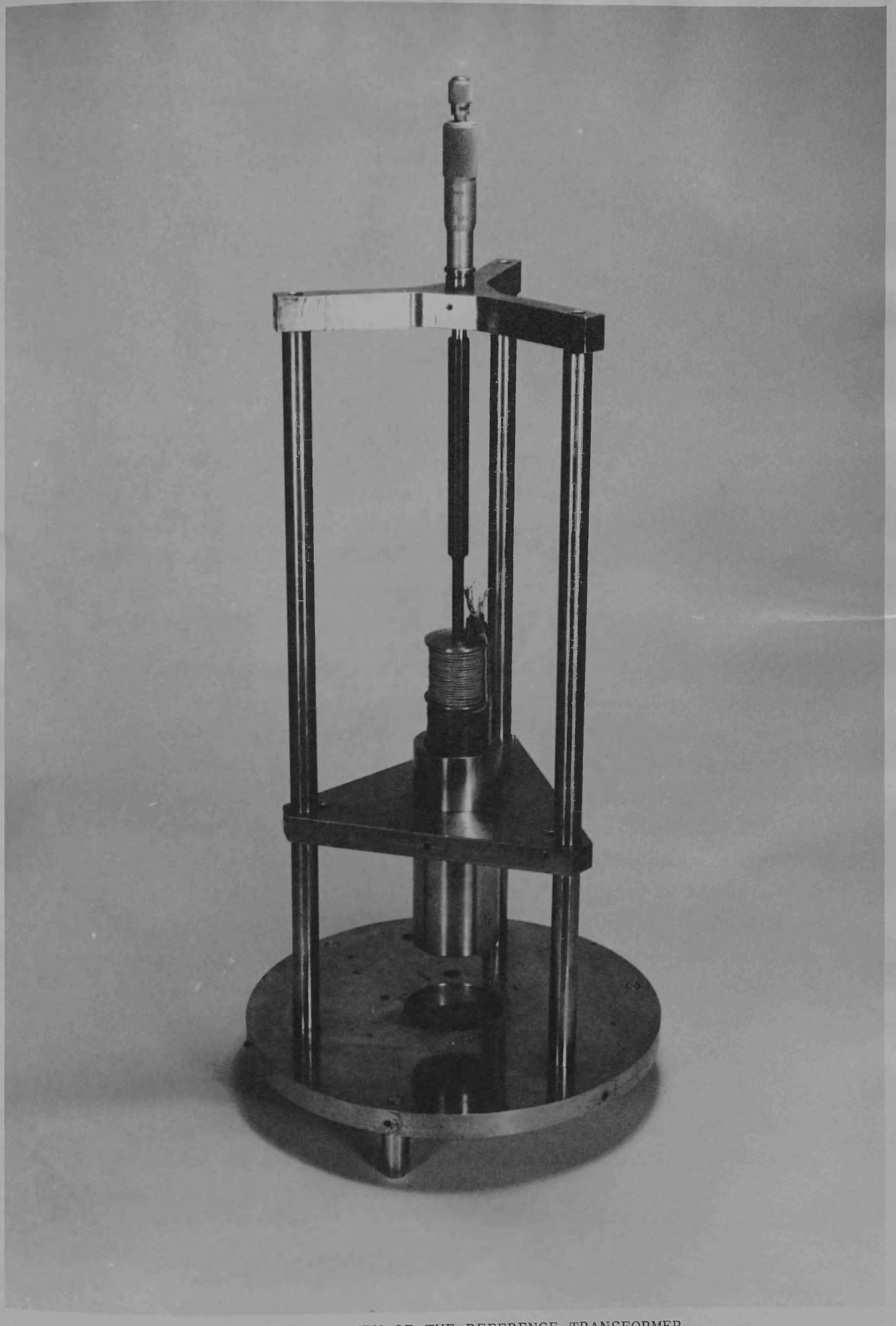

FIG. 6.4. VIEW OF THE REFERENCE TRANSFORMER

to the lower end of the brass connecting rod. The reference transformer which was wound with the same number of turns as the bellows transformer is rigidly attached to the base of the frame. A compression spring acts on the brass square section so that the micrometer is always in firm contact with the ball bearing.

6.1.1b Electrical system

A block diagram of the electronic system is given in Fig. 6.5. A crystal oscillator generates a 10 kHz continuous sinusoidal signal. This signal is passed through a buffer amplifier (A) and applied to the primary windings of the transformers which are connected in series. The total e.m.f. produced in the secondaries of both transformers is fed into a second buffer amplifier (B). The signal from the buffer amplifier is applied to a band-pass fitter and the output fed into an amplifier before being displayed on a single-beam oscilloscope. The oscilloscope is synchronised by triggering from the oscillator.

A schematic circuit diagram of the linear transformers is shown in Fig. 6.6. There are two linear differential transformers: the bellows transformer which is inside the pressure vessel, and the reference transformer which is outwith the pressure system. The primary coils of the two transformers are connected in series as shown. The secondary coils of the individual transformers are wound so that their fields oppose each other and the outputs from both transformers are connected in opposition. The field directions are illustrated by the arrows in Fig. 6.6. A displacement of the iron core attached to the bellows can be compensated by a displacement of the reference iron core by means of a micrometer so that the net voltage of the secondaries is reduced to a null.

i 10 kHz oscillator

A crystal controlled oscillator is used to achieve high stability. The crystal is an X-Y flexure type (Marconi type 1652D). A circuit diagram is given in Fig. 6.7.

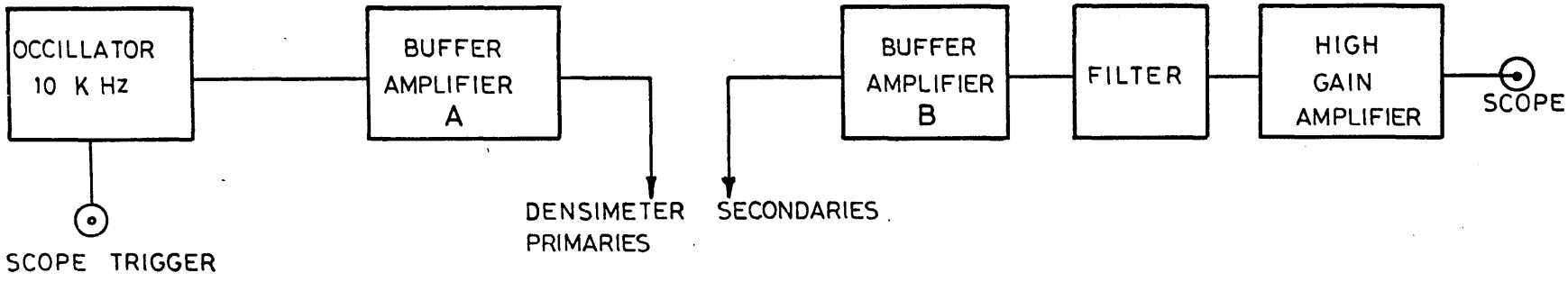

Fig 6.5 Densimeter block diagram

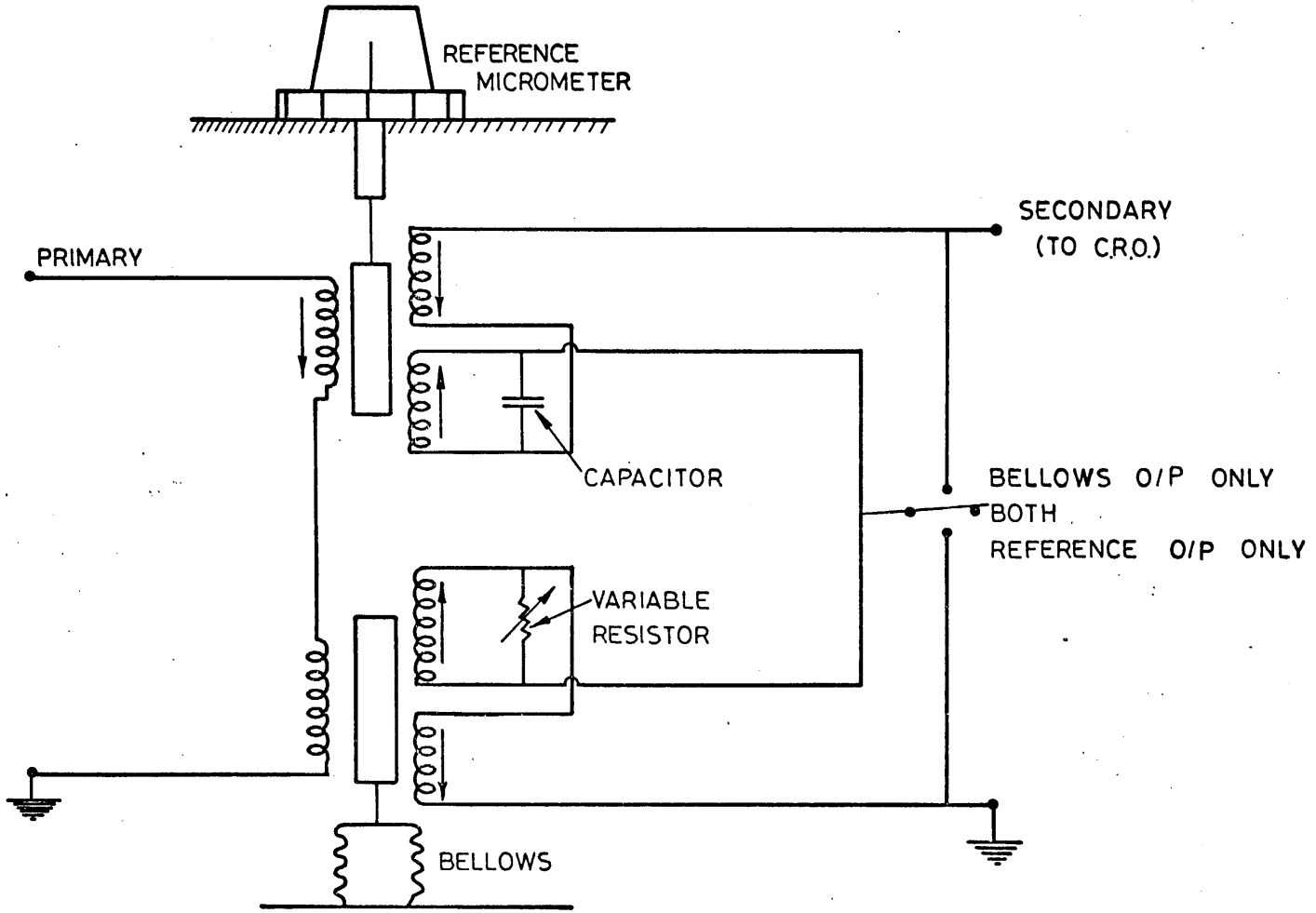

Fig 6.6 Schematic circuit diagram of linear transformer arrangement

ii Buffer amplifier A

This amplifier provides impedance matching between the oscillator and the differential transformers. The loading on the oscillator is minimised to ensure stability of signal amplitude. A 40:1 turns ratio transformer is used to provide the required matching. The circuit diagram is shown in Fig. 6.8.

iii Buffer amplifier B

This amplifier has a high input impedance of about 0.5 MΩ to provide minimal loading on the transformers. The circuit diagram is given in Fig. 6.9.

iv Filter

The filter has a pass-band of 9,900-10,100 Hz and is passive. The iterative impedances are 600Ω. Its function is to reduce harmonics and minimise the effect of stray signals.

v Output amplifier

A circuit diagram of the amplifier is shown in Fig. 6.10. Its purpose is to amplify the out-of-balance signal from the transformers for display on the oscilloscope which is used as a null-detector. It was found that improved precision of balancing was possible from the visual display of the oscilloscope set at 10 mV/cm rather than with an electronic voltmeter as the latter proved excessively sensitive to stray pick-up and interference from other equipment in the laboratory.

vi Transformer coils

The dimensions of the two transformers are identical and every care was made to wind the coils similarly. The coils were wound by hand with PTFE insulated multistrand wire. The primary was first wound with 203 turns. One of the secondaries was then wound in the same direction and then the other secondary was wound in the opposite direction, each with 203 turns. Both transformers were wound in the same manner.

Minor differences between the transformers and slight variations in the distributions of the windings prevented a perfect null from being obtained.

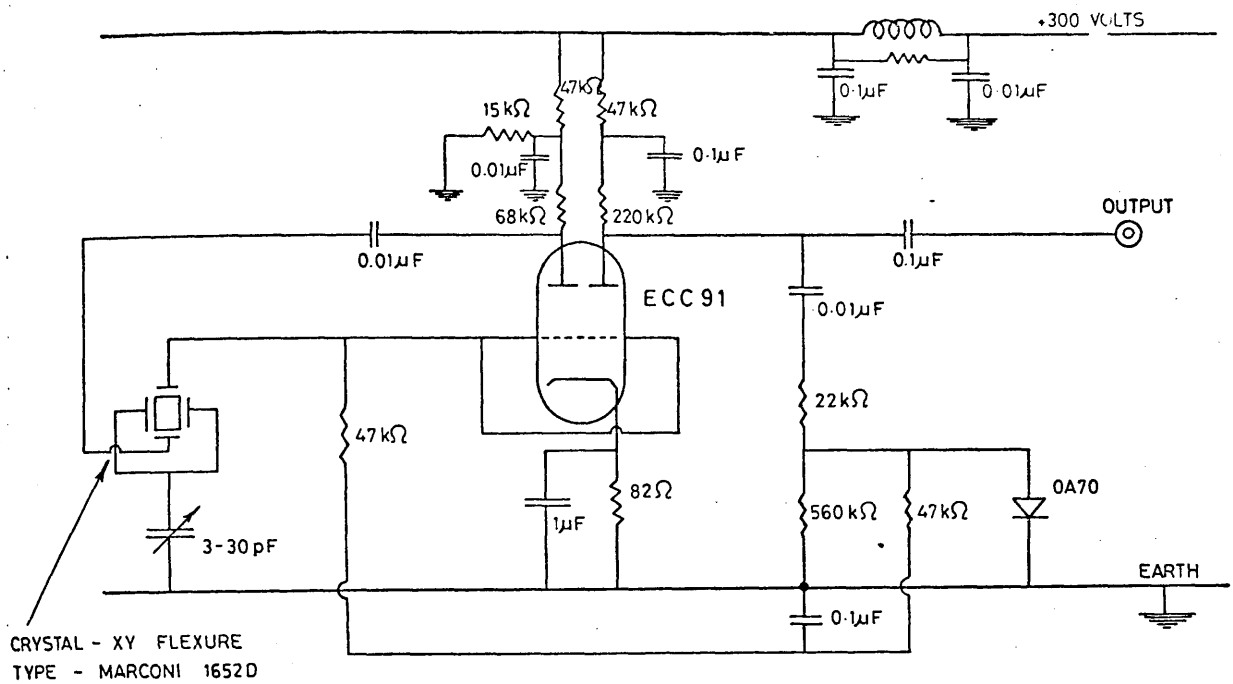

Fig 6.7 10 kHz oscillator

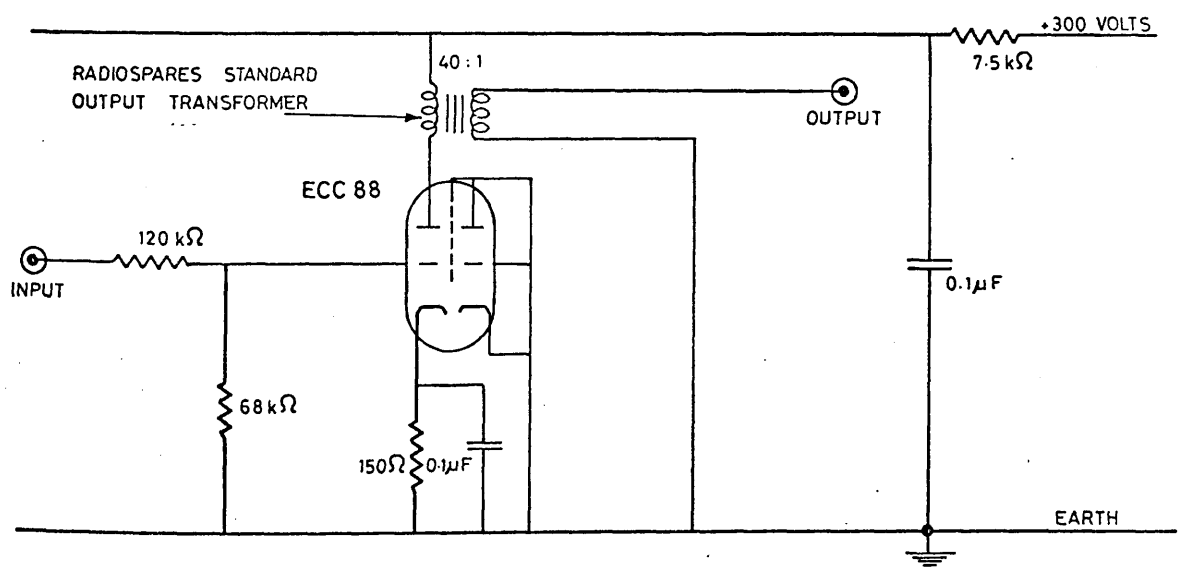

FIG 6.8 Buffer amplifier 'A'

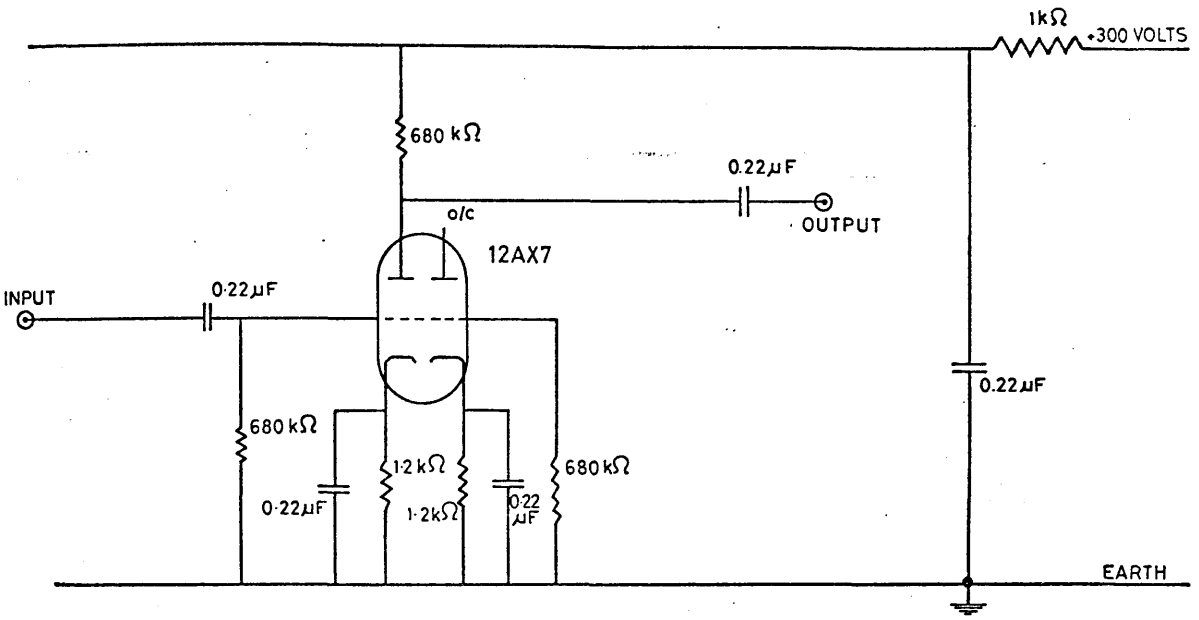

Fig 6.9 Buffer amplifier 'B'

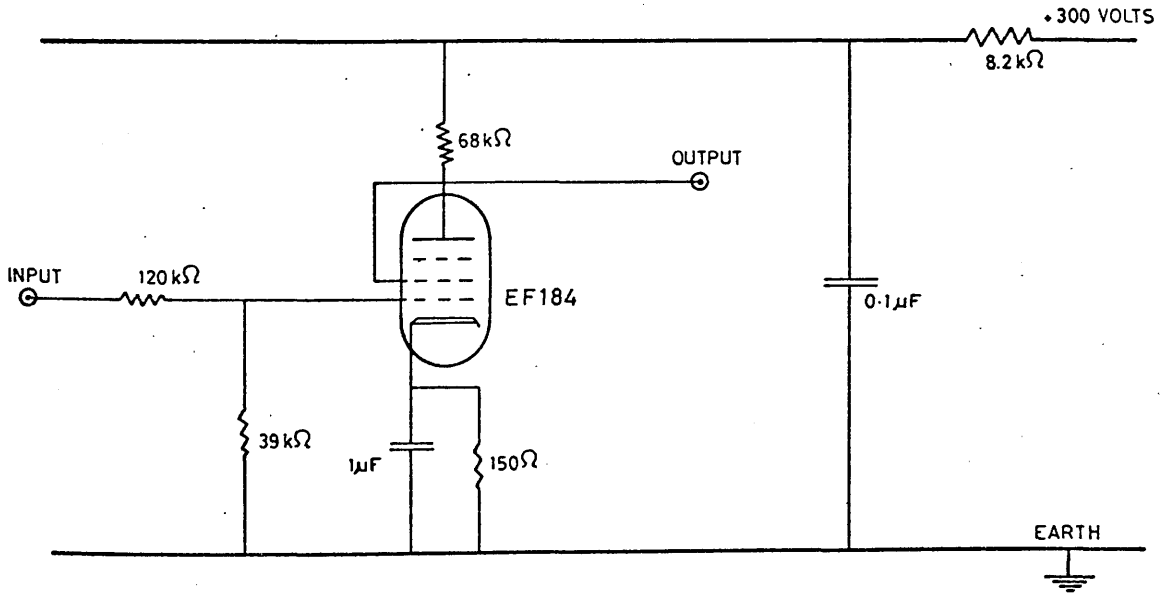

Fig 6.10 High gain output amplifier

A fixed capacitance across one of the secondaries of the reference transformer is used to establish a perfect out-of-phase relationship. A variable resistor of 200 Ω in parallel with one of the secondaries is necessary to maintain exact out-of-phase balance. Thus by alterately adjusting the reference core position and this resistance a well-defined balance point is achieved. For every change in bellows core position this procedure is adopted. The balance point obtained by this tuning method is unique. This was confirmed over the entire travel of the bellows core.

6.1.2 Differential transformer calibration

If the transformers were identical then a movement of the bellows iron core would be compensated by an equal movement of the reference core to provide balance at the circuit output. In practice, due to the transformers not being perfectly identical and other contributary factors such as the effect of the permeability of the pressure vessel on the bellows transformer, the ideal 1:1 core movement ratio does not exist. It is therefore necessary to calibrate bellows core movement against the movement of the reference core. The position of the reference core is defined by the reading on the reference transformer micrometer, so that once a calibration of one core movement against the other has been obtained then, at balance, the position of the bellows core is uniquely defined by the micrometer reading.

The bellows transformer assembly was placed in the high pressure vessel and immersed in the hydrostatic pressurising fluid. The bellows was empty and its sealing screw absent to allow the bellows to be compressed. A micrometer acted upon the bellows core via a connecting rod to provide definite movement. For every position of the bellows core the corresponding reference core position was found by adjusting the latter for minimum output voltage, and final tuning obtained by adjusting the variable resistor and reference core position in turn for out-of-phase balance.

Calibration was carried out with the pressure vessel at 30 ± 0.1°C. Calibration over a range of 7 mm downward movement of the bellows core was carried out and this corresponds to approximately 20 per cent

compression of the bellows. The bellows core was moved by increments of 0.0125 inch and after the calibration in the downward direction, the core was raised in equal steps by rotating the micrometer in the opposite direction. The elasticity of the bellows was sufficient to raise the core to its initial position. No hysteresis was observed in the return of the core to its original position.

The calibration figures are shown in Table 6.1. Inspection of table values shows that linearity is not achieved so that a definite increment in bellows core position does not correspond to a fixed increment of reference core position; that is to say, positional changes vary according to the absolute core locations. Initially a calibration curve of bellows/reference position was drawn but, while accurate, this proved to be a laborious method of converting reference core movement into the corresponding bellows core movement. As an alternative, the equation of the calibration curve was found. This was done by fitting several polynomial equations to the calibration data, increasing the number of coefficients by one each time. Polynomials of more than fifth order showed only a marginal improvement of fit and the fourth order of fit was therefore selected. The polynomial gives the bellows core position as a function of reference core position:

$$y = a + bx + cx^2 + dx^3 + ex^4 \qquad (6.1)$$

$a = 0.329\ 4309$

$b = 0.026\ 0479$

$c = 0.002\ 1079$

$d = 0.000\ 0977$

$e = 0.000\ 0018$

The r.m.s. error is 0.000 11 inch (0.000 28 cm).

The recalculated values of bellows position and the differences are shown in Table 6.1. The maximum error is 0.000 21 inch (0.000 53 cm), and this, with the very small r.m.s. error, indicates that the bellows core position can be determined with very high precision. The errors are random, not systematic, and the accuracy of overall measurement, including estimates of bellows core resolution are further discussed in section 6.1.7.

By using a polynomial the calculation of results from measurements can be effected without recourse to graphical means which reduces the probability of human error.

Table 6.1

Recalculation of bellows position from equation 6.1

Reading No	Bellows position (in)	Ref. micr. reading (mm)	Bellows position (Recalc. by eqn. 6.1)	Error (in)
1	0.0000	8.645	-0.00006	-0.000 06
2	0.0125	8.365	0.01255	5
3	250	8.085	2511	11
4	375	7.805	3760	10
5	500	7.530	4979	- 21
6	625	7.245	6234	- 16
7	750	6.955	7503	3
8	875	6.665	8762	12
9	0.1000	6.375	0.10010	10
10	125	6.085	1247	- 3
11	250	5.790	2492	- 8
12	375	5.485	3766	16
13	500	5.190	4984	- 16
14	625	4.875	6267	17
15	750	4.570	7492	- 8
16	875	4.255	8738	- 12
17	0.2000	3.930	0.20002	2
18	125	3.600	1260	10
19	250	3.270	2493	- 7
20	375	2.925	3752	2
21	500	2.575	4997	- 3
22	625	2.210	6258	8
23	750	1.840	7496	- 4

6.1.3 Determination of the effective cross-sectional area of bellows

To translate changes in bellows length into changes of volume it is necessary to know the effective cross-sectional area of the bellows. A calibration apparatus, Fig. 6.11, was used by which changes in bellows length could be accurately determined as follows.

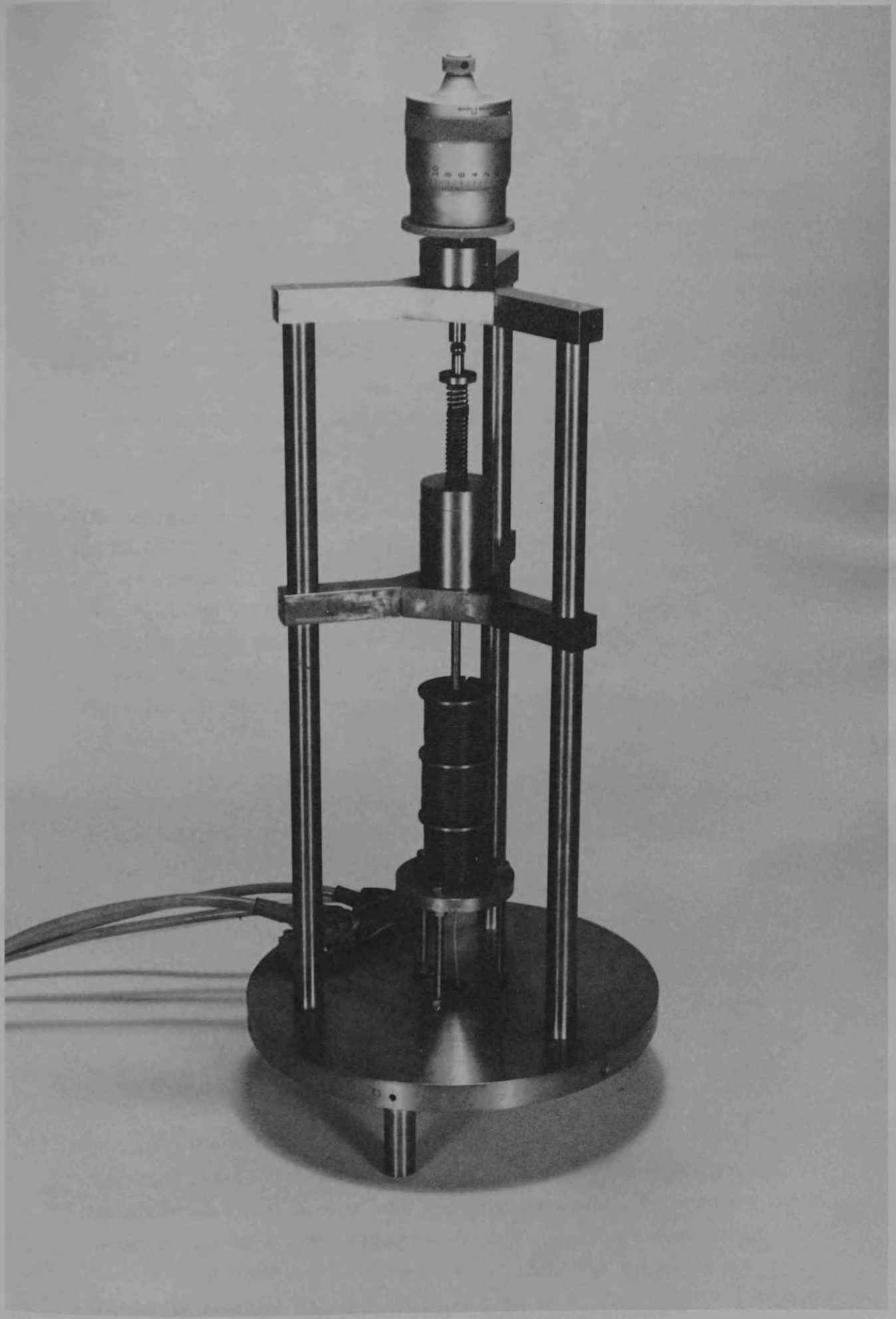

FIG. 6.11. VIEW OF APPARATUS FOR DETERMINING CROSS-SECTIONAL AREA OF THE BELLOWS

The bellows was filled under vacuum with distilled water and then carefully dried on the outside, and weighed. It was then assembled in the differential transformer and placed in the calibration apparatus which has a micrometer with a tufnol rod extension to bear on the iron core on the bellows. After the micrometer reading was taken, the bellows was removed from the apparatus and the sealing screw loosened enough to allow about 0.5 ml of water to be expelled from the bellows before resealing the bellows. After drying and weighing the apparatus was re-assembled and the change of bellows length was obtained directly from the new reading of the micrometer. This procedure was repeated until the bellows had been compressed by 7 mm.

The measurements were carried out at 23.4 ± 0.2°C. The density of water at 23.4°C is 0.9974 g cm^{-3}, (Kell and Whalley) (1965), and this knowledge allows change of weight to be expressed as change of volume. In Fig. 6.12 the decrease in volume is plotted as a function of decrease in length which produces a straight line, the gradient of which (Δ volume/Δ length) is the effective cross-sectional area of the bellows. The value of the effective cross-sectional area of the bellows is 4.000 cm^2.

This compares well with the value of Yazgan and that of the manufacturers of the bellows. Their values are 3.989 and 4.00 cm^2 respectively.

6.1.4 Dimensional corrections due to pressure

Due to the compression of the component parts of bellows transformer assembly there is a slight differential movement between the iron core and the transformer windings. The correction due to the pressure may be estimated by considering the assembly in three parts as follows:

i The bellows

The upper and lower brass seals, which constitute the major portion of the cross-sectional area of the bellows, are subject to pressure and therefore suffer a small reduction in cross-sectional area. This results in an increase in bellows length since the volume of the bellows is constant at any particular pressure. The relative increase

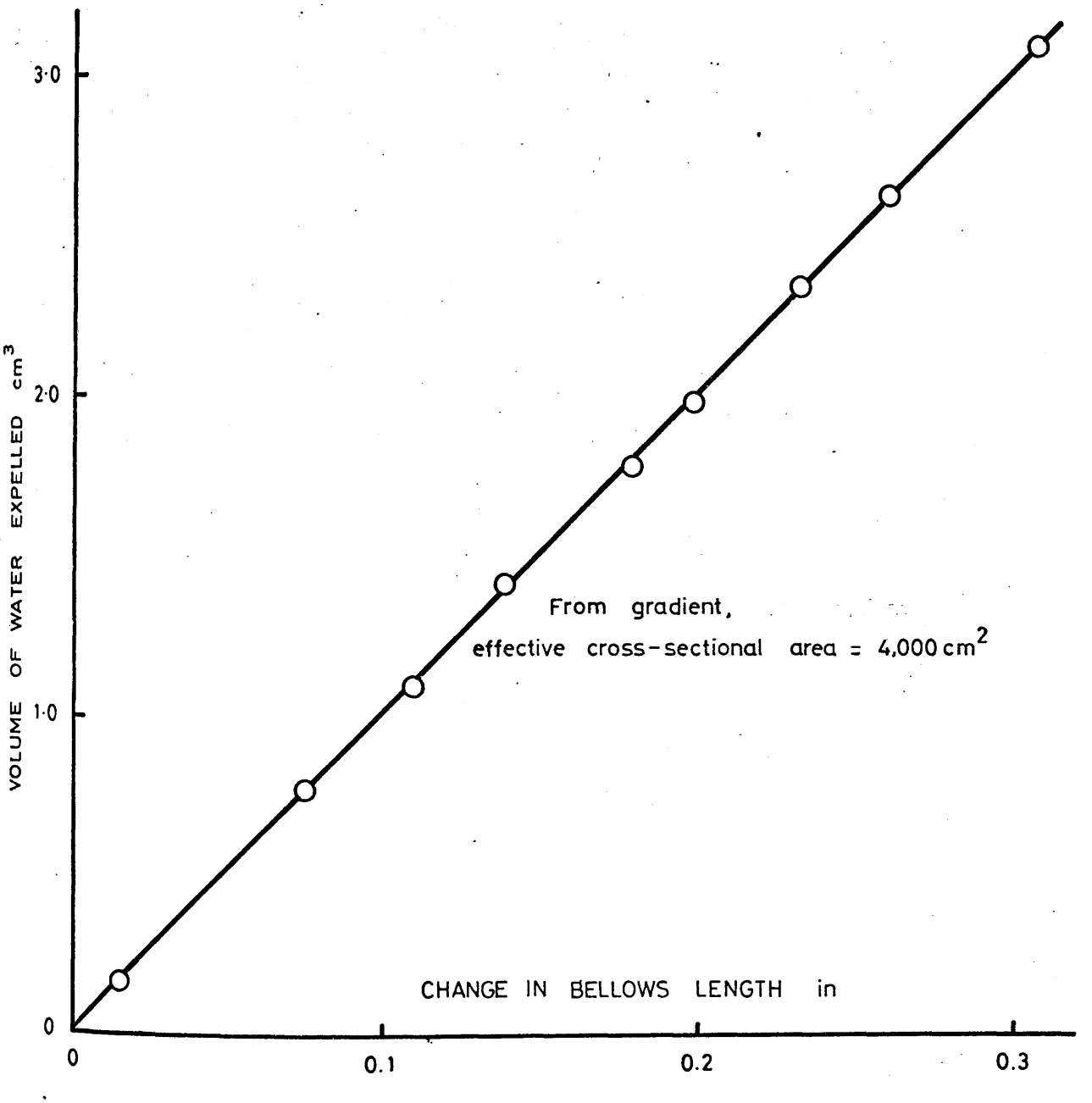

Fig 6.12 Determination of the cross-sectional area of the bellows

in length is equal to the relative reduction in cross-sectional area. That is

$$\frac{\Delta l_{\ell}}{l_{b\ell ws}} = \frac{\Delta A}{A} = 2\varepsilon_b \tag{6.1}$$

where ε_b is the linear compression of brass, $l_{b\ell ws}$ is the length of the bellows, and Δl_{ℓ} is the change in liquid length.

Along the length of the bellows the brass housing is compressed so that

$$\frac{\Delta l_h}{l_{b\ell ws}} = \varepsilon_b \tag{6.2}$$

where Δl_h is the shortening of the bellows housing.

The total apparent increase in bellows length is therefore

$$\Delta l_{\ell} + \Delta l_h = l_{b\ell ws} 2\varepsilon_b + l_{b\ell ws}\varepsilon_b = 3 l_{b\ell ws}\varepsilon_b. \tag{6.3}$$

ii Brass slider

In this section the slider and the surrounding casing are of the same material, so there is no differential movement.

iii The iron core

The iron core is compressed by an amount given by

$$\frac{\Delta l_c}{l_c} = \varepsilon_i \tag{6.4}$$

where l_c is the iron core length, and ε_i the linear compression of iron. The relative change of the brass coil former at the same section is

$$\frac{\Delta l_f}{l_c} = \varepsilon_b. \tag{6.5}$$

Since $\varepsilon_b > \varepsilon_i$ there is a net upward movement of the core with respect to the transformer:

$$\Delta l_f - \Delta l_c = l_c\varepsilon_b - l_c\varepsilon_i = l_c(\varepsilon_b - \varepsilon_i). \tag{6.6}$$

The real effect will be half this value since the mid-point of the iron core has half the relative movement of the top of the core.

The upward movement of the core, Δl, is the sum of the two upward increments described by equations 6.3 and 6.6.

$$\Delta l = 3 l_{b\ell ws} \varepsilon_b + 0.5\, l_c (\varepsilon_b - \varepsilon_i). \qquad (6.7)$$

The values of ε_b and ε_i are given in section 2.4.1, where the values are given as 2.42×10^{-7} and 1.98×10^{-7} bar^{-1} respectively. The length of the iron core is 2.2 inch which allows the movement of the core as a function of applied pressure to be calculated. By equation 6.7,

$$\Delta l = (7.26\, l_{b\ell ws} + 1.23) \times 10^{-7} \times P \text{ cm}. \qquad (6.8)$$

This correction is a function of bellows length and is directly proportional to the hydrostatic pressure (bar). It is subtracted from the displacement of the bellows core which takes place when the test liquid is compressed.

A sample calculation for water at 4868 bar is shown:

$$l_{b\ell ws} = \frac{\text{mass}}{\text{area} \times \rho_o} - \text{(bellows movement with respect to P = 0 position)}$$

$$= \frac{14.9306}{4.000 \times 0.9957} - 0.4813$$

$$= 3.2675 \text{ cm}.$$

By equation 6.8

$$\Delta l = (7.26 \times 3.2675 + 1.23) \times 10^{-7} \times 4846$$

$$= 0.0121 \text{ cm } (= 0.37 \text{ per cent of } l_{b\ell ws})$$

The corrected length is

$$l_{corr} = l_{b\ell ws} - \Delta l$$

$$= 3.2554 \text{ cm}$$

Finally $$\rho = \frac{\text{mass}}{\text{area} \times l_{corr}}$$

$$= 1.1466 \text{ g cm}^{-3}.$$

The densimeter described in the ASME Report (1953) makes use of a bellows with a potentiometric slider mounted on top. On page 51 (Vol. 1) the report has an expression for correcting for the compressibility of the apparatus. By re-arranging the expression and stating it in terms of the notation already used the correction to the displacement is

$$\Delta l = 3\, l_{b\ell ws}\varepsilon_b + l_c(\varepsilon_b - \varepsilon_i). \qquad (6.9)$$

This is similar to the expression in equation 6.7 which was derived independently.

6.1.4a Other pressure effects

The effect of pressure on the dimensions of the apparatus immersed in the pressure vessel has been analysed in section 6.1.4. There is in addition a reduction in the resistance of the transformer windings due to pressure, but the change in inductance is negligible. The reduction of resistance causes a decrease in coil impedance, which results in more current in the bellows transformer primary winding, but since the same current flows in the reference transformer primary, this pressure effect will increase the sensitivity of the transformers equally. The change of resistance in the secondary winding of the bellows transformer has no appreciable effect on the null point since there is little or no current circulating in the secondary circuit at balance.

The effect of pressure on the permeability of the iron core was examined by Yazgan who found that there was negligible change in the apparent core position under pressure.

6.1.5 Measurement method

Before introducing a test liquid, the bellows are cleaned thoroughly both inside and outside, and the bellows, sealing screw and O-ring are weighed on a chemical balance. The bellows are filled by a vacuum technique and particular care is taken to avoid pockets of air being trapped in the convolutions of the bellows. When viscous liquids are being used, for

example castor oil, heating the liquid in the bellows facilitates the expulsion of air bubbles. Once filled, the bellows are sealed with the screw and O-ring. Any test liquid on the outside of the bellows is cleaned off and the bellows re-weighed. By subtraction, the weight of test liquid in the bellows is found.

The bellows transformer arrangement is assembled and the bellows housing is screwed on to the coil former until the iron core is at the top end of the calibration range. This initial positioning of the core need not be precise as the exact starting position is immediately defined by the reference micrometer once circuit balance is achieved. The four leads of the bellows transformer are soldered on to the pressure vessel seal which is then lowered into position and screwed down. The pressure vessel is thermostatically controlled and a period of at least 30 minutes is allowed for thermal equilibrium to be reached.

The first measurement is at atmospheric pressure to define the starting position of the bellows core. The pressure is then increased in steps of approximately 400 bar. After each pressure increment, a period of at least 3 minutes is allowed before the pressure chart reading, and the reference micrometer reading are recorded. This period is allowed for equilibrium to be reached after the heating caused by increasing the pressure. Readings are taken for increasing pressure, and then as the pressure is decreased by similar intervals back to atmospheric pressure.

At the end of a run the bellows are removed from the pressure vessel and are cleaned and dried. They are re-weighed and compared with the weight before measurement. This provides a check that liquid has not leaked from the bellows, or been drawn into it.

In order to calculate the density of a liquid under pressure from the measured change in volume the liquid density at atmospheric pressure is required. Liquid density is measured in a 25 cm^3 density bottle by the standard method. The volume of the density bottle was initially measured using mercury; at $30^{\circ}C$ ρ = 13.5218 g cm^{-3}, (American Institute of Physics Handbook, 1957).

6.1.6 Computation of results

To establish the change in volume of the test liquid in the bellows it is sufficient to know the position of the bellows core with respect to its original starting position at atmospheric pressure. Since the effective cross-sectional area of the bellows is known the change in volume may be readily found.

In mathematical terms the calculation of density is

$$\rho = \frac{\text{mass}}{\text{area} \times l_{corr}}$$

$$l_{corr} = l_{b\ell ws} - \Delta l$$

$$l_{b\ell ws} = \frac{\text{mass}}{\text{area} \times \rho_o} - \text{(bellows movement with respect to P = 0 position)}$$

$$\Delta l = (7.26\ l_{b\ell ws} + 1.23) \times 10^{-7} \times P \text{ cm} \qquad (6.8)$$

ρ = liquid density at pressure P (g cm^{-3})
mass = mass of test liquid (g)
area = cross-sectional area of bellows (4.000 cm^2)
l_{corr} = corrected bellows length (cm)
$l_{b\ell ws}$ = measured bellows length (cm)
ρ_o = liquid desntiy at zero gauge pressure (g cm^{-3})
Δl = correction term due to differential compressibilities (cm)
P = gauge pressure (bar).

A computer program was used to perform the density calculations. The input information required is as follows:

1 the mass of test liquid in the bellows,

2 the liquid density at atmospheric pressure, and

3 the reading of pressure from the Foxboro gauge on the high pressure apparatus along with the corresponding reference micrometer reading.

The fifth order equation which defines the bellows core position as a function of the reference micrometer reading (equation 6.1) is contained in the program with the pressure gauge calibration constant (14.67 lb/in^2 per bar) which converts the pressure readings into bar.

At each pressure the corresponding density, specific volume, and linear secant bulk modulus is computed and tabulated. The linear secant bulk modulus is approximately linear with pressure for liquids. Thus

$$\bar{K} = \frac{PV_o}{V_o - V} = K_o + mP \qquad (6.10)$$

where V_o equals the specific volume at atmospheric pressure. The subject of bulk moduli and density-pressure equations is fully discussed in section 6.3. The constants K_o and m are computed by a least-squares procedure thus giving an equation by which specific volume, or density, may be recalculated for a given pressure.

An example of the results computed from measurements on di-(2-ethylhexyl) phthalate is produced in Table 9.4. In the table correction terms are also shown. The linear secant bulk modulus is evaluated for this liquid as

$$\bar{K} = 14710 + 4.666 \times P. \qquad (6.11)$$

From this the specific volume is recalculated with an r.m.s. error of 0.0036 cm^3 g^{-1}.

The results of all density measurements are in chapter 9.

6.1.7 Error analysis

At a given pressure density is calculated from

$$\rho = \frac{\text{mass}}{\text{area} \times l_{corr}}.$$

By making specific volume V, the inverse of density, the subject of the equation and substituting the full expression for l_{corr} the volume can be

stated in terms of the parameters which are subject to uncertainties.

$$V = \frac{\text{area}}{\text{mass}}\left[\left(\frac{\text{mass}}{\text{area} \times \rho_o} - B\right)(1 - 3\varepsilon_b) - 0.5\, l_c(\varepsilon_b - \varepsilon_i)\right].$$

The overall effect upon V, of uncertainties in the parameters at 5 kbar is found by substitution of typical values, and then by a perturbation upon these values.

area = $4.000 - 0.001$ cm^2

mass = $14.000 + 0.0025$ g

ρ_o = $1.0000 - 0.0004$ g cm^{-3}

B = $0.4 - 0.000\ 85$ cm (bellows movement)

ε_b = $2.42 \times 10^{-7} - 3\%$ bar^{-1}

ε_i = $1.98 \times 10^{-7} + 5\%$ bar^{-1}

l_c = $5.588 - 0.0056$ cm.

With no errors, $V = 0.851\ 81$ cm^3 g^{-1}.

By arranging the errors so that they have a cumulative effect, $V = 0.854\ 12$ cm^3 g^{-1}, which corresponds to an error of 0.27 per cent. The probability that the errors on ε_b and ε_i are as large as 3 per cent and 5 per cent, and that they are in opposite directions is small. The uncertainty on the bellows movement, B, is taken as three times the r.m.s. error of the recalculated bellows position as a function of micrometer reading. The probability of all errors being cumulative is small also, and therefore the error of 0.28 per cent is pessimistic. Therefore a realistic estimate of the error in specific volume or density measurement is ±0.14 per cent at 5 kbar. At pressures of higher than 5 kbar the uncertainty will be greater and therefore by the above analysis a realistic value for the uncertainty in this region is ±0.25 per cent at worst.

6.2 Equations of Density as a Function of Pressure

It is desirable to describe the behaviour of liquid density under pressure in the simplest possible manner, that is, with as few constants as possible. In analysing liquid behaviour, for example in applying the free-volume concept to describe viscosity under pressure, density is required with minimum computation. It is also required for liquid model calculations, and to determine the buoyancy corrections applicable to all types of falling body viscometers.

The subject of liquid compressibility is a straightforward one which has unfortunately been obscured largely due to varying definitions of the bulk modulus. Hayward (1967) has presented a comprehensive survey of most equations used and has rationalised the subject.

6.2.1 Bulk moduli

i Tangent bulk modulus

$$K = -V \frac{dP}{dV}. \tag{6.12}$$

The tangent bulk modulus is the inverse of compressibility which is defined as the fractional volume change per unit change in pressure.

ii Secant bulk modulus

$$\bar{K} = \frac{V_o P}{V_o - V}. \tag{6.13}$$

This may be considered as the average bulk modulus over the range from 0 to P. The term V_o is the specific volume at atmospheric pressure (P = 0).

iii 'Mixed' bulk modulus

$$K' = -V_o \frac{dP}{dV}. \tag{6.14}$$

This is a hybrid between the two previous expressions.

6.2.2 The linear secant bulk modulus equation

When K, $\bar{K}$ of K' are plotted as a function of pressure they all are practically linear but becoming more curved at higher pressures. In terms of ease of calculation, $\bar{K}$ in equation 6.13 is most easily obtained.

Thus it is possible to obtain the following equation

$$\bar{K} = \frac{V_o P}{V_o - V} = K_o + mP \qquad (6.15)$$

K_o and m are constants and may be calculated with comparative ease from P-V data. This equation is referred to as the linear secant bulk modulus equation.

6.2.3 The Tait equation

This equation is derived from the mixed bulk modulus and is attributable to a misinterpretation of Tait's original expression (1888). The commonly used, but erroneous equation is derived from the identity:

$$K' = -V_o \frac{dP}{dV} = K_o + m_1 P. \qquad (6.16)$$

Unlike the linear secant bulk modulus, the mixed modulus, being a tangential gradient, cannot be evaluated directly.

Integrating equation 6.16 yields

$$\frac{V_o - V}{V_o} = C \log \frac{B + P}{B} \qquad (6.17)$$

where $C = 1/m_1$ and $B = K_o/m_1$. This is the spurious Tait equation now commonly used. Due to the non-linear form of equation 6.17 performing a least squares fit to obtain B and C is more difficult than finding K_o and m in equation 6.15. This is one disadvantage of the so-called Tait equation.

As pointed out by Hayward (1967), the equation propounded by Tait was actually the linear secant bulk modulus equation, expressed in reciprocal form.

6.2.4 Modified secant bulk modulus equation

Tamman (1907) introduced the equation

$$V = V_{\infty} + \frac{Ak}{k + p}. \tag{6.18}$$

This has intuitive appeal due to the physical significance of the first constant. As pressure tends towards infinity the specific volume of a liquid approaches a constant value asymptotically. This is V_{∞} in the equation. There are three constants in the equation, but by introducing V_o, the specific volume at zero pressure, any one of the constants may be eliminated. Thus by re-arranging equation 6.18 and eliminating V_{∞}

$$\bar{K} = \frac{V_o P}{V_o - V} = \frac{V_o k}{A} + \frac{V_o}{A} P. \tag{6.19}$$

This is in the form of equation 6.15 which therefore illustrates that equation 6.18 is an alternative form of the linear secant bulk modulus equation.

To facilitate manipulation it is proposed to express equation 6.18 in simpler form:

$$V = a + \frac{b}{k + p} \tag{6.20}$$

where $a = V_{\infty}$, $b = Ak$, and k remains unaltered.

6.2.5 Comparison of the Tait and secant modulus equations

In comparing the usefulness of density equations three main factors should be considered:

i The accuracy with which density or specific volume can be calculated from the equation - the primary objective.

ii The number of constants should be minimal for ease of derivation and reclaculation provided that this is compatible with (i).

iii The constants should, if possible, have physical significance.

The constants of the Tait equation, and the constants of equation 6.20 were found by least-squares procedures using a digital computer. The three liquids studied are n-pentadecane (PSU 532), 9(2-phenylethyl) heptadecane (PSU 87), for which data were obtained from the measurements of Cutler et al. (1958), and di(2-ethylhexyl) phthalate from the data for the 1953 ASME Report.

Table 6.2

Pressure-density equation constants

Liquid	Temp	1 Tait Eqn		2 Lin.Sec.Eqn		3 Modified Eqn			V_o
	(°C)	B	C	K_o	m	a	b	k	($cm^3\ g^{-1}$)
PSU 532	37.8	978.7	0.2058	11 420	4.4057	1.022	778	2592	1.3224
	60.0	874.9	0.2058	10 508	4.2321	1.031	792	2483	1.3499
	79.4	762.3	0.2058	9 745	3.8715	1.018	894	2517	1.3751
	98.9	678.3	0.2058	9 702	3.5000	0.996	1110	2772	1.4015
	115.0	607.8	0.2058	9 521	3.3013	0.986	1246	2884	1.4263
	135.0	533.6	0.2058	9 124	3.1550	0.982	1336	2892	1.4575
PSU 87	37.8	1313	0.2058	16 565	3.9496	0.8836	1258	4194	1.1847
	60.0	1168	0.2058	15 829	3.6813	0.8750	1408	4300	1.2054
	79.4	1037	0.2058	15 645	3.4092	0.8597	1648	4589	1.2243
	98.9	933	0.2058	15 124	3.2665	0.8547	1763	4630	1.2438
di(2-eh) phthalate	0.0	1573	0.2058	20 242	3.7898	0.7364	1410	5341	1.0005
	25.0	1521	0.2058	18 671	4.0291	0.7651	1172	4634	1.0190
	37.8	1424	0.2058	18 159	3.8463	0.7599	1263	4721	1.0290
	98.9	1021	0.2058	16 392	3.2370	0.7389	1688	5064	1.0790

1 Tait equation $$\frac{V_o - V}{V_o} = C \log \frac{B + P}{B} \qquad (6.17)$$

2 Linear secant equation $$\frac{V_o P}{V_o - V} = K_o + mP \qquad (6.15)$$

3 Modified secant equation $$V = a + \frac{b}{k + P} \qquad (6.20)$$

A tabulation of the constants for a range of temperatures are produced in Table 6.2. The constants of the linear secant bulk modulus equation are also produced, these being calculated from the constants of equation 6.20. The value of C in the Tait equation is reported by Cutler to be 0.2058 for a large number of hydrocarbons and independent of temperature. The values of C are reproduced in the table for the three liquids and are remarkably constant, none showing any deviation from 0.2058.

Table 6.3

Comparison of r.m.s. errors in specific volume and maximum percentage errors for the two equations

Liquid	Temp	Tait Eqn		Lin.Sec. Eqn		P_{max}
	(^{o}C)	r.m.s.	max %	r.m.s.	max %	(bar)
PSU 532	37.8	0.003	-0.04	0.0	-0.0	689
	60.0	0.0002	-0.04	0.0004	-0.06	1723
	79.4	0.0003	-0.04	0.0010	-0.14	2756
	98.9	0.0004	0.09	0.0022	0.37	4479
	115.0	0.0004	0.09	0.0032	0.61	5513
	135.0	0.0010	0.15	0.0046	0.93	6546
PSU 87	37.8	0.0003	-0.07	0.0007	0.09	4135
	60.0	0.0003	-0.05	0.0011	0.24	5513
	79.4	0.0013	-0.19	0.0018	0.45	6891
	98.9	0.0013	-0.19	0.0024	0.68	8269
di(2-eh)	0.0	0.0017	-0.28	0.0007	0.16	3154
phthalate	25.0	0.0009	0.26	0.0010	-0.25	5254
	37.8	0.0005	0.10	0.0008	0.15	6088
	98.9	0.0008	-0.17	0.0028	0.63	10 232

The accuracy of the two equations is compared in Table 6.3. The maximum errors as well as the r.m.s. errors in specific volume are listed. It is evident from the table that the Tait equation is more accurate than the modified equation in nearly every case. With both equations the errors become greater with rising temperature because the pressure ranges are greater at higher temperatures, as shown in the table by the P_{max} figures. This confirms a previous statement which is that the bulk modulus becomes more non-linear at higher pressures.

On closer examination the Tait equation,

$$\frac{V_o - V}{V_o} = C \log \frac{B + P}{B}, \qquad (6.17)$$

is not consistent with physical behaviour at elevated pressures because as pressure tends to infinity, the equation forces V towards a large negative quantity. Thus the Tait equation is not physically realistic in its prediction of behaviour and should not therefore be used for extrapolation.

The modified linear secant bulk modulus equation (Tamman's equation) has constants which do comply with physical behaviour in that the volume tends asymptotically to a constant specific volume a ($= V_\infty$). This equation may therefore be used for extrapolation with more confidence than the Tait equation, but this should be done with caution beyond a thousand bars or so because of the increasing curvature, although slight, of the secant bulk modulus as pressure increases. For an improved fit, and hence more reliable prediction, a second or higher order polynomial may be used, of the form

$$\bar{K} = K_o + mP + nP^2 + \ldots \qquad (6.21)$$

In conclusion the linear secant bulk modulus equation is preferable because it is accurate (r.m.s. error in specific volume is not greater than 0.0046 $cm^3\ g^{-1}$ in the data sampled), and it has only two disposable constants both of which may be readily found. The equation may also, with care, be used for limited extrapolation.

CHAPTER 7

HIGH PRESSURE SYSTEMS

List of Figures

List of Tables

CHAPTER 7

HIGH PRESSURE SYSTEMS

7.1 Introduction

In this work three different pressure systems were used. For preliminary work a 1000 bar system was used. A 3000 bar system was also built, and measurements at very high pressures were made in apparatus capable of 200 000 lb in^{-2} (14 000 bar).

7.2 1000 Bar System

The general arrangement of the system is shown in Fig. 7.1. The pressure vessel stands 14 inches high overall and has an effective inner working space of 8 by 2 inches diameter. Pressure is transmitted by a hydraulic hand pump using aircraft mineral hydraulic oil as the working fluid. The vessel sits upon two mild steel stubs which are firmly attached to the base of the constant temperature bath. The top seal of the pressure vessel can be unscrewed while the vessel is sitting in the tank, thus avoiding the considerable inconvenience of removing it in order to undo the top seal.

The fluid in the constant temperature bath is Shellsol T (Shell Chemical Company). It is an aliphatic hydrocarbon solvent of low vapour pressure and is suitable for an open bath. A temperature of $30^{\circ}C \pm 0.1$ is maintained by a 750 W heater operated by a Sunvic thermal relay with a mercury-in-glass contact thermometer. An extra heater is used to raise the bath temperature initially.

7.2.1 Closure seals

A drawing in Fig. 7.2 shows the pressure vessel seal and the means whereby electrical leads are introduced. The closure screws into the vessel body and a seal is effected by an O-ring which rests on a smooth seat, and is held by a circular groove in the closure. The closure has an axial hole

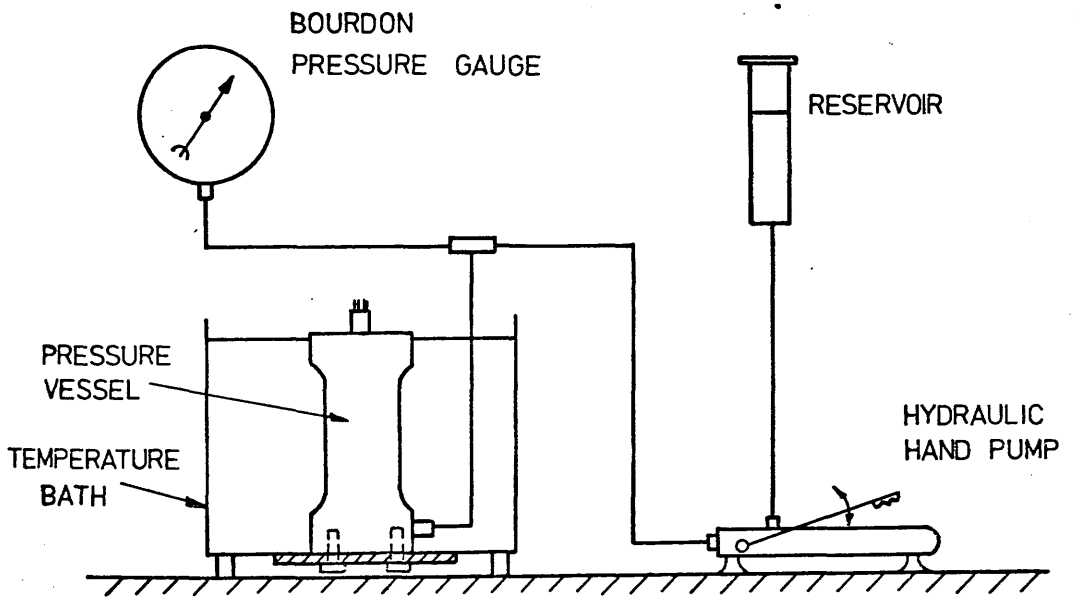

FIG 7.1 1000 bar pressure system

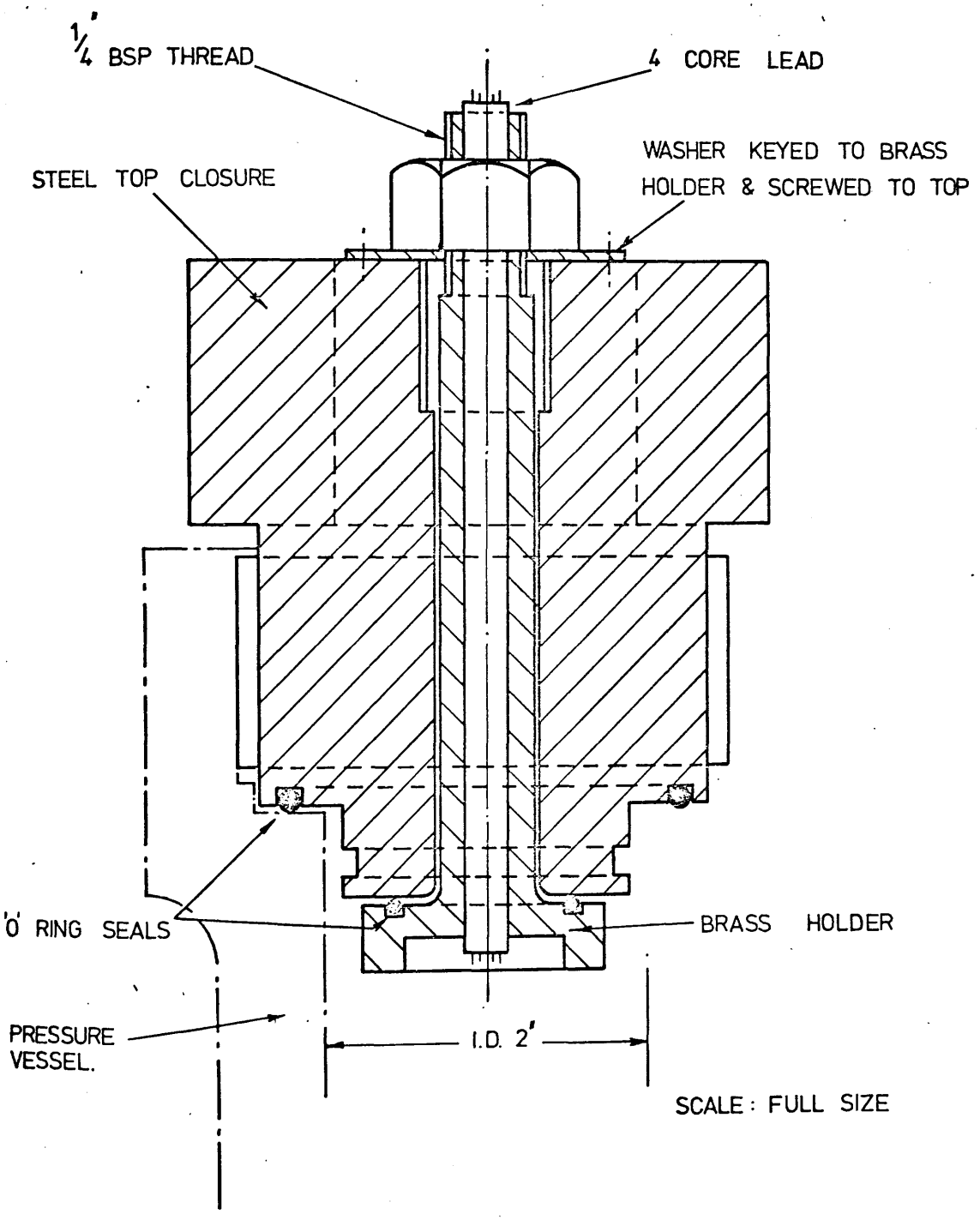

FIG 7.2 Pressure seals for 1000 bar vessel.

through which the leads are taken in a brass holder which is sealed by a second O-ring as shown. A copper sheathed four lead Pyrotenax thermocouple cable is soldered along its entire length into the holder. Both ends of the cable are sealed with epoxy resin to prevent moisture or pressurising fluid from entering the magnesium oxide insulation.

After connecting the viscometer or densimeter to the leads of the brass holder, it is lowered into the pressure vessel. The steel closure is then placed over the brass holder and tightened without rotating the holder, to avoid damage to the connecting wires. The holder is then raised, keyed by a washer attached to the closure, but before tightening the holding nut the pressure transmitting fluid is pumped to displace any remaining air in the vessel.

The O-rings, of nitrile rubber, are as follows:

	Edwards No	Walker No	BS No*	i.d.	Section
Pressure vessel	VOR 1161	50-228	-	2.25 in	0.139 in
Brass holder	VOR 0212	50-212	OS 17	0.859 in	0.139 in

*British Standard, BS 1806 (1951). In 1969 a new standard was published, BS 4518, after all design and manufacture of apparatus had been completed. The later O-ring standard specifications differ from the earlier ones, and consequently none of the rings used is now standard, but they are still manufactured.

7.2.2 Pressure measurements and calibration

A Bourdon type pressure gauge, graduated at intervals of 50 atmospheres from 0 to 2000 atmospheres is used. The gauge was calibrated, and carries a National Physical Laboratory certificate. The gauge requires to be tapped vigorously before each observation.

7.3 3000 Bar System

The pressure vessel has an effective working space of 8 by 1½-inch diameter. Like the 1000 bar apparatus, pressure is produced by an hydraulic hand pump. Steel pressure tubing (0.0625 in bore, 0.25 in o.d.) is used throughout and fine control of pressure decrease is effected by a release valve.

The vessel is attached to the base of the constant temperature bath thus enabling the top seal to be unscrewed in situ. The bath is controlled in a similar manner to the 1000 bar constant temperature bath. It has two 1 kW heaters one of which is regulated by an auto-transformer so that the heating period is made roughly equal to the off period; this improves stability. The bath is stirred by a motor-driven paddle. As a safety measure there is a normally closed thermally-activated switch which isolates all heaters in the event of overheating.

7.3.1 Closure seals

The pressure vessel is sealed with a screwed steel closure, the electrical connections being through an axial brass holder. As with the 1000 bar system the seals are of the grooved O-ring type. The closure is shown by the photograph in Fig. 7.3 where the separate components are clearly seen. In this arrangement the thermocouple cable is soldered into the lower cylindrical section of the holder which is 2.5 inches long.

The nitrile rubber O-rings are as follows:

	Edwards No	Walker No	i.d.	Section
Pressure vessel	VOR 1149	50-224	1.75 in	0.139 in
Brass holder	VOR 1130	50-118	0.875 in	0.103 in

7.3.2 Pressure measurement and calibration

Pressure is measured by a Budenberg gauge, graduated at intervals of 50 atmospheres from 0 to 3000 atmospheres. The gauge was calibrated in the laboratory against a deadweight tester which allows pressure to be measured to within ±5 bar (1 atm = 1.013 25 bar, exactly).

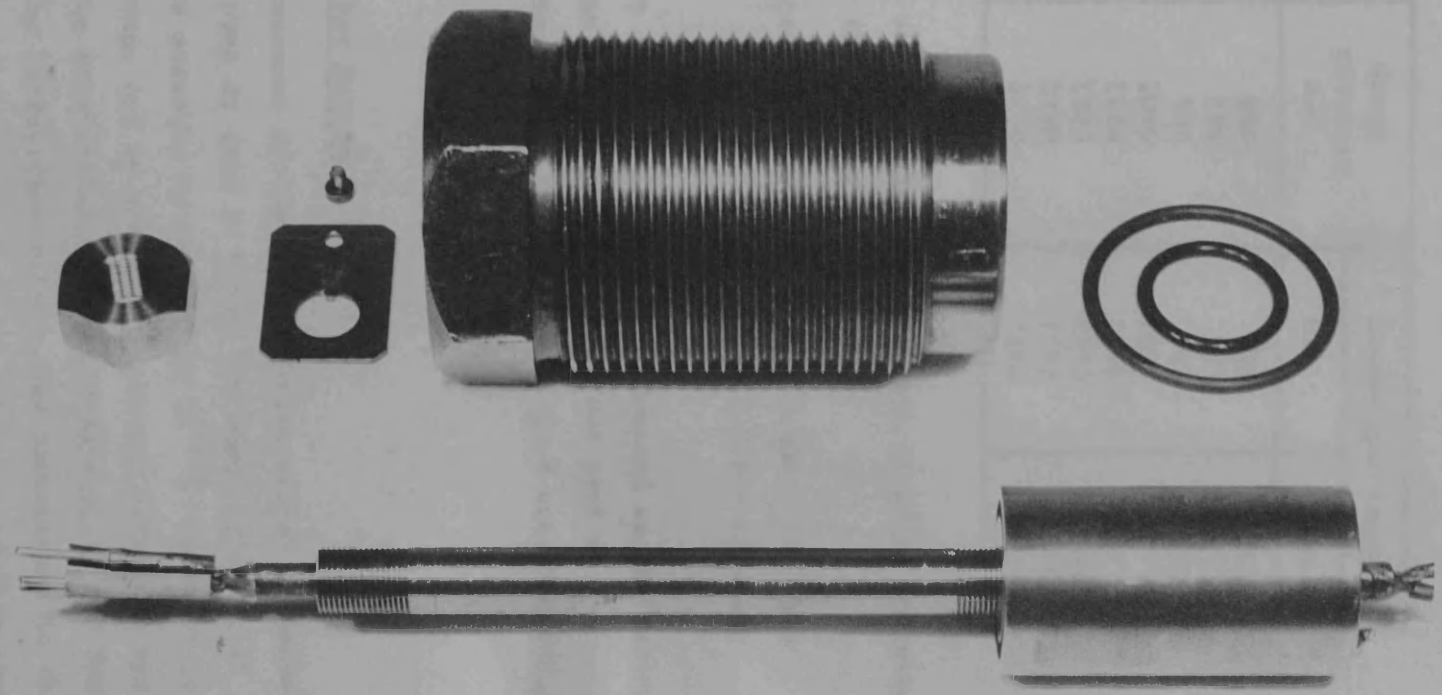

FIG. 7.3. CLOSURE FOR 3000 BAR PRESSURE VESSEL

Table 7.1

Budenberg pressure gauge calibration

Gauge pressure atm	Deadweight tester	
	bar	atm
800	793	783
896	893	881
996	993	980
1090	1093	1079
1186	1193	1177
1285	1293	1276
1780	1793	1770
2270	2293	2263

By least-squares analysis the true pressure is given in terms of the gauge reading by the following

$$\text{Actual pressure} = \text{gauge} \times 1.006 - 19.3 \text{ atm}$$
$$= \text{gauge} \times 1.019 - 19.6 \text{ bar}$$

For the above fit the gauge reading was treated as the dependent variable. The average percentage deviation is 0.18 per cent with a maximum error of 3.3 atm. The linearity is therefore very good over the range of calibration.

7.4 14 000 Bar System

The general arrangement of the high pressure system is shown in Fig. 7.4. A hand operated pump is used to prime the upper cylinder of a 100:1 ratio intensifier. Low pressure up to 2000 lb in^{-2} (~ 140 bar) is generated by a motor driven pump, and by means of a control valve the hydraulic fluid is directed to the intensifier. Thus pressure up to 200 000 (~ 14 000 bar) is obtained at the intensifier output, and transmitted to the pressure vessel through a uni-directional check valve. A similar check valve is used to isolate the low pressure side. A release valve is fitted in the high pressure side to allow fine control of pressure decrease.

The pressure vessel has thick walls to withstand the very high pressure, having an outside diameter of 10 inches and an effective working space of

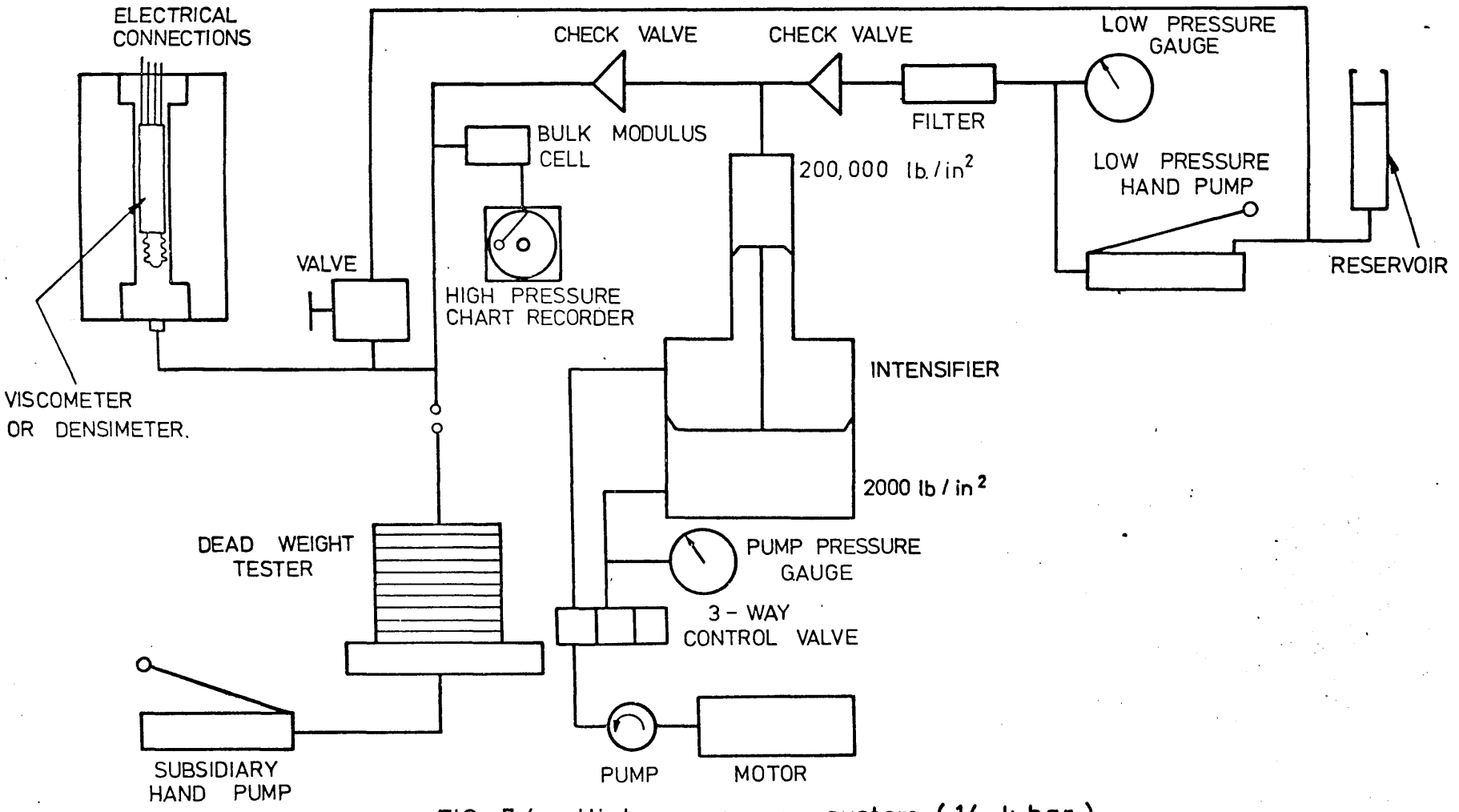

FIG 7.4 High pressure system (14 k bar)

1.25 inch diameter by 8 inches long. It sits in a cylindrical tank, containing a silicone fluid (ICI Fluid F 111/20) which is maintained at $30^{\circ}C \pm 0.1^{\circ}C$. The pressure transmitting fluid is an equal parts mixture of Aeroshell Fluid 4 and petroleum ether.

A full description of the entire system, and the procedure for operating it is described in the PhD thesis of W C Pursley (1968).

7.4.1 Pressure measurement and calibration

Pressure is recorded on a Foxboro chart recorder (0 to 200 000 lb in^{-2}) which is driven by a 'bulk modulus' cell transducer. It was calibrated by a deadweight tester (Budenberg Co Ltd). Unfortunately, the tester can be used only for calibration purposes, due to the unavoidable leak of pressure transmitting fluid past the top piston. It would have been preferable to use a resistance type measuring device such as a manganin coil which is capable of higher accuracy, but this was impracticable because all the electrical leads from the pressure vessel are required for the viscometer or densimeter.

The so-called bulk modulus cell consists of a steel stem, the movement of which is a function of the applied pressure. The cell stem moves 0.01-inch for a pressure of 200 000 lb in^{-2}. This movement by means of a lever and bellows system, modulates a compressed air supply, delivering to a pneumatic receiver in the chart recorder a pressure of between 3 and 15 lb in^{-2} in proportion to the pressure in the high pressure system. The circular chart of the recorder is rotated by a clock and is graduated in steps of 2000 lb in^{-2} from 0 to 200 000 lb in^{-2}, and can be read with an error of not greater than ± 400 lb in^{-2} (~ 25 bar). The linearity of the response of the pneumatic receiver was checked by applying direct air pressure of 3 to 15 lb in^{-2} and reading the corresponding chart pressure. In Fig. 7.5 there is a graph showing the excellent linear response of the receiver, from these experimental measurements.

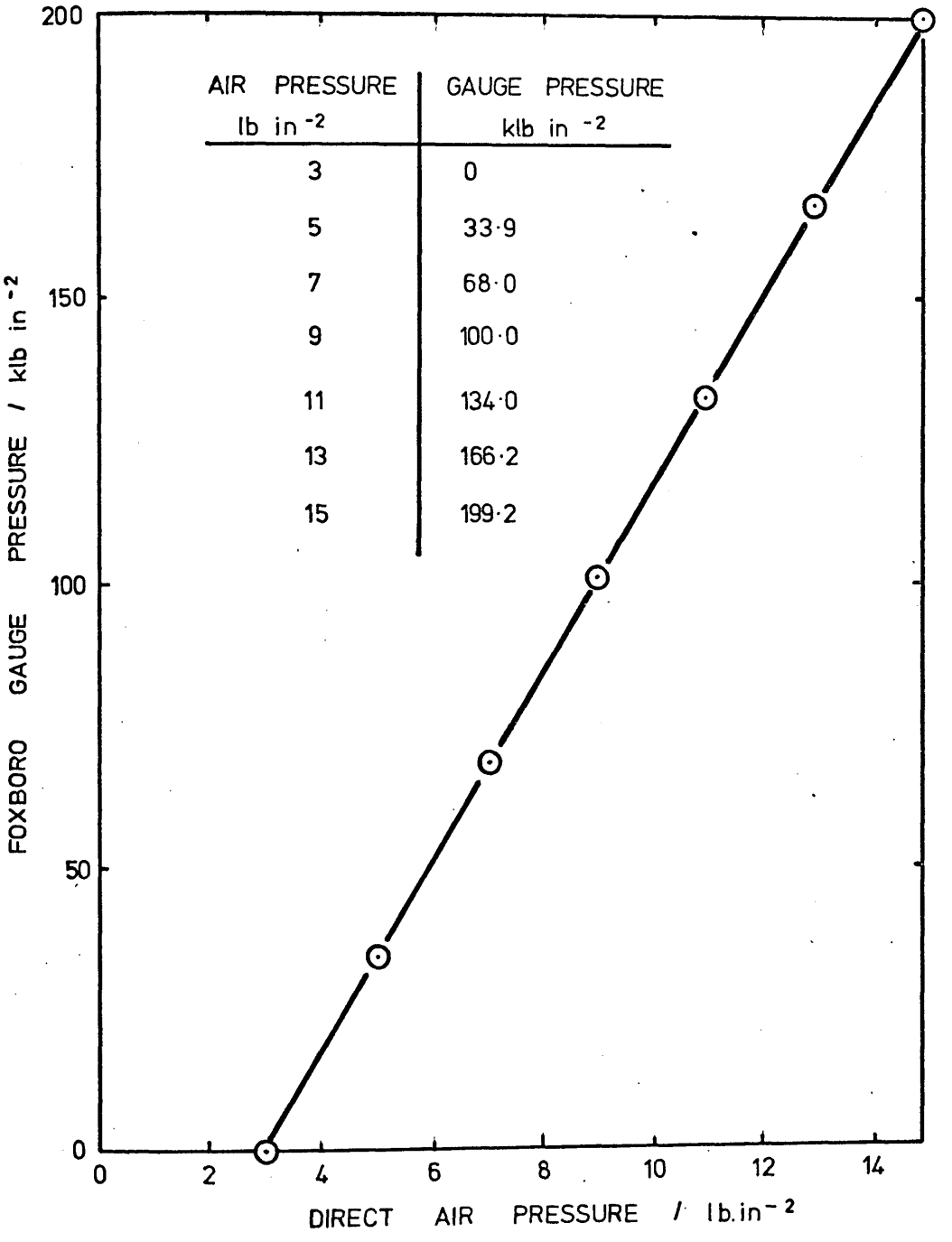

FIG 7.5 Foxboro gauge response

The chart recorder was calibrated with the deadweight tester to its limit of 8 kbar. Due to the slow leak of fluid past the top piston of the tester a very slight loss of accuracy is incurred. Calibration measurements, at intervals of 500 bar, were plotted on a large scale and straight line drawn through all the points, and no point was found to deviate by more than the uncertainty in reading the chart recorder. The gradient was found by the method of least squares to be 14.67 lb in^{-2}/bar. Although it was not possible to calibrate beyond 8 kbar the validity of a linear extrapolation to 14 kbar can be safely assumed, because there is no systematic deviation from linearity up to 8 kbar, and the linearity of the receiver is established over the entire range.

Pressure = chart pressure (lb in^{-2})/14.67 bar (±25 bar).

7.5 Units of Pressure

Many different units of pressure are commonly used, as illustrated by the equipment described in this chapter: gauges graduated in atmospheres, the chart recorder graduated in lb in^{-2}, and the deadweight tester with the bar unit.

Although the SI and MKS unit of pressure is pascal (Pa = N/m^2 = 10^{-5} bar) the practical unit is the bar.

Table 7.2

Conversion table for pressure

	atm	kgf/cm^2	lbf/in^2	bar	MN/m^2
1 atmosphere =	1	1.033 23	14.6959	1.013 25	0.101 325
1 kgf/cm^2 =	0.967 841	1	14.2233	0.980 665	0.098 0665
10 lbf/in^2 =	0.680 460	0.703 070	10	0.689 476	0.068 9476
1 bar =	0.986 923	1.019 72	14.5038	1	0.1
1 MN/m^2 =	9.869 23	10.1972	145.038	10	1

Factors underlined are exact.

In some European countries the kfg/cm^2 is called the Technische atmosphare (at) which can easily be mistaken for the atmosphere (atm).

CHAPTER 8

RESULTS: VISCOSITY UNDER PRESSURE

List of Figures

Page

List of Tables

CHAPTER 8

RESULTS: VISCOSITY UNDER PRESSURE

8.1 Liquids Studied

tri-m-tolyl phosphate

1000 cSt polydimethyl siloxane (MS 200)

bis (m-(m-phenoxy phenoxy)-phenyl)ether (Monsanto OS 138)

castor oil (0311 First) Supplied by Department of Mechanical Engineering, The Queen's University, Belfast

di-n-butyl phthalate

di-(2-ethylhexyl) phthalate.

8.2 Experimental Results of Viscosity Under Pressure

Measurements of viscosity were made for all the above liquids at $30.0 \pm 0.1^{\circ}C$ according to the procedure described in chapter 4. The densities of the test liquids at the same temperature and pressures are given in the following chapter. Two corrections were applied:

a The correction for the change of sinker and tube dimensions under pressure. This correction is applied to the fall time; it increases with increase in pressure, and for sinker 1 is about 1 per cent at 3 kbar, the maximum pressure used for this sinker. For sinker 2 this correction is much less, being about 0.1 per cent at 7 kbar. This correction is fully described in section 2.4.2.

b A correction is applied for the change in density of the sinker. The relative decrease in volume of the mild steel sinker is $3 \times 1.98 \times 10^{-7}$ per bar (c.f. section 2.4.1), and this corresponds to a correction of 0.2 per cent at 7 kbar.

Dynamic viscosity is calculated by evaluating the following expression

$$\eta = KT(\rho_1 - \rho_2),$$

where K = viscometer constant,

T = corrected fall time,

ρ_1 = sinker density, corrected for compression, and

ρ_2 = liquid density under pressure.

8.2.1 Tri-m-tolyl phosphate

This liquid was measured in the 3 kbar pressure vessel with sinker 1. At 1.52 kbar the viscosity value is slightly above the calibration range, and therefore may be less accurate. The liquid density was estimated by J D Isdale (1974) with an error of not greater than ± 2 per cent. Experimental density measurements were not made for tri-m-tolyl phosphate because it was considered to be less important than the other liquids in the programme of study.

The viscosity results are contained in Table 8.1, and plotted in Fig. 8.1.

Table 8.1

Measured Viscosity of Tri-m-tolyl phosphate at 30°C

Gauge pressure		Fall time T/second	Corrected T	ρ_1/g cm^{-3} compress. corrected	ρ_2/g cm^{-3}	η /cP
atm	bar					
0	0	448.4	448.4	7.823	1.1675	42.1
500	507	1284	1282	7.824	1.186	120.1
1000	1013	3931	3916	7.825	1.202	366
1500	1520	13,466	13,390	7.826	1.216	1250*

K = 0.014 11 (sinker 1) Measurements in 3 kbar apparatus

*Slightly above calibration range

8.2.2 1000 cSt polydimethyl siloxane

Measurements were made in the 3 kbar pressure vessel with sinker 2. Two sets of measurements were made on the same sample.

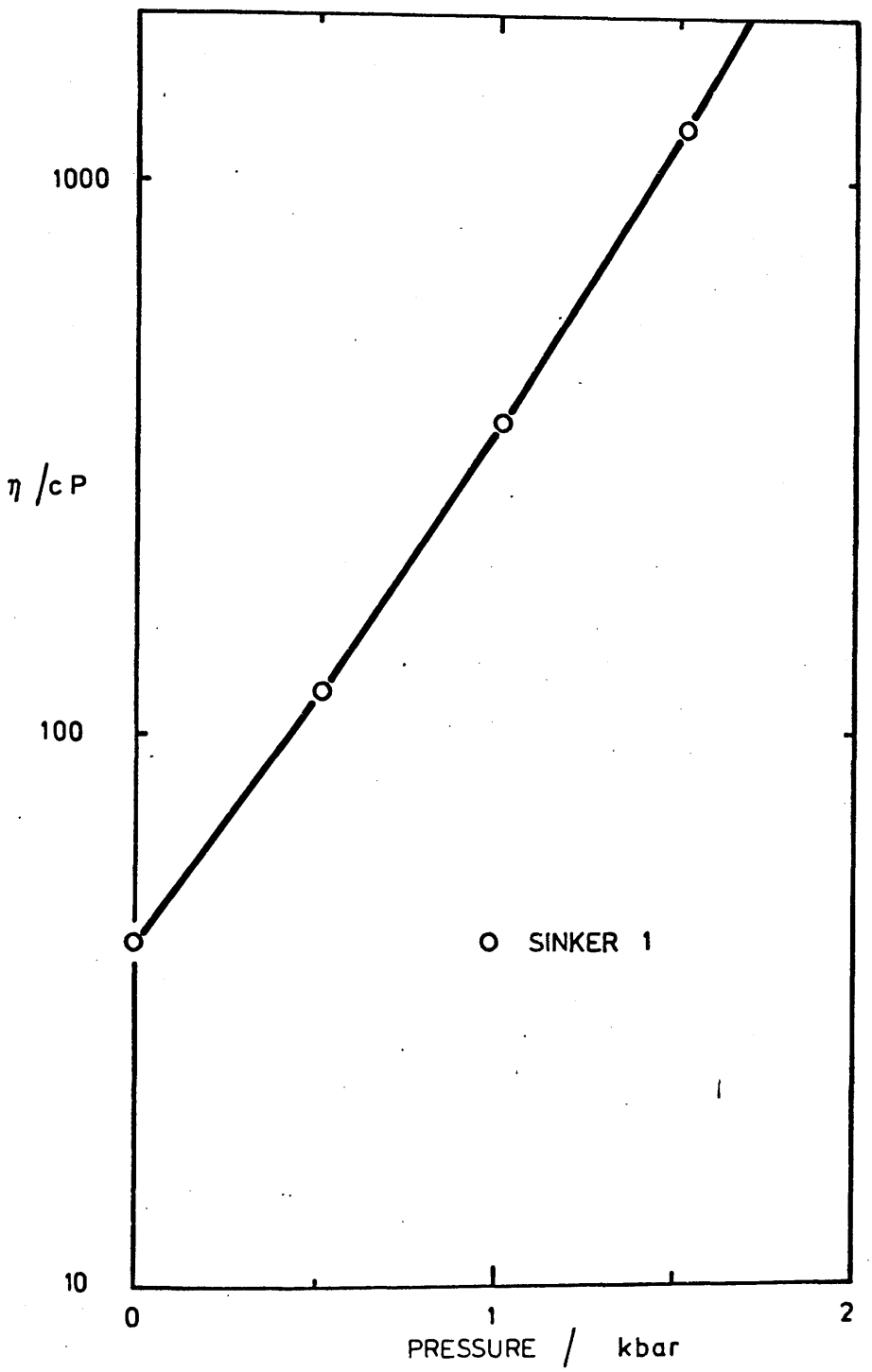

FIG 8.1 Measured viscosity of tri-m-tolyl phosphate at 30° C.

Table 8.2

Measured viscosity of 1000 cSt siloxane at 30°C

Gauge pressure		Fall time T/second	Corrected T	ρ_1/g cm^{-3} compress. corrected	ρ_2/g cm^{-3}	η/cP
atm	bar					
0	0	20.95	20.95	7.805	0.965	904.5
200	203	31.0	31.0	7.805	1.006_5	1330
500	507	51.0	51.0	7.806	1.032_5	2180
700	709	68.1	68.1	7.807	1.046	2910
900	912	88.0	88.0	7.807	1.059	3750
1300	1317	148.5	148.5	7.808	1.082	6300
1600	1621	213.1	213.0	7.809	1.097_5	9020
0	0	20.96	20.96	7.805	0.965	904.9
1000	1013	102.0	102.0	7.807	1.065	4340
1300	1317	148.9	148.9	7.808	1.082	6320
1700	1723	237.1	237.0	7.809	1.102	10000
1140	1155	120.0	120.0	7.808	1.073	5100

K = 6.3119 (sinker 2) Measurements in 3 kbar apparatus

The curve of log η as a function of pressure is shown in Fig. 8.2.

8.2.3 Bis (m-(m-phenoxy phenoxy)-phenyl) ether (OS 138)

This liquid has a comparatively high viscosity at atmospheric pressure, 7951 cP. Measurements were made using sinker 2 in the 3 kbar apparatus. The results in Table 8.3 show that at 405 bar the viscosity of the sample exceeds the range for which it was practicable to establish linearity for this sinker, and therefore the viscosities at this pressure and at 507 bar may be less accurate.

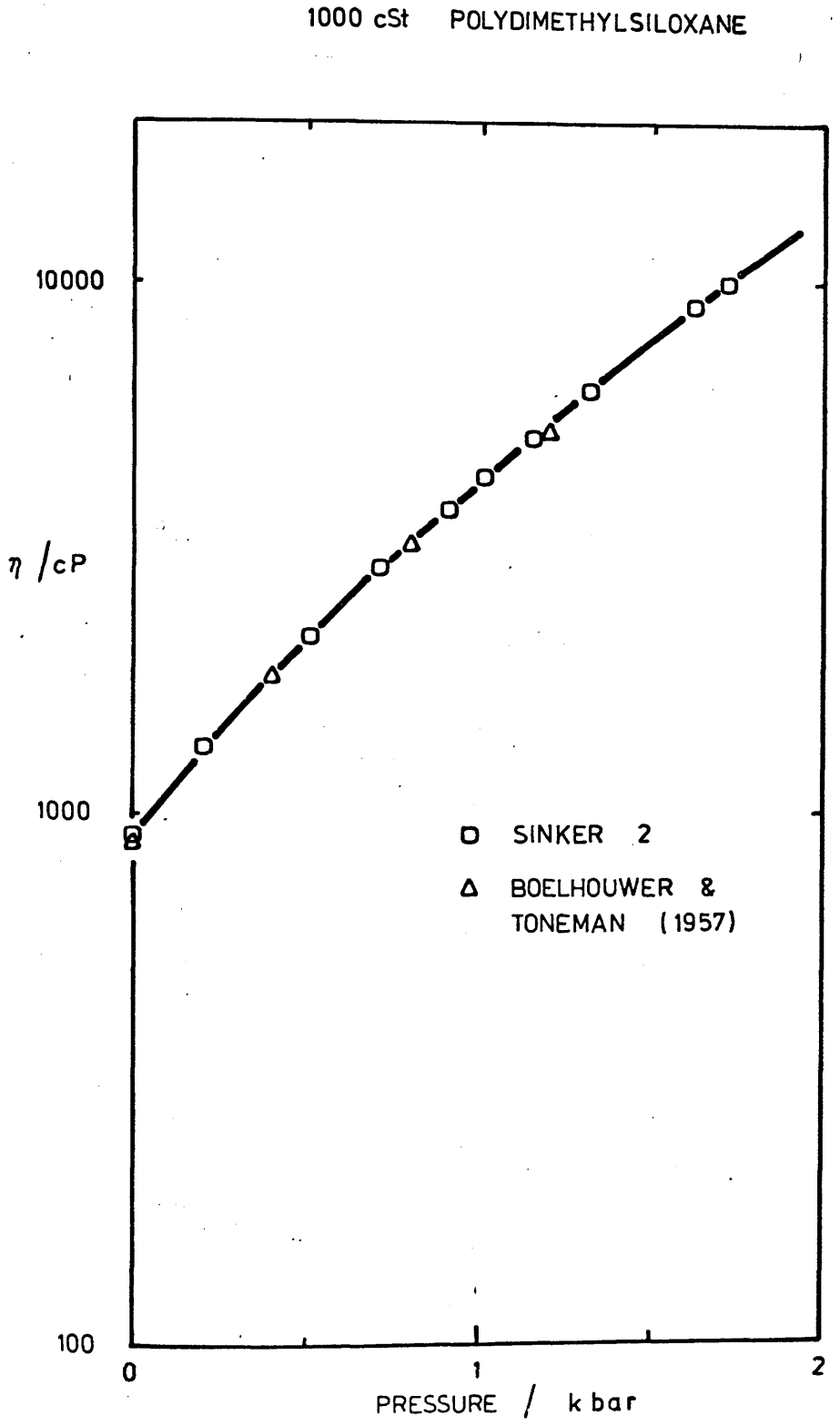

FIG 8.2 Measured viscosity of 1000 cSt siloxane at 30°C

Table 8.3

Measured viscosity of OS 138 at 30°C

Gauge pressure		Fall time T/second	Corrected T	ρ_1/g cm^{-3} compress. corrected	ρ_2/g cm^{-3}	η/cP
atm	bar					
0	0	190.7	190.7	7.805	1.205	7,944
100	101	348	348	7.805	1.211	14,500
180	182	597	597	7.805	1.215_5	24,800
200	203	683	683	7.805	1.216_5	28,400
300	304	1402	1402	7.806	1.221	58,300
400	405	2982	2982	7.806	1.225	124,000*
500	507	6260	6260	7.806	1.229	260,000*

K = 6.3119 (sinker 2) Measurement in 3 kbar apparatus

*Measurements outwith range of calibration

Two unusual features are evident in Fig. 8.3 where log η is plotted as a function of pressure. Firstly, the curve is convex towards the pressure axis whereas most liquids are concave. This is attributable to entanglement of the comparatively complex OS 138 molecules. Secondly, the viscosity of this liquid is more sensitive to pressure than any of the other liquids measured. For OS 138 viscosity increases tenfold during the first 350 bar. For the same increase in viscosity di-n-butyl phthalate and 1000 cSt siloxane require pressures of 1750 bar and 1620 bar respectively.

8.2.4 Castor oil

Two sets of measurements were made, the first in the 14 kbar pressure vessel, the second in the 3 kbar vessel. Both measurements were made using sinker 2, and a fresh sample of oil was used in each case.

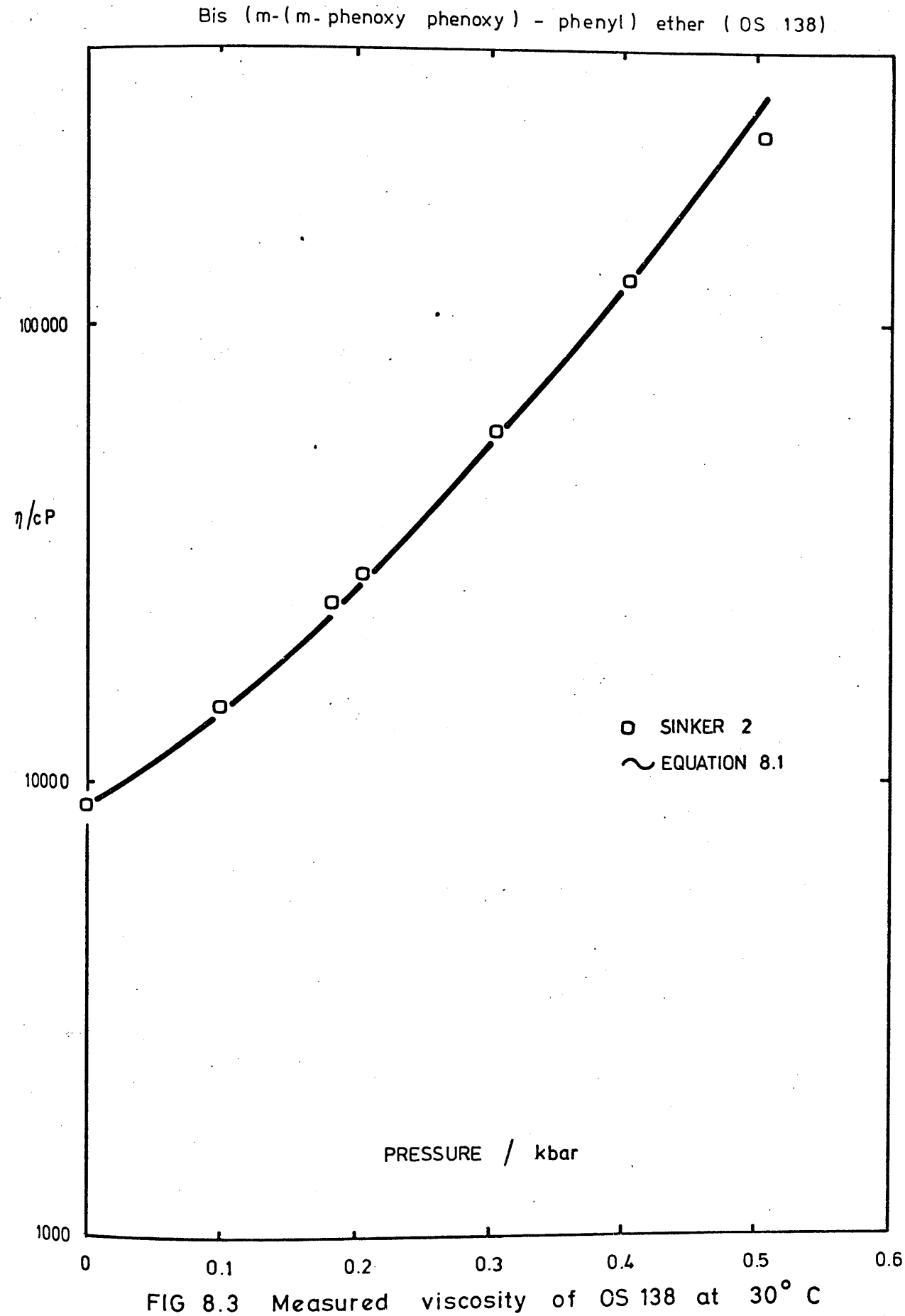

FIG 8.3 Measured viscosity of OS 138 at 30° C

Table 8.4

Measured viscosity of castor oil at 30°C

Gauge pressure		Fall time T/second	Corrected T	ρ_1/g cm^{-3} compress. corrected	ρ_2/g cm^{-3}	η/cP
atm	bar					
-	0	11.31	11.31	7.805	0.9527	489
-	1300	78.34	78.32	7.808	1.013	3,360
-	2740	461.9	461.7	7.811	1.051_5	19,700
-	2730	453.4	453.2	7.811	1.051_5	19,300
-	3410	972.0	971.5	7.813	1.067	41,400
-	4040	1960	1959	7.814	1.081	83,200
-	1490	99.2	99.2	7.808	1.019_5	4,250
0	0	11.61	11.61	7.805	0.9527	502
200	203	16.39	16.39	7.805	0.968	707
510	516	27.52	27.52	7.806	0.983	1,190
510	516	27.23	27.23	7.806	0.983	1,170
700	709	36.30	36.30	7.807	0.991	1,560
1000	1012	55.68	55.67	7.807	1.002_5	2,390

K = 6.3119 (sinker 2)

First group of measurements in 14 kbar apparatus, second group in 3 kbar apparatus

Measurements cover the range 500 cP to 83,200 cP, the latter viscosity corresponding to a pressure of just over 4 kbar. The variation of viscosity with pressure is shown in Fig. 8.4.

8.2.5 Di-n-butyl phthalate

Measurements were made on this liquid using sinker 1 in the 3 kbar apparatus, and sinker 2 in the 14 kbar apparatus. The highest pressure reached was 7.1 kbar, and the range of viscosity measured is from 13.4 cP to 74,950 cP.

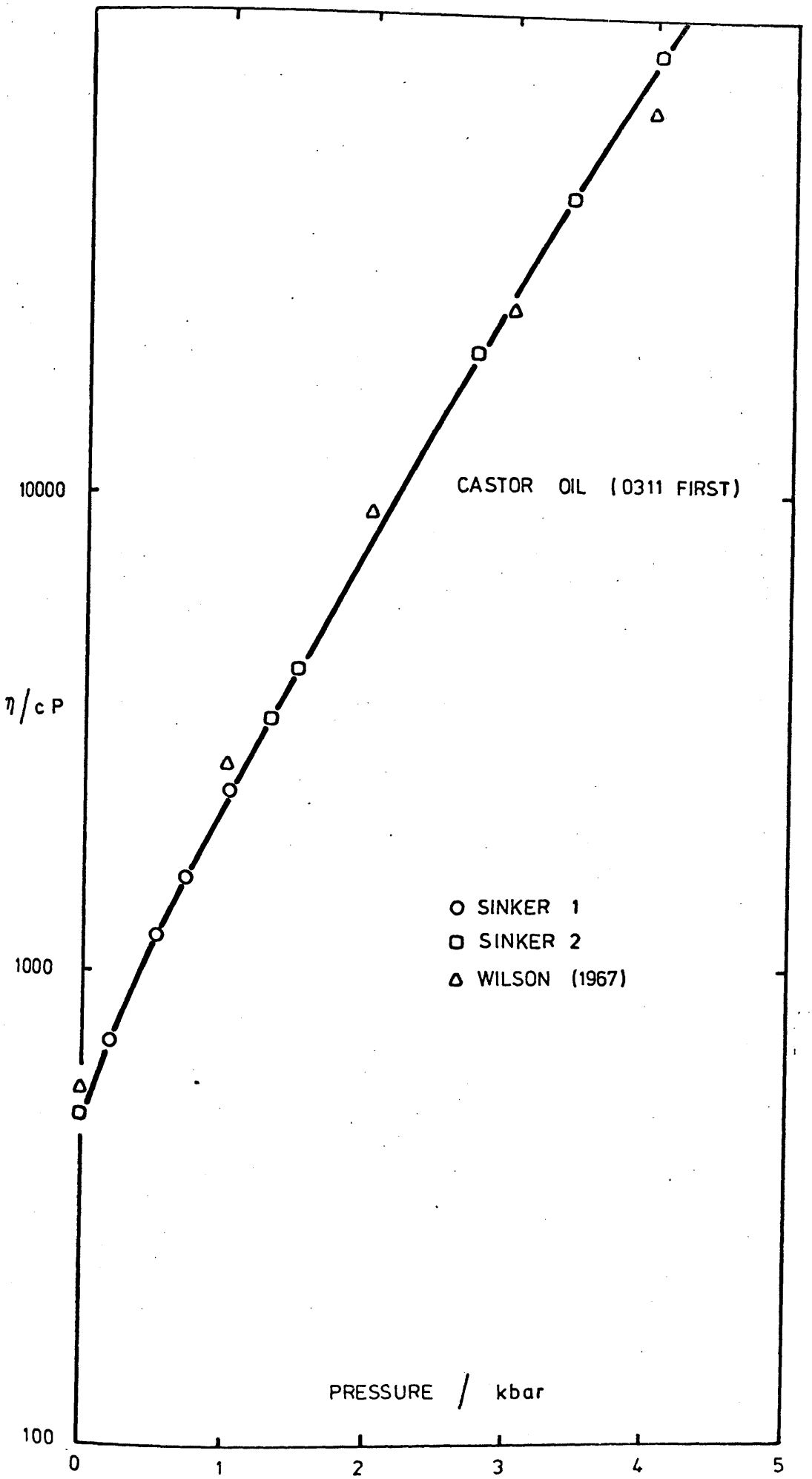

FIG 8.4 Measured viscosity of castor oil at 30° C

Table 8.5

Measured viscosity of di-n-butyl phthalate at 30°C

Gauge pressure		Fall time T/second	Corrected T	ρ_1/g cm^{-3} compress. corrected	ρ_2/g cm^{-3}	η/cP
atm	bar					
-	0	133.5	133.5	7.823	1.0371	13.36
-	532	285	284	7.824	1.067	28.3
-	1140	673	671	7.826	1.095	66.6
-	1760	1416	1407	7.827	1.117	139
-	2300	2796	2772	7.828	1.133	274
-	3170	8240	8144	7.830	1.156	802

K = 0.014 748 (sinker 1) Measurements made in 14 kbar apparatus

Gauge pressure		Fall time T/second	Corrected T	ρ_1/g cm^{-3} compress. corrected	ρ_2/g cm^{-3}	η/cP
atm	bar					
-	3070	16.5	16.5	7.812	1.153	694
-	4090	51.0	50.95	7.814	1.178	2,130
-	4430	77.5	77.4	7.815	1.185	3,240
-	5070	160	159.8	7.817	1.197	6,680
-	5860	387	386	7.818	1.210	16,100
-	6400	734	733	7.820	1.218	30,500
-	7100	1804	1801	7.821	1.227_5	74,950

K = 6.3119 (sinker 2) Measurements made in 14 kbar apparatus

The viscometer tube was replaced due to its being distorted when a lifting coil overheated and had to be recalibrated. The new value for K was obtained from a two point calibration with this liquid and di-(2-ethylhexyl) phthalate. It has already been argued (c.f. section 4.8) that a sinker with a proven linear calibration need not be recalibrated over its entire viscosity range.

The shape of the log η as a function pressure curve for di-n-butyl phthalate, Fig. 8.5, is unusual in that it concaves towards the pressure axis but passes through a gentle inflection to become convex at higher pressures. This type of behaviour has, however, been reported earlier, particularly in the ASME Report (1957), and by Bridgman (1926).

The curve also shows an overlap of measurements with the two sinkers,

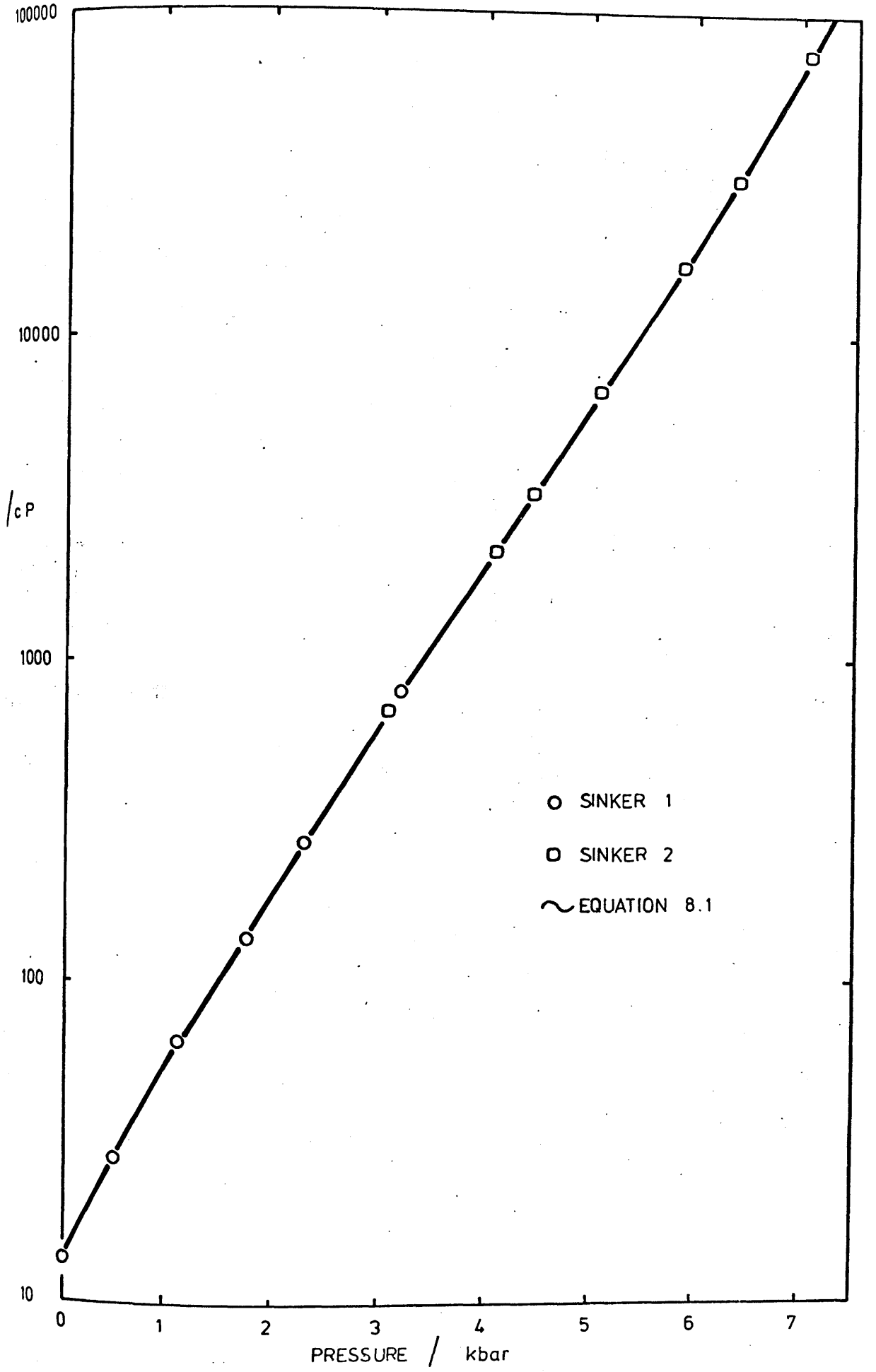

FIG 8.5 Measured viscosity of di-n-butyl phthalate at 30°C

and it is seen that the agreement is excellent thus giving further validity to both these measurements and to the calibration method.

8.2.6 Di-(2-ethylhexyl) phthalate

Measurements on this liquid were made using sinker 1 in the 3 kbar pressure vessel and sinker 2 in the 14 kbar vessel, both at 30°C.

Table 8.6

Measured viscosity of di-(2-ethylhexyl) phthalate

Gauge pressure		Fall time T/second	Corrected T	ρ_1/g cm^{-3} compress. corrected	ρ_2/g cm^{-3}	η/cP
atm	bar					
0	0	429.6	429.6	7.823	0.976	43.4
200	203	660.4	659.9	7.823	0.989	66.5
400	405	1011	1009.5	7.824	1.000	102
550	557	1361	1358	7.824	1.007	137
800	811	2156	2150	7.825	1.018	216
1000	1013	3143	3131	7.825	1.027	314
1300	1317	5468	5441	7.826	1.037	545
1550	1571	8233	8185	7.827	1.046	819

K = 0.014 748 (sinker 1) Measurements made in 3kbar apparatus

Gauge pressure		Fall time T/second	Corrected T	ρ_1/g cm^{-3} compress. corrected	ρ_2/g cm^{-3}	η/cP
atm	bar					
-	2410	68.0	68.0	7.811	1.071	3,495
-	2940	152.3	152.2	7.812	1.085	7,810
-	3820	536	535.5	7.814	1.105	27,400
-	4050	751	750	7.814	1.109	38,400
-	4770	2100	2097	7.816	1.125	107,000
-	4850	2310	2307	7.816	1.126	118,000*
-	5390	5020	5013	7.817	1.136	255,000*
-	5500	5850	5842	7.818	1.138	298,000*

K = 7.6266 (sinker 2) Measurements made in 14 kbar apparatus

*Beyond calibration range

In the second set of measurements with sinker 2, the fall times were outwith the range of calibration for this sinker, that is, beyond the range for which linearity has been experimentally confirmed. These

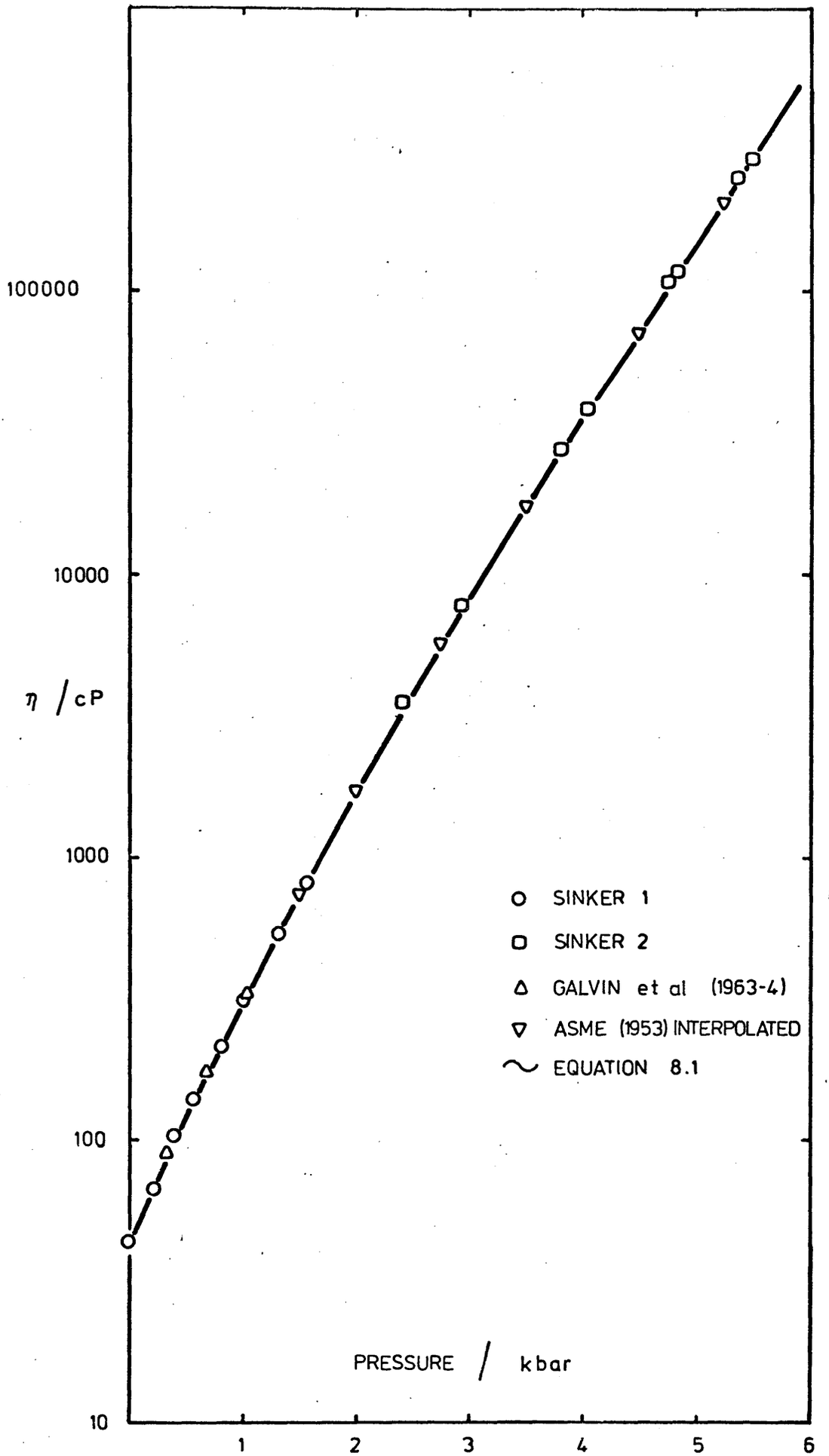

FIG 8.6 Viscosity of di-(2-ethylhexyl) phthalate at 30° C

points may therefore be less precise than the rest of the data. The shape of the log η curve as a function of pressure in Fig. 8.6 is concave towards the pressure axis.

8.3 Assessment of Accuracy

Viscosity is calculated from the calibration equation

$$\eta = KT(\rho_1 - \rho_2). \qquad (2.43)$$

By the Law of Propagation of Errors, the variance of viscosity is given by

$$\sigma\eta^2 = \left[\frac{\partial\eta}{\partial K}\right]^2 \sigma_K{}^2 + \left[\frac{\partial\eta}{\partial T}\right]^2 \sigma_T{}^2 + \left[\frac{\partial\eta}{\partial\rho_1}\right]^2 \sigma\rho_1{}^2 + \left[\frac{\partial\eta}{\partial\rho_2}\right]^2 \sigma\rho_2{}^2$$

Therefore $$\left[\frac{\sigma\eta}{\eta}\right]^2 = \left[\frac{\sigma K}{K}\right]^2 + \left[\frac{\sigma T}{T}\right]^2 + \left[\frac{\sigma\rho_1}{(\rho_1 - \rho_2)}\right]^2 + \left[\frac{\sigma\rho_2}{(\rho_1 - \rho_2)}\right]^2$$

Variance is the square of one standard deviation, and for a normal distribution the standard deviation, σ, corresponds to a confidence interval of 68.3 per cent, and 2σ corresponds to a confidence interval of 95.5 per cent. For purposes of error calculation, the uncertainty of the variables is entered for one standard deviation, so that for the sinker constant, for example, which was shown to be within about ± 1 per cent, a value for $\sigma K/K$ of 0.0068 is the approximate input value. When $\sigma\eta/\eta$ is calculated, it will give the 68.3 per cent confidence interval for viscosity, but in quoting a figure for the uncertainty in viscosity it is more realistic to use $2 \times \sigma\eta/\eta$.

Fall time is repeatable to within 0.6 per cent for both sinkers, except for long fall times. The figure of 0.6 per cent is the worst value encountered over nearly all the calibration range, and therefore the standard deviation is approximately $\sigma T/T = 0.006 \times 0.683 = 0.004$.

In Chapter 6 it was shown that at 5 kbar the uncertainty in liquid density is 0.14 per cent rising to about 0.25 per cent at higher pressures. The latter, which is the worst possible case, is used. The contribution of error due to uncertainty in ρ_2 is therefore

$0.0025/(7.823 - 1.1) = 0.000\ 37$, where 1.1 g cm^{-3} is a typical ρ_2 value.

The sinker density, ρ_1, was ascertained from a cylindrical section of soft iron cut from the same stock from which the sinker was made. The sample was polished in the same way as the sinkers for minimum surface irregularities, its length and diameter measured by a micrometer, and its weight was determined by an analytical balance, sensitive to ± 0.1 mg

$$\rho_1 = \frac{\text{mass}}{\text{volume}} = \frac{m}{\pi a^2 l}.$$

By the Law of Propagation of Errors

$$\left[\frac{\sigma\rho_1}{\rho_1}\right]^2 = \left[\frac{\sigma m}{m}\right]^2 + \left[\frac{2\sigma_a}{a}\right]^2 + \left[\frac{\sigma l}{l}\right]^2$$

$$= \left[\frac{0.004}{5.9668}\right]^2 + \left[\frac{2 \times 0.0005}{0.311}\right]^2 + \left[\frac{0.001}{0.6127}\right]^2$$

$$= 0.449 \times 10^{-8} + 1034 \times 10^{-8} + 266 \times 10^{-8}$$

Therefore $\frac{\sigma\rho_1}{\rho_1} = 0.0036$ (ie 0.36 per cent).

Thus $\sigma\rho_1 = 0.0282$, and the sinker density error contribution is $0.0282/(7.823 - 1.1) = 0.0042$.

By substitution of these separate errors, the variance in viscosity is

$$\left[\frac{\sigma\eta}{\eta}\right]^2 = 0.0068^2 = 0.000\ 046 \quad \text{(sinker constant)}$$
$$+0.004^2 \quad 0.000\ 016 \quad \text{(fall time)}$$
$$+0.0042^2 \quad 0.000\ 017\ 6 \quad \text{(sinker density)}$$
$$+0.0004^2 \quad 0.000\ 000\ 16 \quad \text{(liquid density)}$$
$$= 0.000\ 080$$

Therefore $\frac{\sigma\eta}{\eta} = 0.009$ (ie 0.9 per cent).

This analysis shows that 68.3 per cent of viscosity values calculated from equation 2.43 are accurate to within ± 0.9 per cent, but it is more realistic to use the 95.5 per cent confidence interval giving an accuracy of ± 1.8 per cent. This accuracy applies to fall times of less than about 2 hours. There is no reason to question the continued linearity of calibration, but extrapolation does increase the possibility of larger

error, and where long fall times are encountered there is poorer repeatability. It is not possible to quantify these errors, but they are estimated to be less than twice the probable error, that is, less than ±3.6 per cent.

The above analysis does not include uncertainties being introduced by the correction factor which is applied to the fall time to allow for dimensional changes under pressure since these are very small. This factor, derived in section 2.4 is negligible for sinker 2, and a maximum of 1 per cent for sinker 1 at 3 kbar which is the maximum pressure used with this sinker, and can be calculated with high accuracy. This is because the errors in sinker and tube dimensions are extremely small, even although the value of ϵ may not be well defined. For example, the radius of the brass tube b at 3 kbar is given by

$$b = b_{P=0}(1 - \epsilon)$$

$$= 0.31525\ (1 - 2.42 \times 10^{-7} \times 3000)$$

$$= 0.315\ 021\ 1 \text{ cm.}$$

When a +5 per cent uncertainty is placed upon ϵ, the b value is 0.315 009 7 cm, and therefore the uncertainty in b is only 0.004 per cent. Calculation showed that the resultant uncertainty in the correction factor is less than 0.1 per cent, and the analysis is not given here because it is comparatively complicated, and only shows what is intuitively obvious.

In summary, the measurements of viscosity have a probable error of up to ±1.8 per cent. This calculation takes into account errors due to uncertainties in calibration, fall time measurement, liquid and sinker densities, and correction factor; it is therefore the assessment of performance of this viscometer under pressure, using unguided sinkers.

8.3.1 The effect of pressure and temperature measurement upon viscosity

Since viscosity is a property which is sensitive to changes in both pressure and temperature, accurate viscosities must be associated with accurate values of pressure and temperature if the combined data is to be classed as accurate.

a Pressure

With the exception of OS 138, the viscosity of the liquids studied varies by up to 0.2 per cent per bar. The effect on OS 138 is 0.6 per cent per bar. Pressure is measured to within ±3 per cent absolute in the 3 kbar vessel, and therefore the maximum error is 0.6 per cent for most of the liquids studied, and 1.8 per cent for OS 138.

In the case of the 14 kbar vessel the uncertainty in absolute pressure measurement is as high as 25 bar, with a proportionally adverse effect upon viscosity. Pressure measurement in this vessel to within ±8 bar has been achieved using a manganin gauge, Pursley (1968), but it was not possible to use this type of transducer because the four electrical leads into the pressure chamber were required for the viscometer.

b Temperature

The effect of temperature upon the viscosity of a liquid is quite well represented by the equation

$$\ln \eta = A'' + \frac{B''}{T - T_o}$$

For di-(2-ethylhexyl) phthalate $A'' = -9.421$, $B'' = 1305$ K, $T_o = 150.6$ K, Barlow, Lamb, and Matheson (1966). The temperatures of the constant temperature baths were monitored with mercury-in-glass thermometers, calibrated to the specification of BS 593, or ASTM E77-70, and therefore accurate to within ±0.05°C. The baths were controlled at a mean absolute temperature of 30.0 ± 0.05°C, but with a temperature fluctuation of up to ±0.1°C. Due to the high thermal inertia of the thick-walled pressure vessels this fluctuation is smoothed, and the temperature of test fluid did not depart by more than ±0.02°C from the absolute value of 30 ± 0.05°C. Thus the maximum possible error in temperature is ±0.07°C, but the probable error is somewhat less than this, say ±0.05°C. Hence it is easily shown that di-(2-ethylhexyl) phthalate viscosity varies by no more than 0.27 per cent. The effect of temperature on viscosity is more pronounced as pressure increases, and from ASME (1953) data on di-(2-ethylhexyl) phthalate where several isotherms are reported, it can be shown that at 4 kbar the effect on viscosity of a 0.05°C temperature excursion is 0.60 per cent.

For the other five liquids of this study there are less data for viscosity as a function of temperature and pressure, and an approximate assessment of error must be made. The data of Barlow et al. (1966) show that for many different liquids an uncertainty of $\pm 0.05^{\circ}C$ at atmospheric pressure would cause a change in viscosity of less than 0.25 per cent. The limited data at pressure suggest that the uncertainty in viscosity of the liquids studied will be similar to that calculated for di-(2-ethylhexyl) phthalate.

8.4 Comparison with Published Data

Data on the viscosity of liquids at pressures greater than 1 kbar are still scarce when compared with the prolific data to be found for liquid viscosity as a function of temperature, at atmospheric pressure. Two sources of data stand out because of the quality and the quantity of the work. Bridgman (1926) produced viscosity data up to 12 kbar at $30^{\circ}F$ and $75^{\circ}F$ for 43 pure liquids, and in the ASME report (1953) there are data on 44 liquids over a wider temperature range to 10 kbar. The accuracy of these data is high, and both use the falling body viscometer.

Of the liquids measured in this study, the viscosities of di-(2-ethylhexyl) phthalate, 1000 cSt siloxane and castor oil, have previously been determined under pressure.

8.4.1 Tri-m-tolylphosphate

The viscosity of this liquid when measured at atmospheric pressure using sinker 1 was found to be 42.1 cP. This is 0.24 per cent higher than the value found by Erginsav (1969).

8.4.2 1000 cSt polydimethyl siloxane

This siloxane was one of the three liquids used to calibrate sinker 2, and therefore the value calculated from fall time measurement is a measure of the quality of calibration. The difference from the suspended-level viscosity value is +0.35 per cent. After a series of measurements were made up to 1.6 kbar, a repeat measurement was made at

atmospheric pressure: the value was 904.9 compared with 904.5 cP.

The viscosity of Dow Corning DC 200 of 1000 cSt nominal viscosity at 25°C has been measured by Boelhouwer & Toneman (1957) at 30°C, at pressures up to 1.2 kbar. The method used was the unguided falling needle viscometer. A viscosity of 880 cP at atmospheric pressure was reported. Their results under pressure are consistently lower by about 3 per cent, which means although the agreement in absolute terms is only moderate, there is very good agreement in terms of the relative effect of pressure. The discrepancy in absolute values is probably due to the liquid samples being from different suppliers.

8.4.3 Bis(m-(m-phenoxy phenoxy)-phenyl) ether (OS 138)

This is a very viscous liquid having a viscosity of about 8000 cP at 30°C, at atmospheric pressure. No other viscosity-pressure data are known to exist, and at atmospheric pressure the data of Erginsav (1969) and Cochrane and Harrison (1972) are not at 30°C. Extrapolation of their data is inadvisable because OS 138 is so sensitive to temperature that large errors are likely.

8.4.4 Castor oil

The oil sample was supplied by Dr W R D Wilson of the Department of Mechanical Engineering, the Queen's University of Belfast. Dr Wilson made measurements up to 12 kbar on this oil with his novel flat plate viscometer, at temperatures of 25.1, 44.5, 69.2, and 91.0°C. The oil supplied by the Castrol Oil Co is designated '0311 First Castor Oil'.

In his thesis (1967), Wilson gives preliminary results for this oil in graphical form on a logarithmic scale of viscosity. In order to compare his results with this work, his viscosity values were taken at 1 kbar intervals from the graph and tabulated. These were then re-plotted as a function of temperature in order to find the 30°C isotherm values by interpolation.

Table 8.7

Viscosity of castor oil from Wilson's Graph

Press (kbar)	Viscosity/cP				Interpolated	JBI	Diff %
	25.1°C	44.5°C	69.2°C	91.0°C	30°C	30°C	
0	796	210	49.0	21.9	560	489	14.5
1	3,800	915	170	64.5	2,700	2,380	13.4
2	13,500	2,900	485	160	9,100	8,100	12.3
3	35,500	7,900	1250	356	24,000	26,100	- 8.0
4	96,000	19,800	2900	740	63,000	80,000	-21.3
5	330,000	46,500	6300	1450	190,000	-	-
5.5	700,000	71,000	9200	1950	365,000	-	-

The error introduced in the graphical interpretation of Wilson's data is estimated to be within ±2.5 per cent. The agreement between this work and that of Wilson is poor; the errors vary from +14.5 per cent at atmospheric pressure, to -21.3 per cent at 4 kbar. The errors are systematic as shown in Fig. 8.4, and in Table 8.7.

Two separate samples of castor oil were obtained from Belfast 6 months apart, and the kinematic viscosity of each was measured by suspended-level viscometer at 30.0 ± 0.1°C. Different viscometers were used on each occasion, the viscometers being NPL calibrated with an accuracy of ±0.5 per cent. The density of the first sample was measured in a 10 ml density bottle, and the second in a 25 ml bottle, and a value of 0.9527 g cm^{-3} was obtained in each case. Density was used to convert to dynamic viscosity and the values are 490.5 cP and 491.8 cP (diff = 0.26 per cent). The difference between these viscosity values and that of Wilson at atmospheric pressure strongly suggest inaccuracy in the latter, although Wilson states that his value is in excellent agreement with results obtained by Castrol Ltd using more conventional techniques.

The flat plate viscometer developed by Wilson is novel, and the results obtained by it are described as preliminary. No assessment of accuracy is given for the viscosity data reported. In comparing his absolute values with the values obtained by this falling body viscometer (relative method), the conclusion can be drawn that errors of 17 per cent

or more may be encountered with the plate viscometer, even allowing for a ±4 per cent error in the falling body measurements.

Since castor oil is a vegetable product, its quality and therefore its properties vary, and it is not possible to compare the results of this work with results obtained from measurements on a different stock. For example Hersey and Shore (1928) made measurements of viscosity under pressure using two different castor oil samples. At atmospheric pressure the first had a viscosity of about 740 cP at 22°C, the second a viscosity of about 600 cP at 25°C.

A different sample of castor oil, designated 'Castrol III Press', was purchased direct from the Castrol Oil Co. Its viscosity was measured at 30°C and found to be 604 cP which is also markedly higher than the 490.5 cP of the Belfast sample.

8.4.5 Di-n-butyl phthalate

No viscosity-pressure data for this liquid were found in the literature. The atmospheric pressure viscosity of 13.36 cP is in good agreement with the value of 13.43 cP of Barlow, Lamb, and Matheson (1966).

8.4.6 Di-(2-ethylhexyl) phthalate

The data published in the ASME Report (1953) at 32, 77, and 100°F were carefully interpolated graphically to produce viscosities at 30°C which are compared with the measured viscosities in the following table.

The interpolated values are estimated to be within ±3 per cent. The agreement between the results is very satisfactory; the r.m.s. difference is 2.6 per cent and only two of the differences are greater than 3 per cent. The measured values are also in good agreement with those of Galvin, Naylor, and Wilson (1963-64), obtained at 30°C and at pressures up to 1.03 kbar.

The measured results, the ASME interpolated results, and the values of Galvin et al can be seen in Fig. 8.6.

Table 8.8

Comparison of viscosity data for di-(2-ethylhexyl) phthalate

Pressure bar	Measured P	ASME P	diff %
0	0.434	0.441	1.6
203	0.665	0.665	0.0
405	1.02	0.992	-2.8
557	1.37	1.33	-2.9
811	2.16	2.15	-0.5
1013	3.14	3.11	-1.0
1317	5.45	5.36	-1.7
1571	8.19	8.29	1.2
2410	34.95	32.8	-6.2
2940	78.1	74.3	-4.9
3820	274	273	-0.4
4050	384	381	-0.8
4770	1070	1050	-1.9
4850	1180	1180	0.0
5390	2550	2490	-2.4
5500	2980	2900	-2.7

8.5 The Double Exponential Equation

Up to pressures of 1 kbar or so it is common practice to assume that log viscosity is a linear function of pressure; this is usually a reasonable assumption. However at pressures in excess of this the behaviour of viscosity on a logarithmic scale may be concave towards the pressure axis, convex, or both. An example of each type may be seen in Fig. 8.7 where all six liquids measured are drawn on one graph. Castor oil is concave, tri-m-tolyl phosphate is convex, and di-n-butyl phthalate is initially concave before passing through a gentle inflection to become convex.

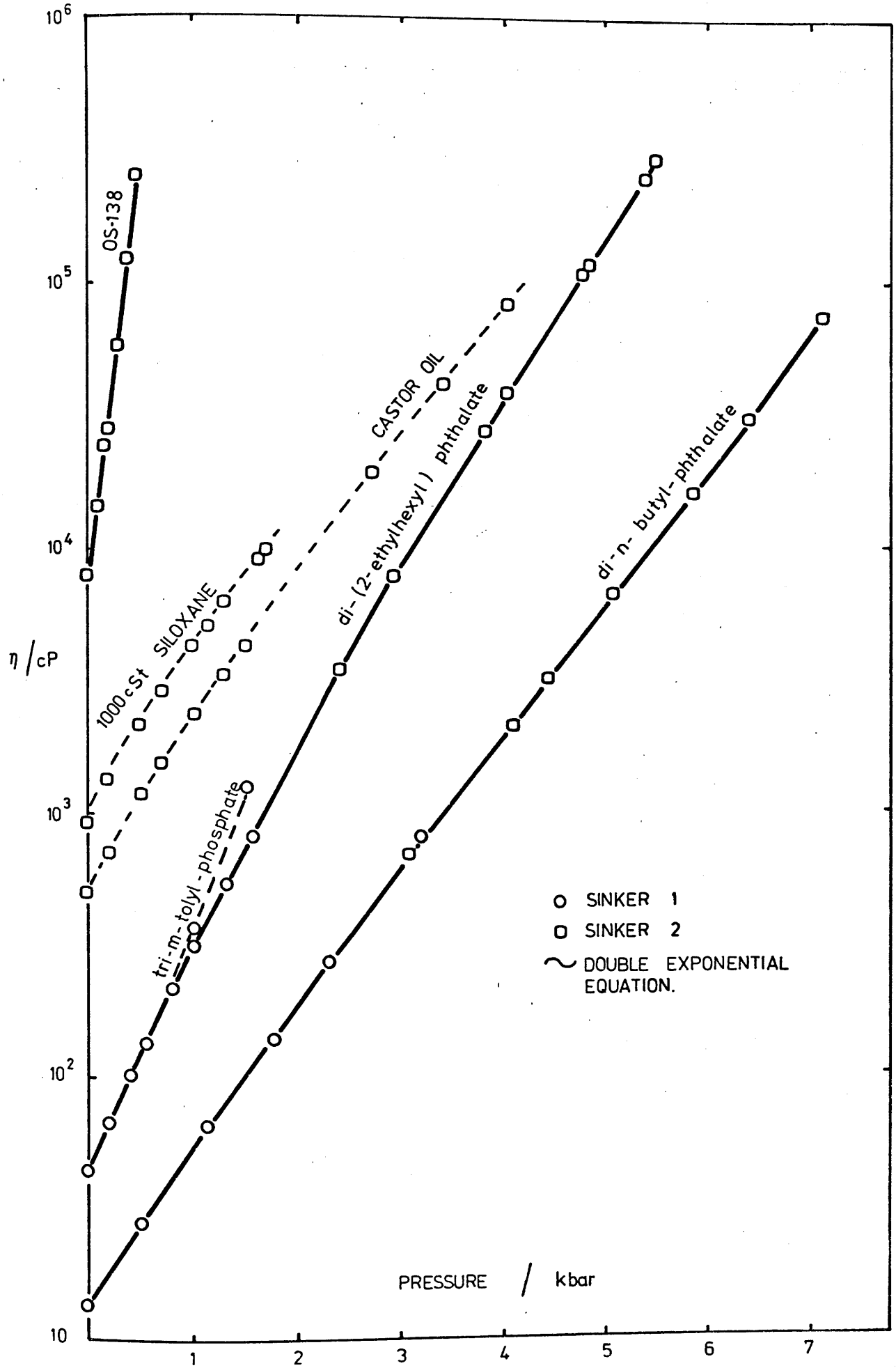

FIG 8.7 Viscosity at 30° C of six liquids under pressure.

Several different descriptive equations, mostly empirical or at best semi-theoretical, have been proposed. Perhaps the best of these is that of Roelands (1966), whose one parameter equation is very effective in that it can represent concave or convex curvature, or a straight line. It cannot, however, cope with a curve passing from concave to convex.

The equation proposed here describes all three types of behaviour almost to within experimental error

$$\ln \eta = Ae^{BP} - Ce^{-DP} \qquad (8.1)$$

where P is the gauge pressure, and A, B, C, and D are constants at a given temperature. By imposing the condition that at $P = 0$, $\eta = \eta_0$ the number of disposable constants is reduced to three. The equation is unequivocally empirical.

The method of optimization of equation 8.1, its derivation, and its wider applications, are described more fully in chapter 10.

8.5.1 Fitted data

The viscosity data at 30°C of OS 138, di-n-butyl phthalate, and di-(2-ethylhexyl) phthalate were fitted to equation 8.1. There are insufficient data to fit tri-m-tolyl phosphate and 1000 cSt siloxane.

Table 8.9

The constants of the double exponential equation for three liquids

	A	B/kbar	C	D/kbar
OS 138	4.5992	1.150	0.2242	0.321
di-n-butyl phthalate	2.8095	0.1396	4.8314	0.2282
di-(2-eh) phthalate	6.0029	0.0929	6.8381	0.2229

A close examination of the accuracy of fit of the double exponential may be obtained from Table 8.10 where the errors for each liquid are shown. The fits for di-n- and di(2-ethylhexyl) phthalates are excellent

with r.m.s. errors of 2.3 per cent and 2.2 per cent respectively, and a maximum error of -5.1 per cent. Thus the equation describes the variation of viscosity over four orders of magnitude for both of these liquids almost to within experimental accuracy.

The fit for OS 138 is poorer due to the limited amount of data (to 0.5 kbar), and in Fig. 8.7 it can be seen how rapidly the log η curve rises in comparison with the other liquids. The combination of the limited range, steep curve, and only 7 data points from which to find three constants produces a poor fit to the data. The problem of fitting double exponential type equations has been previously encountered in the analysis of isotope decay measurement, and a warning of the equation being extremely ill-conditioned is mentioned by Acton (1970). Provided, however, that the uncertainties in the data are not too great, and that a sufficient spread of data are used, then good fits can be achieved for log η -pressure data.

Table 8.10

Double exponential fit for experimental data

OS 138

Press/kbar	η_{meas}/P	η_{calc}/P	Diff %
0	79.44	79.44	0
0.101	145	141	- 2.8
0.182	248	235	- 5.3
0.203	284	270	- 4.9
0.304	583	556	- 4.6
0.405	1240	1250	0.8
0.507	2600	3130	20.4

Table 8.10 (Contd)

di-n-butyl phthalate

Press/kbar	η_{meas}/P	η_{calc}/P	Diff %
0	0.1336	0.1324	-0.9
0.532	0.283	0.286	0.9
1.14	0.666	0.650	-2.4
1.76	1.39	1.43	3.0
2.30	2.74	2.76	0.7
3.17	8.02	7.61	-5.1
3.07	6.94	6.79	-2.2
4.09	21.3	21.6	1.4
4.43	32.4	31.7	-2.2
5.07	66.8	65.5	-1.9
5.86	161.0	164.0	1.7
6.40	305.0	312.2	2.4
7.10	749.5	745.4	-0.6

di-(2-ethylhexyl) phthalate

Press/kbar	η_{meas}/P	η_{calc}/P	Diff %
0	0.434	0.434	0.0
0.203	0.665	0.658	-1.1
0.405	1.02	0.985	-3.4
0.557	1.37	1.33	-2.9
0.811	2.16	2.15	-0.5
1.013	3.14	3.13	-0.3
1.317	5.45	5.40	-0.9
1.571	8.19	8.40	2.6
2.410	34.95	33.6	-3.9
2.940	78.1	76.5	-2.0
3.820	274.0	282.0	2.9
4.050	384.0	393.0	2.3
4.770	1070.0	1084.0	1.3
4.850	1180.0	1212.0	2.7
5.390	2550.0	2560.0	0.4
5.500	2980.0	2979.0	0.0

CHAPTER 9

RESULTS: DENSITY UNDER PRESSURE

List of Figures

Page

List of Tables

CHAPTER 9

RESULTS: DENSITY UNDER PRESSURE

9.1 Introduction

The main application in this work on liquid densities under pressure is to apply corrections for buoyancy in the viscosity measurements. For this purpose high accuracy is not required since the liquid density appears with the sinker density and the latter predominates, so that the effect of any error in liquid density under pressure is diminished by a factor of approximately six.

The experimental procedure is described in section 6.1.5.

9.2 Liquids Studied

Measurements were made at 25°C on di-(2-ethylhexyl) phthalate to allow a direct comparison with the results reported in the ASME Report (1953). Subsequent measurements of density were all made at 30°C. The liquids measured were distilled water, di-n-butyl phthalate, and a polydimethyl siloxane (MS 200 series) of nominal viscosity 1000 cSt at 25°C. A sample of castor oil from the Department of Mechanical Engineering, the Queen's University of Belfast was measured; it is designated '0311 First castor oil'. The density of bis(m-(m-phenoxy phenoxy)phenyl) ether, known as OS 138, was also measured as a part of the study on the viscoelastic properties with pressure carried out by Barlow, Harrison, Irving, Kim, Lamb, and Pursley (1972).

9.3 Density Measurements at Atmospheric Pressure

Densities were measured using a 25 cm^3 density bottle which was calibrated at 30°C with mercury according to the procedure described in section 6.1.5. For the one measurement at 25°C a correction term to account for the thermal contraction of the density bottle was applied.

Table 9.1

Measured and literature density values at atmospheric pressure

Liquid	Temperature (°C)	Density (g cm^{-3})	
		Measured	Literature
di-(2-eh)phthalate	25	0.9794	0.981[a] 0.977[b]
di-(2-eh)phthalate	30	0.9760	0.974[b]
water	30	-	0.9957[c,f]
di-n-butyl phthalate	30	1.0371	1.035[b] 1.042[d]
1000 cSt silicone	30	-	0.965[e]
Castor oil (0311 First)	30	0.9527	-
OS-138	30	1.2049	-

a ASME Report (Vol. II)
b Barlow, Lamb and Matheson (1966)
c Engineering Sciences Data Unit, ESDU (1968)
d Bridgman (1931) (by interpolation)
e Harrison (1964)
f National Engineering Laboratory (NEL) Steam Tables (1964).

Measured values and literature values are compared in Table 9.1. The agreement is considered satisfactory except for Bridgman's value for di-n-butyl phthalate which appears to be 0.5 per cent high.

Several other liquids covering a wide viscosity range were used for calibrating the viscometer at atmospheric pressure. It is appropriate to list the density values in this section. The densities are in Table 9.2.

Table 9.2

Density of calibration liquids at 30°C

Liquid	Density (g cm^{-3})	
	Measured	Harrison (1964)
2 cSt silicone		0.8716
5 cSt silicone		0.9018
10 cSt silicone	0.9347	0.933
20 cSt silicone	0.9449	0.942
100 cSt silicone	0.9586	0.959
350 cSt silicone		0.964
12 500 cSt silicone		0.968
30 000 cSt silicone	0.9637	
100 000 cSt silicone		0.966
LVI 260 mineral oil	0.9407	
MVI(N) 170 mineral oil	0.8929	0.895

All the silicones, MS 200, were supplied by Midland Silicones with the exception of the 30 000 cSt sample which was obtained from Hopkin and Williams. The mineral oils were supplied by Shell Research Ltd, Thornton Research Centre, Chester.

9.4 Experimental Results of Density Under Pressure

The results were calculated by computer as described in section 6.1.6. Measurements on di-(2-ethylhexyl)phthalate at 25°C and water at 30°C were made before the program was written and were therefore calculated on a desk calculator.

9.4.1 di-(2-ethylhexyl)phthalate at 25°C

The entire calculation showing bellows length and the correction term Δl are contained in Table 9.3. Two separate tests were made with different samples. A leak in the pressure vessel occurred during the second test. Pressure was released and the leaking top seal tightened without removing

the densimeter. This resulted in a small change in the bellows position at zero gauge pressure from 0.0128 to 0.0244 inch, probably due to vibration in securing the pressure vessel seal. Density as a function of pressure is shown graphically in Fig. 9.1.

9.4.2 di-(2-ethylhexyl)phthalate at 30°C

The computed results are shown in Table 9.4. In this case only, the details of calculation are shown in which bellows position, bellows length and correction are tabulated. This was used to verify that each step of the program was in agreement with the hand calculation. The results for the other liquids are adequately described by an abridged table in which pressure, density, specific volume, specific volume recalculated by the linear secant bulk modulus equation, and the difference are listed. The abridged table is shown for this test in Table 9.5.

The two constants of the linear secant bulk modulus equation for di-(2-ethylhexyl)phthalate at 30°C are included in Table 9.5. The coefficients of the alternative modified secant bulk modulus equation (eq 6.20) are calculated from these two constants.

Density up to 6 kbar is plotted in Fig. 9.2. The measurements for both increasing and decreasing pressure are seen to fall on a smooth single curve. The differences between the measured specific volumes and those calculated from the linear bulk modulus equation show systematic errors (Table 9.5, column 4) which indicates that for such high pressures the secant bulk modulus deviates from a straight line and that it could be better represented by a polynomial.

9.4.3 Water at 30°C

For these density measurements a datum measurement was made at atmospheric pressure and the system then pressurised to 8.68 kbar. A delay of about 30 minutes was made to allow thermal equilibrium to be regained before taking measurements for downward steps of pressure. The results which were calculated by hand are in Table 9.6. The measured density as a

function of pressure was plotted and is shown in Fig. 9.3.

9.4.4 di-n-butyl phthalate at 30°C

The results of density measurements up to 8.7 kbar are given in Table 9.7 and are plotted in Fig. 9.4. The root mean square of the differences between measured and recalculated volumes is 0.0010 $cm^3\ g^{-1}$. Even for this good degree of fit a systematic deviation is evident (Table 9.7) which again indicates that a polynomial would represent the secant bulk modulus better.

9.4.5 1000 cSt silicone at 30°C

This liquid has a high compressibility, its volume being reduced by approximately 17 per cent at 5 kbar. Measurements were discontinued at 5.44 kbar due to an electrical short circuit so that no results could be made while reducing pressure. Preliminary measurements for pressure increasing to 2 kbar and reduced in steps to atmospheric fell on a single curve and were in excellent agreement with the results reported in Table 9.8. Because of the comparatively high compressibility the secant bulk modulus is non-linear. The density-pressure curve is in Fig. 9.5.

9.4.6 OS 138 at 30°C

This liquid is comparatively viscous (7951 cP at 30°C) and consequently greater care was required during filling to ensure that no pockets of air remained in the convolutions of the bellows. The results for measurements made with increasing pressure up to 6.176 kbar are in Table 9.9.

It was found that for pressure excursions greater than about 3 kbar that downward pressure measurements did not coincide with those taken with increasing pressure. This effect is probably due to a mechanical deformation of the bellows caused by the liquid becoming glass-like and ceasing to compress as a liquid. This explanation is borne out by the fact that successive runs to above 3 kbar showed that bellows displacement curves as a function of pressure were parallel. That this effect

was not due to contamination was confirmed by weighing the bellows containing the OS 138 before and after measurements; no discrepancies were found. By making measurements on di-(2-ethylhexyl)phthalate in between tests on OS 138 it was shown that the apparatus was working satisfactorily and that the effective cross-sectional area had not been affected by the behaviour of OS 138 at pressure.

A graph of density as a function of pressure is shown in Fig. 9.6.

The points fall on a smooth curve which flattens to a nearly horizontal line above 3 kbar unlike any of the other liquids. Examination of the viscosity behaviour of this liquid indicates that, by extrapolation, OS 138 has a viscosity of at least 10^{12} P at 3 kbar. This means that the liquid has reached a glass-like or vitrified state in which molecules are in a closely packed configuration and consequently the sample is relatively incompressible. The glass transition temperature of a liquid is conventionally defined as the temperature at which the viscosity of a liquid is 10^{13} P at atmospheric pressure. Bondi (1968) discusses the pressure dependence of T_g and states that for each temperature $T > T_g$ there is a pressure P_g at which a melt will vitrify and states that the vitrification curve seems to be linear over most of the range. Erginsav (1969) has shown that for this liquid at atmospheric pressure $T_g = -10^{\circ}C$, and if the vitrification curve is linear then it would appear as in Fig. 9.7. This shows that at $10^{\circ}C$ P_g could be as low as 1 kbar.

9.4.7 0311 First castor oil at $30^{\circ}C$

The results for this liquid are listed in Table 9.10. Measurements were made for increasing and decreasing pressure with a maximum of 3.272 kbar. As shown in Fig. 9.8 the scatter of measurements is greater than for the other reported liquids, although below 1 kbar the agreement among measurements made with increasing and decreasing pressure is excellent.

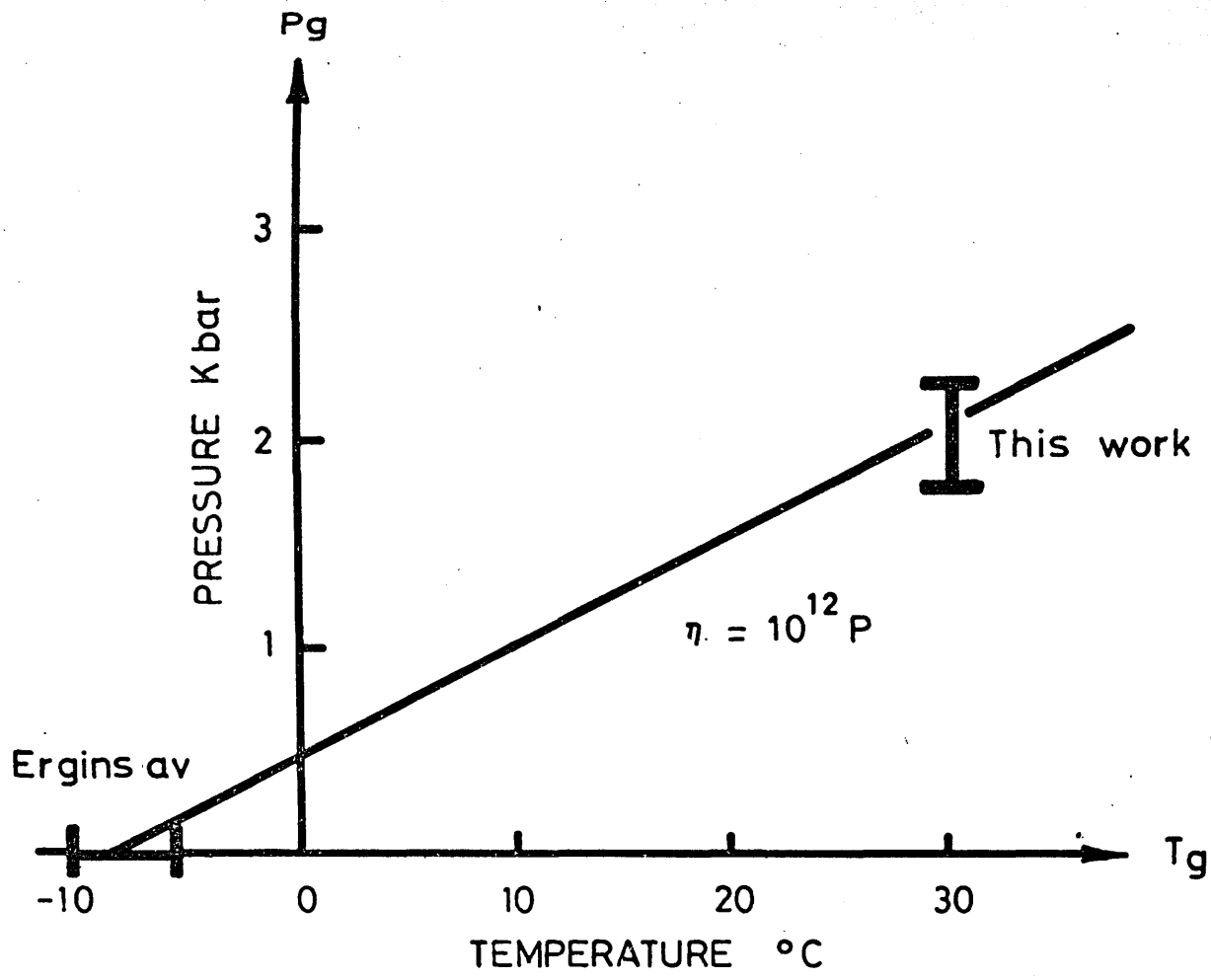

Fig 9.7 Vitrification curve for OS 138

9.5 Comparison with Published Data

Sources of data are available on di-(2-ethylhexyl)phthalate, water and di-n-butyl phthalate. Reliable data have not been located for 1000 cSt silicone, OS 138, and 0311 First castor oil.

9.5.1 di-(2-ethylhexyl)phthalate

Density values at 25°C are reported in the ASME Report. They are plotted on the same graph as this work in Fig. 9.1. The published data are shown by the solid line and agreement with this work is good, the maximum difference being 0.003 g cm^{-3}. For a true comparison of the agreement under pressure, the ASME data were recalculated with reference to an atmospheric density of 0.9794 g cm^{-1} instead of their value of 0.981 g cm^{-3}. The density values fall on or below the ASME values.

9.5.2 Water

There are many sources of density data on water particularly in the range 0 to 1000 kbar. Within this range measurements have been made to within 0.001 per cent as reported in the Engineering Sciences Data Unit (ESDU) tables of 1968 which are recommendations based largely on the work of Kell and Whalley (1965). Sources of other reliable density data below 1 kbar are to be found in a work by Hayward (1971).

These measurements were made with reference to an atmospheric density at 30°C of 0.9957 g cm^{-3} which is the internationally agreed value recommended by ESDU and by the National Engineering Laboratory (NEL) Steam Tables (1964).

In the range 1 to 10 kbar published measurements and recommended values are mostly within ±0.2 per cent although reproducibility of ±0.3 per cent is claimed by Koster and Franck (1969) with an uncertainty of ±1.0 per cent. An equation of state by Juza (1966) has uncertainties of up to ±1.0 per cent at 10 kbar. The recommendations of ESDU are based largely on the equation of Juza and his measured values. With these comparatively large uncertainties it is surprising that independent measurements which

include the work of Bridgman (1935) should be within ±0.2 per cent of one another. Bridgman's relative volume measurements are with reference to his value of 0.9949 g cm^{-3} at atmospheric pressure.

In Fig. 9.3 the above-mentioned published data are plotted along with the results of this work up to 8.7 kbar. At pressures up to about 2 kbar agreement between this work and other published data is excellent. At higher pressures the agreement is less good with measurements higher than the published data, but nevertheless falling well within the above-mentioned uncertainties of ±1.0 per cent. A measurement by Yazgan (1966) at approximately 2 kbar which was made on a similar apparatus is also slightly higher than the published data.

9.5.3 di-n-butyl phthalate

Bridgman (1931) measured the density of di-n-butyl phthalate up to 12 kbar at 0°C, 50°C and 95°C. Values at 30°C were found by careful graphical interpolation and these are compared with this work in Fig. 9.4. The agreement is very good up to 3 kbar. Between 3 kbar and 6 kbar Bridgman's values are up to 0.3 per cent lower, and from 6 kbar his values are higher by 0.48 per cent. The agreement over the comparatively large pressure range of 8 kbar is quite satisfactory particularly as the values of Bridgman are interpolated.

Table 9.3

Calculation of density from pressure measurements on di-(2-ethylhexyl)phthalate at 25°C

TEST 1 $\rho_{P=0}$ = 0.9794 g cm^{-3} mass = 14.7393 g

Press. (bar)	Bellows position (in)	$\Delta l_{bellows}$ (cm)	$l_{bellows}$ (cm)	Δl (cm)	$l_{corr} = l_{liq} - \Delta l$	ρ (g cm^{-3})	V (cm^3 g^{-1})
0	0.0265	0.0	3.7623	0.0	3.7623	0.9794	1.0210
634	0.0694	0.1090	3.6533	0.0018	3.6516	1.0091	0.9910
1360	0.1087	0.2088	3.5535	0.0037	3.5498	1.0380	0.9634
2040	0.1342	0.2736	3.4887	0.0054	3.4833	1.0578	0.9453
2730	0.1580	0.3340	3.4283	0.0071	3.4212	1.0771	0.9284
4090	0.1946	0.4270	3.3353	0.0104	3.3249	1.1082	0.9023
5450	0.2221	0.4968	3.2655	0.0136	3.2519	1.1331	0.8825
6800	0.2430	0.5499	3.2124	0.0167	3.1957	1.1531	0.8673
8040	0.2594	0.5916	3.1707	0.0195	3.1512	1.1693	0.8552

TEST 2 $\rho_{P=0}$ = 0.9794 g cm^{-3} mass = 14.7162 g

Pressure (bar)	ρ (g cm^{-3})	V (cm^3 g^{-1})
Run 1		
0	0.9794	1.0210
395	1.0001	0.9999
729	1.0169	0.9833
1400	1.0429	0.9589
1895	1.0581	0.9451
Run 2		
0	0.9794	1.0210
4090	1.1089	0.9018
7020	1.1552	0.8656
8070	1.1692	0.8553
3240	1.0915	0.9162
1870	1.0562	0.9468

Table 9.4

Detailed calculation of specific volume from pressure measurements on di-(2-ethylhexyl)phthalate at 30°C

No	Press. (bar)	Bellows position (in)	$l_{b\ell ws}$ (cm)	Δl (cm)	$l_{corr} = l_{liq} - \Delta l$	V ($cm^3\ g^{-1}$)
1	136	0.0369	3.6584	0.0004	3.6580	1.0144
2	273	0.0472	3.6325	0.0008	3.6317	1.0071
3	409	0.0567	3.6083	0.0011	3.6072	1.0003
4	532	0.0652	3.5865	0.0014	3.5851	0.9942
5	682	0.0742	3.5638	0.0018	3.5619	0.9878
6	818	0.0820	3.5439	0.0022	3.5417	0.9821
7	954	0.0896	3.5246	0.0026	3.5221	0.9767
8	1077	0.0954	3.5098	0.0029	3.5070	0.9725
9	1241	0.1038	3.4886	0.0033	3.4853	0.9665
10	1363	0.1087	3.4761	0.0036	3.4725	0.9630
11	1636	0.1201	3.4471	0.0043	3.4428	0.9547
12	1909	0.1309	3.4198	0.0050	3.4149	0.9470
13	2181	0.1410	3.3940	0.0056	3.3883	0.9396
14	2454	0.1495	3.3725	0.0063	3.3662	0.9335
15	2727	0.1581	3.3507	0.0070	3.3437	0.9273
16	3115	0.1698	3.3209	0.0079	3.3130	0.9187
17	3545	0.1808	3.2931	0.0089	3.2842	0.9107
18	4070	0.1935	3.2607	0.0101	3.2506	0.9014
19	4772	0.2083	3.2231	0.0118	3.2113	0.8905
20	5433	0.2209	3.1911	0.0133	3.1778	0.8812
21	6040	0.2312	3.1649	0.0146	3.1503	0.8736
22	5862	0.2290	3.1704	0.0142	3.1562	0.8753
23	5303	0.2187	3.1968	0.0130	3.1838	0.8829
24	4635	0.2058	3.2294	0.0114	3.2180	0.8924
25	3954	0.1916	3.2657	0.0099	3.2558	0.9029
26	3204	0.1720	3.3153	0.0081	3.3072	0.9171
27	2249	0.1423	3.3908	0.0058	3.3850	0.9387
28	873	0.0853	3.5356	0.0023	3.5333	0.9798
29	504	0.0628	3.5927	0.0014	3.5913	0.9959
30	0	0.0226	3.6947	0.0000	3.6947	1.0246

Table 9.5

Measured density of di-(2-ethylhexyl)phthalate at 30°C

Press. (bar)	ρ (g cm^{-3})	V (cm^3 g^{-1})	Recalc. V (cm^3 g^{-1})	Diff. (meas-calc)
ATMOS	0.9760	1.0246		
136	0.9858	1.0144	1.0155	-0.0011
273	0.9929	1.0071	1.0071	0.0000
409	0.9997	1.0003	0.9994	0.0010
532	1.0058	0.9942	0.9929	0.0013
682	1.0124	0.9878	0.9855	0.0022
818	1.0182	0.9821	0.9793	0.0028
954	1.0238	0.9767	0.9736	0.0032
1077	1.0283	0.9725	0.9687	0.0039
1241	1.0346	0.9665	0.9626	0.0039
1363	1.0385	0.9630	0.9583	0.0047
1636	1.0474	0.9547	0.9496	0.0052
1909	1.0560	0.9470	0.9418	0.0052
2181	1.0643	0.9396	0.9348	0.0048
2454	1.0713	0.9335	0.9285	0.0050
2727	1.0785	0.9273	0.9227	0.0045
3115	1.0884	0.9187	0.9154	0.0033
3545	1.0980	0.9107	0.9084	0.0024
4070	1.1094	0.9014	0.9008	0.0006
4772	1.1229	0.8905	0.8924	-0.0018
5433	1.1348	0.8812	0.8856	-0.0044
6040	1.1447	0.8736	0.8803	-0.0067
5862	1.1425	0.8753	0.8818	-0.0065
5303	1.1326	0.8829	0.8869	-0.0040
4635	1.1206	0.8924	0.8939	-0.0015
3954	1.1076	0.9029	0.9024	0.0005
3204	1.0904	0.9171	0.9139	0.0032
2249	1.0653	0.9387	0.9331	0.0056
873	1.0206	0.9798	0.9770	0.0028
504	1.0041	0.9959	0.9943	0.0016
0	0.9760	1.0246	1.0246	0.0000

Linear secant bulk modulus, $\frac{V_o P}{V_o - V} = 14710 + P \times 4.666$

Modified equation (eq 6.20) $V = 0.8050 + \frac{692.1}{3151.8 + P}$

Table 9.6

Measured density of water at 30°C

$\rho_{P=0}$ = 0.9957 g cm^{-3} mass = 14.9306 g

Pressure (bar)	ρ (g cm^{-3})	V (cm^3 g^{-1})
0	0.9957	1.0043
626	1.0216	0.9788
1505	1.0532	0.9495
2245	1.0781	0.9275
3016	1.0993	0.9097
3624	1.1160	0.8960
4226	1.1324	0.8831
4846	1.1466	0.8721
5435	1.1570	0.8643
6098	1.1710	0.8540
7277	1.1943	0.8373
8108	1.2067	0.8287
8680	1.2159	0.8224

Table 9.7

Measured density of di-n-butyl phthalate at 30°C

Press. (bar)	ρ (g cm^{-3})	V (cm^3 g^{-1})	Recalc. V (cm^3 g^{-1})	Diff. (meas-calc)
ATMOS	1.0371	0.9642		
273	1.0523	0.9503	0.9504	-0.0001
750	1.0774	0.9281	0.9296	-0.0015
1227	1.0969	0.9117	0.9123	-0.0006
1472	1.1056	0.9045	0.9044	0.0001
2747	1.1450	0.8734	0.8720	0.0014
3647	1.1674	0.8566	0.8552	0.0014
4485	1.1862	0.8430	0.8425	0.0005
5726	1.2090	0.8271	0.8276	-0.0004
5331	1.2025	0.8316	0.9319	-0.0003
4035	1.1766	0.8499	0.8490	0.0009
3252	1.1574	0.8640	0.8621	0.0019
2147	1.1277	0.8867	0.8857	0.0010
1384	1.1027	0.9068	0.9072	-0.0004
5876	1.2110	0.8258	0.8260	-0.0002
7812	1.2386	0.8074	0.8091	-0.0018
8725	1.2467	0.8021	0.8029	-0.0008
6844	1.2227	0.8179	0.8168	0.0010

Linear secant bulk modulus, $\frac{V_o P}{V_o - V} = 17970 + P \times 3.916$

Modified equation (eq 6.20) $V = 0.7180 + \frac{1129.9}{4589.2 + P}$

Table 9.8

Measured density of 1000 cSt silicone at 30°C

Press. (bar)	ρ (g cm^{-3})	V (cm^3 g^{-1})	Recalc. V (cm^3 g^{-1})	Diff. (meas-calc)
ATMOS	0.9650	1.0363		
136	0.9976	1.0024	1.0148	-0.0125
273	1.0136	0.9866	0.9966	-0.0101
409	1.0248	0.9758	0.9810	-0.0052
545	1.0356	0.9657	0.9674	-0.0017
682	1.0444	0.9575	0.9554	0.0020
941	1.0610	0.9425	0.9364	0.0061
1227	1.0776	0.9279	0.9195	0.0084
1500	1.0916	0.9161	0.9064	0.0097
1772	1.1051	0.9049	0.8954	0.0095
2059	1.1169	0.8953	0.8857	0.0096
2345	1.1283	0.8863	0.8774	0.0089
2584	1.1377	0.8790	0.8714	0.0076
2993	1.1518	0.8682	0.8625	0.0056
3408	1.1647	0.8586	0.8550	0.0035
3817	1.1761	0.8502	0.8488	0.0014
4213	1.1873	0.8422	0.8436	-0.0014
4622	1.1983	0.8345	0.8390	-0.0045
5037	1.2076	0.8281	0.8348	-0.0067
5440	1.2161	0.8223	0.8313	-0.0090

Linear secant bulk modulus, $\frac{V_o P}{V_o - V} = 6053 + P \times 3.942$

Modified equation (eq 6.20) $V = 0.7734 + \frac{403.6}{1535.4 + P}$

Table 9.9

Measured density of OS 138 at 30°C

Press. (bar)	ρ (g cm^{-3})	V (cm^3 g^{-1})	Recalc. V (cm^3 g^{-1})	Diff. (meas-calc)
ATMOS	1.2049	0.8299		
136	1.2130	0.8244	0.8244	-0.0001
273	1.2193	0.8202	0.8195	0.0006
409	1.2256	0.8159	0.8151	0.0008
559	1.2311	0.8123	0.8108	0.0015
668	1.2353	0.8095	0.8079	0.0017
927	1.2444	0.8036	0.8018	0.0018
1213	1.2551	0.7967	0.7961	0.0006
1636	1.2681	0.7886	0.7893	-0.0007
1909	1.2752	0.7842	0.7856	-0.0014
1895	1.2756	0.7839	0.7858	-0.0018
2413	1.2875	0.7767	0.7799	-0.0032
2761	1.2943	0.7726	0.7766	-0.0041
3095	1.2980	0.7704	0.7739	-0.0035
3436	1.3011	0.7686	0.7715	-0.0029
3763	1.3030	0.7675	0.7694	-0.0019
4090	1.3051	0.7662	0.7675	-0.0013
4444	1.3068	0.7652	0.7657	-0.0004
4751	1.3080	0.7645	0.7642	0.0003
5078	1.3090	0.7639	0.7628	0.0011
5010	1.3094	0.7637	0.7631	0.0006
5467	1.3115	0.7625	0.7613	0.0012
5842	1.3125	0.7619	0.7600	0.0019
6176	1.3136	0.7613	0.7589	0.0024

Linear secant bulk modulus, $\frac{V_o P}{V_o - V} = 19410 + P \times 8.544$

Modified equation (eq 6.20) $V = 0.7328 + \frac{220.7}{2271 + P}$

Table 9.10

Measured density of 0311 First castor oil at 30°C

Press. (bar)	ρ (g cm^{-3})	V (cm^3 g^{-1})	Recalc. V (cm^3 g^{-1})	Diff. (meas-calc)
ATMOS	0.9527	1.0496		
259	0.9711	1.0298	1.0320	-0.0022
409	0.9783	1.0222	1.0232	-0.0009
545	0.9840	1.0163	1.0159	0.0003
668	0.9893	1.0108	1.0100	0.0008
954	0.9996	1.0004	0.9977	0.0027
1207	1.0094	0.9907	0.9885	0.0021
1452	1.0194	0.9810	0.9807	0.0003
1772	1.0294	0.9714	0.9718	-0.0004
2195	1.0385	0.9629	0.9629	0.0009
2454	1.0447	0.9572	0.9568	0.0004
2733	1.0514	0.9511	0.9518	-0.0007
2999	1.0577	0.9455	0.9475	-0.0020
3272	1.0634	0.9404	0.9435	-0.0031
2986	1.0558	0.9471	0.9477	-0.0006
2727	1.0502	0.9522	0.9519	0.0003
2727	1.0506	0.9519	0.9519	-0.0001
2100	1.0345	0.9667	0.9641	0.0026
1431	1.0150	0.9852	0.9813	0.0039
661	0.9895	1.0106	1.0103	0.0003
409	0.9788	1.0216	1.0232	-0.0015

Linear secant bulk modulus, $\frac{V_o P}{V_o - V} = 13910 + P \times 5.640$

Modified equation (eq 6.20) $V = 0.8636 + \frac{458.9}{2466 + P}$

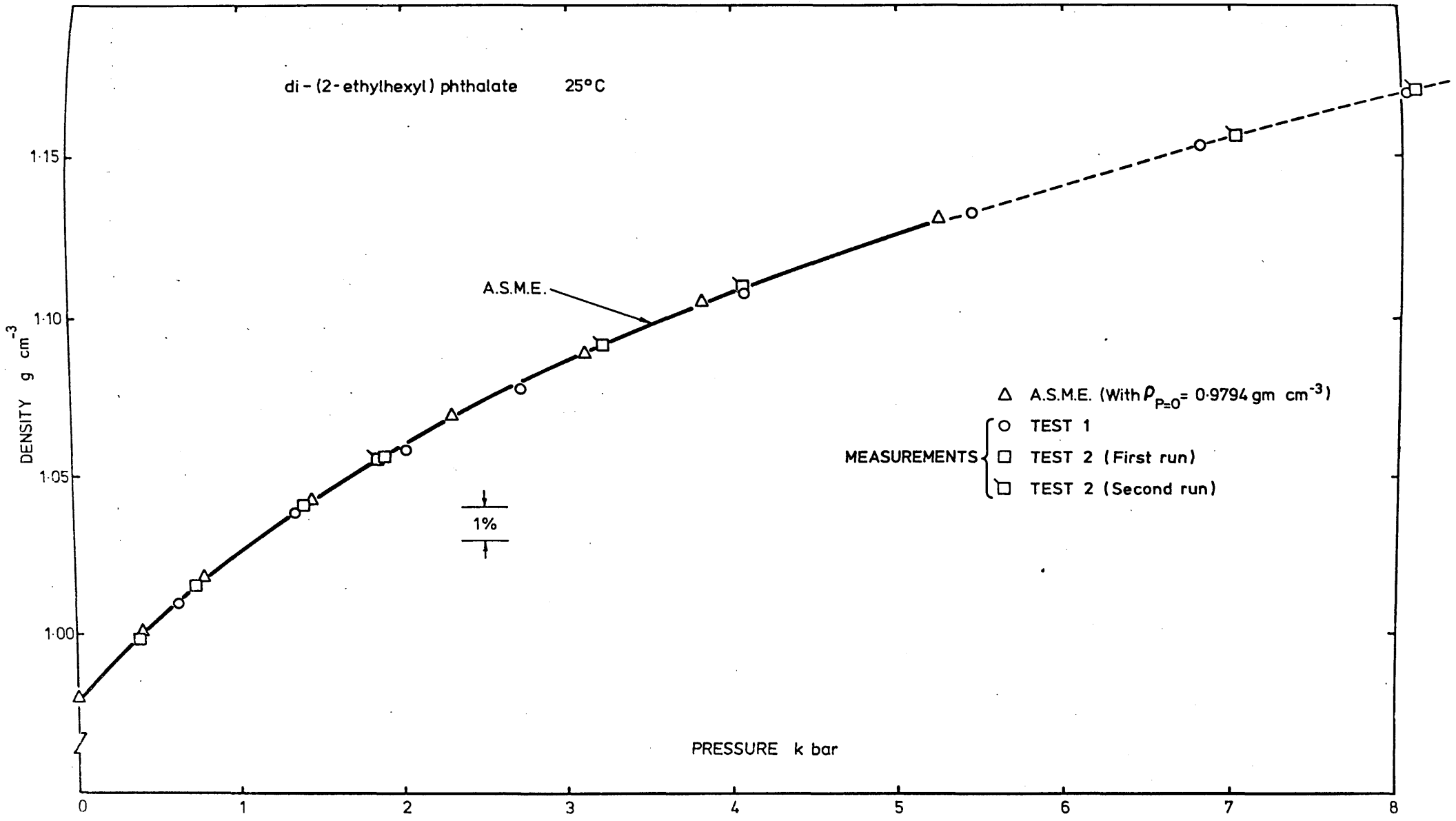

Fig 9.1 di-(2-ethylhexyl) phthalate: density as a function of pressure at 25°C

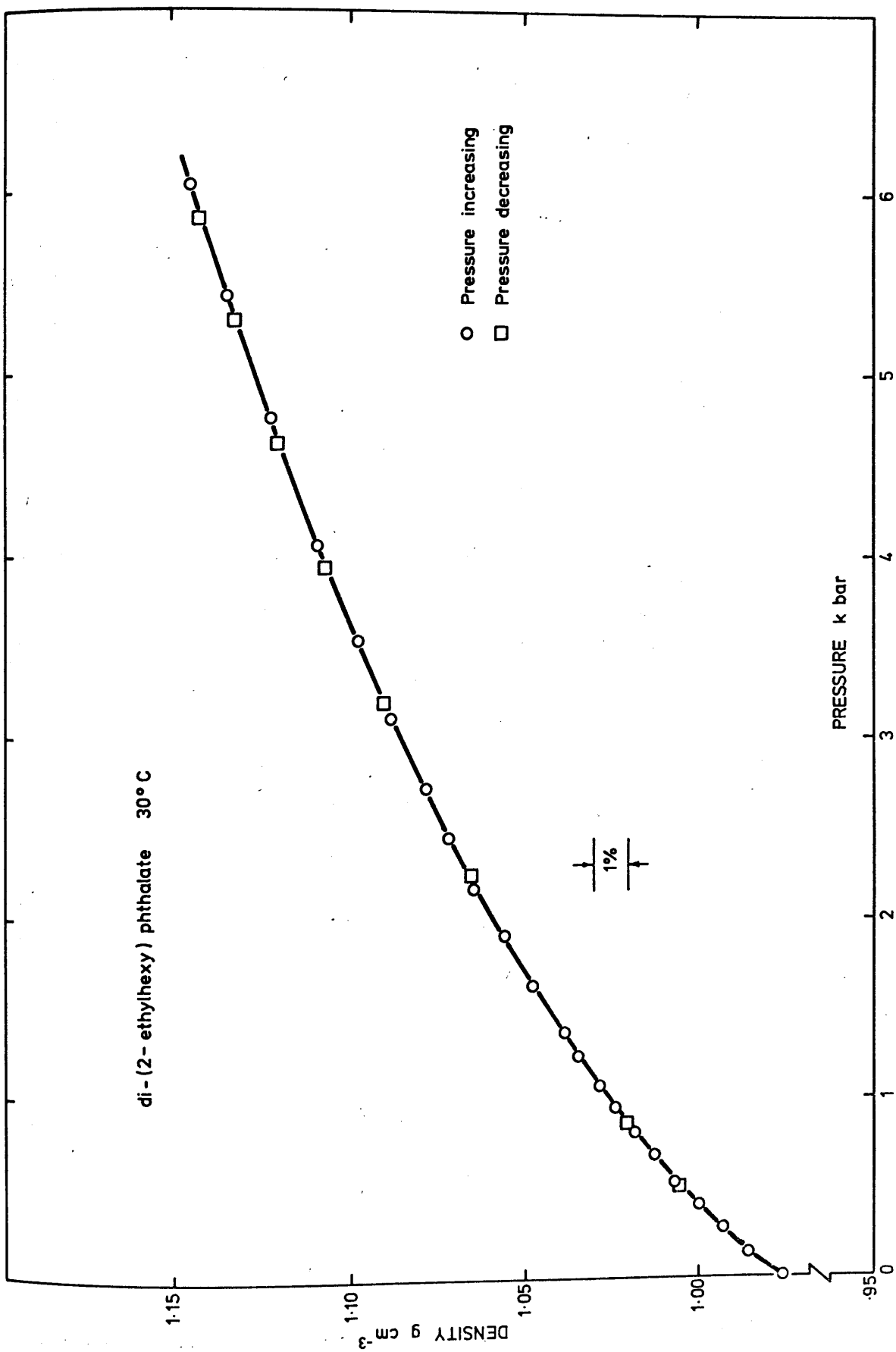

Fig 9.2 di-(2-ethylhexyl) phthalate: density as a function of pressure at 30°C

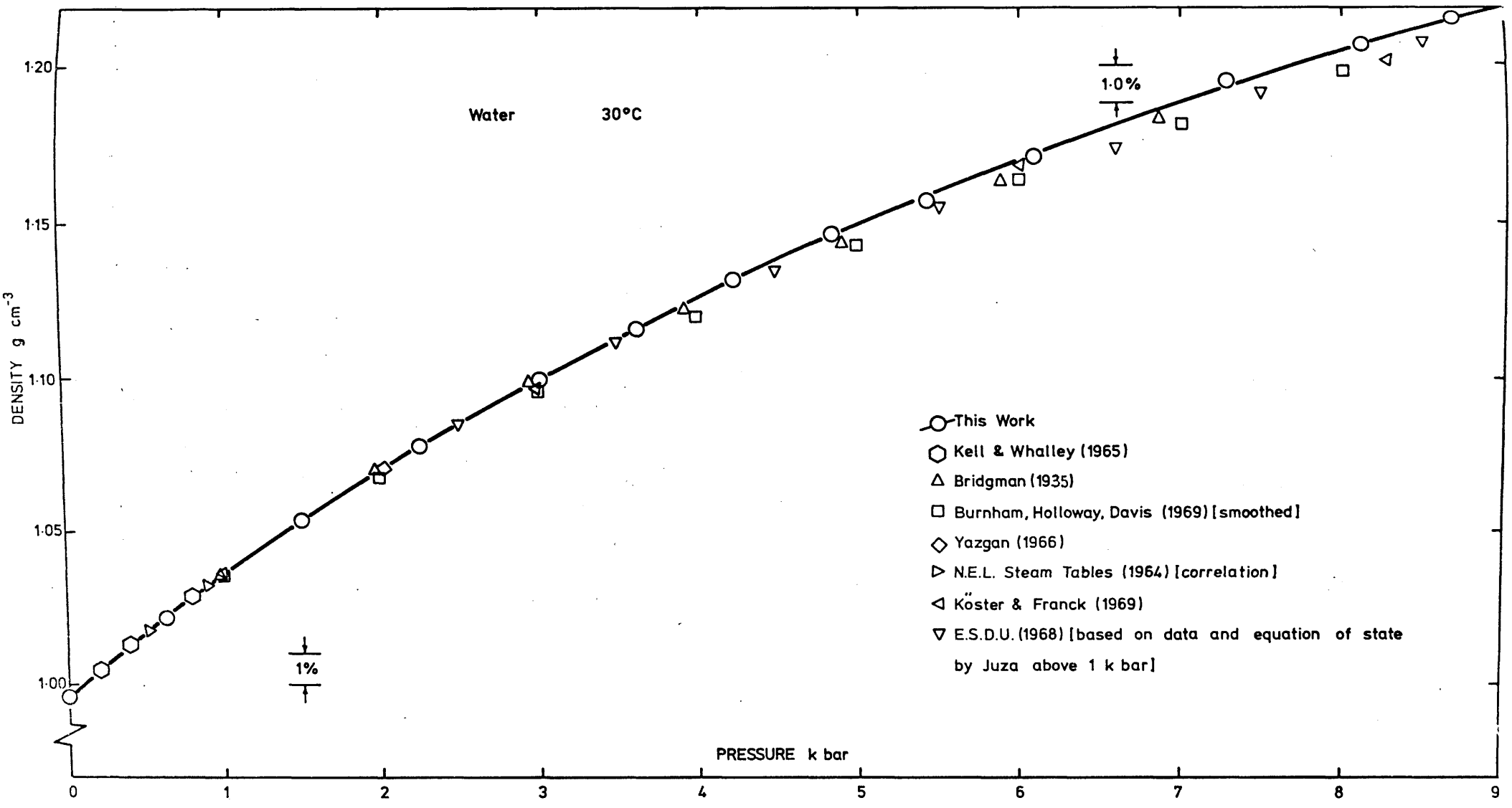

Fig 9.3 Water: density as a function of pressure at 30°C

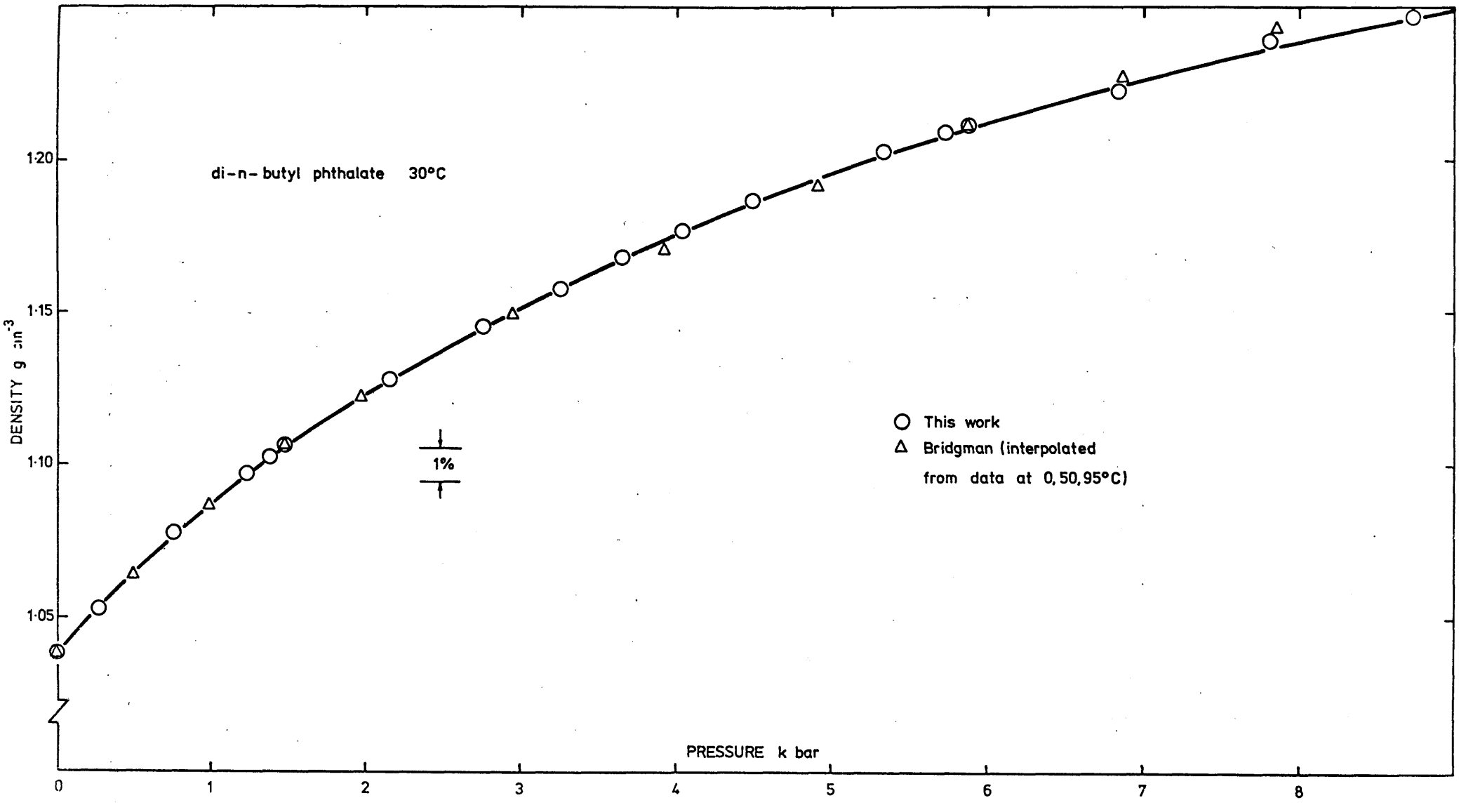

Fig 9.4 di-n-butyl phthalate: density as a function of pressure at 30°C

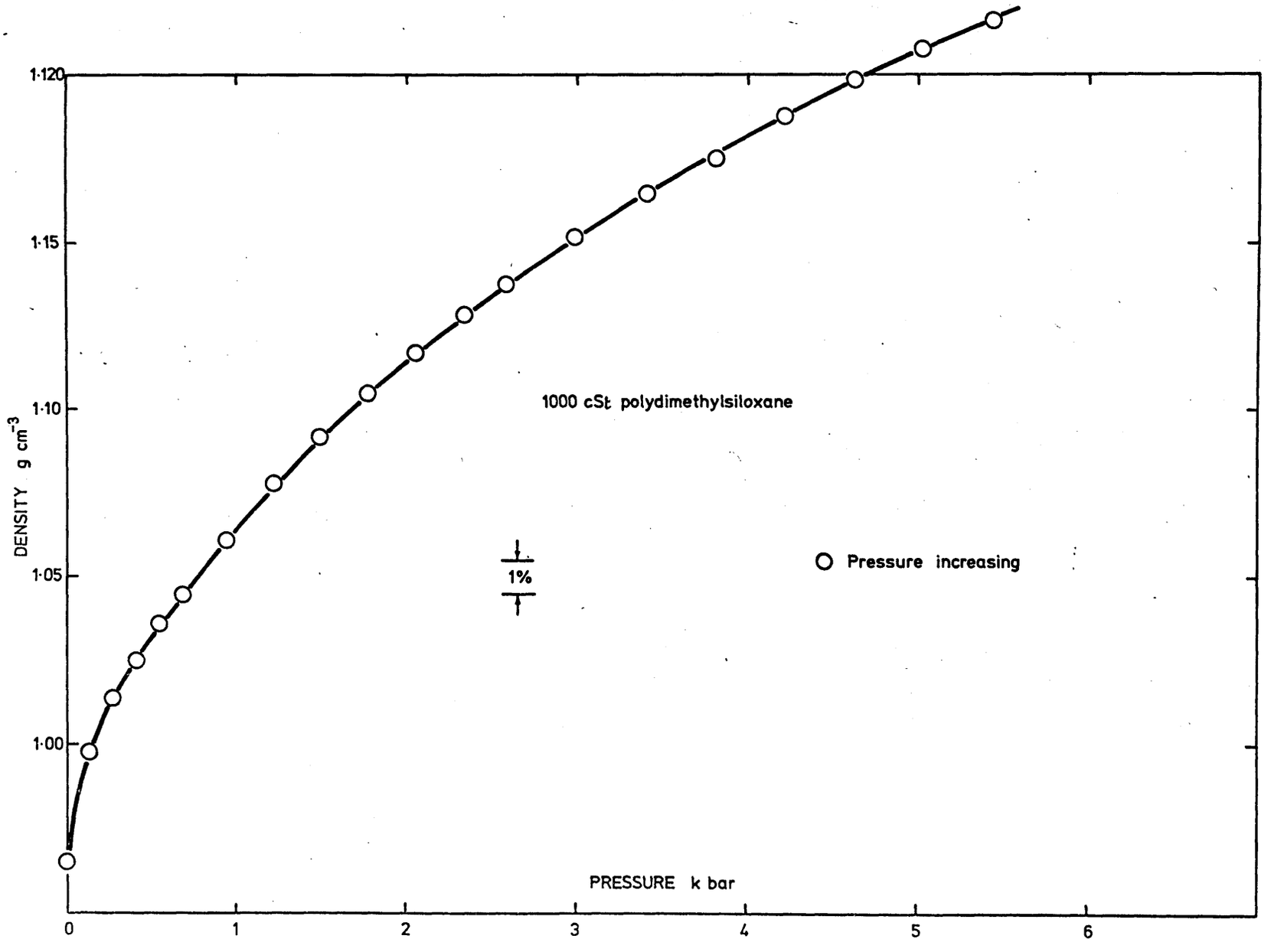

Fig 9.5 1000 cSt polydimethylsiloxane: density as a function of pressure at 30°C

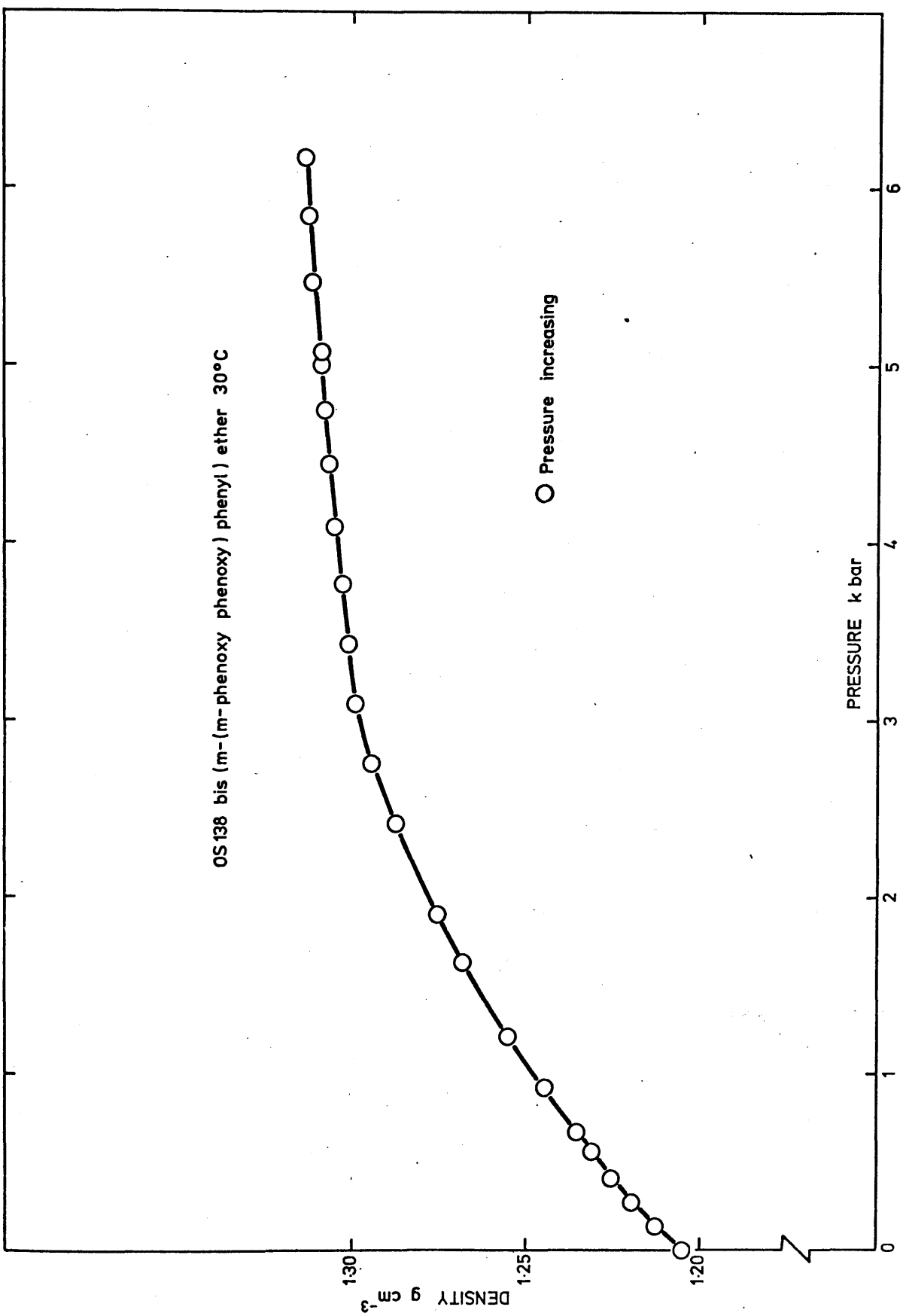

Fig 9.6 OS138: density as a function of pressure at 30°C

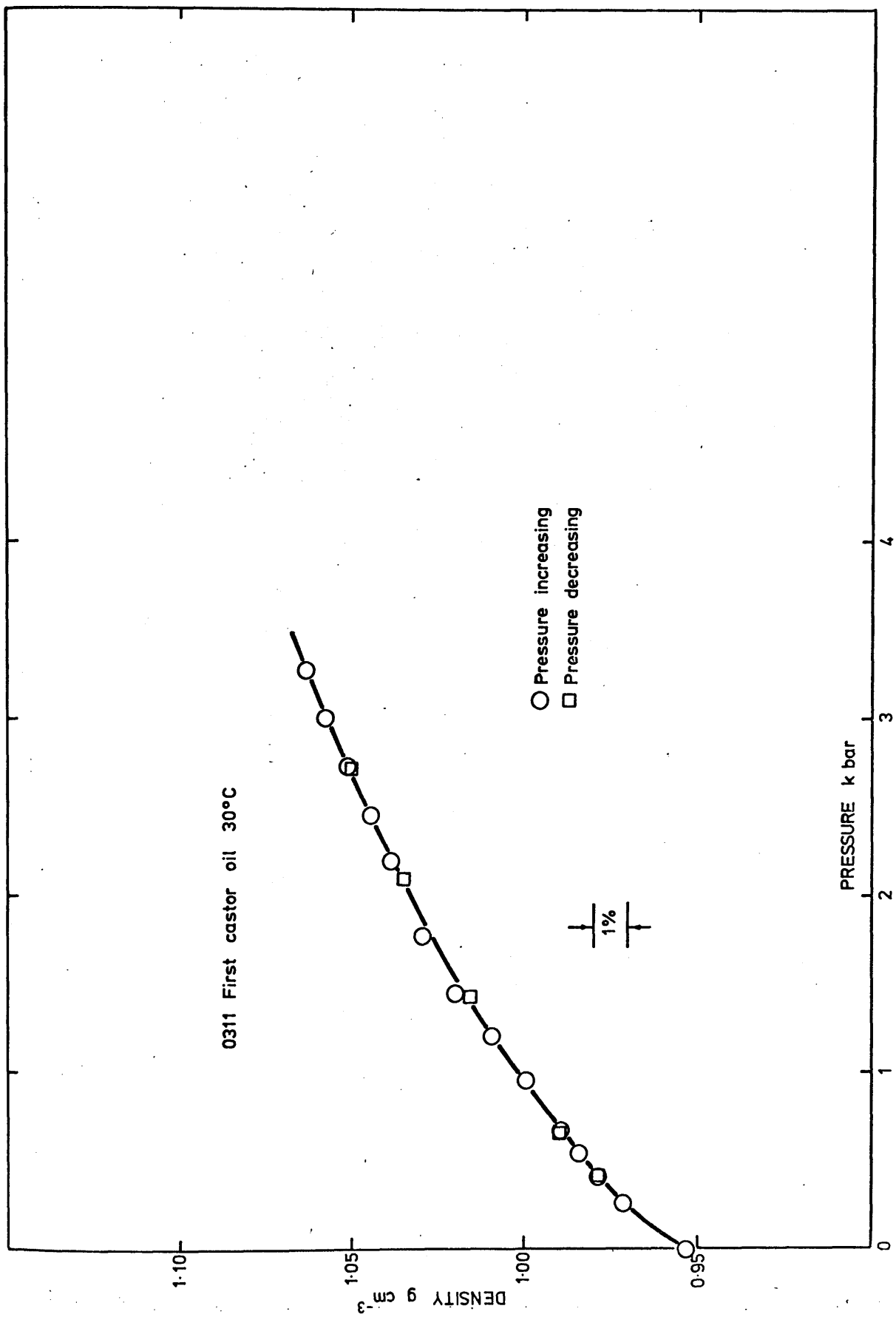

Fig 9·8 0311 First castor oil: density as a function of pressure at 30°C

CHAPTER 10

EMPIRICAL AND SEMI-THEORETICAL VISCOSITY-PRESSURE EQUATIONS

Page

List of Figures

List of Tables

CHAPTER 10

EMPIRICAL AND SEMI-THEORETICAL VISCOSITY EQUATIONS

The behaviour of gases and solids is fairly well understood, and satisfactory theories exist. In contrast, however, the behaviour of the liquid phase is not nearly so well understood, and no precise theory has so far been developed. As long ago as 1924, for example, Lennard-Jones was able to deduce the force law for various atoms from gas viscosity, but since then this has still not been done from liquid viscosity data.

Many different theories of liquid viscosity have been proposed, but none has been successful in predicting viscosity without introducing adjustable parameters. In his paper 'Theories of liquid viscosity' Brush (1962) reviews the position in critical detail. While warning against empirical formulae, he does admit that they do fulfil a role in that they provide a convenient means for presenting experimental data in a form which is useful to others, as well as providing physical chemists with profitable employment.

In the absence of adequate fundamental theories, many empirical relationships to describe transport and other liquid properties have been proposed. Many of these work surprisingly well and some have been lent respectability by having been derived theoretically from simple models. As such, it is more correct to describe these derivations as 'semi-theoretical'. Until such time as a proper molecular theory is produced, an event viewed with pessimism by Goldstein (1969) and others, the only course open for treating liquid viscosity data is to employ the best semi-theoretical relationship or empirical equation available.

In this chapter the free volume equation is used to describe viscosity data as a function of pressure. It is shown to fit data over many decades of viscosity accurately, and a new but straightforward application of the free volume equation overcomes inconsistencies found by earlier workers.

A completely new empirical equation with three constants is offered in Section 10.6. This equation relates viscosity to pressure for all the experimental data tested, to within experimental accuracy.

10.1 The Free Volume Theory

"If you knows a better 'ole, go to it"
C B Bairnsfather (1915)

The free volume equation has been used to describe liquid viscosity as a function of specific volume for many liquids, especially for temperature variation in the non-Arrhenius region. The concept of free volume was introduced by Batschinski (1913), modified by Macleod (1923), and adopted by Doolittle in 1951. The free volume equation that Doolittle proposed is

$$\ln \eta = A' + B' \frac{v_o}{v_f}, \tag{10.1}$$

where A' and B' are constants for a single substance, and v_o/v_f at fixed pressure is a function of temperature only. Doolittle originally defined v_o as the specific volume of liquid extrapolated to absolute zero, but he later modified this in 1957. The free volume v_f is the difference between specific volume v, and v_o.

The free volume equation was later derived by Cohen and Turnbull (1959) who related the diffusion constant D in a liquid of notionally hard spheres with free volume, and used the Stokes-Einstein inverse relationship between D and dynamic viscosity to produce an equation similar to equation (10.1). The mechanism assumed by Cohen and Turnbull is that occasionally there is a fluctuation in density which opens up a hole within a cage large enough to permit a considerable displacement of the molecule contained by it. Such a displacement gives rise to diffusive motion only if another molecule jumps into the hole before the first can return to its original position.

It is now generally held that v_o is the limiting specific volume of the liquid, that is the volume occupied by a molecule when in a close-packed glasslike condensed phase. It is more than the specific volume of the sphere itself since there are always small pockets between spheres when

they are closely packed, and each sphere has its share of the pockets included in v_o.

A paper by Hogenboom, Dixon and Webb in 1967 clearly sets out the advances and applications of the free volume equation up to that time, with particular emphasis on the effects of pressure. Further advances are proposed in this chapter in Sections 10.1.2 et seq.

10.1.1 Free volume and temperature

For most liquids it is found experimentally that, at atmospheric pressure, density varies linearly with temperature below the vicinity of the boiling point. Thus

$$\rho = \rho_r\{1 - a(T - 273.2)\}. \tag{10.2}$$

When temperature T_o is defined as the temperature corresponding to the limiting specific volume v_o, Barlow, Lamb and Matheson (1966) showed that by combining equations (10.1) and (10.2) the following equation is derived by simple algebraic manipulation

$$\ln \eta = A'' + \frac{B''}{T - T_o}, \tag{10.3}$$

where A'', B'' and T_o are constants. This equation is referred to by Barlow et al as the modified free volume equation. The two equations (10.1) and (10.3) are precisely equivalent in liquids where density is a linear function of temperature. Equation (10.3) is the same as the empirical equation found by Vogel (1921), Fulcher (1925), and Tamman and Hesse (1926), apparently independently of one another, according to Goldstein (1969).

10.1.2 Free volume and pressure

Whereas liquid density at atmospheric pressure is found to vary linearly with temperature, under pressure the experimental data show that specific volume varies linearly with temperature. Thus

$$v = v_o\{1 + \alpha(T - T_o)\}, \tag{10.4}$$

where v_o is the limiting specific volume, and T_o the corresponding temperature. The linear temperature coefficient of specific volume is defined as α. Since free volume is $v - v_o$ it follows from the above

relation that $v_f = v_o\alpha(T - T_o)$, and substitution into equation (10.1), the free volume equation yields

$$\ln \eta = A' + \frac{B'''}{(T - T_o)}, \qquad (10.5)$$

which has exactly the same form as equation (10.3). Here $B''' = B'/\alpha$.

Thus, by using the linear relationship between specific volume and temperature at a given pressure, the modified free volume equation is again derived. It is paradoxical that the same type of modified free volume equation can be derived by taking either density or specific volume as a linear function of temperature.

Equations (10.5) and (10.1) are equivalent when specific volume is a linear function of temperature.

10.1.3 The variation of v_o and T_o with pressure

It is proposed here that it is valid to use the free volume equation to describe the effect of pressure on viscosity, provided that the equation is applied isobarically. This is in contrast to earlier workers such as Hogenboom, Dixon and Webb (1967) who applied it as a function of pressure along the isotherms. For this proposed application, the free volume equation is stated more precisely as

$$[\ln \eta]_p = A' + B' \frac{v_o}{v_f}. \qquad (10.1a)$$

If the linear specific volume relationship $v = v_o\{1 + \alpha(T - T_o)\}$ is applied at a fixed pressure, then the modified free volume equation is derived, and this is re-stated more precisely as

$$[\ln \eta]_p = A' + \frac{B'''}{(T - T_o)}. \qquad (10.5a)$$

It is of interest to consider how the parameters A', B', B''', and in particular how v_o and T_o vary with pressure. Examination of specific volume as a function of temperature shows a series of straight lines whose gradients decrease with pressure as shown in Fig. 10.1. If T_o remains constant as pressure is increased, then v_o will become less, taking values falling on line AB in the figure, implying that v_o is

compressible. On the other hand, if v_o is incompressible, then T_o would assume values at the intercepts of line AC with the volume isobars which is not possible, since this would produce high T_o values at elevated pressures.

Thus v_o appears to vary with pressure, although T_o does not necessarily remain constant.

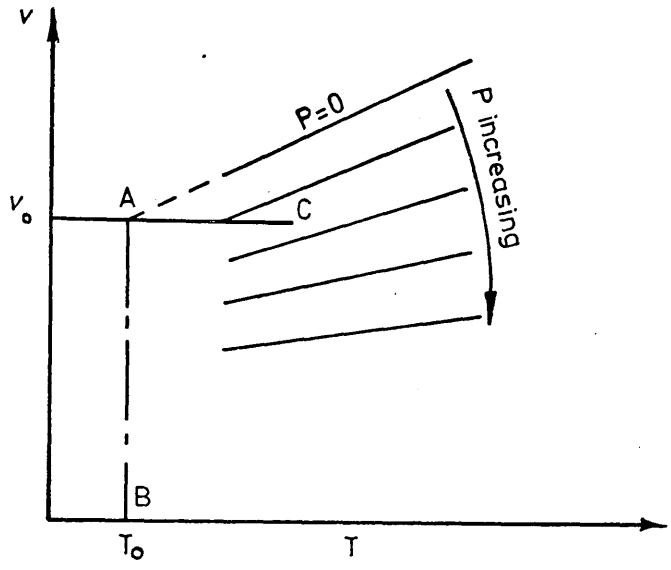

FIG 10·1 Isobaric specific volume as a function of temperature

That the limiting specific volume should become less under pressure is a realistic supposition. In addition to the argument above, it has been suggested by others, including Matheson (1966).

10.1.4 Methods of finding the variation of v_o with pressure

At any fixed pressure v_o is constant, and therefore if viscosity and density data are available over a range of temperature then v_o can be found with A′ and B′ by optimization, from equation (10.1a) (the free volume equation).

Alternatively, viscosity-temperature data can be fitted to equation (10.5a) (the modified free volume equation) to find A′, B‴ and T_o, along the isobars. By using the linear specific volume temperature correlation, the value of v_o at temperature T_o is found by extrapolation, at each pressure.

Since both equations are equivalent, the method adopted is arbitrary except in the case where the precision in specific volume data is poor, in which case equation (10.5a) is preferable. Both methods involve

considerable effort in the preparation of data because viscosity data are usually presented as a function of pressure at a few fixed temperatures, but to apply the free volume equations as proposed here requires viscosity as a function of temperature at fixed pressure, and therefore the data require to be plotted, smoothed, and values taken along isobars of viscosity-temperature curves. This is time consuming when done accurately.

10.2 Free Volume Calculations

Some data from the ASME Report (1953) were used to test the effectiveness of the proposed interpretation of the free volume model. The data are among the best available since viscosity and density values of fairly high accuracy are reported over a wide range of pressure and temperature. Smoothed data from the paper by Hogenboom, Webb and Dixon (1967) are also used.

10.2.1 Di-(2-ethylhexyl) phthalate

a Preparation of data

For this liquid the ASME data are from 32 to 425°F (0 to 218.3°C) up to pressures of 145 klb/in^2 ($\sim$10 kbar). The isothermal curves of viscosity as a function of pressure are shown in Fig. 10.2 where it is seen the curves are concave towards the pressure axis, with those at the lower temperatures tending towards linearity at higher pressures. Viscosity values were taken from this graph at 10 klb/in^2 pressure intervals in readiness for fitting to the free volume equation. These isobaric values of viscosity are plotted as a function of temperature in Fig. 10.3 and show that the curves are roughly parallel to the atmospheric pressure curve. While not necessary to the procedure of fitting data to the free volume equation, this figure is shown in order to obtain a better understanding of viscosity-pressure-temperature behaviour.

To find the corresponding density data, the ASME values were plotted on a large scale and densities were read from the graph at the same isobars as for viscosity.

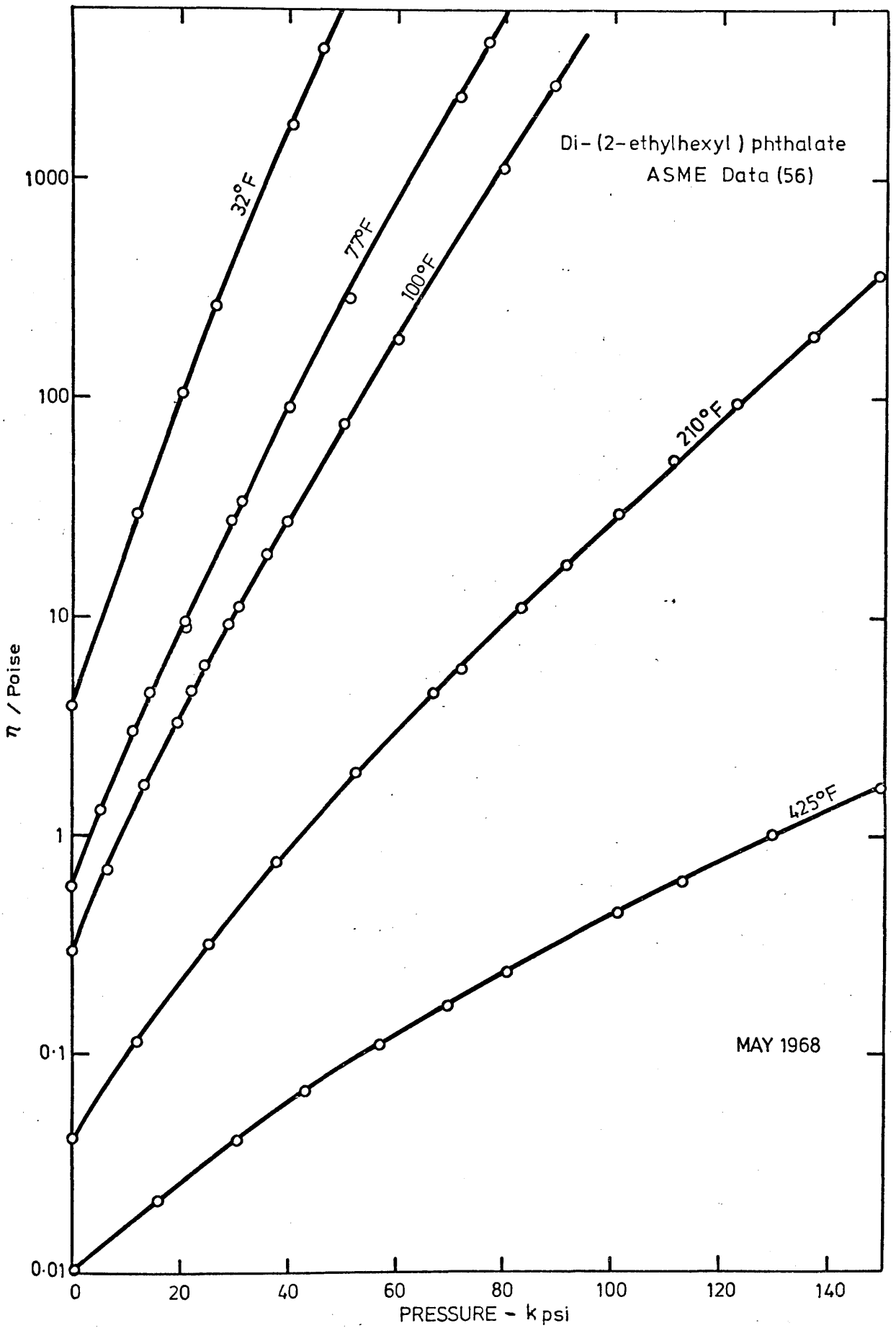

FIG 10·2 Log viscosity - pressure isotherms for di-(2-ethylhexyl) phthalate

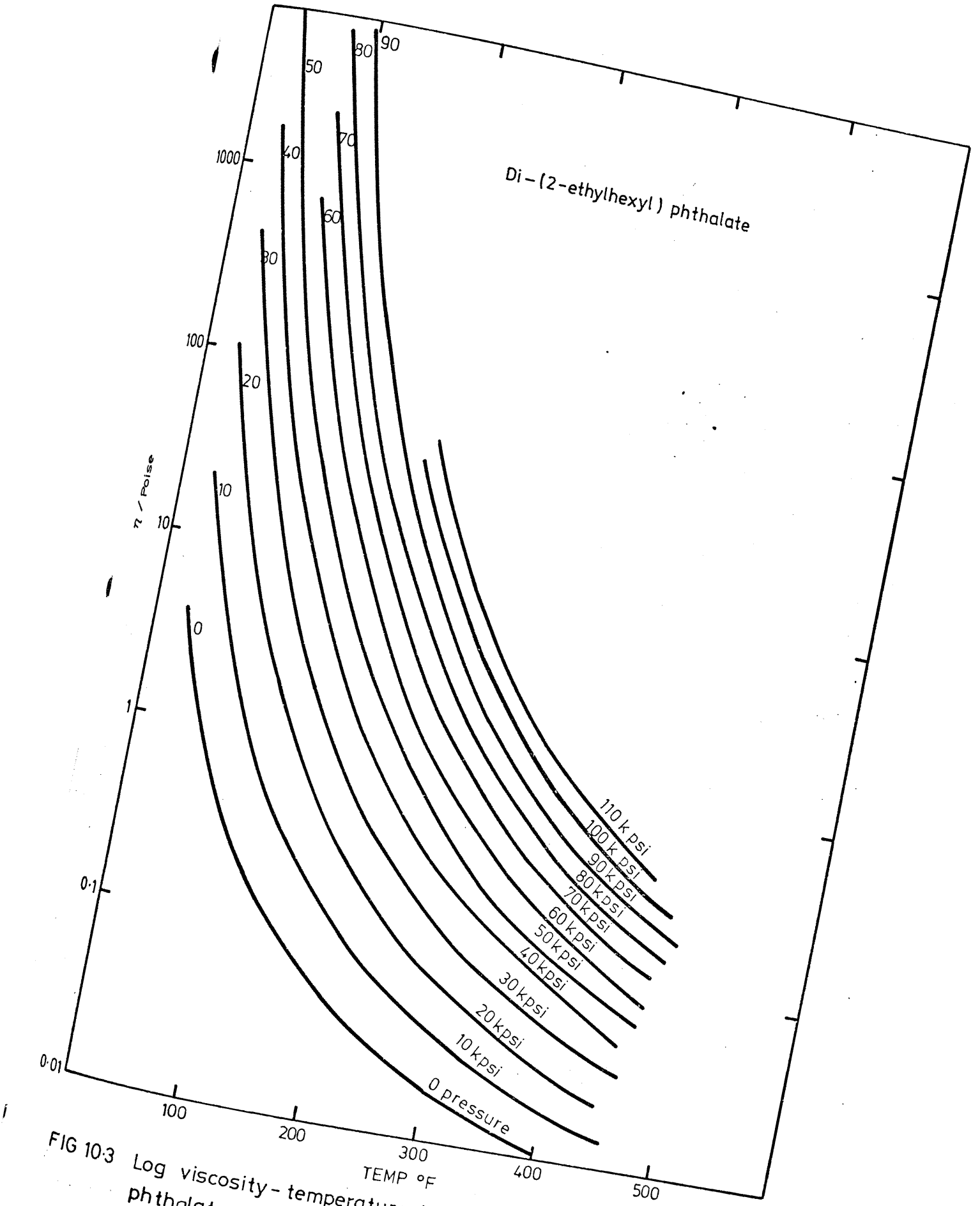

FIG 10·3 Log viscosity-temperature isobars for di-(2-ethylhexyl) phthalate

b Fitting data to the free volume equation

The viscosity and density data were fitted, at pressure intervals of 20 klb/in^2, up to 100 klb/in^2, to the free volume equation:

$$[\ln \eta]_p = A' + B' \frac{v_o}{v_f}. \qquad (10.1a)$$

The parameters A′, B′, and v_o were calculated by digital computer using an optimization procedure proposed by R Jefferyes (1967). The following table summarises the results.

Table 10.1

The parameters A′, B′, and v_o of the free volume equation for di-(2-ethylhexyl) phthalate

Pressure klb/in^2	No of points	A′	B′	v_o cm^3 g^{-1}	Max error in η %
0	6	-6.27	0.412	0.952	2.1
20	6	-6.67	0.523	0.907	-2.2
40	6	-6.77	0.563	0.880	-5.6
60	6	-7.08	0.569	0.863	-7.2
80	6	-6.73	0.454	0.855	-8.6
100	3	-6.61	0.382	0.847	-

Data are fitted from 100 to 425°F to obtain the above parameters. It was found that the values from 32 to 100°F do not conform to the free volume equation. This small range where free volume does not apply is discussed later.

The table shows that A′ does vary from pressure to pressure, but only slightly, and this could be attributable to some extent to the uncertainty of the experimental data. The parameter B′ also varies with pressure, first increasing, and then decreasing in a systematic manner. The limiting specific volume, v_o, decreases smoothly with increase in pressure which shows that it is compressible. These first results are promising in that the parameters are shown in principle to conform to the general model of free volume, and v_o is seen to be compressible as one would expect from physical considerations. Using

the isobaric approach, the errors on recalculation over a range of five decades of viscosity are all within +2.1 per cent to -8.6 per cent, as shown in Table 10.1. The errors are not systematic.

The free volume equation is strikingly simple in that when viscosity is plotted on a logarithmic scale as a function of v_o/v_f, a straight line should result. The equation is independent of temperature because this is accounted for in the specific volume behaviour contained in v_f. These results suggest that while A′ and B′ are independent of temperature, as originally proposed by Doolittle (1951), they are not independent of pressure. This is illustrated to advantage in Fig. 10.4 where log η is plotted as a function of v_o/v_f for the isobars 0, 20, 40, 60, 80 and 100 klb/in^2. A fan of converging straight lines results. The effect of pressure upon B′ (the gradient) is clearly seen; the gradient increases with pressure to a maximum at 40 klb/in^2 and then decreases thereafter to 100 klb/in^2.

c Fitting data to the modified free volume equation

The viscosity-temperature data for di-(2-ethylhexyl) phthalate were fitted at pressure intervals of 20 klb/in^2 to the modified free volume equation

$$[\ln \eta]_p = A' + \frac{B'''}{(T - T_o)}. \qquad (10.5a)$$

The results are in the following table, in which v_o is calculated from the optimised T_o using the linear specific volume relation of equation (10.4).

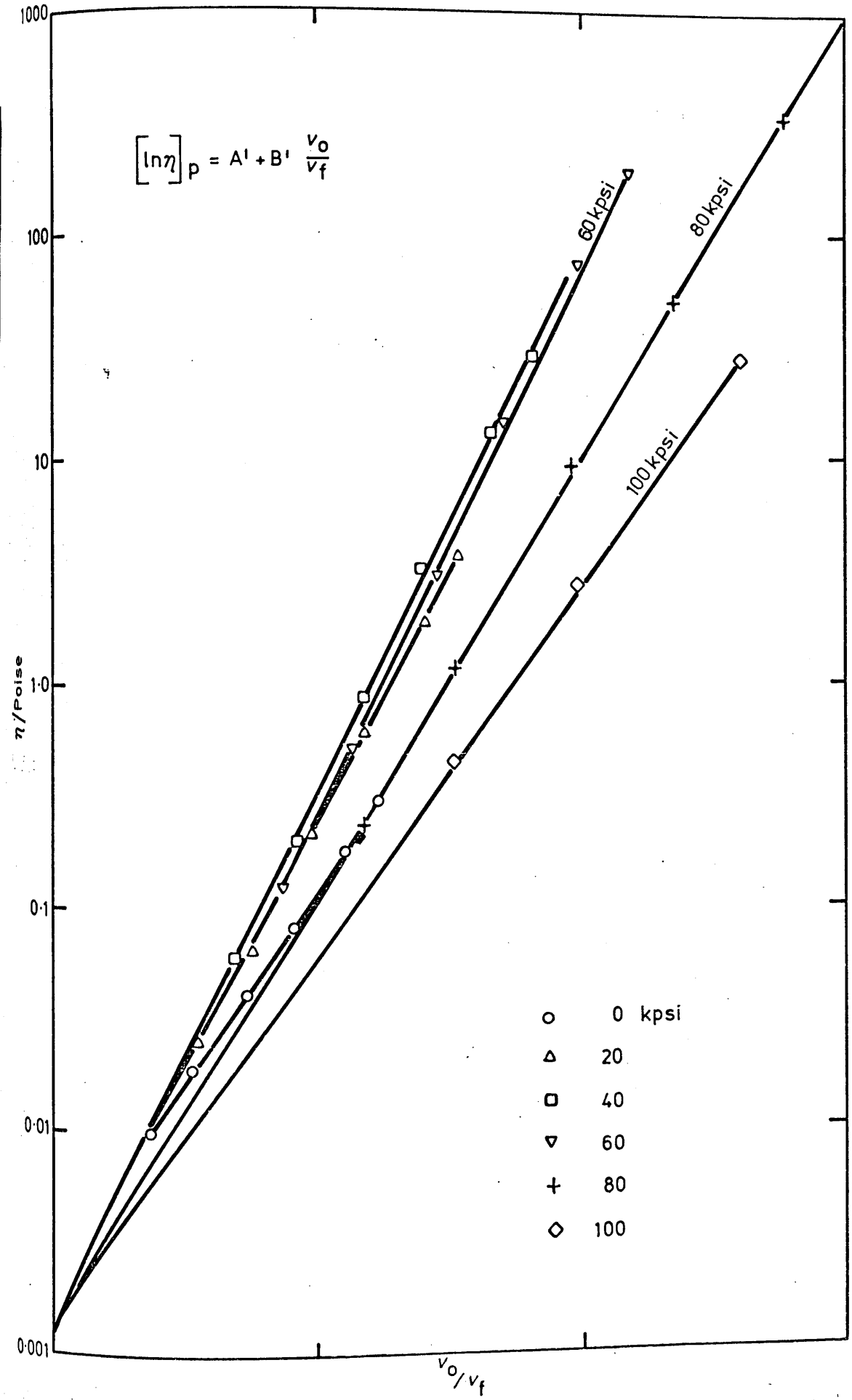

FIG 10·4 Log η as a function of v_o/v_f for di-(2-ethylhexyl) phthalate

Table 10.2

The parameters A', B''', and T_o of the modified free volume equation for di-(2-ethylhexyl) phthalate

Pressure klb/in^2	No of points	A'	B''' K	T_o K	v_o cm^3 g^{-1}
0	7	-6.71	598	202	0.951
20	7	-6.73	888	201	0.906
40	7	-6.79	1175	196	0.880
60	7	-6.88	1411	195	0.865
90	7	-6.84	1655	200	0.854

Data were fitted over the range 100 to 425°F, the same range as used for fitting the free volume equation. Parameter B''' varies rapidly with pressure, increasing linearly, while A' and T_o are virtually constant. The agreement between the v_o values calculated from T_o and those found from the free volume equation given in Table 10.1 is excellent. This is not surprising since the two forms of equation are exactly equivalent.

The most significant results is that T_o is found to be constant within experimental error for di-(2-ethylhexyl) phthalate, and this was established without placing any constraints on A' and B'''.

10.2.2 Di-(2-ethylhexyl) sebacate

Viscosity and specific volume data from the ASME Report were prepared in the same way as for di-(2-ethylhexyl) phthalate, and fitted to the free volume equation. The results are tabulated below.

Table 10.3

The parameters A′, B′, and v_o of the free volume equation for di-(2-ethylhexyl) sebacate

Pressure klb/in^2	No of points	A′	B′	v_o cm^3 g^{-1}	Max error in η %	T_o* K
0	5	-6.802	0.603	0.9798	3.3	165
10	5	-6.602	0.540	0.9684	2.3	165
20	5	-6.390	0.485	0.9572	9.7	166
30	5	-6.469	0.519	0.9398	9.2	164
40	5	-6.458	0.531	0.9270	9.6	162
50	5	-6.248	0.490	0.9197	-6.7	166
60	5	-6.209	0.483	0.9103	8.4	167
70	5	-6.554	0.538	0.8989	-6.9	160
90	5	-6.561	0.548	0.8831	-33.4	156
110	4	-6.986	0.620	0.8657	-20.1	147
130	4	-7.777	0.717	0.8518	-12.9	-
150	4	-7.697	0.707	0.8411	-36.9	-

*Found from v_o by linear extrapolation

All the data were used, unlike the previous case where values below 100°F were omitted, and this is reflected in the poorer fit shown by the maximum errors in the table above. Even so, this constitutes a very good fit since the viscosity range covers five decades.

The limiting specific volume decreases smoothly with pressure, while A′ is essentially constant except at very high pressures, but B′ varies with pressure in a different manner from di-(2-ethylhexyl) phthalate. Fig. 10.5 is a graph of log η as a function of v_o/v_f, and the straight lines for each isobar are contained in a narrow spread, especially within the range 0 to 90 klb/in^2.

It has been shown that equations (10.1a) and (10.5a) are equivalent when isobaric specific volume varies linearly with temperature.

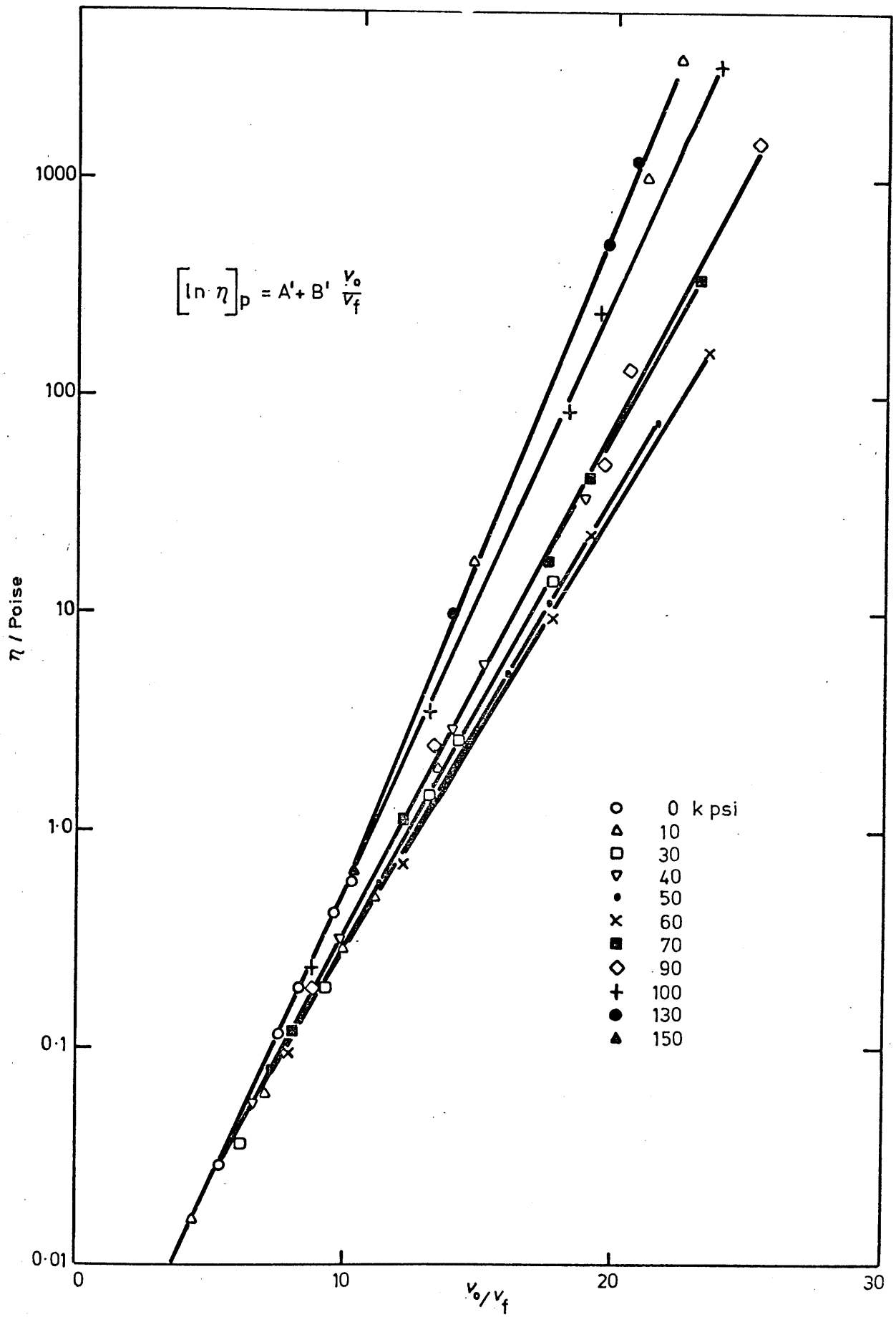

FIG 10·5 Log η as a function of v_o/v_f for di-(2-ethylhexyl) sebacate

Rather than fit viscosity-temperature data to equation (10.5a), T_o is found in this case by linear extrapolation of specific volume to find the temperature, T_o, which corresponds to v_o for each isobar. The T_o values are added in the last column of Table 10.3. Up to 70 klb/in^2, T_o is constant at 165 ± 2 K to within accuracy of calculation, but above this pressure it decreases to about 147 K. At these higher pressures it is difficult to assess how much of this apparent drop in T_o is real, and how much is due to there being less data with which to optimise.

At this point no conclusions will be drawn as to the significance of the behaviour of A′, B′, v_o (and T_o), but it is worth comparing the trends shown by them for the two liquids studied so far. The variation of v_o for both di-(2-ethylhexyl) phthalate and di-(2-ethyhexyl) sebacate is similar; it decreases with pressure, corresponding to the behaviour one expects intuitively. Under pressure, A′ shows some variation but this is comparatively small, being more at zero pressure for the phthalate, but more marked at high pressures for the sebacate. The variation of B′ differs from one liquid to the other. The effect of pressure is less on the sebacate as can be seen by comparing Figs 10.4 and 10.5 which are drawn to the same scale.

10.2.3 1-cyclopentyl-4(3-cyclopentylpropyl) dodecane (ASME liquid No 10)

This liquid is a pure hydrocarbon of high molecular weight, 348.6, and the data are from the ASME Report (1953). Viscosity and specific volume data are given from 32 to 400°F (0 to 204.4°C) at pressures up to 151 klb/in^2 (∿ 10 kbar). For this liquid, viscosity varies by less than four decades. Data were prepared as before up to 36.8 klb/in^2, above which there are no further measurements at 32°F. The results of fitting the data to the free volume equation follow.

Table 10.4

The parameters A′, B′, and v_o of the free volume equation for ASME liquid No 10

Pressure		No of points	A′	B′	v_o	Max error in η	T_o*
klb/in^2	kbar				$cm^3\ g^{-1}$	%	K
0	0	5	-6.173	0.386	1.079	-9.3	196
7.4	0.5	5	-6.561	0.498	1.049	-12.4	183
14.7	1.0	5	-6.959	0.564	1.032	8.8	167
22.1	1.5	5	-7.202	0.626	1.015	-8.7	156
29.4	2.0	5	-7.590	0.717	0.999	9.9	146
36.8	2.5	5	-7.035	0.640	0.993	-21.2	159

*Found from v_o by linear extrapolation

The maximum errors in recalculated viscosity occur at the low temperature region near 0°C, and had the data at this temperature been discarded, an even better fit would have been found. Nevertheless, the quality of fit of the free volume equation along these isobars is still quite good.

As for the previous two liquids, v_o shows a decrease with pressure, and the corresponding temperature T_o is given in the table. In this case T_o decreased with temperature; the uncertainty in these T_o values is about ±5 K.

In Fig. 10.6 log η is plotted as a function of v_o/v_f, and a fan of converging straight lines is seen.

10.3 Interpretation of Free Volume Results

Viscosity and specific volume data have been fitted to the free volume equation along isobars for three liquids, allowing complete freedom in A′, B′, and v_o. Other investigators have also applied free volume to interpret viscosity-pressure-temperature data but have done so by taking data along the isotherms. Among these investigators are Dixon and Webb (1962), and later Hogenboom, Webb and Dixon (1967) who found that v_o tended to increase with decreasing

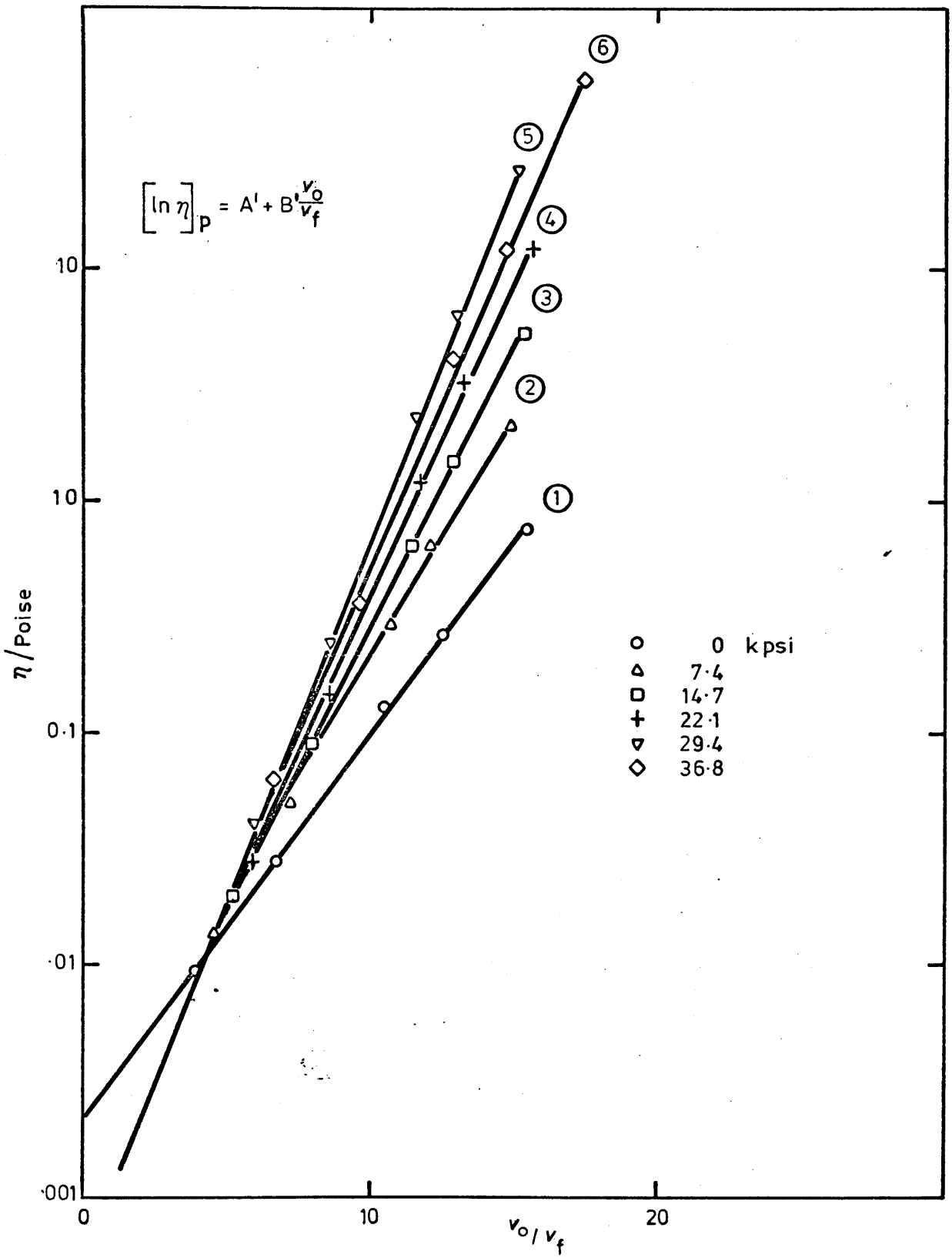

FIG 10·6 Log η as a function of v_o / v_f for ASME liquid no. 10

temperature, which is opposite to normal behaviour, and for which no explanation could be offered. Matheson (1966) adopted a different approach by supposing that v_o is a function of pressure and temperature but regarded A′ and B′ as independent of both.

This new approach does not claim to produce a better fit to the data, but does show that the parameters of the free volume model do vary in a physically realistic manner.

10.3.1 Limiting specific volume, v_o

In Fig. 10.7, v_o is plotted as a function of pressure for the three liquids, and in each case the limiting specific volume decreases, rapidly at first and then flattening off at elevated pressures.

In Chapter 6 it was shown that the modified secant modulus equation provides an excellent fit to specific volume as a function of pressure:

$$v = a + \frac{b}{k + p}, \qquad (6.20)$$

where $a = v_\infty$, the value to which specific volume tends asymptotically as pressure approaches infinity. Data were fitted to this equation for di-(2-ethylhexyl) phthalate from 0 to 98.9°C (Table 6.2) and it was found that v_∞ lies between 0.736 and 0.765 $cm^3\ g^{-1}$. When v_o is extrapolated towards infinite pressure in Fig. 10.7, it is seen that it agrees fairly well with the v_∞ predicted from v - T data. This suggests that from a physical standpoint both v_o and v_∞ both tend toward a common realistic value, which is the ultimate limit of specific volume.

For di-(2-ethylhexyl) sebacate, v_∞ was found by fitting to be between 0.761 and 0.816 $cm^3\ g^{-1}$. This agrees very well with v_o when graphically extrapolated towards infinite pressure, Fig. 10.7. Specific volume data for ASME liquid No 10 were not fitted to the equation above, but the v_o values show a similar shape to the other two liquids.

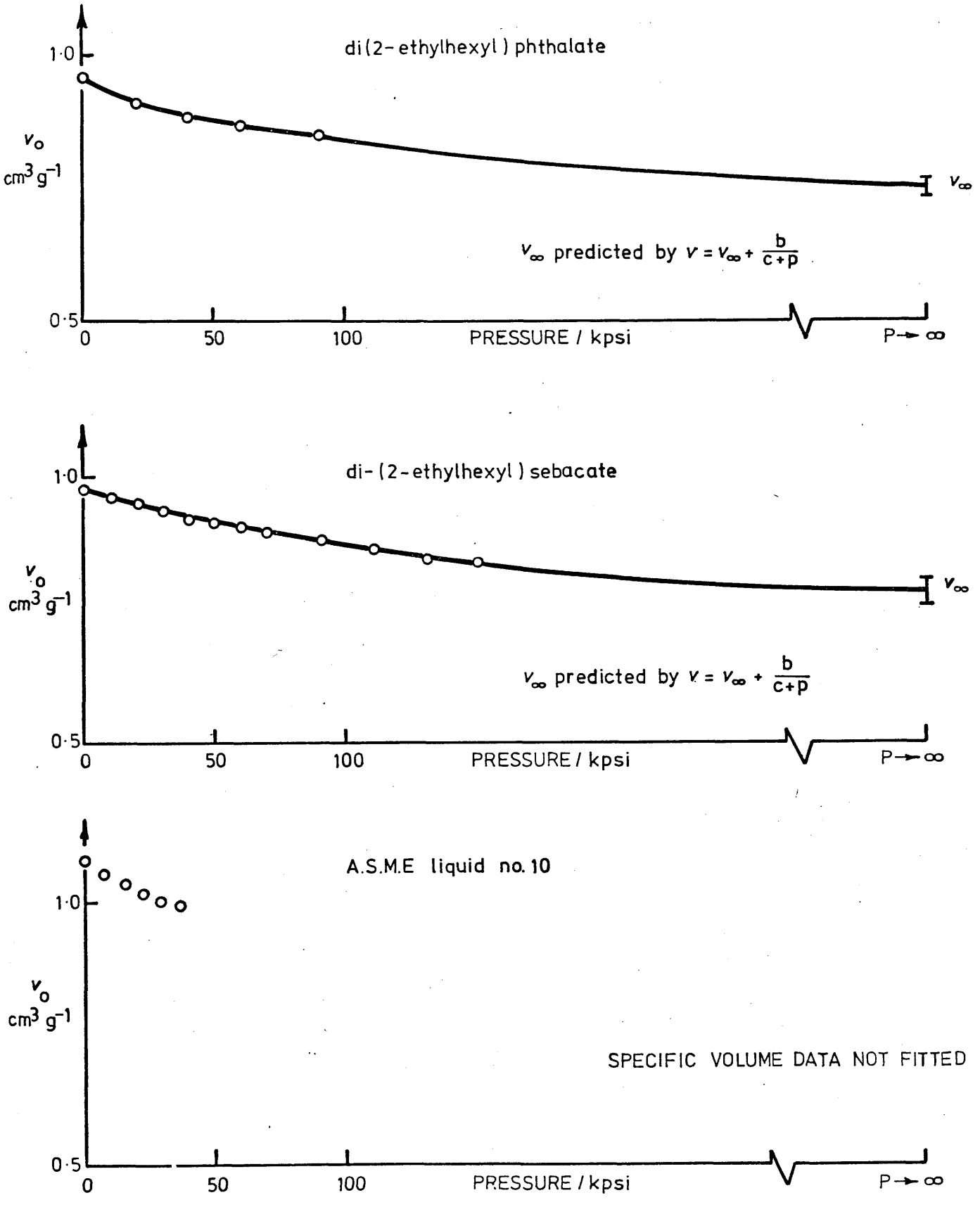

FIG 10·7 Variation of v_o with pressure for three liquids

10.3.2 The variation of A′ and B′ with pressure

In his original proposal of the free volume equation Doolittle (1951) stated that "A′ and B′ = constants for a single substance", and that at fixed pressure v_o/v_f is a function of temperature only. He did not specify whether or not v_o itself is constant for a single substance, but did state that "presumably changes in relative free-space (v_f/v_o) result from changes in pressure ... but data have not so far been obtained that could be used in a similar study of the pressure variable". This statement tells us nothing about v_o, because it is obvious that v_f is a function of pressure since it contains specific volume, v. None of his subsequent papers in the series 'Studies in Newtonian Flow' (1952a), (1952b) and (1957) discusses the effects of pressure.

In his treatment, Matheson (1966) considered A′ and B′ as constants and allowed v_o to be a function of pressure and temperature, giving it the characteristics of a solid. Earlier Dixon and Webb (1962) fitted data to the free volume equation along isotherms, and thus considered A′, B′ and v_o as functions of temperature, and later Hogenboom, Webb and Dixon (1967) reported the results of the same approach, but did not publish the A′ and B′ values.

The plots of log η as a function of v_o/v_f are shown for the three liquids where the data were fitted along isobars in Figs 10.4 to 10.6. Although these three liquids are different types, when they are plotted on one graph they show a remarkable similarity as seen in Fig. 10.8.

With the exception of di-(2-ethylhexyl) phthalate at 100 klb/in^2, all the lines converge at one point where η = 1 cP and $v_o/v_f \approx 4$. This exception is at the highest pressure where there is only limited data; and the line has been extrapolated back by about two decades of viscosity so that small errors are amplified.

That the three liquids should have log η versus v_o/v_f lines which so nearly converge is quite striking, but this pattern could be fortuitous. Whether or not this is so, the fact that each family does converge immediately allows A′ and B′ to be readily correlated.

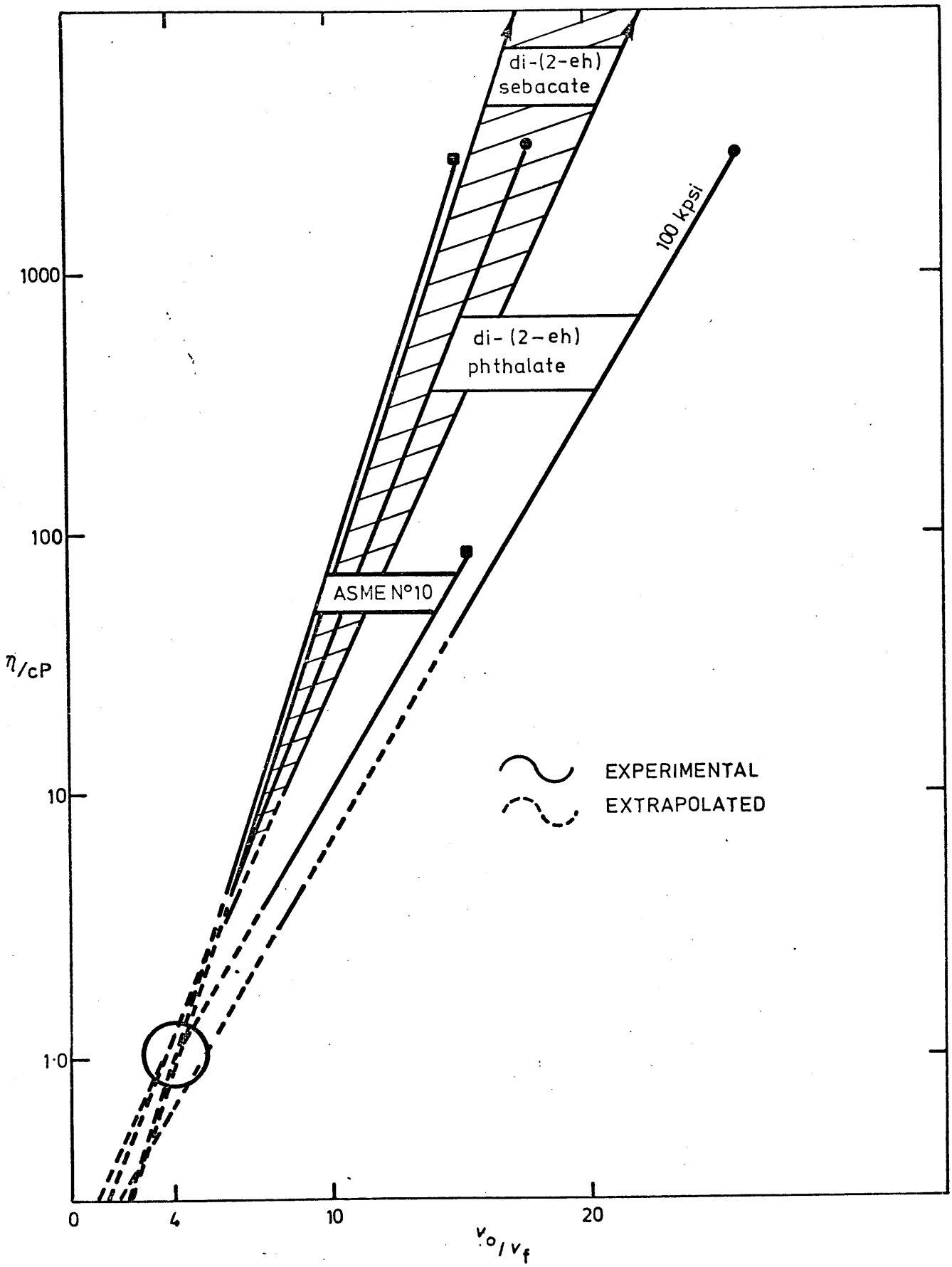

FIG 10·8 Log η as a function of v_o/v_f – convergence at 1cP

Before doing so, however, a verification of this behaviour was sought.

Hogenboom et al (1967) have fitted atmospheric pressure data to the free volume equation for nine liquids and reported A', B' and v_o values. The convergence of the three liquids being studied here showed a focal point at η = 1 cP, and $v_o/v_f \approx 4$. This implies, on substitution into the free volume equation that:

$$\ln \eta_o = A' + 4B', \tag{10.6}$$

where η_o is the reference viscosity which is approximately equal to 1 cP.

From this equation

$$\eta_o = \exp\ (A' + 4B'). \tag{10.7}$$

The value of η_o was calculated for each of the liquids in the paper of Hogenboom et al, using their values of A' and B'. The values of A', B', and η_o are in Table 10.5 where it may be seen that the average value of η_o is 0.87 cP, with a standard deviation of ±0.09 cP. This value of 0.87 cP is gratifyingly close to the figure of 1 cP which, after all, was an approximate value taken from the graph of Fig. 10.8. The same procedure was applied to the three liquids using the A' and B' values already calculated at various pressures, as well as at atmospheric pressure to show exactly the variation of η_o. The results in Table 10.6 show the phthalate, sebacate, and ASME liquid No 10 to have average viscosities of 0.88, 1.08 and 0.97 cP respectively. If the 100 klb/in^2 isobar of di-(2-ethylhexyl) phthalate η_o is omitted, then the average value is increased from 0.88 to 0.94 cP.

These results, therefore, show that to a fairly good first approximation, many liquids of greatly differing structures all converge at about 1 cP for $v_o/v_f = 4$, or, in other words, that at 1 cP the liquids have about 20 per cent free volume. This generalisation holds at high pressures as well as at atmospheric pressure.

Table 10.5

Test for viscosity convergence at $v_o/v_f = 4$ for nine liquids at atmospheric pressure

	A′	B′	(A′ + 4B′)	$\eta_o = e^{(A' + 4B')}$ cP
1. cis-decahydronaphthalene (0 to 100°C)	-2.719	0.668	-0.047	0.95
2. trans-decahydronaphthalene (0 to 100°C)	-2.753	0.653	-0.139	0.87
3. spiro (4,5) decane (0 to 100°C)	-2.541	0.608	-0.111	0.90
4. spiro (5,5) undecane (0 to 100°C)	-2.671	0.628	-0.158	0.85
5. cis-octahydroindene (15.6 to 115°C)	-2.942	0.637	-0.396	0.67
6. trans-octahydroindene (15.6 to 115°C)	-2.852	0.696	-0.068	0.93
7. $n\text{-}C_{12}$ (0 to 100°C)	-2.773	0.646	-0.190	0.83
$n\text{-}C_{12}$ (90 to 210°C)	-3.130	0.946	+0.653	1.92 *
8. $n\text{-}C_{15}$ (30 to 150°C)	-2.550	0.598	-0.157	0.86
$n\text{-}C_{15}$ (110 to 250°C)	-3.069	0.977	+0.838	2.31 *
9. $n\text{-}C_{18}$ (30 to 150°C)	-2.494	0.624	+0.004	1.00
$n\text{-}C_{18}$ (160 to 250°C)	-3.089	1.104	1.327	3.77 *

Average $\eta_o = 0.874 \pm 0.09$ cP (excluding *values). * High temperature region

A′ and B′ from Table VI of paper by Hogenboom, Webb and Dixon (1967)

Liquids 1 to 4. Data from Pennsylvania State University Project 42 (1962)

Liquids 5 and 6. Data by Hogenboom et al (above)

Liquids 7 to 9. Rossini et al (1953). Data also used by Doolittle (1951)

Table 10.6

Test for viscosity convergence at $v_o/v_f = 4$ for three liquids, along their isobars

Pressure klb/in^2	A′	B′	(A′ + 4B′)	$\eta_o = e^{(A' + 4B')}$ poise
di-(2-ethylhexyl) phthalate				
0	-6.27	0.412	-4.62	0.010
20	-6.67	0.523	-4.54	0.011
40	-6.77	0.563	-4.52	0.011
60	-7.08	0.569	-4.80	0.008
80	-6.73	0.454	-4.91	0.007
100	-6.61	0.382	-5.08	0.006
				0.008_8 = average
di-(2-ethylhexyl) sebacate				
0	-6.80	0.603	-4.39	0.012
10	-6.60	0.540	-4.44	0.012
30	-6.47	0.519	-4.39	0.012
50	-6.25	0.490	-4.29	0.014
70	-6.55	0.538	-4.40	0.012
90	-6.56	0.548	-4.73	0.009
110	-6.99	0.620	-4.51	0.011
130	-7.78	0.717	-4.91	0.007
150	-7.70	0.707	-4.87	0.008
				0.010_8 = average
ASME liquid No 10				
0	-6.17	0.386	-4.63	0.010
7.4	-6.56	0.498	-4.57	0.010
14.7	-6.96	0.564	-4.70	0.009
22.1	-7.20	0.626	-4.70	0.009
29.4	-7.59	0.717	-4.72	0.009
36.8	-7.04	0.640	-4.48	0.011
				0.009_7 = average

10.4 A Tentative Simplification of the Free Volume Equation

In the previous section it was shown that for several different liquids,

$$\ln \eta_o = A' + 4B'.$$

By combining this with the free volume equation, and eliminating A′ the following relationship is derived

$$[\ln \eta]_p - \ln \eta_o = B' \left(\frac{v_o}{v_f} - 4\right). \qquad (10.8)$$

Since η_o = 1 cP to a good approximation, and provided that cPoise units are used then equation (10.8) reduces to

$$[\ln \eta]_p = B' \left(\frac{v_o}{v_f} - 4\right). \qquad (10.9)$$

10.4.1 A test of the simplified free volume equation at atmospheric pressure

One set of viscosity-density data ($v = 1/\rho$) was chosen at random from the paper by Hogenboom et al (1967). Their A′, B′, and v_o values were used to recalculate viscosity, and the results are in Table 10.7 for later comparison. The results show an r.m.s. error of 0.25 per cent.

A fit to the new equation (10.9) was carried out. This simplified equation has only two disposable parameters, namely B′ and v_o. From the point of view of optimization, however, the equation is very non-linear indeed, and B′ and v_o were therefore found by trial and error using a pocket calculator. After five iterations an r.m.s. error in viscosity of 0.44 per cent was achieved which is almost to within experimental error. Results of the calculation are in Table 10.7 where it is seen that there is a slight systematic error. Further calculation would probably reduce the r.m.s. error but this was not considered worthwhile.

This result shows that the proposed two-constant simplified free volume equation describes viscosity-specific volume data at atmospheric pressure with almost the same accuracy as the three-constant free volume equation.

Table 10.7

Viscosity data fitted to the simplified free volume equation at atmospheric pressure

$\ln \eta = -2.852 + \frac{0.6960 \times 0.960}{v - 0.960}$					$\ln \eta = 0.7228 \left(\frac{0.9553}{v - 0.9553} - 4\right)$		
Temp ^{o}C	η cP	v $cm^3\ g^{-1}$	η_{calc} cP	Diff %	v_o/v_f	η_{calc} cP	Diff %
15.56	1.81	1.1539	1.81	0.0	4.810	1.796	0.8
37.78	1.225	1.1787	1.225	0.0	4.276	1.221	0.4
60.00	0.885	1.2050	0.883	0.3	3.826	0.882	0.4
79.44	0.698	1.2282	0.697	0.1	3.501	0.697	0.1
98.89	0.565	1.2523	0.568	-0.5	3.216	0.567	-0.4
115.00	0.487	1.2737	0.486	0.3	3.000	0.485	0.3

Free volume equation r.m.s. error in η = 0.25%

Simplified equation r.m.s. error in η = 0.44%

trans-octahydroindene, data from Hogenboom et al (1967)

The value of v_o in the free volume equation is 0.960, and in the simplified free volume equation it is 0.9553 $cm^3\ g^{-1}$, a difference of 0.5 per cent. Accuracy to the fourth decimal place is required for v_o to maintain precision. The value of B′ differs from one equation to the other; in the simplified equation it is 3.9 per cent higher. It is clear, therefore, that the B′ and v_o values obtained by fitting data to the free volume equation cannot be applied to the simplified equation without sacrificing accuracy.

10.4.2 A test of the simplified free volume equation at pressure

Viscosity-specific volume data at several pressures were fitted to the equation $[\ln \eta]_p = B(v_o/v_f - 4)$ for three liquids. A program was written to optimise for B and v_o.

The detailed results for di-(2-ethylhexyl) phthalate are in Table 10.8 and the individual errors are listed as well as the r.m.s. percentage error for each isobar. The r.m.s. errors vary from 1.3 to 9.0 per cent, the latter occurring at 80 klb/in^2. This constitutes an excellent fit for a two-constant equation, and at 80 klb/in^2 the viscosity

Table 10.8

Di-(2-ethylhexyl) phthalate data fitted to the simpliefied free volume equation at different pressures

Pressure klb/in^2	Temperature ^oC	η cP	v $cm^3\ g^{-1}$	B′	v_o $cm^3\ g^{-1}$	η_{calc} cP	Diff %	r.m.s. % error
0	37.8	29.2	1.0290	0.431	0.9488	29.3	-0.4	1.2
	48.9	18.0	1.0377			17.8	1.1	
	71.1	8.40	1.0554			8.28	1.4	
	98.9	4.06	1.0790			4.13	-1.7	
	148.9	1.84	1.1231			1.86	-1.3	
	218.3	0.97	1.1913			0.96	0.7	
20	as	365.0	0.9666	0.534	0.9066	378.0	-3.6	1.8
	above	190.0	0.9722			190.0	0.1	
		60.0	0.9844			59.6	0.6	
		21.4	0.9998			21.3	0.4	
		6.50	1.0272			6.55	-0.7	
		2.56	1.0653			2.50	2.5	
40	as	2 900.0	0.9290	0.618	0.8773	3 021.0	-4.2	3.3
	above	1 300.0	0.9337			1 260.0	3.0	
		320.0	0.9431			320.0	-0.1	
		88.0	0.9550			90.5	-2.9	
		20.0	0.9760			20.5	-2.6	
		6.0	1.0060			5.70	5.0	

Table 10.8 (contd)

Pressure klb/in^2	Temperature ^oC	η cP	v $cm^3\ g^{-1}$	B′	v_o $cm^3\ g^{-1}$	η_{calc} cP	Diff %	r.m.s. % error
60	as above	18 600.0	0.9022	0.493	0.8665	22 000.0	-18.3	8.3
		7 000.0	0.9061			6 760.0	3.4	
		1 400.0	0.9132			1 310.0	6.4	
		300.0	0.9225			287.0	4.5	
		50.0	0.9391			50.1	-0.1	
		12.1	0.9615			12.5	-2.4	
80	37.8	117 000.0	0.8829	0.389	0.8579	129 000.0	-10.0	9.0
	48.9	32 000.0	0.8855			36 800.0	-14.9	
	71.1	5 000.0	0.8911			4 810.0	3.7	
	98.9	950.0	0.8981			840.0	11.6	
	148.9	120.0	0.9106			118.0	1.8	
	218.3	23.7	0.9280			24.5	-3.5	
100	98.9	2 860.0	0.8796	0.301	0.8517	2 980.0	-4.0	3.5
	148.9	864.0	0.8898			252.0	4.3	
	218.3	44.0	0.9030			44.5	-1.4	

Data from ASME Report (1953)

has changed by nearly four decades. The limiting specific volume, v_o, decreases with pressure as was found for the free volume equation, and B' is also a function of pressure, starting at 0.431 at 0 klb/in^2, increasing to 0.618 at 80 klb/in^2 and then falling to 0.301 at the maximum pressure of 100 klb/in^2. These parameters are plotted in Fig. 10.9.

It is significant that for each isobar the maximum difference between experimental viscosity and the recalculated value occurs at the minimum temperature where viscosity is greatest. For example, along the 60 klb/in^2 isobar (r.m.s. error = 8.3 per cent), the maximum error is -18.3 per cent at 37.8°C. This error is contributed to mainly by the low specific volume which is 0.9022 cm^3 g^{-1}, and an uncertainty in this value of as little as ±0.0005 cm^3 g^{-1} leads to a relatively large error in $v_f = v - v_o$. In this instance the resulting errors in v_f for v_o = 0.8665 cm^3 g^{-1} is 1.4 per cent, which causes a difference in recalculated viscosity of 15 per cent. This is important, because it means that where specific volume is low, that is at low temperature and at high pressure, any free volume equation is extremely sensitive to small errors of as little as 0.05 per cent, and therefore the efficacy of this equation cannot be properly assessed without very good quality specific volume data.

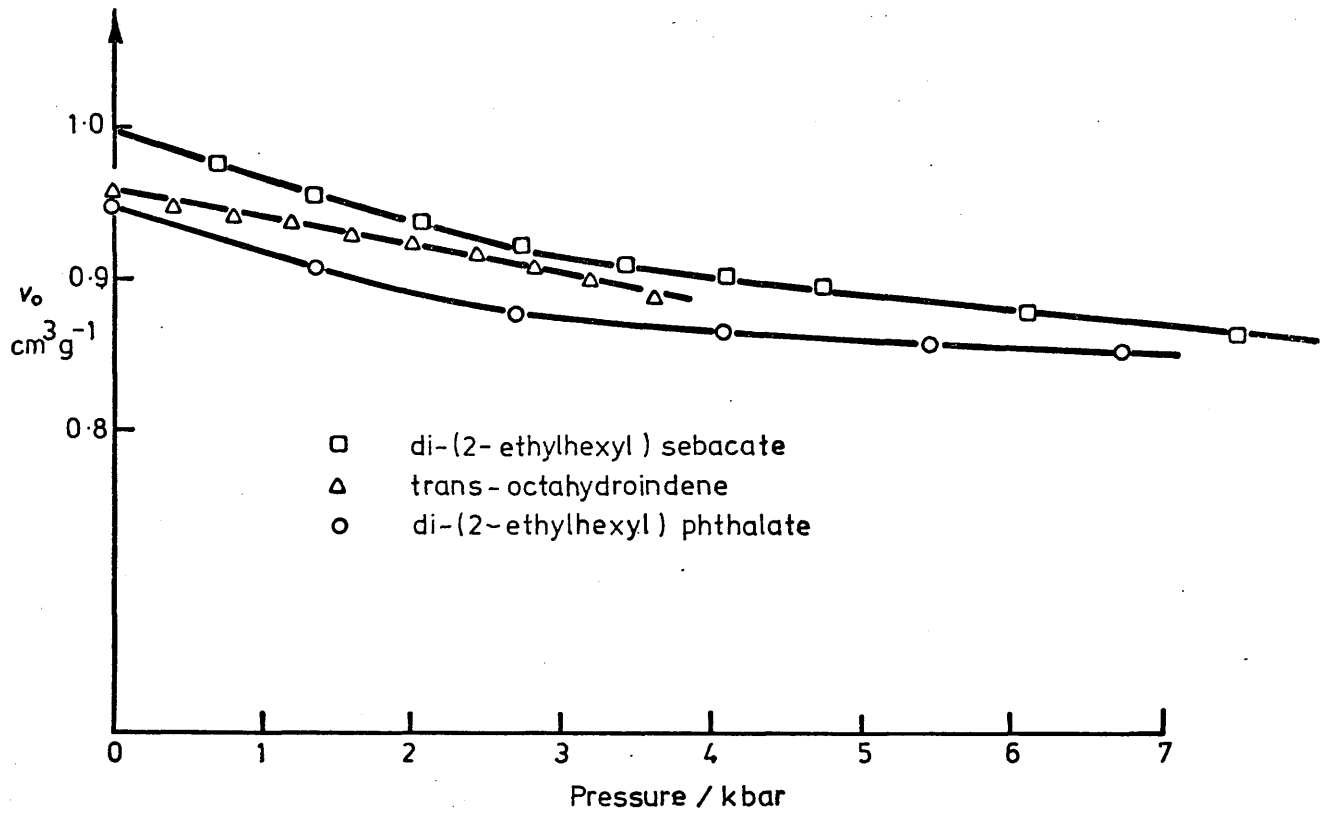

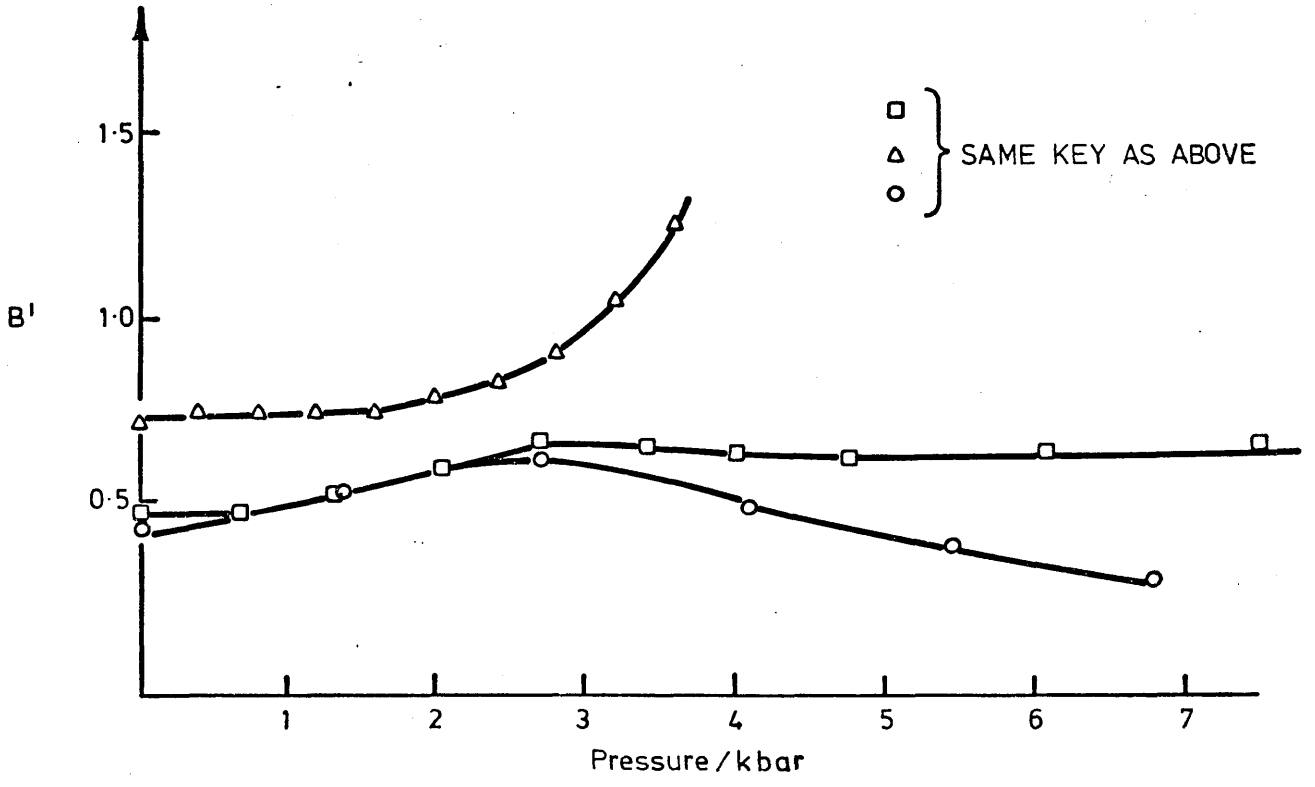

FIG 10·9 Variation with pressure of v_o and B' in equation $\ln\eta = B'(v_o/v_f - 4)$

The smoothed trans-octahydroindene data of Hogenboom et al (1967) were fitted. It should be noted that their values cover a 200°C temperature range, at pressures from 0 to 3.6 kbar, and the viscosity varies by less than one decade for each isobar. The results are summarised in Table 10.9 where values for B′ and v_o are given. The r.m.s. errors for each isobar are not greater than 2.9 per cent, with an overall maximum error of 5.1 per cent. This constitutes an excellent fit.

Table 10.9

Trans-octahydroindene data fitted to the simplified free volume equation at different pressures

Pressure kbar	B′	v_o $cm^3\ g^{-1}$	r.m.s. % error
0	0.727	0.9555	0.3
0.4	0.748	0.9486	1.6
0.8	0.751	0.9425	1.8
1.2	0.747	0.9372	2.5
1.6	0.750	0.9324	2.8
2.0	0.789	0.9255	2.9
2.4	0.0832	0.9185	2.6
2.8	0.913	0.9101	1.6
3.2	1.048	0.8999	1.6
3.6	1.260	0.8880	2.9

Data from Hogenboom et al (1967)

Data for di-(2-ethylhexyl) sebacate were also fitted to the simplified free volume equation. The values of viscosity change up to four decades within the temperature range 0 to 218.3°C, along each isobar up to 110 klb/in^2 (∿7.5 kbar). This is a much more severe test of the equation than the previous liquid because it covers such a wide range of viscosity, pressure, and temperature. The results are in Table 10.10. All the r.m.s. errors are within 10.1 per cent except for the 90 klb/in^2 isobar.

Table 10.10

Di-(2-ethylhexyl) sebacate data fitted to the simplified free volume equation at different pressures

Pressure klb/in^2	B′	v_o cm^3 g^{-1}	r.m.s. % error
0	0.481	0.9959	6.5
10	0.491_5	0.9755	9.8
20	0.544	0.9540	10.1
30	0.604	0.9352	9.5
40	0.666	0.9197	9.4
50	0.648	0.9107	8.4
60	0.634	0.9020	9.6
70	0.634	0.8939	8.3
90	0.644	0.8786	20.1
110	0.660	0.8643	9.3

10.4.3 Conclusions on the effectiveness of the simplified free volume equation

The proposed simplified free volume equation is

$$[\ln \eta]_p = B' \left(\frac{v_o}{v_f} - 4 \right). \qquad (10.9)$$

It has two disposable parameters B′ and v_o which are functions of pressure, and the equation was derived from the observation that when log η is plotted as a function of v_o/v_f, then a fan of straight lines is found which converge approximately at $v_o/v_f = 4$, where $\eta \approx 1$ cP.

This behaviour was noted for twelve different liquids with atmospheric pressure data, and also with pressure data up to 15 kbar for three liquids.

When B′ and v_o were found by optimization, using trans-octahydroindene data the r.m.s. error in recalculated viscosity varied from 0.3 per cent for the atmospheric pressure isobar, up to 2.9 per cent for the 3.6 kbar isobar. Although this is a very good fit, the data do not impose a very severe test on the equation because the temperature range of 100°C is not large, and having a fairly symmetrical molecular structure the liquid viscosity is not as sensitive as other more complex liquids to variations of pressure.

A more exacting test of the equation was with di-(2-ethylhexyl) phthalate data for temperatures from 37.8 to 218.3°C, for pressures up to 10 kbar. The equation describes the data well, with r.m.s. errors of 3.5 per cent or less for four out of six isobars. The maximum error is -18.3 per cent at 60 kbar, but this occurs where an uncertainty of only 0.0005 $cm^3\ g^{-1}$ in specific volume gives rise to a 15 per cent error in viscosity. This shows that the equation requires accurate data where $v_f (= v - v_o)$ is small.

Lastly, the equation was tested against di-(2-ethylhexyl) sebacate using the available data down to 0°C. The errors are larger, due in part to the uncertainty of specific volume data, with r.m.s. errors of about 10 per cent except at 90 klb/in^2 where it is 20 per cent. The fit is still considered to be quite good in view of the fact that it covers a viscosity range of almost six decades, that is from 0.73 to 630 000 cP.

The effectiveness of the simplified equation is limited, although not to a great extent for the three liquids which have been considered, by small specific volume errors producing large variations in viscosity. These errors occur at high pressure combined with low temperature - less than about 35°C for the phthalate, for example. The region where viscosities become dangerously inaccurate can be quantified by differentiating equation (10.9) to give the identity

$$\frac{\Delta\eta}{\eta} = \frac{B' v_o \Delta v}{(v - v_o)^2}. \qquad (10.10)$$

If the acceptable limit of viscosity error is set at say 10 per cent (ie $\Delta\eta/\eta = 0.1$), then for $\Delta v = 0.0005$ cm^3 g^{-1} we have

$$v - v_o = \sqrt{\left(\frac{B'v_o\ 0.0005}{0.1}\right)}$$

thus

$$v - v_o = \sqrt{(0.005B'v_o)}. \qquad (10.11)$$

Both B' and v_o are slowly varying functions of pressure, and for di-(2-ethylhexyl) phthalate the average value of $B'v_o$ is 0.44, with a standard deviation of ±0.11. But $v - v_o$ equals the free volume, and so for this liquid it may be stated that where v_f is less than 0.047 cm^3 g^{-1}, then errors of 10 per cent or more will be encountered for viscosity.

For trans-octahydroindene the v_f minimum value is about 0.06 cm^3 g^{-1}, and for the sebacate, it is 0.05 cm^3 g^{-1}.

The variation of the parameters v_o and B' with pressure are shown for the three liquids in Fig. 10.9. As before v_o decreases with pressure asymptotically towards an ultimate specific volume in the same way as it was found to vary for the original free volume equation. Therefore this isobaric interpretation of the free volume concept not only fits the data very well, but also shows that v_o behaves in a physically realistic manner. The variation of B' shown for the three liquids in Fig. 10.9 is smooth, and passes through a maximum for the two phthalates, and for the trans-octahydroindene it increases rapidly at higher pressures. The variation of B' with pressure is systematic and too large for it to be attributed to experimental errors. Insufficient data are presented here to be able to surmise the significance of the behaviour of B'. It could be a molecular packing factor which occurs due to an overlap of the free volumes of adjacent spheres, or in the context of the theory of Cohen and Turnbull (1959) an overlap of the cages which they define as being occupied by each molecule. Their free volume is defined as the cage volume less the volume of the molecule. That B' appears to increase and then decrease could be explained by the cages being squeezed closer together under pressure, until the repulsive forces between molecules prevent further overlap. The behaviour of B'

leaves room for further investigation not only to explain it, but also to establish the effect upon B′ of the range of data used in its derivation.

The simplified free volume equation has been shown to describe data almost as well as the free volume equation, and it has two pressure dependent parameters as opposed to three. The simplified equation is offered as a purely empirical extension of the free volume equation which was derived by Cohen and Turnbull using a hard-sphere model. That such a simple equation as the simplified equation (or the free volume equation for that matter) expresses the data to such high accuracy is surprising, because the molecules of the liquids tested here lack sphericity and any significant symmetry.

10.5 Free Volume - Discussion

It is customary to treat Doolittle's original free volume equation,

$$\ln \eta = A' + B' \frac{v_o}{v_f}, \tag{10.1}$$

as viscosity on a logarithmic scale as a function of v_o/v_f, which of course yields a straight line relationship in the region where it is valid. The independent variable is not v_o/v_f, however, but specific volume, v. Equation (10.1) may be expressed more fully as follows

$$\ln \eta = A' + \frac{B'v_o}{v - v_o}. \tag{10.12}$$

On rearrangement this becomes

$$\ln \eta = \frac{(A' - B') - \frac{A'}{v_o} v}{1 - \frac{v}{v_o}}. \tag{10.13}$$

This is of the form

$$Y = \frac{P + QX}{1 + RX}, \quad \text{when } Y = \ln \eta, \text{ and } X = v, \tag{10.14}$$

which is the general equation of the rectangular hyperbola. The asymptotes of the hyperbola are given by $\bar{X} = -1/R$, and $\bar{Y} = Q/R$. Thus

from equation (10.13) it is deduced that when ln η is plotted as a function of specific volume, v, then the asymptotes are at v_o and at A'. This becomes clearer in Fig. 10.10. As v approaches v_o the curve rises steeply towards the v_o asymptote so that any small deviation in specific volume results in a rapid change in viscosity which is on a logarithmic scale.

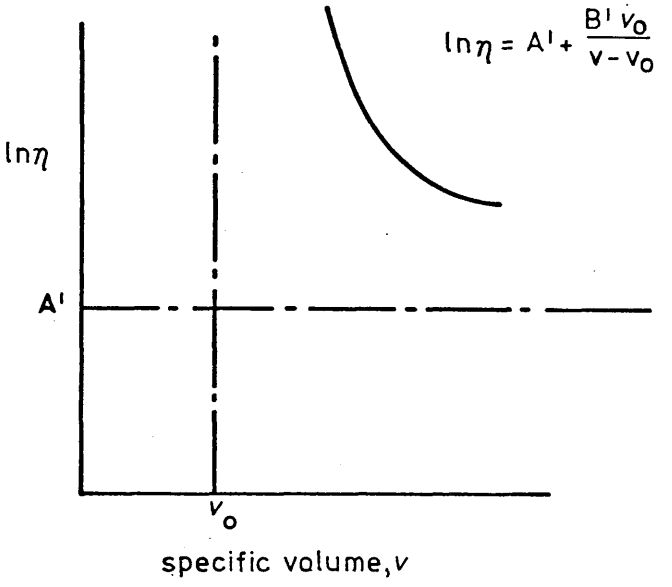

FIG10·10 The hyperbolic form of the free volume equation

The hyperbola is a useful and flexible equation, and it occurs in many fields as the proper relationship, although it is often not recognised. For example, the modified secant bulk modulus equation used in Chapter 6 to relate specific volume and pressure is also a hyperbola. Hohmann and Lockart (1972) state that in many instances the hyperbola with its three constants can fit data more precisely than a five-constant polynomial. It has the additional advantage that the constants often have physical meaning.

10.5.1 Comparison with other equations

The relative merits of the free volume model and other types of models for describing viscous behaviour have been compared by several workers including Hogenboom, Dixon, and Webb (1967), Gubbins and Tham (1969), and Hutton (1972). In the context of this thesis, the most important models are, briefly:

a The reaction rate model proposed by Glasstone, Laidler, and Eyring in 1941 which resulted in an equation of the Arrhenius form

$$\eta = Ae^{B/T}. \qquad (10.15)$$

Although this equation has severe limitations, it is nevertheless still useful, mostly at high temperatures.

b The free volume equation of Doolittle (1951) which is adapted from the earlier models of Batchinski (1913) and Macleod (1923). The equation has already been discussed in this chapter.

c The Cohen and Turnbull hard-sphere diffusion model produced in 1959 yields the following equation

$$\ln (\eta/T^{\frac{1}{2}}) = A''' + B'''/(v - v_o). \qquad (10.16)$$

This derivation provided the theoretical justification of Doolittle's empirical equation, since $\ln (T^{\frac{1}{2}})$ in the above equation, where T is the absolute temperature, is a slowly varying function compared with $\ln \eta$, and may usually be regarded as constant.

d The Eyring and Ree significant-structure theory - Eyring and Marchi (1963), Ree, Ree, and Eyring (1964) - produced an equation which bears similarities to the previous equations. At atmospheric pressure the equation is

$$\ln \{\eta(v - v_s)/T^{\frac{1}{2}}\} = A + \{Bv_s/(v - v_s)T\}. \qquad (10.17)$$

Here v_s is the specific volume of the solid phase.

A careful comparison of the effectiveness of the last three equations has been made by Hogenboom et al (1967) for nine compounds at atmospheric pressure. It was found that all three equations provide excellent fits to the data. This confirms that no single model is unique in accurately describing the data, and is a warning against accepting any one hypothetical model as successful simply because it fits the data well. This point has been discussed in a definitive paper by Brush (1962). Hutton and Phillips (1970) also observed that liquid model theories cannot be unequivocally tested using viscosity data.

Each of the equations has its limit of applicability; in particular the free volume equation has deficiencies in accounting for Arrhenius behaviour in liquids. To overcome this, Macedo and Litovitz (1965) combined the rate theory of Glasstone et at (1941) with the free volume theory of Cohen and Turnbull. This quite logical merging of models to obtain the virtues of both was not entirely successful and has been

criticised on theoretical grounds by Brummer (1965), and also by Barlow, Lamb, and Matheson (1966), Hogenboom, Webb, and Dixon (1967), and Bloomfield (1971). More recently another equation which combines two flow processes has been proposed by Breitling and Magill (1974). Their equation is capable of reducing data for several polymers to a single master curve which extends over 16 orders of magnitude.

Many different liquids of varying molecular complexity have been shown to exhibit behaviour that can be described by various models. In the main, the successes have been in describing the viscosity of liquids as a function of temperature. It was noted by Dixon and Webb (1962) that it is surprising that the relatively simple free volume equation describes data with precision even for complex molecules which lack both sphericity and symmetry. The accuracy with which the free volume equation describes data has been confirmed here and elsewhere, but this is not by any means conclusive evidence that this particular hard-sphere model is more correct than all others. That the free volume equation in all its simplicity does perform as well for pressure as well as temperature variations suggests that it should be maintained as an extremely useful tool until significant advances in liquid theory have been made to provide a practical and convincing alternative.

One of the strongest critics of the simplistic models is Goldstein (1969) who considers the pursuit of these models misguided. In his view they are crude and naive and suggests for the present that investigations should be of a qualitative or at best semiquantitative nature until a rigorous molecular theory of viscosity can be developed. Of this he is pessimistic.

10.5.2 The effect of pressure on v_o

By applying the free volume equation along viscosity isobars it has been shown in this chapter that the limiting specific volume, v_o, does behave in a physically realistic way, that is, it is compressible. In their treatment of pressure data Hogenboom et al showed that the free volume equation provides an excellent description of data, but they applied the equation to isotherms with the result that v_o was found to decrease with increasing temperature in defiance of the expected, and impossible to explain in physical terms.

It is not difficult to understand why this second isothermal treatment produces curious effects. This is because it implies that the limiting specific volume (the volume in the close-packed state) is not a function of pressure, but solely a function of temperature. However, when a liquid is subjected to high pressures and to excursions in temperature the effects of the former are known to be dominant upon its specific volume, simply by examining liquid P-V-T data.

The main argument often used against the free volume approach is that the resulting equation predicts that if pressure and temperature are increased simultaneously to maintain the specific volume of the liquid constant, then it predicts that the viscosity will remain constant, whereas it is found experimentally that viscosity decreases under these conditions. The argument assumes that v_o is independent of pressure and temperature. This assumption is incorrect as mentioned above, and it is difficult to find its origin in view of several early references to v_o as not being immune to these external variables. As early as 1937, for example, Bernal asserted that v_o, the occupied volume in the model of Batchinski, 'cannot be considered to be independent of temperature and pressure'. He then showed that by allowing v_o to vary with pressure and to have the same compressibility as solid lead - no solid mercury compressibilities were available then - that Bridgman's mercury viscosity measurements were well described by the Batchinski equation up to 12 kbar. Bernal therefore recognised that v_o is a function of pressure.

In his first paper on free volume, Doolittle (1951) implied that v_o could be a function of pressure, and Cohen and Turnbull (1959), in their well-known derivation of the free volume equation, suggested that for liquid metals the temperature coefficient of v_o is small compared with that of the free volume whereas the reverse is true of the pressure coefficients. In 1964 Naghizadeh found good agreement of the pressure and temperature dependence of the self-diffusion coefficients of the rare-gas liquids with the free volume model by allowing for the 'softness' of molecular cores. Jhon, Klotz, and Eyring (1969) have discussed the effects of pressure and temperature on their significant structure equation which uses v_s which is conceptually very similar to v_o, and they considered the compressibility

of v_s and not its thermal expansion because the expansion is negligible. The allowance that Matheson (1966) made for the effects of pressure and temperature on v_o were mentioned in Section 10.3.2. In his approach he found that v_o increases with temperature and decreases with increasing pressure by amounts which correspond with solid behaviour. The importance of core 'softness' when pressure dependence of transport rates is interpreted in terms of free volume was mentioned again by Turnbull and Cohen in 1970.

Although Hogenboom et al fitted isothermal viscosity-pressure data and hence obtained v_o as a function of temperature, they also discussed other ways of applying the free volume equation. In their paper (1967) they modified the Cohen and Turnbull equation to allow v_o to be a function of pressure, and found the variation of v_o with pressure, and also found that v_o has solid-like compressibility. The $T^{\frac{1}{2}}$ term was included in the calculation. The fit to the data was comparatively poor because they used the atmospheric values of A''' and B''' (equation (10.16)). Hogenboom et al did not pursue this treatment.

In this chapter it has been demonstrated that v_o does vary with pressure if viscosity data are fitted along isobars. It shows compressibility which agrees with the ultimate specific volume, deduced from P-V-T data alone. It has been shown above that other workers in this field have recognised the dependence of v_o upon pressure, and to a lesser degree upon temperature, but none has used this approach. It is emphasised that the agreement of v_o with expected behaviour was obtained without placing any restraint on A', B', or v_o during optimization.

10.5.3 The range of applicability of the free volume equation

The modified free volume equation has been used to describe viscosity as a function of temperature fairly successfully by many different workers. It is not valid to apply this equation in the Arrhenius region, that is at higher temperatures. This subject is discussed by Davies and Matheson (1966) who also observed that the liquids that do show Arrhenius behaviour over the whole liquid range are confined to those composed of spherical atoms or molecules which are free to rotate in the liquid.

The free volume theory is gaining acceptance by polymer scientists such as Cukierman, Lane, and Uhlmann (1973), and Breitling and Magill (1974). Cukierman et al. found that the range of close description is from 10^{-2} to 10^{4} P for simple organic liquids, and also noted that the free volume model ceases to provide a useful description of viscosity for fractional free volumes of smaller than about 0.015.

In Section 10.2.1 a limit to the successful description by the free volume equation of viscosity-pressure data was found, in the region of high pressure and low temperature. For di-(2-ethylhexyl) phthalate this meant that the temperature range was 100 to 425°F rather than from 32 to 425°F. Larger errors at low temperatures are inevitable with the free volume equation, especially at high pressure, for here the specific volume, v, and the limiting specific volume, v_o, become closer in magnitude and small errors are amplified when the two quantities are subtracted to calculate v_f. This was demonstrated quantitatively in Section 10.4.3 where it was calculated that when v_f is less than 0.047 $cm^3\ g^{-1}$ then the error in viscosity is 10 per cent for an error in specific volume of only 0.0005 $cm^3\ g^{-1}$. This analysis is for the simplified free volume equation, but the argument holds for the free volume equation also, to a lesser extent. Along the 20 kbar isobar the free volume v_f for di-(2-ethylhexyl) phthalate is 0.05 $cm^3\ g^{-1}$ at 32°F; this point was discarded. This shows at 20 kbar that v_f is small enough to cause large errors in viscosity; the situation is worse at the higher isobars.

The free volume equation has been shown in this chapter to describe the effect of pressure on viscosity, for viscosity ranges of up to six decades. Care has to be exercised in the low temperature, high pressure region to avoid errors at small v_f values.

10.6 The Double Exponential Equation

Over the years many empirical viscosity-pressure equations have been proposed. Wilson (1967) reviewed the subject. The nine empirical equations that he cited are briefly:

Barus (1892) suggested a law of the form

$$\eta = \eta_a e^{A(P - P_a)}. \qquad (10.18)$$

It is by far the most common approach to use an exponential relationship. In the equation, η_a is the viscosity at atmospheric pressure, P_a, and A is a constant.

Kiesskalt (1927a,b) used an alternative form,

$$\eta = \eta_a B^{(P - P_a)}, \tag{10.19}$$

where B is another empirical constant.

Bridgman (1931) suggested

$$\log \eta = CP + D, \tag{10.20}$$

where C and D are constants.

Suge (1937) found that the constant A of the Barus equation varied exponentially with temperature

$$A = A_o e^{E\left(\frac{1}{T} - \frac{1}{T_o}\right)}, \tag{10.21}$$

where A_o is the value of the constant at temperature T_o, and E is an empirical constant.

Dow, McCartney and Fink (1941) worked on mineral oils and produced the equation

$$\eta = F\eta_a^{GP}, \tag{10.22}$$

with the two empirical constants F and G.

Hersey and Snyder (1932) used a modified exponential equation to obtain a better fit with experimental results.

$$\eta = \eta_a e^{(HP - JP^K)}, \tag{10.23}$$

where there are three constants, H, J, and K.

Skinner (1938) and Block (1951) suggested

$$\eta = \eta_a(1 - L + Me^{NP}). \tag{10.24}$$

Cragoe (1933) proposed that viscosity obeys the relationship

$$\eta = Qe^{R/S}, \tag{10.25}$$

where Q and R are empirical constants, and S is a function of temperature and pressure for a given oil:

$$S = S_a/\{1 + U(P - P_a)\},$$

where, at constant temperature, S_a is the value at atmospheric pressure and U is a constant. Dow (1948) investigated this equation and concluded that U is not constant, but varies with pressure.

Karlson (1926) developed an equation for use in his work on gear lubrication

$$\eta = \eta_o\left(\frac{P + W}{W}\right)^X, \tag{10.26}$$

where he gave X a value of 2. In the general form above, the equation was used by Blok (1950), Hersey and Lowdenslager (1950), and by Hersey and Long (1951).

In addition to these there are several comparatively recent equations, such as that of Chu and Cameron (1962),

$$\frac{\eta}{\eta_o} = \{1 + 10^a(1 - b)\eta_o{}^{-(1 - b)P}\}^n. \tag{10.27}$$

The empirical equation proposed by Roelands (1966) has only one disposable parameter and holds generally up to 5 kbar and often higher. It is

$$\log \eta + 1.2 = (\log \eta_o + 1.2)\left(1 + \frac{P}{2000}\right)^Z. \tag{10.28}$$

This equation is more accurate and certainly simpler than most other equations. The units for the equation are cP and kgf cm^{-2}. This equation, like the others, does not hold far beyond the log η-pressure transition, that is, where the curve changes from concave to convex towards the pressure abcissa.

The double exponential equation proposed here does permit all the known types of viscosity-pressure behaviour to be described almost to within experimental accuracy. The equation which is purely empirical is,

$$\ln \eta = Ae^{BP} - Ce^{-DP}. \tag{10.29}$$

In Chapter 8, viscosity results are fitted to this equation satisfactorily.

To begin with, data were fitted to the equation using a graphical method. As pressure increases the second term becomes insignificant, and by plotting log log η as a function of pressure, A and B can be found. If the lower pressure values are subtracted from the back-extrapolation of the first straight line to P = 0, then a log plot of the difference yields exponent D. This method is a trial and error process because the high pressure line is asymptotic and the gradient is not well defined, so that different lines have to be tried until the low-pressure differences plot is linear. The preliminary fits to several liquids provided such good results that a computer program was written.

10.6.1 Optimization method

Viscosity data are fitted equally well by a variation of equation (10.29). The alternative equation, given below, was used since it simplifies the calculation of optimized constants

$$\ln (\eta/\eta_o) = A(e^{BP} - e^{-KP}). \tag{10.30}$$

For ease of manipulation let $y = \ln (\eta/\eta_o)$, where η_o is the viscosity at zero gauge pressure. Thus

$$y = A(e^{BP} - e^{-KP}). \tag{10.31}$$

The constants A, B and K cannot be found directly by least squares fit. It is necessary to give starting values and obtain the constants by iteration.

Let the values for optimum fit be $A + \alpha$, $B + \beta$, and $K + \gamma$, where A, B and K are given starting values, and α, β, and γ are found by optimization. The equation can now be written as

$$y = (A + \alpha)\{e^{(B + \beta)P} - e^{-(K + \gamma)P}\}. \tag{10.32}$$

By expanding the exponentials, and discarding square or higher terms in α, β or γ the equation becomes

$$\begin{aligned} y &= (A + \alpha)\{e^{BP}(1 + \beta P) - e^{-KP}(1 - \gamma P)\} \\ &\approx A\{e^{BP}(1 + \beta P) - e^{-KP}(1 - \gamma P)\} + \alpha(e^{BP} - e^{-KP}). \end{aligned} \tag{10.33}$$

The sum of the squares of the differences between the experimental values of y and the values calculated by equation (10.33) is therefore given by

$$S^2 = \sum_{i=1}^{n} [y_i - A\{e^{BP_i}(1 + \beta P_i) - e^{-KP}(1 - \gamma P_i)\} - \alpha(e^{BP_i} - e^{-KP_i})]^2 . \qquad (10.34)$$

By differentiating with respect to α, β and γ the following equations are obtained.

$$\frac{\partial S^2}{\partial \alpha} = 2 \sum_{i=1}^{n} [y_i - A\{\ldots\} - \alpha(\ldots)](e^{BP_i} - e^{-KP_i}) \qquad (10.35)$$

$$\frac{\partial S^2}{\partial \beta} = 2 \sum_{i=1}^{n} \{ \qquad \}(-Ae^{BP_i}P_i) \qquad (10.36)$$

$$\frac{\partial S^2}{\partial \gamma} = 2 \sum_{i=1}^{n} \{ \qquad \}(Ae^{-KP_i}P_i) \qquad (10.37)$$

To minimise errors the differentials given by equations (10.35), (10.36) and (10.37) are each equated to zero giving three simultaneous equations linear in α, β and γ. The values of these are found by normal computing methods.

The values obtained are added to the starting values and the optimization procedure is repeated until the value of the squares of the errors, S^2, has converged, or is sufficiently small to be accepted as a solution.

By optimizing on $\ln (\eta/\eta_o)$ (=y) the errors are in proportion to the magnitude of viscosity and not to viscosity itself. This is important since viscosity often changes by four or five orders of magnitude over the pressure range, and percentage errors in viscosity measurements are of similar magnitude over the entire range.

10.6.2 Evaluation of the double exponential equation

The data in the ASME Report (1953) have been fitted to the double exponential equation. An overall experimental accuracy of ±3 per cent is justifiably claimed, but there are a few points which are clearly in error by up to ±10 per cent. These have been discarded. The double exponential fits the isotherms which range from 0 to 218.3°C to within experimental accuracy in nearly every case. The 44 liquids reported in the ASME Report fall into various categories: synthetic lubricants, pure hydrocarbons (American Petroleum Institute, API), gear oils, high rate of shear test oils (API), Navy oils, special samples prepared for ASME, and additional synthetics. The optimized constants for equation (10.30), and the r.m.s. errors on recalculated viscosity for samples from each group are given in Table 10.11.

The r.m.s. errors in recalculated viscosity are small being not greater than 3.5 per cent, and usually about 2.5 per cent. The maximum errors are less than twice the r.m.s. errors. Isotherms may be either concave or convex towards the pressure axis, or be concave and then convex passing through a point of inflection, and cover a change of viscosity of up to five decades. Behaviour of liquids with long chains exhibit convex curvature more than less complex liquids as illustrated by the isotherms of Dow Corning '550 silicone' shown in Fig. 10.11. At temperatures of 32, 77 and 100°F the curves are convex, while the curves at 210 and 425°F start by being concave and then become convex. The double exponential equation describes all of these curves with r.m.s. errors of less than 3.5 per cent.

The values of A, B and K of the equation vary with temperature, but not smoothly, and it is therefore inadvisable to interpolate them in order to calculate viscosities at other temperatures. The variations with temperature are mainly due to the form of the double exponential equation, since equations with two or more exponents have a notorious tendency towards being ill-conditioned, Acton (1970). It is probable, however, that this non-regular variation with temperature could be resolved by taking a set of A, B, or K values for one liquid, smoothing it, and re-optimizing for the remaining two parameters at each

Table 10.11

Optimised constants for selected liquids from the ASME Report (1953)

Liquid	ASME sample No	A	B $kbar^{-1}$	K $kbar^{-1}$	r.m.s. error in viscosity per cent	Temp ^{o}F	Temp ^{o}C
Synthetic lubricant	1	4.769 72	0.095 71	0.291 80	2.49	32	0.0
di-(2-ethylhexyl) sebacate		4.978 17	0.071 42	0.238 30	1.69	77	25.0
		4.725 22	0.068 06	0.234 99	1.62	100	37.8
		3.020 50	0.078 16	0.285 03	2.53	210	98.9
		2.267 89	0.067 08	0.379 12	3.01	425	218.3
Pure hydrocarbon (API)	9	0.991 78	0.587 43	1.681 38	0.56	32	0.0
9-n-octylheptadecane		2.235 26	0.191 14	0.659 85	0.66	68	20.0
		3.381 84	0.093 98	0.358 95	0.15	100	37.8
		3.539 56	0.057 77	0.247 75	0.90	210	98.9
		3.491 48	0.032 34	0.200 15	1.32	400	204.4
Gear oil REO-26-48	19	2.405 69	0.204 91	0.636 29	0.80	32	0.0
2-ethylhexyl sebacate		2.858 23	0.153 29	0.443 05	0.45	77	25.0
		3.517 09	0.105 29	0.323 90	0.59	100	37.8
		3.221 61	0.072 68	0.264 34	1.58	210	98.9
High rate of shear test oil	27	4.979 42	0.205 64	0.339 04	2.25	32	0.0
petroleum oil plus high		6.040 89	0.129 33	0.225 06	3.01	77	25.0
molecular weight polymer		4.604 55	0.147 26	0.292 77	2.48	100	37.8
		5.096 76	0.081 78	0.167 93	3.16	210	98.9
		2.640 07	0.081 48	0.325 27	3.04	425	218.3

Table 10.11 (contd)

Liquid	ASME sample No	A	B $kbar^{-1}$	K $kbar^{-1}$	r.m.s. error in viscosity per cent	Temp °F	Temp °C
Navy oil	28	1.753 50	0.527 00	1.066 86	0.0	77	25.0
Navy gear test oil		2.983 01	0.257 97	0.572 58	0.21	100	37.8
		3.268 06	0.137 44	0.410 32	1.22	210	98.9
		3.599 00	0.057 86	0.190 49	1.31	425	218.3
Special ASME sample	50	2.456 59	0.295 59	0.683 85	0.31	100	37.8
paraffinic oil		3.528 18	0.116 63	0.349 14	1.00	210	98.9
		3.468 23	0.058 70	0.211 66	1.13	425	218.3
Synthetic	53	2.704 99	0.707 77	0.551 85	1.09	32	0.0
Dow Corning '550 silicone'		2.184 90	0.556 74	0.607 15	1.94	77	25.0
		2.256 11	0.472 22	0.426 00	2.01	100	37.8
		1.918 96	0.295 25	0.639 28	1.67	210	98.9
		2.125 94	0.144 49	0.659 25	3.48	425	218.3
Synthetic	56	3.826 49	0.222 59	0.489 25	1.56	32	0.0
di-(2-ethylhexyl) phthalate		4.499 67	0.142 78	0.362 59	0.56	77	25.0
		4.380 42	0.129 24	0.350 42	1.39	100	37.8
		4.645 51	0.071 24	0.214 03	1.93	210	98.9
		3.248 36	0.053 35	0.187 99	1.34	425	218.3

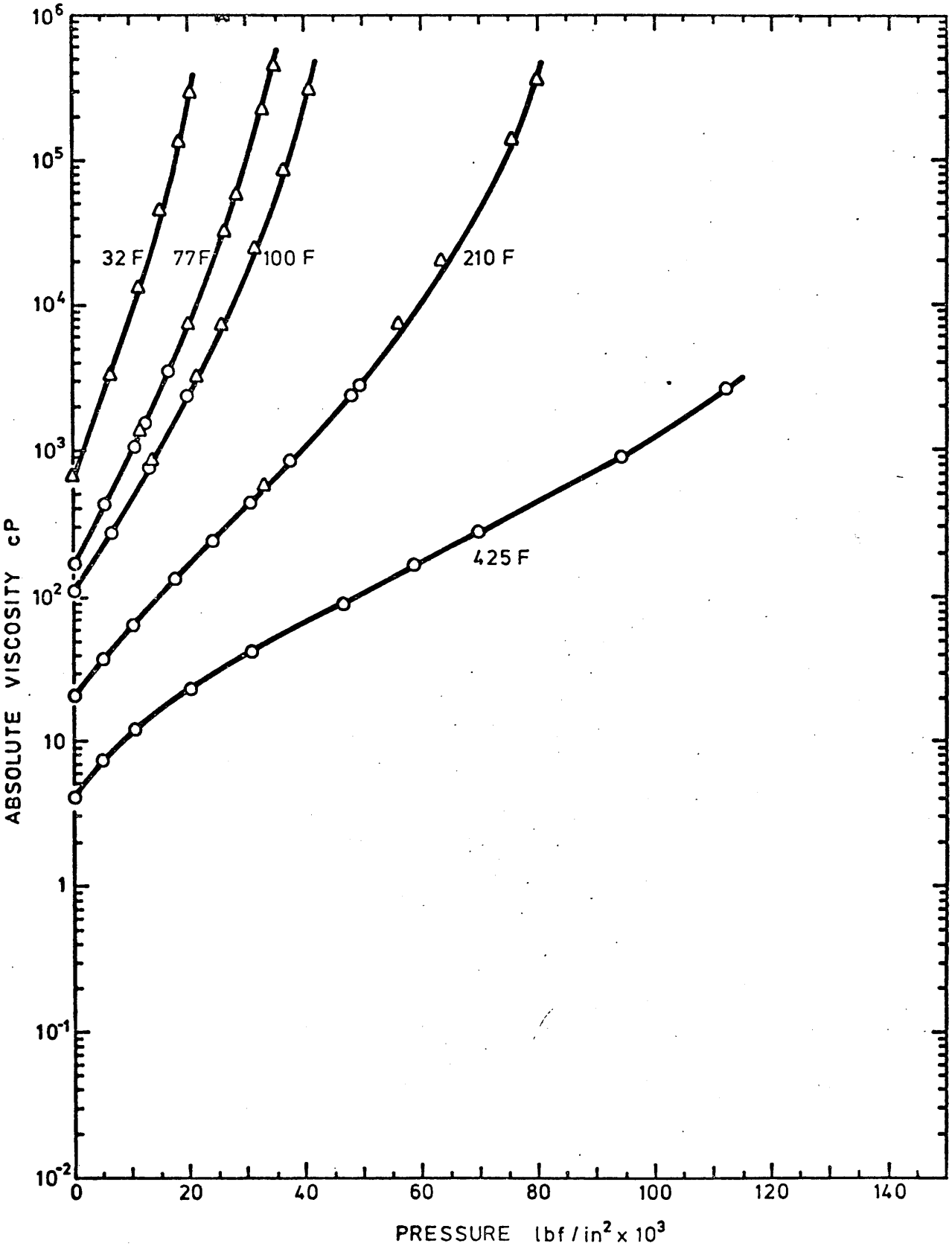

FIG 10·11 The viscosity pressure isotherms for A.S.M.E. measurement on Dow Corning 550 silicone (53-H)

temperature. In this way it may be possible to force A, B, and K to be each a smooth function of temperature without seriously impairing the accuracy of the double exponential equation.

Some effort was made to correlate the parameters, and it was found that B and K are approximately proportional for each liquid.

10.6.3 Extrapolation using the double exponential equation

The double exponential equation $\ln \eta/\eta_o = A(e^{BP} - e^{-KP})$ can be used to extrapolate to viscosity values at higher pressures.

Viscosity-pressure data at 32, 77, 210 and 425°F for di-(2-ethylhexyl) phthalate from the ASME Report were fed into the double exponential optimization program, but the data were curtailed at higher pressures by up to about 4 kbar. For example, the ASME data at 425°F reach 10 kbar, but values were only optimised up to 5.6 kbar. The values found for A, B and K were used to calculate viscosities up to 10 kbar, and these were compared with the ASME data. For the 425°F isotherm the maximum error is 15 per cent (below the measured value) which is quite good for an extrapolation of 4.4 kbar.

At high temperatures the viscosity-pressure isotherms are less steep, and therefore the likelihood of error is least, Fig. 10.11. For the 77°F isotherm, on the other hand, an error of +44 per cent was found for a 2.8 kbar extrapolation. AT lower temperatures such as 32, 77 and 100°F extrapolation should be limited to about 1 kbar if errors of greater than 20 per cent are to be avoided, whereas at higher temperatures such as 210 and 425°F extrapolations up to about 4 kbar are possible without serious loss of accuracy.

10.6.4 Range of applicability

When a liquid is subjected to pressures above about 1 kbar the assumption that the logarithm of viscosity is a linear function of pressure becomes invalid in many cases. The several empirical equations which describe viscosity as a function of pressure are inadequate, especially at higher pressures than this. The double exponential equation proposed here has been demonstrated to describe the behaviour of viscosity of eleven markedly different types of liquids to within experimental error.

The range of applicability of the proposed equation is also wide. It has been demonstrated to describe changes in viscosity up to four decades at pressures ranging from atmospheric to 10 kbar. The maximum liquid viscosity with which the equation has been tested is about 5000 Poise, this being, at the moment, the upper limit of accurate viscosity measurement attainable by conventional high-pressure viscometry techniques. When the range is extended by future experimentalists it is expected that the data will be fitted to the double exponential with similar precision, provided that the viscosity measurements are well distributed over the pressure range and that the scatter is no greater than ±3 per cent or so.

REFERENCES

1 ACTON F S. 1970
Numerical methods that work. New York, Evanston and London: Harper and Row, p 253.

2 AMERICAN INSTITUTE OF PHYSICS HANDBOOK. 1957
New York: McGraw Hill.

3 AMERICAN SOCIETY OF MECHANICAL ENGINEERING (ASME). 1953
Pressure-viscosity report. Vols I and II.

4 API PROJECT 42. 1962
Properties of hydrocarbons of high molecular weight synthesized by Research Project 42 of the API. Coll. of Sci., Pennsylvania State University.

5 API PROJECT 44. 1953
Selected values of physical and thermodynamic properties of hydrocarbons and related compounds. Pittsburg: Carnegie Press.

6 BARLOW A J. 1959
Ph.D. Thesis. University of London.

7 BARLOW A J, ERGINSAV A and LAMB J. 1967
Proc. R. Soc. A, 298, 481.

8 BARLOW A J, LAMB J and MATHESON A J. 1966
Proc. R. Soc. A, 292, 322-42.

9 BARLOW A J, HARRISON G, IRVING J B, KIM M G, LAMB J and PURSLEY W C. 1972
Proc. R. Soc. A, Lond., 327, 403-12.

10 BARR G. 1931
A monograph of viscometry. London: Humphrey Milford.

11 BARUS. 1892
Proc. Am. Acad., 19, 13.

12 BATSCHINSKI A J. 1913
Z. phys. Chem., 84, 643-706.

13 BERNAL J D. 1937
Proc. R. Soc., Lond., VA 163, 320-3.

14 BESSOUAT R and ELBERG S. 1964
J. de Phys., Supp. No 3, 25, 23-30a (in French).

15 BOELHOUWER J W M and TONEMAN L H. 1957
Proc. Conf. Lubr. and Wear, Paper 38, 214.

16 BOLAROVICH M P. 1940
Bull. Acad. Sci., 3, 27.

17 BONDI A. 1968
Physical properties of molecular crystals, liquids and glasses.
New York, London and Sydney: J Wiley & Sons Inc.

18 BLOK H. 1951
Ann. New York Acad. Sci., 53(4), 779.

19 BLOOMFIELD V A and DEWAN R K. 1971
J. phys. Chem., 75(20), 3113-9.

20 BRADBURY D, MARK M and KLEINSCHMIDT R V. 1951
Trans. ASME, 72, 667-76.

21 BREITLING S M and MAGILL J H. 1974
J. appl. Phys., 45(10), 4167-71.

22 BRIDGMAN P W. 1926
Proc. Am. Acad. Arts & Sci., 61(3), 57-99.

23 BRIDGMAN P W. 1935
J. chem. Phys., 3, 597-605.

24 BRIDGMAN P W. 1940
Ibid, 74, 11-20.

25 BRUMMER S B. 1965
J. chem. Phys. (letter), p 4317.

26 BRUSH S G. 1962
Chem. Review, 62, 513-48.

27 BRUSH S G. 1968
Arch. Hist. Exact Sci., 5(1), 1-36.

28 BURNHAM C W, HOLLOWAY J R and DAVIS N F. 1969
US Dept of Interior, Office of Saline Water. R & D Report 414,
pp 89.

29 CAPPI J B. 1964
Ph.D. Thesis. University of London.

30 CHAUDHURI P M, STAGER R A and MATHUR G P. 1968
J. chem. Engng Data, 13(1), 9-10.

31 CHEE K K and RUDIN A. 1970
Can. J. chem. Engng, 48(4), 362-72.

32 CHEN M C S, LESCARBOURA J A and SWIFT G W. 1968
AIChE Jl, 14(1), 123-7.

33 CHEN M C S and SWIFT G W. 1972
Ibid, 18(1), 146-9.

34 COCHRANE J and HARRISON G. 1972
J. Phys. E (Scientific Instruments), 5, 48-51.

35 COHEN M H and TURNBULL D. 1959
J. Chem. Phys., 31(5), 1164-9.

36 CRAGOE C S. 1933
Proc. first world petr. congress, London, 11, 529-41.

37 CUKIERMAN M, LANE J W and UHLMANN D R. 1973
J. chem. Phys., 59(7), 3639-44.

38 CUTLER W G, McMICKLE R H and SCHIESSLER. 1958
Ibid, 29(4), 727-40.

39 DAVIES D B and MATHESON A J. 1966
J. Chem. Phys., 45(3), 1000-6.

40 DIXON J A and WEBB W. 1962
Am. Pet. Inst. mid-year meeting, 14 May 1962.

41 DOOLITTLE A K. 1951
J. appl. Phys., 22(8), 1031-5.

42 DOOLITTLE A K. 1952a
Ibid, 23(2), 236-9.

43 DOOLITTLE A K. 1952b
Ibid, 23(4), 418-26.

44 DOOLITTLE A K and DOOLITTLE D B. 1957
Ibid, 28(8), 901-5.

45 DOW R B, McCARTNEY J S and FINK C E. 1941
Rheol. Bull., 12(3), 34.

46 DOW R B. 1948
J. Coll. Sci., 3, 99.

47 ENGINEERING SCIENCES DATA UNIT (ESDU). 1968
Density of water substance. Item No 68010, London.

48 ERGINSAV A. 1969
Ph.D. Thesis. University of Glasgow.

49 EYRING H and MARCHI R P. 1963
J. chem. Ed., 40, 562.

50 FLOWERS A E. 1914
Proc. ASTM, 14(2), 565-616.

51 FULCHER. 1925
J. Am. Ceram. Soc., 8, 339.

52 GABIBOV A B and TSATURYANTS A B. 1968
Dokl. Akad. Nauk Azerb. SSR, 24(7), 19-23 (in Russian).

A translation is held at NEL, East Kilbride, Glasgow.

53 GALVIN G D, NAYLOR H and WILSON A R. 1964
Proc. Instn mech. Engrs, 178(3N), Paper 14, 283-90.

54 GALVIN G D, JONES B and NAYLOR H. 1968
Experimental methods in tribology. Instn mech. Engrs, Report 28.

55 GLASSTONE S N, LAIDLER K and EYRING H. 1941
New York: McGraw Hill.

56 GOLDSTEIN M. 1969
J. chem. Phys., 51(9), 3728-39.

57 GOLIK A Z, ADAMENKO I I and VARETSKII V V. 1976
Ukr. Fiz. Zh., 21(2), 177-180 (in Russian).

58 GUBBINS K E and THAM M J. 1969
AIChE Jl, 15(2), Parts I and II, 264-9, 269-71.

59 HARRISON G. 1964
Ph.D. Thesis. University of London.

60 HAWKINS G A, SOLBERG H L and POTTER A A. 1935
Trans. ASME, 57, 395-400.

61 HAYWARD A T J. 1967
NEL Report No 295, East Kilbride, Glasgow.

62 HAYWARD A T J. 1971
NEL Report No 486, ibid.

63 HEIKS J R and ORBAN E. 1956
J. phys. Chem., 60(8), 1025-7.

64 HEINZE. 1925
Thesis. Berlin (in German).

65 HERSEY M D and SHORE. 1928
Mech. Engng, 50(3), 221.

66 HERSEY M D and SNYDER G H S. 1932
J. Rheol., 3(3), 298.

67 HERSEY M D and LOWDENSLAGER. 1950
Trans. ASME, 72, 1035.

68 HERSEY M D and LONG O M. 1951
Ibid, 72, 673.

69 HOGENBOOM D L, WEBB W and DIXON J A. 1967
J. Chem. Phys., 46(7), 2586-98.

70 HOHMANN E C and LOCKART F J. 1972
Chem. tech., 614-9.

71 HUANG E T-S. 1966
Ph.D. Thesis. University of Kansas.

72 HUBBARD R M and BROWN G G. 1943
Ind. Eng. Chem. Anal. Ed., 15, 212.

73 HUTTON J F and PHILLIPS M C. 1970
Amorphous materials. Proceedings of the 3rd Internat. Conf. on the physics of non-crystalline solids. London, New York and Sydney, Toronto: Wiley, 215-23.

74 HUTTON J F. 1972
Conf. on Rheol. of Lubricants, Trent Poly., Nottingham, 1-14.

75 IRVING J B and BARLOW A J. 1971
J. Phys. E (Scientific Instruments), 4, 232-6.

76 IRVING J B. 1972
J. Phys. D (Applied Physics), 5, 214-24.

77 IRVING J B. 1977
NEL Report No 630, East Kilbride, Glasgow.

78 IRVING J B. 1977
NEL Report No 631, ibid.

79 ISDALE J D. 1974
Private communication.

80 ISDALE J D and SPENCE C M. 1975
NEL Report No 592, East Kilbride, Glasgow.

81 JEFFERYES R. 1967
Private communication.

82 JHON M S, KLOTZ W L and EYRING H. 1969
J. chem. Phys., 51(9), 3692-4.

83 JOBLING A and LAWRENCE A S C. 1951
Proc. Roy. Soc., 206, 257-74.

84 JONES W R, JOHNSON R L, WINER W O and SANBORN D M
Trans. ASLE, 18(4), 249-62.

85 JŮZA J. 1966
Řada Technických Věd. Ročknick 76 Sěsitl, Academia Praha.

86 KARLSON K G. 1926
Teknisk Tidskrift, 56, Mekanik No 1, 1.

87 KELL G S and WHALLEY E. 1965
Phil. Trans. Roy. Soc. A, Lond., 258, 565-617.

88 KÖSTER VON H and FRANCK E U. 1969
Ber. der Bunsen, 73(7), 716-22.

89 KOZLOV YU V, YAKOVLEV V F and MALYAVIN I G. 1966
Russ. J. phys. Chem., 40(9), 1265-6.

90 KIESSKALT S. 1927a
VDI Forschungsarbeiten, 291.

91 KIESSKALT S. 1927b
VDI Z., 71, 218.

92 KÜNZEL W. 1969
Expl. Tech. der Physik., 17(6), 531-42 (in German).

A translation is held at NEL, East Kilbride, Glasgow.

93 KÜNZEL W. 1971
Private communication.

94 LAWACZECK F. 1919
VDI Z., 63(29), 677-82.

95 LENNARD JONES. 1924
Proc. R. Soc., Lond., A106, 441.

96 LESCARBOURA J A and SWIFT G W. 1968
AIChE Jl, 14(4), 651-2.

97 LOHRENZ J, SWIFT G W and KURATA F. 1960
Ibid, 547-50.

98 LOHRENZ J and KURATA F. 1962
Ibid, 8(2), 190-3.

99 MACEDO P B and LITOVITZ T A. 1965
J. Chem. Phys., 42(1), 245-56.

100 MACLEOD. 1923
Trans. Faraday Soc, 19(6).

101 MASON C C. 1935
Proc. Roy. Soc., 47, 519-20.

102 MATHESON A J. 1966
J. Chem. Phys., 44(2), 695-9.

103 McDUFFIE G E and BARR T. 1969
Rev. scient. Instrum., 40(5), 653-5.

104 McLACHLAN R J. 1975
J. Phys. E (Scientific Instruments), 9, 391-4.

105 MITSUISHI N and ADYAGI Y. 1973
J. chem. Engng, Jap., 6(5), 402-8.

106 NAGHIZADEH. 1964
J. appl. Phys., 35(4), 1162-5.

107 NATIONAL ENGINEERING LABORATORY (NEL) STEAM TABLES, 1964. 1964
Edinburgh: HMSO.

108 NEL STEAM TABLES. 1964
See above.

PSU PROJECT 42 (PENNSYLVANIA STATE UNIVERSITY). 1953
See under API Project 42.

PSU PROJECT 44 (PENNSYLVANIA STATE UNIVERSITY). 1962
See under API Project 44.

109 PURSLEY W C. 1968
Ph.D. Thesis. University of Glasgow.

110 REE T S, REE T and EYRING H. 1964
J. phys. Chem., 68, 3262.

111 ROELANDS C J A. 1966
Thesis. Technical University of Delft.

ROSSINI et al. 1953
See under API Project 44.

112 ROWE G W. 1966
ASME Paper No 66 - Lub. 2.

113 SABERSKY R H and ACOSTA A J. 1964
Fluid flow. London and New York: Macmillan.

114 SCOTT R. 1959
Ph.D. Thesis. University of London.

115 SEEDER W A. 1943
Thesis. University of Utrecht.

116 SHAKHOVSKOI G P, LAVROV I A, PUSHKINSKII M D and GONIKBERG M G. 1962.
Inst. Org. Chem. Acad. Sci., USSR, 1, 181-3.

117 SKINNER S M. 1938
J. appl. Phys., 9, 409.

118 SMITH G S. 1957
J. Inst. Petrol., 43(404), 227-30.

119 STAKELBECK H. 1933
Zeit. ges Kälte-Ind., 40, 33-40 (in German).

STEAM TABLES, 1964. 1964
See under National Engineering Laboratory (NEL).

120 STEINER L A. 1949
Chemical Age, 60, 638-44.

121 SUGE Y. 1937
General discussion on lubricants and lubrication. IME, 2, 412.

122 SWIFT G W, CHRISTY J A and KURATA F. 1959
AIChE Jl, 5(1), 98-102.

123 SWIFT G W, LOHRENZ J and KURATA F. 1960
Ibid, 6(3), 415-9.

124 TAMMANN G. 1907
On the relation between internal forces and the properties of solutions. Hamburg: Leopold Voss (in German).

125 TAMMANN G and HESSE W. 1926
Z. anorg. allgem. Chem., 156, 245 (in German).

126 TRACHMAN E G. 1975
Trans. ASME, 486-93.

127 TROMBETTA M L. 1971
Int. J. Heat Mass Transfer, 14(8), 1161-73.

128 TSIKLIS D S. 1968
Handbook of techniques in high-pressure research and engineering. (Trans. from Russian by A Bobrowsky.) New York: Plenum Press.

129 TURNBULL D and COHEN M H. 1970
J. Chem. Phys., 52(6), 3038-41.

130 VAIDYA S N and KENNEDY G C. 1970
J. Phys. Chem. Solids, 31, 2329-45.

131 VOGEL H. 1921
Phys. Z., 22, 645.

132 WILSON W R D. 1967
Ph.D. Thesis. Queen's University, Belfast.

133 YAZGAN E. 1966
Ph.D. Thesis. University of Glasgow.